

UNCLASSIFIED

AD NUMBER
AD901770
NEW LIMITATION CHANGE
TO Approved for public release, distribution unlimited
FROM Distribution authorized to U.S. Gov't. agencies only; Test and evaluation; Sep 1971. Other requests shall be referred to Air Force Flight Dynmaics Laboratory, Wright-Patterson AFB, OH 45433.
AUTHORITY
AFFDL ltr, 29 Dec 1978

THIS PAGE IS UNCLASSIFIED

7
AD901270
AFFDL-TR-70-169
VOLUME I

**AIRCRAFT LANDING GEAR
DYNAMIC LOADS INDUCED
BY SOIL LANDING FIELDS**

VOLUME I. PREDICTION MODEL AND WHEEL LOADS

B. M. CRENSHAW

LOCKHEED-GEORGIA COMPANY

TECHNICAL REPORT AFFDL-TR-70-169, VOLUME I

JUNE 1972

D D C
JUN 1972
10 3

Distribution limited to U. S. Government agencies only; test and evaluation; statement applied September 1971. Other requests for this document must be referred to AF Flight Dynamics Laboratory, (FY), Wright-Patterson AFB, Ohio 45433.

AIR FORCE FLIGHT DYNAMICS LABORATORY
AIR FORCE SYSTEMS COMMAND
WRIGHT-PATTERSON AIR FORCE BASE, OHIO

NOTICE

When Government drawings, specifications, or other data are used for any purpose other than in connection with a definitely related Government procurement operation, the United States Government thereby incurs no responsibility nor any obligation whatsoever; and the fact that the Government may have formulated, furnished, or in any way supplied the said drawings, specifications, or other data, is not to be regarded by implication or otherwise as in any manner licensing the holder or any other person or corporation, or conveying any rights or permission to manufacture, use, or sell any patented invention that may in any way be related thereto.

Copies of this report should not be returned unless return is required by security considerations, contractual obligations, or notice on a specific document.

**AIRCRAFT LANDING GEAR
DYNAMIC LOADS INDUCED
BY SOIL LANDING FIELDS**

VOLUME I. PREDICTION MODEL AND WHEEL LOADS

B. M. CRENSHAW

LOCKHEED-GEORGIA COMPANY

Distribution limited to U. S. Government agencies only; test and evaluation; statement applied September 1971. Other requests for this document must be referred to AF Flight Dynamics Laboratory, (FY), Wright-Patterson AFB, Ohio 45433.

FOREWORD

This report was prepared by the Lockheed-Georgia Company, Marietta, Georgia, under USAF Contract F33615-69-C-1349, "Aircraft Landing Gear Dynamic Loads Induced by Soil Landing Fields." The contract was initiated under Project 1370, "Dynamic Problems in Military Flight Vehicles, "Task No. 137008, "Prediction of Dynamic Loads in Military Aircraft." The work was administered under the direction of the Air Force Flight Dynamics Laboratory, Air Force Systems Command, Wright Patterson Air Force Base, Ohio. Mr. Roger J. Aschenbrenner of the Aerospace Dynamics Branch was project engineer for the laboratory.

This report covers work conducted from February 1969 to June 1971.

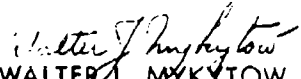
This volume was submitted by the author in June 1971.

Volume I of this report contains an analytical prediction model and wheel loading results. Volume II of this report, prepared by the IIT Research Institute contains the results of the soil tests and soil rate of loading response studies. The work reported in this volume was performed by the Aeromechanics Division of the Lockheed-Georgia Company under the direction of Mr. L. A. Tolve and in cooperation with the IIT Research Institute, the NASA Landing Loads Track at the Langley Research Center, the U. S. Army Waterways Experiment Station, and the U. S. Air Force Computer Center and Flight Dynamics Laboratory.

The author wishes to express his appreciation to the Lockheed and IIT Research Institute personnel who have contributed to this program. These include Messrs. C. K. Butterworth, A. L. Clough, Leroy Davis, C. H. Griffin, and G. K. Williams of the Lockheed-Georgia Company; Messrs. P. J. Huck, E. H. Scharres, W. B. Truesdale, and J. A. Tysiak of the IIT Research Institute.

Special recognition is due the personnel of the NASA Langley Research Center, the Waterways Experiment Station, and the Air Force Computer Center for their cooperation and support of the program. The test and data reduction portions of this program were conducted at the NASA Langley Research Center under the direction of Mr. T. J. W. Leland. The field measurements team furnished by the Waterways Experiment Station was under the direction of Mr. A. J. Joseph. The analog computer program development at the Air Force Computer Center was directed by Mr. B. J. Doody.

This technical report has been reviewed and is approved.


WALTER J. MYKYTOW
Asst. for Research & Technology
Vehicle Dynamics Division

ABSTRACT

A mathematical model to predict sinkage and the resulting loads for aircraft wheels operating on bare soil surfaces is presented together with experimental results for a 29 x 11-10 8PR Type III tire. Four primary factors which determine soil rutting and drag have been identified. They consist of the tire spring rate, the soil load deflection relation, a drag inertia force, and a lift inertia force. Soil load deflections are based on the mobility number concept developed by the U. S. Army Corps of Engineers Waterways Experiment Station. Empirical constants obtained from tests conducted at the NASA Langley Landing Loads Track were used to compute the inertia forces. Comparisons of predicted and measured rut depths and drag loads are made for a clay soil with CBR's ranging from 1.5 to 2.3 and speeds from 0 to 90 knots for tire inflation pressures of 30, 45, and 70 psi. Similar comparisons are made for sand having a surface strength of CBR 1.5. The experimental program included 173 tests with a single wheel and 39 tests with two wheels in tandem on buckshot clay and 24 single wheel tests on sand. Overall average differences in predictions and test data for rut depths were the following: 11% on CBR 1.5, less than 1% on CBR 2.3, and 1.5% on sand. Overall average differences for drag loads were the following: 6% on CBR 1.5, 9% on CBR 2.3, and 12% on sand. Average positive and negative differences were somewhat higher and were between 11% and 36%. An alternate computation using a spring-mass-damper model as used in vibrating foundation studies is also included. This alternate model is not recommended as it does not account for drag load interaction and thus is not representative of the physical system. Methods for improvement of the alternate model are discussed. A computer program is described which incorporates the soil/wheel interaction model with a simulation of the C-130 aircraft during taxi and take-off. Analyses with this program show that moderate roughness has negligible effect on take-off distance for either soft fields or hard surfaces.

TABLE OF CONTENTS

Section		Page
I	INTRODUCTION	1
II	SOIL/WHEEL INTERACTION MODEL	5
	1. Definition of Terms	7
	2. A Recommended Model for the Free Rolling Single Wheel	20
	3. A Model for Braking	46
	4. A Second Pass Model	48
	5. Landing Impact	49
	6. Comparisons of the Soil Model Results with Test Data	50
	7. An Alternate Soil Model	69
III	TEST RESULTS	77
	1. Tests with a Single Wheel	77
	2. Tests with a Tandem Wheel	88
	3. Tests with a Rigid Tire	98
IV	INCORPORATION OF THE SOIL MODEL INTO AN AIRCRAFT TAXI SIMULATION	103
	1. Take-off Distance Determination	103
	2. Wing Load Peak Counts for Take-Off	107
	3. Wing Load Peak Counts for Constant Speed Taxi	107
	4. Incremental Gear Loads for (1 - cosine) Shaped Bumps	107
	5. Recommendations for Further Computer Simulation	114
V	CONCLUSIONS	115
APPENDIX A	TABULATIONS OF TEST DATA AND TYPICAL TEST LOAD HISTORIES	119
	1. Single Wheel Tests	119
	2. Tandem Wheel Tests	119
	3. Rigid Wheel Tests	119
	4. Typical Test Load Histories	126

Section	Page
APPENDIX B ACQUISITION OF TEST DATA	148
1. Description of the Test Track	148
2. Wheel Support Devices	151
3. Data Recording System	151
APPENDIX C COMPUTER PROGRAM LISTINGS FOR SOIL MODELS	156
APPENDIX D A SAMPLE CALCULATION FOR RUT DEPTH AND DRAG LOAD	159
1. Input Data	159
2. Calculations	160
REFERENCES	171

ILLUSTRATIONS

No.	Title	Page
1.	Typical Rut Depths and Drag Loads on a Soft Soil Surface	6
2.	The Linear Relationship of Rut Depth and Drag Load	8
3.	Tire Geometric Properties	13
4.	Tire Rolling Radius as a Function of Inflation Pressure	15
5.	Tire Load-Deflection Curve	16
6.	Tire Footprint Length as a Function of Sinkage and Tire Pressure	19
7.	Load Pulse Times as a Function of Wheel Forward Velocity	21
8.	Diagram of the Soil Wheel Interaction Model	23
9.	Static Sinkage Predictions for Clay as a Function of Soil Strength	25
10.	Static Sinkage Predictions for Sand as a Function of Soil Strength	26
11.	Hypothesized Pressure Distributions underneath a Wheel at Low Forward Velocity	28
12.	Hypothesized Pressure Distributions underneath a Wheel at High Forward Velocity	30
13.	Incremental Rut Depth Caused by Drag Load	31
14.	Lift Coefficient as a Function of Soil Strength	34
15.	Incremental Rut Depth Caused by Inertial Lift Force	35
16.	Drag Coefficient as a Function of Wheel Forward Velocity	36
17.	Equivalent Tire Footprint Area Reduction with Center of Pressure Shift	38
18.	Static Pressure-Sinkage Relation for CBR 1.5 Buckshot Clay	40
19.	Predicted Sinkage vs. Dynamic Mobility Number, Clay Surface, $CI = 75$	41
20.	Predicted Sinkage vs. Dynamic Mobility Number, Clay Surface, $CI = 115$	42
21.	Flow Chart of the Soil Model Computation	45
22.	Drag Coefficient for a Braked Wheel	47
23.	Comparison of Analytical and Test Rut Depths for CBR 1.5 Clay	53

ILLUSTRATIONS (Continued)

	Page
24. Comparison of Analytical and Test Drag Loads for CBR 1.5 Clay	54
25. Comparison of Analytical and Test Rut Depths for CBR 2.3 Clay	55
26. Comparison of Analytical and Test Drag Loads for CBR 2.3 Clay	56
27. Analytical Predictions of Rut Depths for CBR 4.4 Clay	58
28. Comparison of Analytical and Test Drag Loads for CBR 4.4 Clay	59
29. Comparison of Analytical and Test Rut Depths on Sand	60
30. Comparison of Analytical and Test Drag Loads on Sand	61
31. Comparison of Analytical and Test Rut Depths for Braking on CBR 1.5 Clay	63
32. Comparison of Analytical and Test Drag Loads for Braking on CBR 1.5 Clay	64
33. Comparison of Analytical and Test Rut Depths for Braking on CBR 2.3 Clay	65
34. Comparison of Analytical and Test Drag Loads for Braking on CBR 2.3 Clay	66
35. Predictions of Second Pass Rut Depths, CBR 1.5 Clay	67
36. Predictions of Second Pass Drag Loads, CBR 1.5 Clay	68
37. Proposed Alternate Spring-Mass-Damper Soil Model	70
38. Pressure Pulse Forcing Functions	72
39. Soil Element Deflection Time Histories	73
40. Maximum Soil Element Deflections vs. Wheel Velocity	74
41. Flow Chart for the Alternate Soil Model Incorporating Drag Force Interaction and Inertia Lift Force	75
42. Free Rolling and Braking Rut Depths for Single Wheel - Zero Degrees Wheel Yaw Angle	78
43. Free Rolling and Braking Rut Depths for Single Wheel - Three Degrees Wheel Yaw Angle	79
44. Free Rolling and Braking Rut Depths for Single Wheel - Six Degrees Wheel Yaw Angle	80
45. Free Rolling and Braking Drag Ratios for Single Wheel - Zero Degrees Wheel Yaw Angle	82

ILLUSTRATIONS

(Continued)

	Page
46. Free Rolling and Braking Drag Ratios for Single Wheel - Three Degrees Wheel Yaw Angle	83
47. Free Rolling and Braking Drag Ratios for Single Wheel - Six Degrees Wheel Yaw Angle	84
48. Comparison of Free Rolling Lateral Load Ratios on Concrete and Clay for Three and Six Degrees Yaw Angle	86
49. Comparison of Lateral Load Ratios for Free Rolling and Braking on Clay at Three and Six Degrees Wheel Yaw Angle	87
50. Free Rolling and Braking Rut Depths for Tandem Wheels - 70 psi Tire Pressure	89
51. Free Rolling and Braking Rut Depths for Tandem Wheels - 45 psi Tire Pressure	90
52. Free Rolling and Braking Rut Depths for Tandem Wheels - 30 psi Tire Pressure	91
53. Free Rolling and Braking Drag Ratios for Tandem Wheels - 70 psi Tire Pressure	93
54. Free Rolling and Braking Drag Ratios for Tandem Wheels - 45 psi Tire Pressure	94
55. Free Rolling and Braking Drag Ratios for Tandem Wheels - 30 psi Tire Pressure	95
56. Comparison of Drag Ratios for 5,300 Lb. and 11,200 Lb. Tandem Wheel Loads	96
57. Comparison of Single and Tandem Wheel Drag Ratios	97
58. Rut Depths for a Single Rigid Wheel	99
59. Drag Load Ratios for a Single Rigid Wheel	100
60. C-130 Aircraft and Assault Landing Gear Schematic	104
61. Hybrid Simulation Flow Chart for Soil - Aircraft Interaction	105
62. Take-off Distance vs. Soil Strength - Rough and Smooth Surfaces	106
63. Shear Peak Counts for Take-off	108
64. Bending Peak Counts for Take-off	109
65. C-130 Aircraft Configuration	110
66. Shear Peak Counts for Constant Speed Taxi	111
67. Bending Peak Counts for Constant Speed Taxi	112

ILLUSTRATIONS
(Continued)

	Page
68. Incremental Gear Load vs. Frequency	113
69. Drag Load Time History for Single Wheel at Six Degrees Yaw - Tow	127
70. Lateral Load Time History for Single Wheel at Six Degrees Yaw - Tow	128
71. Vertical Load Time History for Single Wheel at Six Degrees Yaw - Tow	129
72. Drag Load Time History for Single Wheel at Six Degrees Yaw - 18.1 Knots	130
73. Lateral Load Time History for Single Wheel at Six Degrees Yaw - 18.1 Knots	131
74. Vertical Load Time History for Single Wheel at Six Degrees Yaw - 18.1 Knots	132
75. Drag Load Time History for Single Wheel at Six Degrees Yaw - 28.8 Knots	133
76. Lateral Load Time History for Single Wheel at Six Degrees Yaw - 28.8 Knots	134
77. Vertical Load Time History for Single Wheel at Six Degrees Yaw - 28.8 Knots	135
78. Drag Load Time History for Single Wheel at Six Degrees Yaw - 40.2 Knots	136
79. Lateral Load Time History for Single Wheel at Six Degrees Yaw - 40.2 Knots	137
80. Vertical Load Time History for Single Wheel at Six Degrees Yaw - 40.2 Knots	138
81. Drag Load Time History for Single Wheel at Six Degrees Yaw - 59.2 Knots	139
82. Lateral Load Time History for Single Wheel at Six Degrees Yaw - 59.2 Knots	140
83. Vertical Load Time History for Single Wheel at Six Degrees Yaw - 59.2 Knots	141
84. Drag Load Time History for Single Wheel at Six Degrees Yaw - 77.3 Knots	142

ILLUSTRATIONS (Concluded)

	Page
85. Lateral Load Time History for Single Wheel at Six Degrees Yaw - 77.3 Knots	143
86. Vertical Load Time History for Single Wheel at Six Degrees Yaw - 77.3 Knots	144
87. Drag Load Time History for Single Wheel at Six Degrees Yaw - 87.4 Knots	145
88. Lateral Load Time History for Single Wheel at Six Degrees Yaw - 87.4 Knots	146
89. Vertical Load Time History for Single Wheel at Six Degrees Yaw - 87.4 Knots	147
90. Schematic Diagram of the NASA/Langley Landing and Impact Loads Test Facility	149
91. Landing Loads Track during the Soil Test Program	150
92. Schematic of the Test Fixture Mounted to the Test Carriage	152
93. Schematic of the Single and Tandem Wheel Cantilevered Axle Test Fixtures	153
94. Schematic of the NASA Single Wheel Dynamometer	154
95. Instrumentation Signal Conditioning and Recording System	155
96. Determination of Tire Deflection for a Given Wheel Load and Tire Inflation Pressure	161
97. Determination of Tire Footprint Length for a Given Sinkage and Tire Inflation Pressure	163
98. Determination of the Drag Coefficient, C_D , for a Given Velocity	165
99. Determination of the Drag Interaction Rut Depth for a Given Drag Load	166
100. Determination of the Lift Coefficient, C_L , for a Given Soil Strength	167
101. Determination of the Lift Interaction Rut Depth for a Given Inertia Lift Force	168

LIST OF TABLES

No.	Title	Page
I	Soil Test Beds	3
II	Summary of Single Wheel Free Rolling Tests - Test Bed IV	120
III	Summary of Single Wheel Braking Tests - Test Bed IV	121
IV	Summary of Tandem Wheel Free Rolling Tests - Test Bed IV	122
V	Summary of Tandem Wheel Braking Tests - Test Bed IV	123
VI	Summary of Free Rolling Tests on Concrete - Single and Tandem Wheel	124
VII	Summary of Rigid Wheel Tests - Free Rolling on Concrete and on Test Bed IV	125
VIII	Computer Program Listing for the Recommended Soil Model	157
IX	Computer Program Listing for the Alternate Soil Model	158

NOMENCLATURE

A	Tire footprint area - in. ²
b	Tire width - in. and Footing width in the Bekker Equation - in.
C	Soil damping constant - lb. sec./in.
CBR	California Bearing Ratio - percent
CI	Cone index - lb./in. ²
C _D	Soil drag coefficient - dimensionless
C _L	Inertial lift coefficient - dimensionless
c	Cohesion - lb./in. ²
D	Dynamic factor
d	Tire diameter - in.
F _I	Inertia lift force - lb.
F _{net}	Net vertical force acting in the tire footprint - lb.
F _{spring}	Spring force from the soil load deflection curve - lb.
F _t	Vertical tire force - lb.
F _x	Drag force - lb.
G	Slope of cone index vs. depth curve averaged over a depth equal to the tire width - lb./in. ² /in.
h _t	Tire section height - in.
K _c	Cohesive modulus of sinkage in the Bekker Equation - lb./in. ¹⁺ⁿ
K _c '	Cohesive modulus of sinkage in the Reece Equation - dimensionless
K _d	Empirical drag interaction constant - in./lb.
K _I	Empirical inertia lift constant - in./lb.
K _φ	Frictional modulus of sinkage in the Bekker Equation - lb./in. ²⁺ⁿ
K _φ '	Frictional modulus of sinkage in the Reece Equation - dimensionless
L _t	Tire footprint length - in.
M _e	Effective soil mass - lb. sec. ² /in.
n	Exponent in the Bekker Equation - dimensionless

NOMENCLATURE (Concluded)

p	Applied pressure in the Bekker Equation - lb./in. ²
p_o	Initial tire inflation pressure - lb./in. ²
$p_o(t)$	Time function of applied footprint pressure - lb./in. ²
t_p	Loading pulse time - seconds
R_o	Undelected tire radius - in.
R_r	Tire rolling radius - in.
V	Velocity of the wheel axle - knots or as required
$X_{c.p.}$	Center of pressure shift forward of the axle centerline - in.
Z_a	Axle deflection - in.
Z_s	Rut depth - in.
ΔA	Equivalent footprint area reduction caused by drag load - in. ²
Δp	Tire pressure increment caused by drag load - lb./in. ²
$\Delta Z_{s_{drag}}$	Increment of rut depth caused by drag force - in.
$\Delta Z_{s_{lift}}$	Increment of rut depth caused by inertia lift force - in.
$\Delta Z_{s_{soil spring}}$	Increment of rut depth from soil deflection excluding inertia forces - in.
δ_t	Tire deflection - in.
μ_o	Rigid surface rolling resistance coefficient - dimensionless
ρ	Soil density - lb. sec. ² /in. ⁴
Ω	Soil mobility number - dimensionless
Ω_c	Clay soil mobility number - dimensionless
Ω_s	Sand mobility number - dimensionless
Ω'	Dynamic soil mobility number - dimensionless (used to represent either sand or clay in a general discussion)

SECTION I INTRODUCTION

Operation of large aircraft from unpaved airfields continues to be of concern to military planners. Since 1958 three large cargo transport types, the C-130, the C-141A, and the C-5A, have been operated from or have been tested on unpaved landing surfaces and taxiways. To date the C-130's have been used extensively for routine airlift to and from remote areas by both military and commercial operators by the United States and foreign countries as well. These landing surfaces have ranged from smooth to very rough, hard-baked to muddy, rocky to sand, and gravel to silt surfaces, usually bare but covered with mats in the wetter softer areas.

The C-141A, while designed for operation from paved surfaces only, has been tested on both matted and bare surfaces and has been shown to have a limited capability for operation from unpaved areas.

Repeated operations from unpaved surfaces, without major landing area maintenance, is a design requirement of the C-5A. High flotation, maximum wheel separation, and low operating tire pressures are features of this design intended to provide this capability. To date limited testing from unpaved surfaces has been conducted, but no routine operations from such surfaces have been scheduled.

Military logistics, airplane specifications, and mission flexibility may require that these and future large cargo aircraft be capable of operating repeatedly under increasingly stringent requirements from forward areas with minimal preparation and very limited maintenance expenditures.

Most full scale aircraft tests on soil surfaces are for the determination of performance capabilities; few gather data for improving other designs. In almost all the tests conducted thus far, the aircraft loads and takeoff or landing distance have been of primary importance, and only superficial attention has been given to the effects on the surface so long as operation could be sustained. No single instance where surface ruts have been measured and correlated with wheel loading has been found. No quantitative information about the progressive deterioration of the surface strength

with continued operations using aircraft as the test vehicle is available. As efficiencies must improve in the future STOL and V/STOL air vehicles, it becomes more and more difficult for an aircraft designer to apply the civil engineering soils analysis approach, based primarily on the theory of the failure of building foundations, to the design of gear systems for these aircraft which operate at ground speeds up to and above 100 knots.

In 1967 the Air Force began a series of tests using the Landing Loads Track at the NASA Langley Research Center to study soil/wheel interaction under controlled conditions (Reference 1) to develop better analytical soil models. So far only one tire size, a 29 x 11-10 BPR Type III, has been tested. Parameters investigated include wheel load, speed, tire pressure, soil hardness, and free rolling and braked conditions. These tests and a limited amount of aircraft data comprise almost the entire amount of experimental information available today for wheels operating on unpaved surfaces at speeds above about 20 knots. A summary of the soil conditions and types and the wheel configurations included in the test programs at the Landing Loads Track is shown in Table I.

Soil inertia forces have been found to strongly influence the behavior of wheels at high speed. At 90 knots the wheel used in this program produced little rutting for the same wheel loads and soil strengths that were found to produce several inches rutting at 5 knots. From 30 to 50 knots, rutting increases with increasing velocity; whereas it was previously thought that low speed rut depths were the maximum ever obtained and that it was unnecessary to study the wheel behavior at high velocity. The information gathered in this program proves that consideration must be given to the forces and deformations at high speed.

In the current study soil load-deflection properties have been based on methods developed by the U. S. Army Waterways Experiment Station. Their procedure was chosen as that most representative of wheel loading of soils. It is desirable as more tests are made to improve upon these relations and to eventually develop a general method for calculating soil load-deflection characteristics under moving

TABLE I
SOIL TEST BEDS

Test Series	Soil Bed No.	Average Strength	Wheel Configuration	Date
I	Trial Soil Bed	CBR 8 and CBR 2	Single Wheel	1967
	I Buckshot Clay	CBR 4.4	Single Wheel	1967
	II Buckshot Clay	CBR 1.5	Single Wheel	1967
	III Buckshot Clay	CBR 2.3	Single Wheel	1967
II	Sand	CBR 1.5 Surface	Single Wheel (Tandem Wheel and Landing Gear Drop Test Equipment Checkout)	1968
III	IV Buckshot Clay	CBR 2.4	Tandem Wheel	1969
			Single Wheel and Single Wheel Yawed	
			Single Rigid Wheel	

wheels with a minimum number of empirical constants. Much of the empirical data in this report is the result of a limited range of test data and the lack of suitable instrumentation to measure tire deflections and footprint pressures at high speed. These deficiencies can be corrected in the future through continued research and development programs.

Results of this study of wheel behavior at high speed are encouraging, and it is probable that analytical expressions can be developed for calculating these forces except for semi-analytical determinations of a wheel lift and drag coefficient. Analytical techniques can possibly be developed which relate these coefficients to the geometry of a particular tire.

The soil model has been incorporated into a prototype aircraft taxi and take-off simulation computer program using the C-130 aircraft.

SECTION II

SOIL/WHEEL INTERACTION MODEL

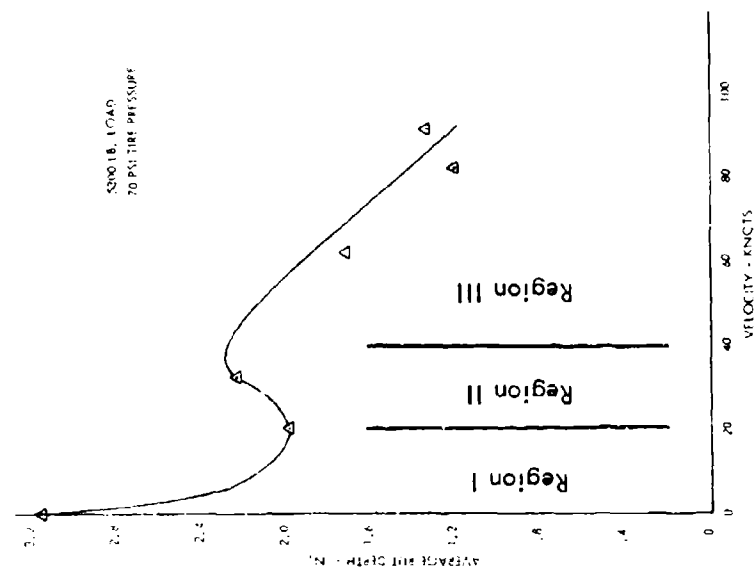
The term "soil/wheel interaction" refers to the rutting of a soil surface over which a wheel rolls and the influence of these ruts upon loads applied to the wheel. Both the ruts and the applied loads are mutually dependent upon the magnitude of each other, and this mutual dependence is called interaction. This interaction occurs between the vertical load and the rut and between the drag load and the rut.

Through a phenomenon called "slip sinkage" (2), a braked wheel produces drag loads higher than a free rolling wheel. These drag loads increase the rut depth over its free rolling value. The increased rut depth then contributes to higher drag loads because of the larger rut cross sectional area. A phenomenon similar to slip occurs on a free rolling wheel as soil inertia forces increase drag loads at high speed.

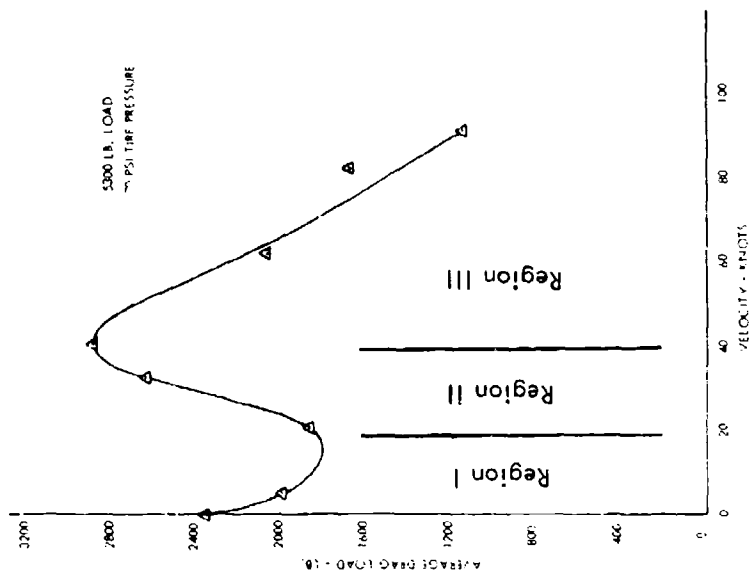
The experimental results for this program were obtained at a constant wheel load rather than at a constant penetration into the soil surface. The results thus contain the types of interaction seen on a vehicle which ruts the surface at a depth determined by the applied loads.

Figure 1a shows how a typical rut for a 30 inch diameter wheel loaded to 5300 lb. varies with velocity between zero and 90 knots. The velocity axis has been arbitrarily divided into three regions. Region I, the low speed region from 0 to about 20 knots, shows that the rut begins at a maximum and decreases to 63% of the zero speed depth. Region II, the intermediate speed region from 20 knots to around 40 knots, indicates an increasing depth with increasing speed to 72.5% of the zero speed depth. Region III, the high speed region above 40 knots, shows that the rut, after reaching a second maximum, continues to decrease with increasing speed. At 90 knots it is only 40% of its zero speed value.

Figure 1b shows the drag loads applied to the wheel as it forms the ruts shown in Figure 1a. The drag load shows behavior similar to the rut depth.



(a) Rut Depth vs. Velocity



(b) Drag Load vs. Velocity

Figure 1. Typical Rut Depths and Drag Loads on a Soft Soil Surface

Clearly the rut depth and drag load quantities are related to each other. By a cross plot they are found to be approximately linearly related as shown in Figure 2. These data points were obtained by taking the average values of rut depth and drag load for a constant speed at each of the points shown, thus representing an equilibrium condition at each speed.

Because of the interaction of the rut depth and the wheel loads, neither quantity is independent of the other, and therefore, in an analytical model they must be calculated simultaneously. Subsequent parts of this section explain how this is accomplished.

1. DEFINITION OF TERMS

There are several terms and definitions used in the development of a soil/wheel model which are not commonly used by aerospace engineers. The most significant of these terms are discussed, and references given for obtaining additional information.

a. Soil Properties

The important properties to be considered are soil strength measurements used to define test conditions, the dimensionless quantities which arise from an analysis of the soil/wheel system, and the parameters used to distinguish different types of soils.

(1) California Bearing Ratio

The expression CBR is an abbreviation for California Bearing Ratio, which is a measurement of soil strength. In simplified form this number is the ratio of the load required to deflect a soil 0.1 in. to the load required to deflect a standard crushed gravel 0.1 in., using a 3 in.² piston. A load of 3,000 lb. (1,000 psi x 3 in.²) is required to deflect the gravel 0.1 in. Since CBR is expressed as a percentage, the ratio is multiplied by 100 to obtain the CBR number. Additional information on CBR measurement is contained in Reference 3.

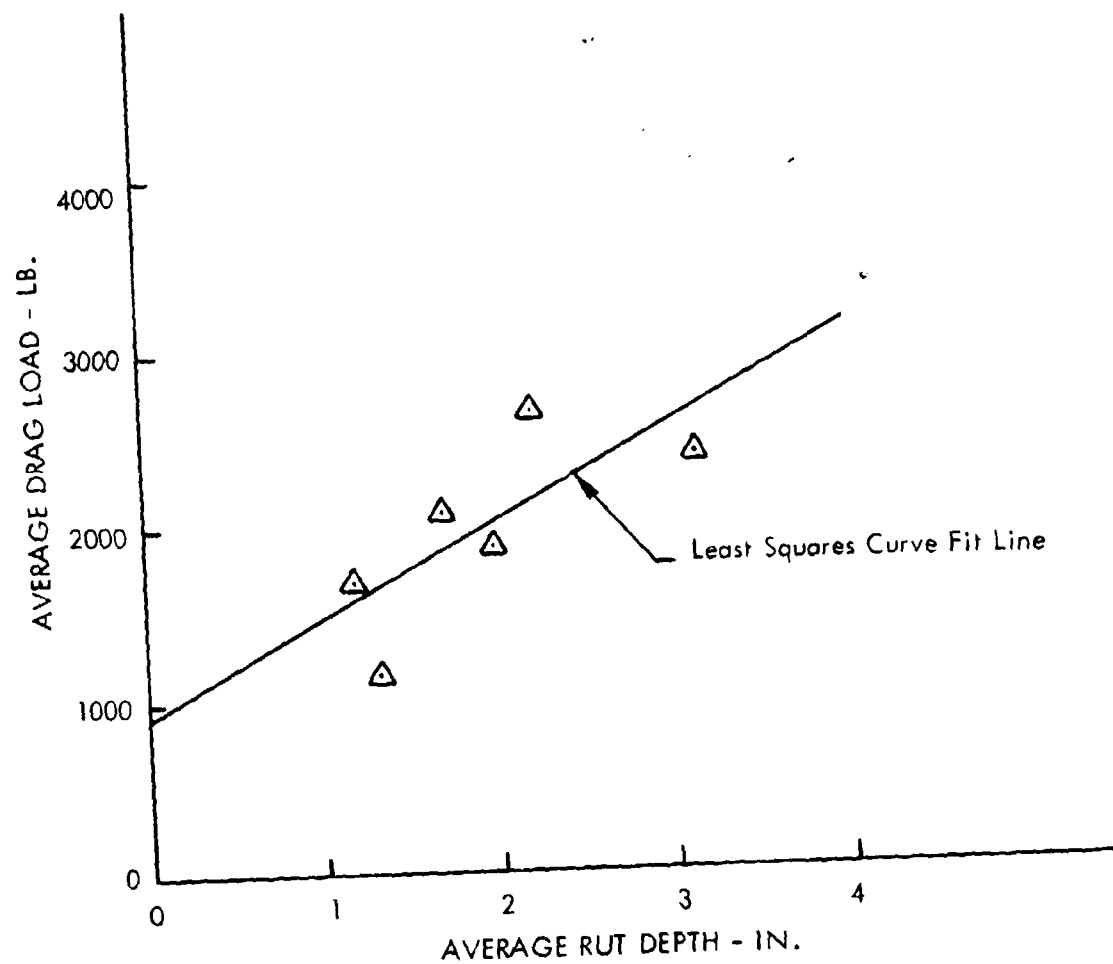


Figure 2. The Linear Relationship of Rut Depth and Drag Load

For the range of clay soil strengths that have been used in the experimental program, the force required to deflect the piston 0.1 in. varied from 45 lb. at CBR 1.5 to 132 lb. at CBR 4.4. These forces represented soil pressures of 15 psi and 44 psi respectively.

(2) Cone Index

Cone index is measured in the field using either a standard penetrometer with a 0.5 in.² base area 30° cone or an airfield cone penetrometer having a 0.2 in.² base area 30° cone. Cone index is obtained by dividing the applied force by the cone base area. Penetrometer measurements are sometimes substituted for CBR tests. Time savings from use of the penetrometer may be as much as 100:1 if excavation is required to obtain the CBR/depth profile. Reference 4 discusses the airfield cone penetrometer. Throughout this report a cone index to CBR ratio of 50:1 is used for conversion. If a different ratio is used for other soils, empirical constants developed herein will have to be adjusted accordingly.

(3) Rut Depth Measurements

Rut depth is the difference in the profile of the undisturbed soil surface and the profile of the center of the track left by wheel passage referenced to a fixed elevation. Both rod and level profiles and continuously recorded profiles have been used. Continuously recorded profiles provide improved results because of the better definitions of transient effects caused by changes in wheel loading.

(4) Mobility Numbers

The Waterways Experiment Station (WES) developed the concept of mobility numbers through dimensional analysis and from cross plots of a large number of tests for a range of tire sizes. Test results were reduced to sinkage ratio, Z_s/d , versus mobility number, Ω , as shown in Reference 5. For clay the mobility number has been defined as:

$$\Omega_c = \frac{CI (bd)}{F_t} \left(\frac{\delta_t}{h_t} \right)^{\frac{1}{2}} \quad (1)$$

For sand the mobility number has been defined as:

$$\Omega_s = \frac{G(bd)^{\frac{3}{2}}}{F_t} \frac{\delta_t}{h_t} \quad (2)$$

Mobility numbers incorporate the important parameters which relate tire properties to soil conditions. So far, these relations have been developed only for cohesive materials as represented by buckshot clay and for frictional materials represented by Yuma sand. Insufficient test data is available to predict accurately the behavior of mixtures of clay and sand, a loose compactible soil, or a hard soil having a wet surface; however, these materials are believed to have response characteristics between those of clay and sand.

Tire properties included in the mobility numbers are discussed below under Item b.

(5) Dimensional Analysis

Relationships which led to the development of the WES mobility numbers were derived by dimensional analysis. Briefly the procedure consists of grouping all of the system variables into feasible relations in which dimensions cancel to produce a "dimensionless" quantity. By further physical reasoning, the number of these relations may be reduced to a minimum. Reference 6 presents a general development of the technique. References 7, 8, and 9 apply the procedure to the problem of a wheel rolling through soil. Reference 9 shows the detailed development of the sand mobility number.

Extension of the dimensional groups to include inertia effects at high speed was discussed in Reference 7, but no additional work was done in this respect on the present program using dimensional analysis in the development of the recommended soil model. The empirical relations obtained are, however, dimensionally correct.

(6) The Dynamic Factor

Experiments have shown that the deformation of soil decreases as the rate of loading increases. Conversely, when a rolling wheel comes to rest it will sink to a greater depth during the first few seconds after it is stopped. This effect takes place at too slow a rate to be considered as inertial resistance of the soil particles and is attributed to time dependent propagation of intergranular stresses and friction.

The Waterways Experiment Station has made plate sinkage tests to determine a dynamic factor which, when multiplied by static sinkage, attenuates the sinkage by an amount which is proportional to the rate of loading. The dynamic factor is described in Reference 5, and shows that there is no attenuation for a load pulse duration of 4 seconds but that the attenuation is $\frac{1}{2.3}$ for a pulse duration time of $\frac{1}{100}$ second. The empirical equation is:

$$D = 1.0 + 1.34 e^{-1.27 t_p} \quad (3)$$

Most of the velocities tested were greater than 5 knots. These velocities correspond to pulse durations of 0.24 seconds or less. The dynamic factor was then always greater than about 2.0. Since Equation 3 has an asymptote at 2.34, it is seen that there is not a large change in the value of D over the velocity range considered compared to the change from zero ($D=1.0$) to 5 knots.

(7) The Bekker Equation

Many investigators have based their calculations of wheel sinkage on the Bekker Equation:

$$p = \left(\frac{K_c}{b} + K_\phi \right) Z_s^n \quad (4)$$

where p is the applied pressure

b is the footing width

Z_s is the rut depth

K_c is the soil cohesive modulus

K_ϕ is the frictional modulus

n is an arbitrary exponent related to the properties of the particular soil being used.

or the modified equation by Reece (10):

$$p = c K_c^{-1} + \left(\frac{b K_\phi}{2} \right) \left(\frac{Z_s}{b} \right)^n \quad (5)$$

The model presented in this report does not utilize these sinkage equations, and the parameters K_c , K_ϕ , and n were not measured as a part of the test program.

By properly choosing the value of n it should be possible to correlate static and towing sinkage test data with Equations 4 and 5; however, they have no velocity dependent relations and cannot, without modification, predict the velocity dependent behavior of the test wheel.

Reference 7 contains equations which relate the value of K_c and K_ϕ to the cone index, CI, and Reference 8 relates these quantities to CBR. In both cases the relations are only approximate.

b. Tire Geometry

The important tire geometric properties have been found to be the tire diameter, width, section height, and deflection under load. These quantities are illustrated in Figure 3 and are obtained from tire manufacturers' published data (11). They are incorporated into the soil sinkage calculations through the mobility number as discussed above under Item a.

(1) Rolling Radius

The rolling radius of a tire has been estimated (12) to be:

$$R_r = R_o - 1/3 \delta_f \quad (6)$$

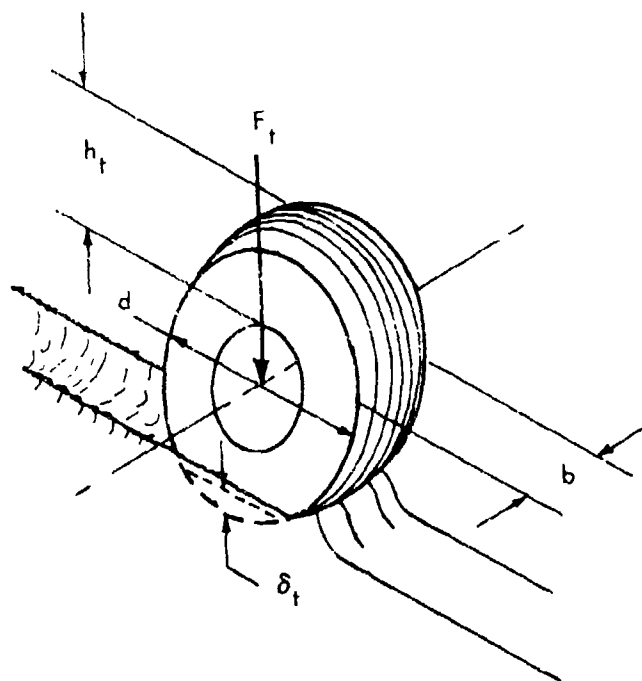


Figure 3. Tire Geometric Properties

for hard surfaces. It is not possible to determine accurately the rolling radius on a soft soil without some measurement of the instantaneous tire deflection, and it was not obtained during these tests. The hard surface approximation is being used until better information becomes available. Rolling radius versus tire inflation pressure using Equation 6 is shown in Figure 4. For the tire pressures tested the radius varies from 13.12 in. for 30 psi to 13.56 in. for 70 psi at a 5300 lb. load.

(2) Tire Load Deflection Curve

The load deflection curve for the 29 x 11-10 8PR type III tire used in this test program is shown in Figure 5. It is re-plotted from manufacturers' published data (13). From these curves the tire deflections, δ_f , used in the computation of the mobility number are obtained. Magnitudes ranged from 2.3 in. at 70 psi to 3.54 in. at 31 psi for a 5300 lb. load.

(3) Footprint Pressure

Soil is deformed by pressure applied inside the tire footprint and is proportional to the magnitude of the applied pressure in a non-linear manner. The pressure sinkage relationship varies with the soil strength and the rate at which it is loaded, decreasing in sinkage with both strength and rate of loading increases. In addition the pressure underneath the tire is non-uniform. No equipment has yet been developed to measure these pressures under pneumatic tires at high speed, but some work has been done on rigid plates, rigid wheels, and pneumatic tires at low speed (14), (2), and (15). These tests have shown that the pressure distribution in the soil is not uniform under a loaded surface, even under flat plates. The pressures under a rolling tire are usually divided into normal pressures perpendicular to the local surface of the tire and shearing stresses along the circumference of the tire. Pressure is assumed to be constant across the width of the tire although this has not been found to be true in the case of rigid wheels (16).

A wheel rolling free at constant velocity is in a condition of rotational equilibrium with all forces and moments balanced. Vertical load is supported by pressure applied

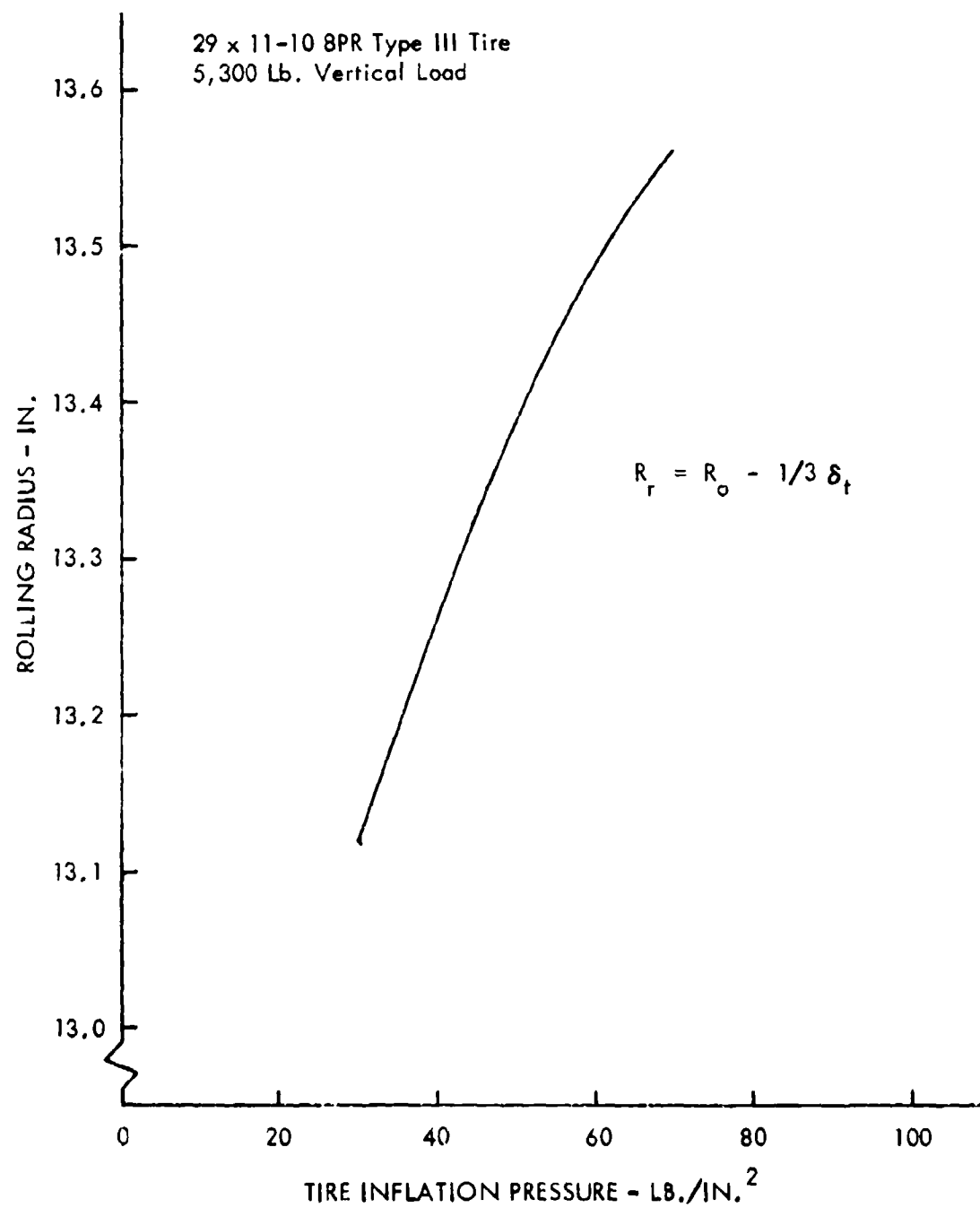


Figure 4. Tire Rolling Radius as a Function of Inflation Pressure

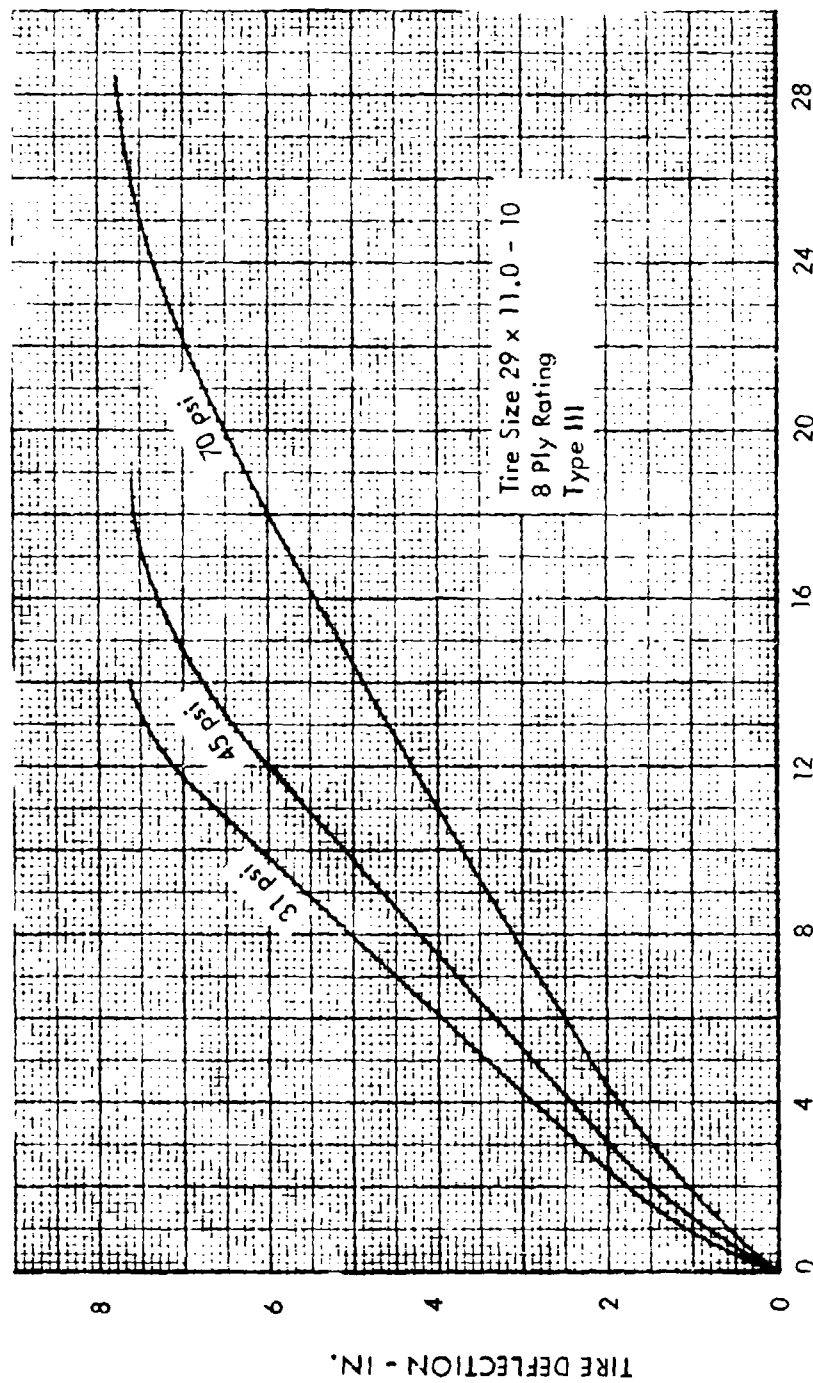


Figure 5. Tire Load-Deflection Curve

in the tire footprint and ultimately through the sidewall. Pressures are not uniform, but the integral of the pressure over the area of contact must equal the applied load. Under high drag load conditions, as encountered in deep ruts, the pressure centroid must shift forward of the axle centerline in order to provide a balancing moment which equals the drag moment and maintain zero angular acceleration. If this condition were not true, the unbalanced drag moment would accelerate the wheel and force it to go faster than the towing vehicle. Obviously this does not happen and the wheel is in a balanced condition.

A forward shift in the pressure centroid increases the pressure under the wheel above the average footprint pressure at zero speed. Increasing pressure ahead of the wheel axle increases the rutting. It is quite evident in the test data as illustrated in Figure 1 and is called drag load interaction. For the 30 inch wheel the amount of rut increase necessary to bring analytical and test results into approximate agreement was found to be 0.28 in. per 1,000 lb. drag load at CBR 1.5.

(4) Tire Footprint Length

Tire footprint length is used for inertial lift calculations and to determine pulse loading time of the soil for calculating a dynamic factor.

This length is:

$$L_f = 2 \sqrt{d(\delta_f + Z_s) - (\delta_f + Z_s)^2} \quad (7)$$

as determined in Reference 5 and is the length of the chord of a circle having a diameter equal to the undeflected tire which has penetrated the ground a distance $(\delta_f + Z_s)$. δ_f must be the hard surface deflection since tire deflections in soil have not been obtained. Reference 12 indicates that tire distortion by vertical load may reduce the footprint length by approximately 15% on a hard surface, but any change caused by vertical load distortion while the tire is rolling in a rut has been neglected.

Figure 6 shows the footprint length of a 29 x 11-10 8PR tire versus sinkage for 3 tire pressures. It varies from a minimum of 15.5 in. to a maximum of 25.2 in. for rut sinkage to 4 in.

(5) Vertical Load

Load applied to the soil surface is equal and opposite to the vertical load applied at the wheel axle. This load is distributed over the surface of the soil in proportion to the local tire footprint pressure. The vertical load is assumed constant for a freely rolling wheel on a smooth surface. Local undulations in the surface will induce oscillations in the vertical load, generally in proportion to the amplitude of the undulations for small amplitudes. Any factor which abruptly affects the rut depth can change vertical load. These factors include changes in soil strength with distance traveled, brake application, and brake release. Usually these load oscillations produce potholes or "washboarding" of the surface with repeated passes.

There is some amount of filtering of both the tire loads and abrupt rut depth changes because of the finite footprint length and because internal inflation pressure limits the radius of curvature of the tire for local deformations (assuming that the forces are not large enough to cause puncture). Interaction of the tire with roughness or surface strength changes over distances less than the tire footprint length are not well understood and are usually neglected. However, since they may be important for some applications, they deserve further study.

(6) Rate of Soil Deformation

Soil deformation takes place from initial contact of a point on the tire with the soil surface until the axle passes over this contact point. The load history of this particular point in the soil is a pulse. Duration of the pulse is proportional to wheel forward speed. The derivative of this pressure vs. time pulse is the instantaneous rate of loading.

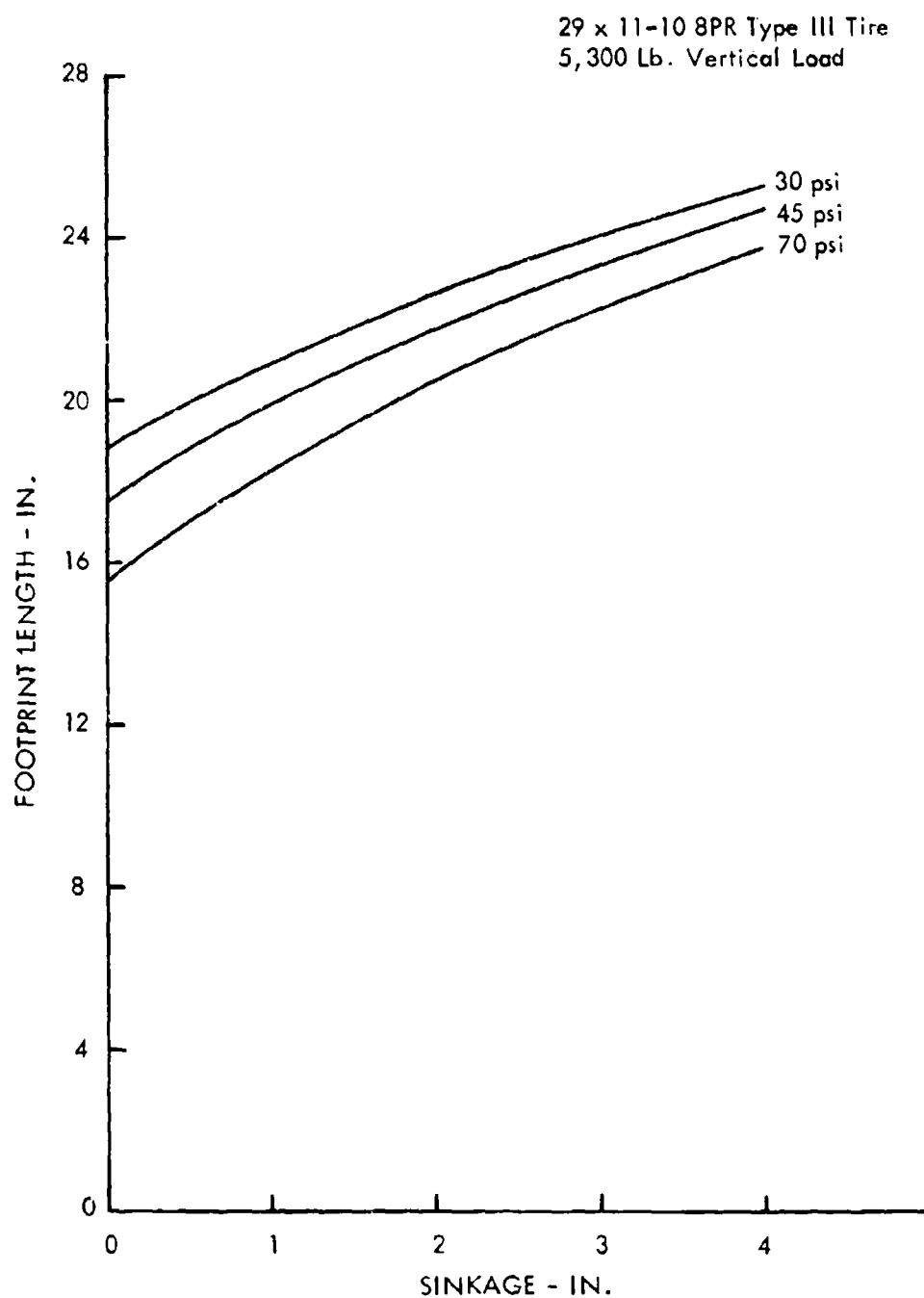


Figure 6. Tire Footprint Length as a Function of Sinkage and Tire Pressure

As a first approximation pulse time is taken as:

$$t_p = \frac{L_t}{V} \quad (8)$$

from Reference 5.

At high speeds this expression may approach a value of:

$$t_p = \frac{L_t}{2V} \quad (9)$$

because the tire is increasingly supported on the front half of the footprint length. Soil inertia forces cause the footprint pressure centroid to move forward and the pressures to become small quite rapidly aft of the axle centerline. Reference 17 assumes pressure to extend only 10° to 15° aft of the axle.

Pulse times are shown in Figure 7 for the test wheel and vary from 0.24 seconds at 5 knots to 0.0076 seconds at 100 knots.

2. A RECOMMENDED MODEL FOR THE FREE ROLLING SINGLE WHEEL

During the development of a rut depth and drag load prediction model, attempts have been made to use mathematical relationships which are consistent with as much of the available experimental results as possible. Three approaches to a soil model have been considered. These are the mobility number relationship (15, 18), the Bekker sinkage equation and its modifications (19), and a spring-mass-damper system (20).

The mobility number concept is chosen to represent the soil load sinkage relationship (excluding inertia forces) because of the considerable amount of experiments carried out with wheels during the development of the mobility numbers. The Bekker equations were excluded because insufficient test information using wheels to establish the load sinkage relation was available and because soil constants, K_c , K_ϕ , and n , necessary to utilize these equations were not measured in the test program. A spring-mass-damper system has been considered as an alternative model and is discussed in more detail below in a separate item.

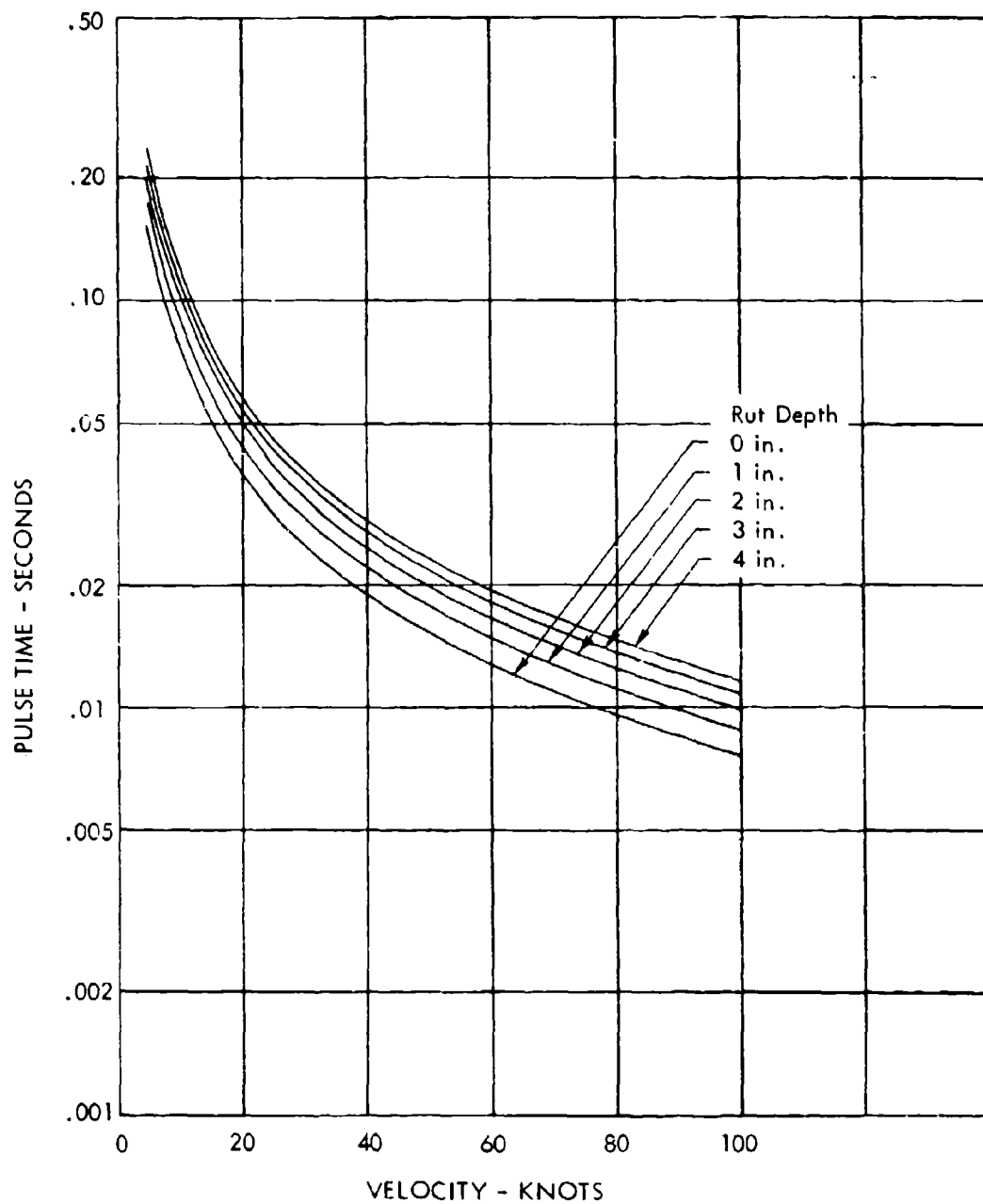


Figure 7. Load Pulse Times as a Function of Wheel Forward Velocity

Inertia forces representing drag and lift have been combined with empirical mobility number load sinkage equations in the model. A drag/rut depth interaction (which can be converted to a pressure sinkage interaction) was observed in the tests. It is also included. A schematic representation of the model is shown in Figure 8. It consists of four forces acting through springs (in the sense of a load deflection relation). Two of the spring forces, the tire spring and the drag interaction spring, act in a direction to increase rut depth. Two other spring forces, the soil resistance and inertia lift, act in a direction to reduce rut depth. Solution is by calculation of steady state equilibrium forces through iteration. This method was recommended in Reference 7.

a. The Tire Spring

The tire spring is represented by its non-linear load deflection curve from Figure 5. There is no damping associated with this spring, and to calculate forces or deflections, the load is assumed to be applied at a point.

b. The Soil Spring

The soil spring is represented by an empirical mobility number relation. This equation indicates that rut depths decrease with increasing mobility number as:

$$\Delta Z_{\substack{s_{\text{soil}} \\ \text{spring}}} = \left[\frac{.1208}{\Omega'_c - .9468} - .0095 \right] d \quad (10)$$

for a clay surface, and

$$\Delta Z_{\substack{s_{\text{soil}} \\ \text{spring}}} = \left[\frac{.3439}{\Omega'_s - .6239} - .0017 \right] d \quad (11)$$

for a sand surface. These quantities show a rapid decrease in sinkage with increasing values of Ω'_c and Ω'_s . The range of mobility numbers encountered during testing was from 2.6 to 7.9 for clay at CBR 1.5 and 2.3.

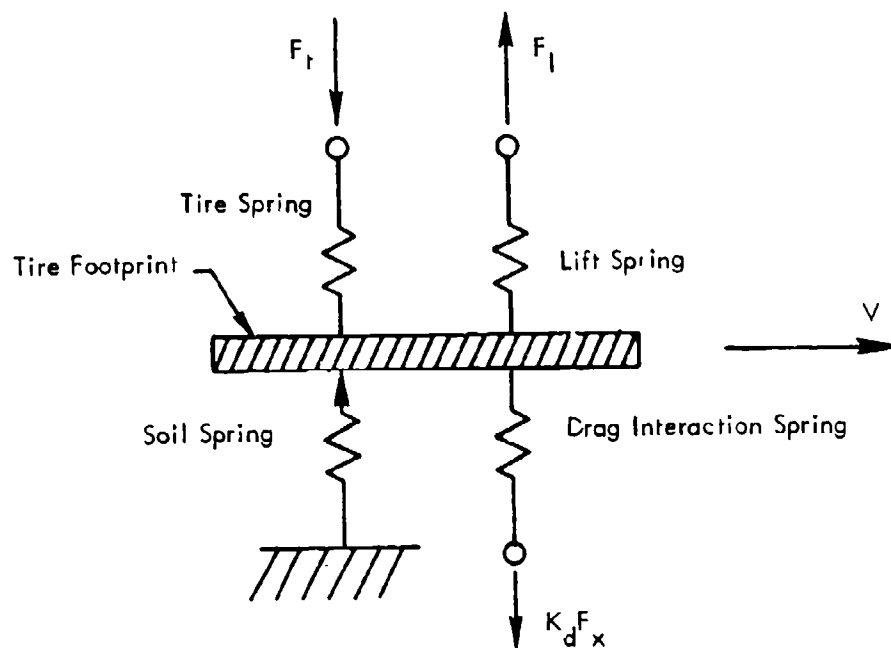


Figure 8. Diagram of the Soil Wheel Interaction Model

For wheel velocities above zero, mobility numbers are multiplied by the dynamic factor. The product of the dynamic factor times the mobility number is called the dynamic mobility number and is designated by the symbol Ω' . Since the dynamic factor is always equal to or greater than one, the dynamic mobility number is greater than the mobility number Ω . Predicted rut depths from Equations 10 and 11 thus show decreasing rut depths above zero speed because of the increasing dynamic factor.

Figure 9 shows predicted sinkages as a function of soil strength using Equation 10. The forward velocity is zero ($D=1.0$ and $\Omega_c = \Omega'_c$), and predicted sinkages are for 70, 45, and 30 psi with cone index values from 25 to 400. These cone indexes represent CBR's from 1.0 to 8.0. Tests were run between a point just above instability due to excessive sinkage to the point of negligible sinkage. This was from CBR 1.5 to CBR 4.4. Predicted sinkages ranged from 2.6 in. to 0.5 in. Maximum measured sinkage at zero forward speed was 3.17 in., and the minimum was below the resolution of the measuring equipment. For a 5,300 lb. load on the test wheel, the range of soil strength that will produce useful test information is quite narrow. The entire range of soil strengths tested represented only 5.3% change in the soil moisture content at 89.5% saturation.

Figure 10 shows the predicted and measured sinkages for a sand surface using Equation 11. Only one sand strength was tested.

As shown in Figures 9 and 10 the WES mobility numbers did not produce as great a spread in sinkage with changing tire pressure as was found in the test data. Since the only variable in the mobility number that changes with tire pressure is the deflection, δ_t , the numerical value of the exponent on δ_t was increased from 0.5 to 1.2 for clay and from 1.0 to 1.5 for sand in order to increase the spread with tire pressure. The revised mobility numbers are:

$$\Omega_c = \frac{CI(bd)}{F_t} \frac{(\delta_t)^{1.2}}{(h_t)^{\frac{1}{2}}} (.534) \quad (12)$$

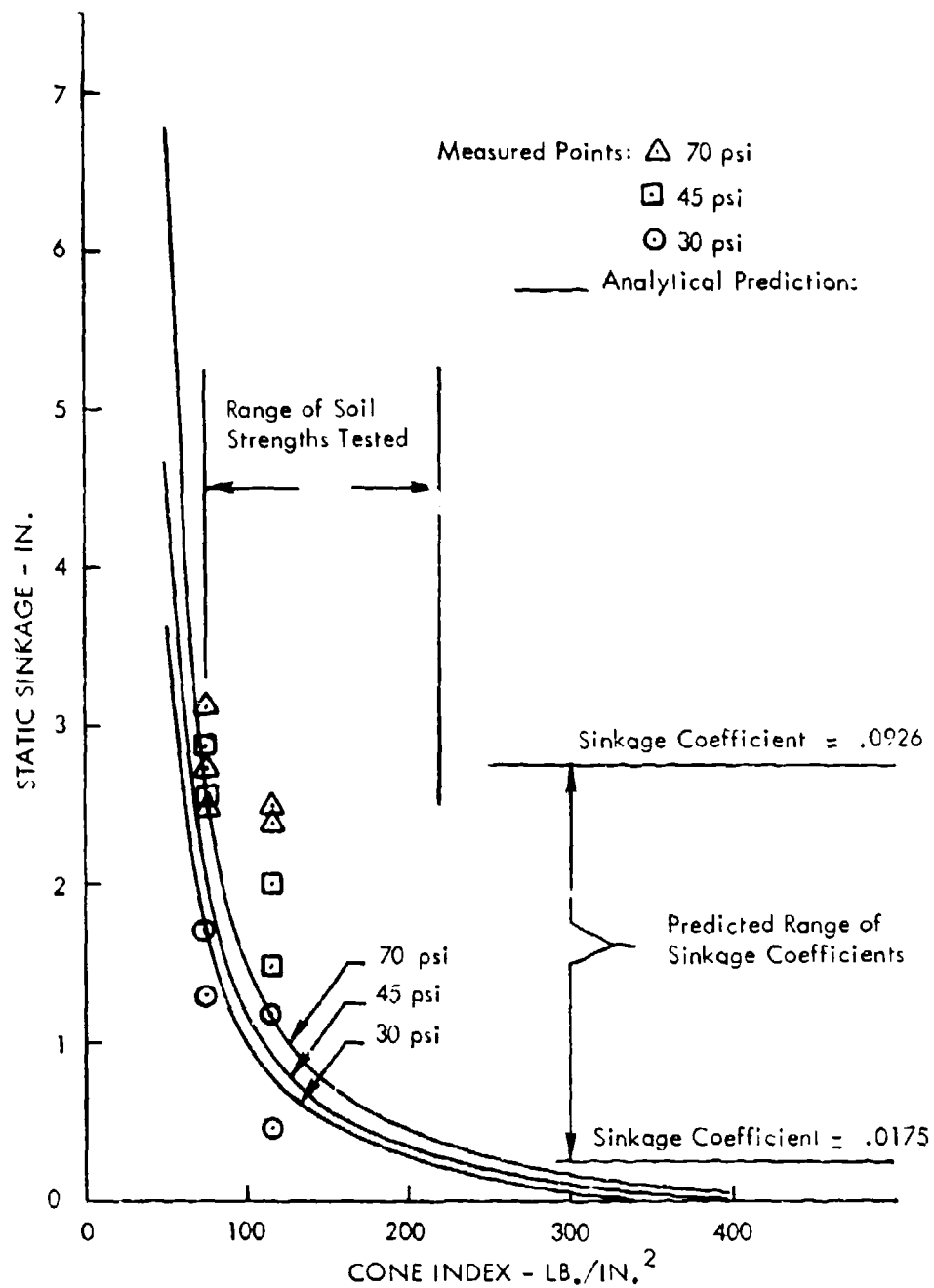


Figure 9. Static Sinkage Predictions for Clay as a Function of Soil Strength

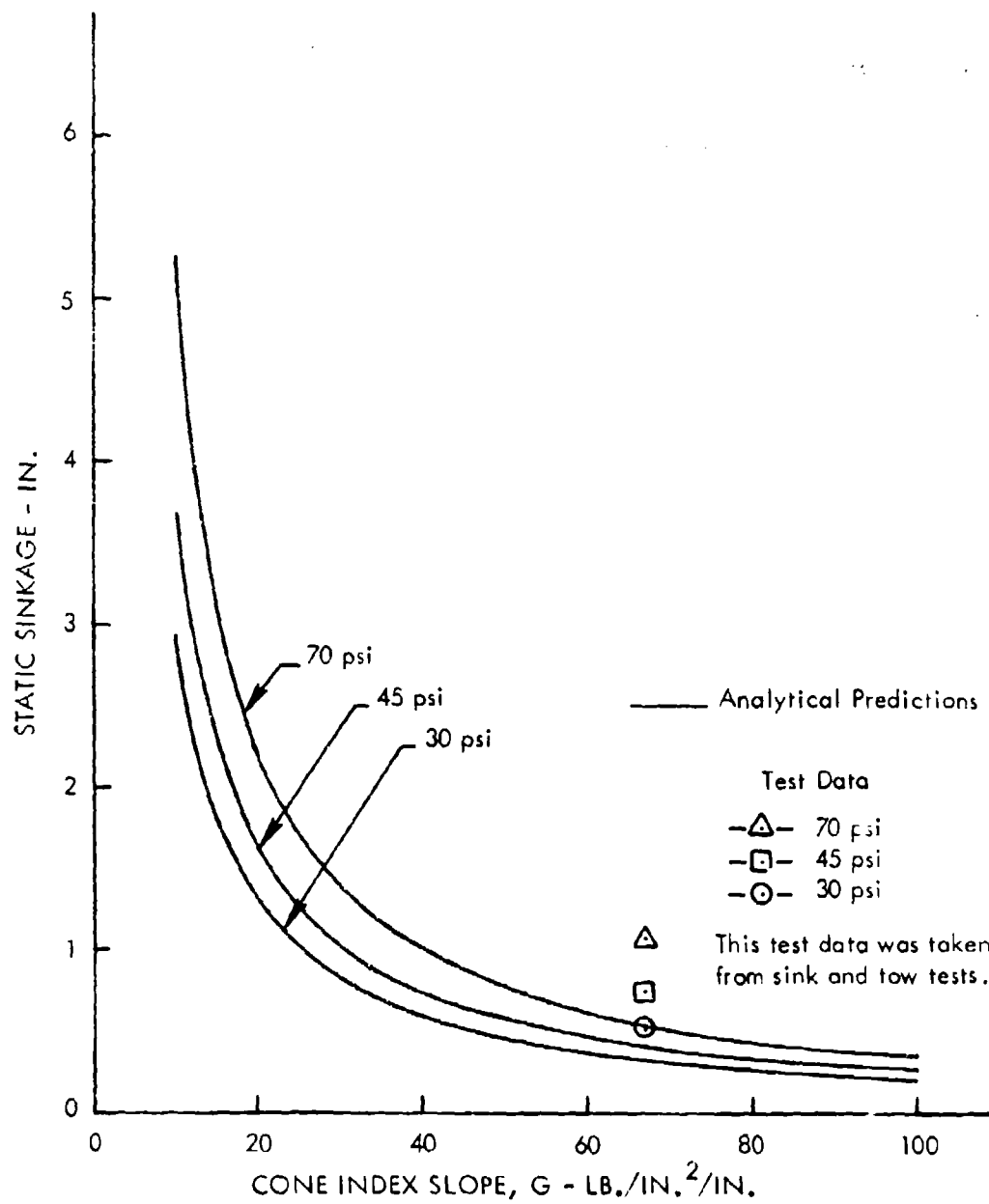


Figure 10. Static Sinkage Predictions for Sand as a Function of Soil Strength

for clay, and

$$\Omega_s = \frac{G (bd)^{3/2}}{F_t} \frac{(\delta_t)^{1.5}}{h_t} (.491) \quad (13)$$

for sand.

The numerical constants in parentheses shown in Equations 12 and 13 adjust the entire mobility number independent of tire pressure so that the rut depth predictions did not change when the exponents on δ_t were increased. The number also contains a 15% adjustment that resulted from a tire ply rating change in the analysis. It was included here to avoid re-calculating all of the empirical constants after a satisfactory comparison had been made at a different ply rating. If it is necessary to change the predictions for all tire pressures by a constant amount, it can be accomplished by an appropriate factor on Equations 12 and 13. The factor is determined by curve fitting.

c. Drag Interaction Spring

The drag interaction spring is the most difficult portion of the soil model to justify. It is based on the hypothesis that the equilibrium rut depth is not dependent upon the wheel vertical loading only, but that it is also dependent upon the drag load reaction in the soil; thus these quantities are inter-related and cannot be determined independently.

Figures 11 and 12 show schematic pressure distributions that are believed to exist in the soil and the resulting force diagrams. At low speeds illustrated by Figure 11, the inertia forces are small and the pressure distribution is not much different from that underneath a static wheel. The rut depths are decreasing in this region with increasing velocity because the effective soil strength is higher due to increasing rate of loading. These soil strength changes are represented by the dynamic factor correction discussed above. Above about 20 knots, inertia forces start to predominate in the drag load. The moment about the wheel axle caused by the drag load has to be balanced by a load generated from a distortion of the footprint pressure. This pressure distortion produces

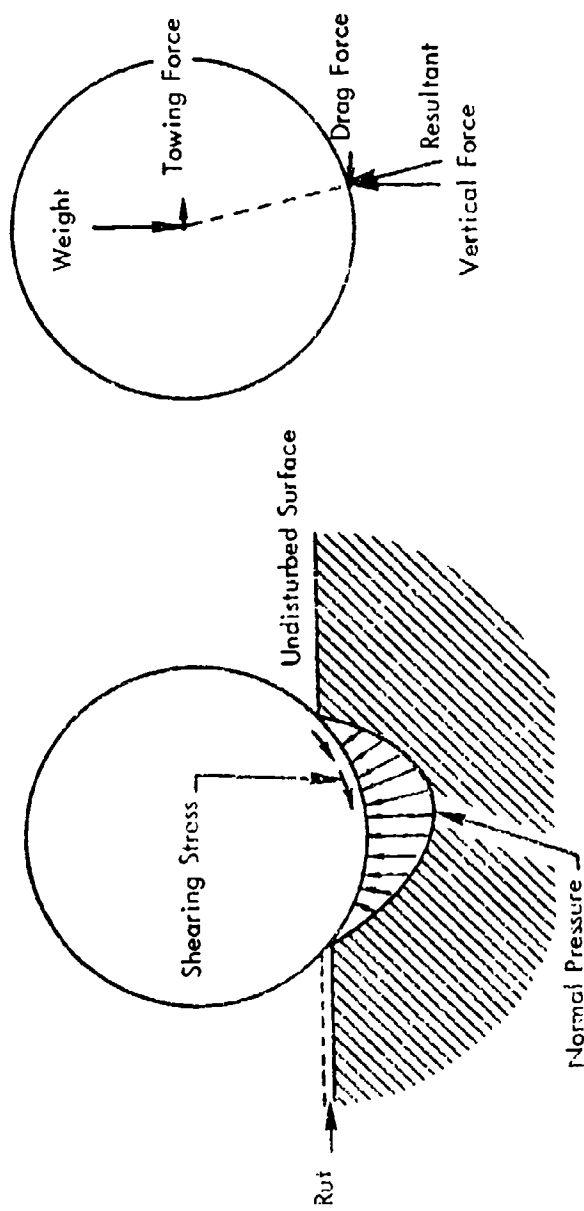


Figure 11. Hypothesized Pressure Distributions underneath a Wheel at Low Forward Velocity

higher normal pressure on the soil and thus deeper ruts. The tire has a tendency to "dig in" as speed is increased. Figure 12 shows a possible pressure distribution for velocities above 20 knots. Although tire deflection is not shown in Figures 11 and 12, it will be greatest at the point where maximum pressure is applied. The tire will be flattened to a greater extent along the slope of the rut than it is directly beneath the axle. Reverse curvature of the tire may occur at the point of maximum pressure. At this time no limit of the local pressure to a value equal to the tire inflation pressure is seen for either soft or hard surfaces.

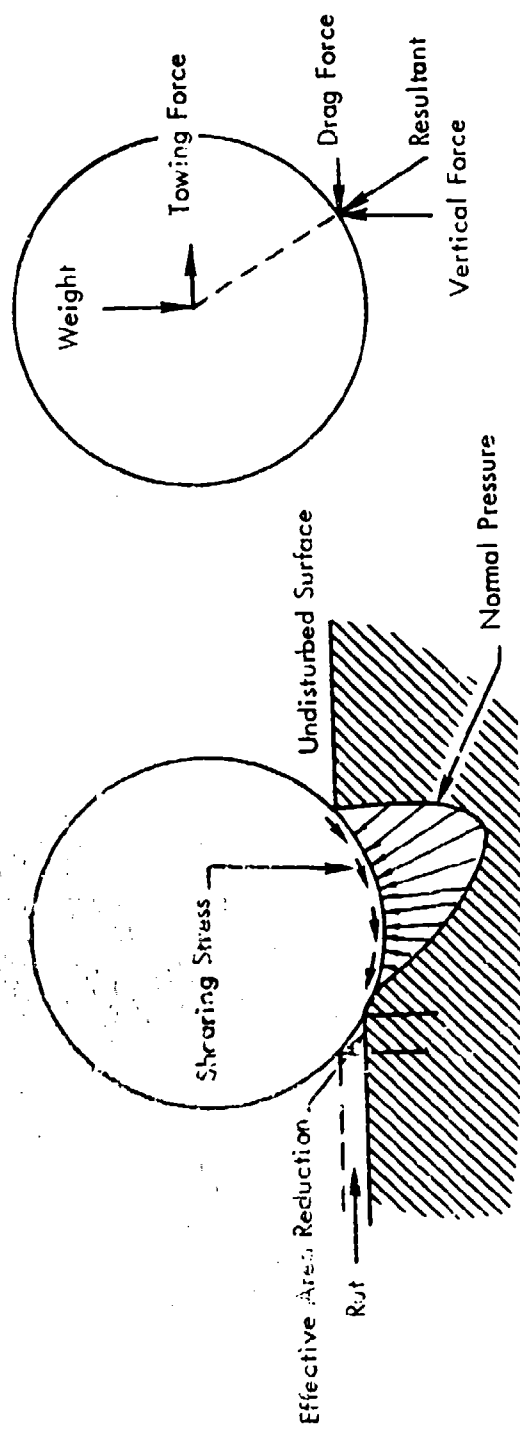
Drag interaction would soon immobilize a wheel except that the wheel drag coefficient, C_D , continuously decreases with increasing velocity. At some speed the continuing reduction in the drag coefficient more than offsets the tendency of the wheel to "dig in", thus resulting in a peak in the drag load and the rut depth.

References 1, 5, and 21 have referred to the speed at which the peak drag occurs as the "planing" velocity. The use of this term to describe the peak should be discontinued, as the wheel is definitely not planing. In fact it is at its deepest point in the soil for any speed except for static and low speed towing conditions. A more appropriate term would be "transition velocity".

There may be a planing speed for wheels on soft soils, but it would have to occur at high enough velocity that the soil inertia lift force would equal the wheel weight. This would probably not occur below 100 knots for most large aircraft tires.

The amount of rutting that is caused by the drag load was first determined empirically from test data. A semi-analytical procedure was later developed and is discussed below under Item f. Figure 13 shows the incremental rut depth caused by interaction as a function of the drag load and as a function of the soil strength. The equation represented is:

$$\Delta Z_{s_{\text{drag}}} = \frac{K_d F_x}{(CI)^{0.8}} \quad (14)$$



The average pressure is increasing and acting over a smaller area.

Figure 12. Hypothesized Pressure Distributions underneath a Wheel at High Forward Velocity

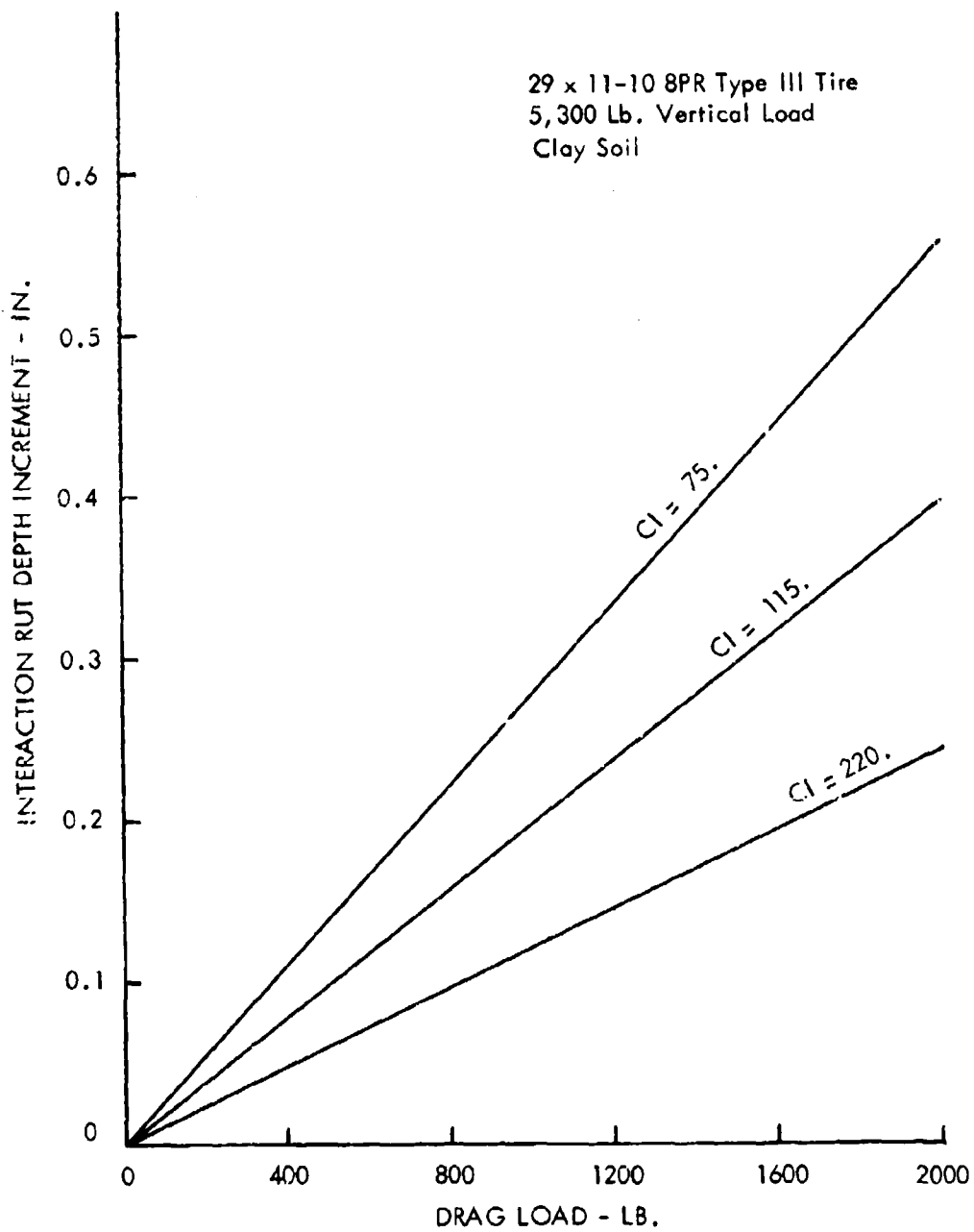


Figure 13. Incremental Rut Depth Caused by Drag Load

It was previously thought that K_d was a function of tire pressure and that $\Delta Z_{s,drag}$ varied inversely with cone index (21), but additional calculations have shown that a better overall fit to experimental data is obtained with Equation 14.

d. The Lift Spring

As wheel speed increases, soil inertia forces are generated and these forces resist deformation of the soil. They are large at high speed and are not included in the mobility number representation of soil sinkage and will not appear in a load deflection curve for soil that is loaded at a slow rate (over several seconds). In the soil model this force is represented as an increment which is proportional to the square of the forward velocity of the wheel. This force is not lift in the sense of circulation about an airfoil but is similar to the force which separates a hydroplaning tire from the pavement surface or the force which supports a planing flat plate on the surface of deep water.

The force generated on the tire is assumed to be of the following form:

$$F_l = 1/2 \rho b L_t C_L V^2 \quad (15)$$

The net force on the wheel which causes penetration into the soil is then:

$$F_{net} = F_t - 1/2 \rho b L_t C_L V^2 \quad (16)$$

Since the rut depth is proportional to the net force applied or the difference of the applied force and the soil resistance to deformation (until depth equilibrium is reached), a rut depth increment is proportional to some factor times the inertia force, or:

$$\Delta Z_{s, lift} = \frac{K_l (1/2 \rho b L_t C_L V^2)}{(CI)^{0.8}} \quad (17)$$

The constant K_l is the form of a reciprocal spring constant since it converts the force into a deflection. The lift coefficient, C_L , cannot be computed directly from the tests because of the way in which they were run. A constant vertical load was used so that the soil reaction is always equal and opposite to this load.

In the absence of any additional data C_L from Reference 5 is used. It is shown in Figure 14. The amount of rut depth reduction from the lift is determined from the value of K_l . Figure 15 shows the magnitude of the rut depth reduction as a function of the lift force and the cone index. The variation of the value of K_l inversely proportional to $(CI)^{0.8}$ is somewhat arbitrary at this time and is used to be consistent with the variation of the drag interaction term.

Figure 15 shows that the lift interaction is quite small for values of lift up to 1,000 lb. The maximum value of $\Delta Z_{s, \text{lift}}$ at 100 knots was, however, 0.246 in. in the analytical solution or a lift of greater than 10,000 lb. Since this magnitude of lift cannot be obtained with a 5,000 lb. ballast load, it indicates that although the product of $K_l C_L$ may be approximately correct C_L actually is too high and K_l is too low.

e. The Drag Load Equation

The equation used to solve for the drag load is:

$$F_x = \left(\mu_o + \frac{Z_s}{L_t} \right) F_t + \frac{1}{2} \rho b Z_s C_D v^2 \quad (18)$$

as was used in Reference 5. The term, $\left(\mu_o + \frac{Z_s}{L_t} \right) F_t$, is the drag which would be expected for a wheel starting from a zero speed condition. The second term is the inertia force caused by the motion of the wheel. It is based on the assumption that soil can be represented in the same way that flow is represented in aerodynamic or hydrodynamic problems. This assumption appears to be satisfactory at least for the soils tested in this program. All material was in a near saturated condition at high moisture contents.

The magnitude of the drag load is highly dependent upon the drag coefficient, C_D , and the manner in which it varies with velocity. Figure 16 shows the C_D used in the

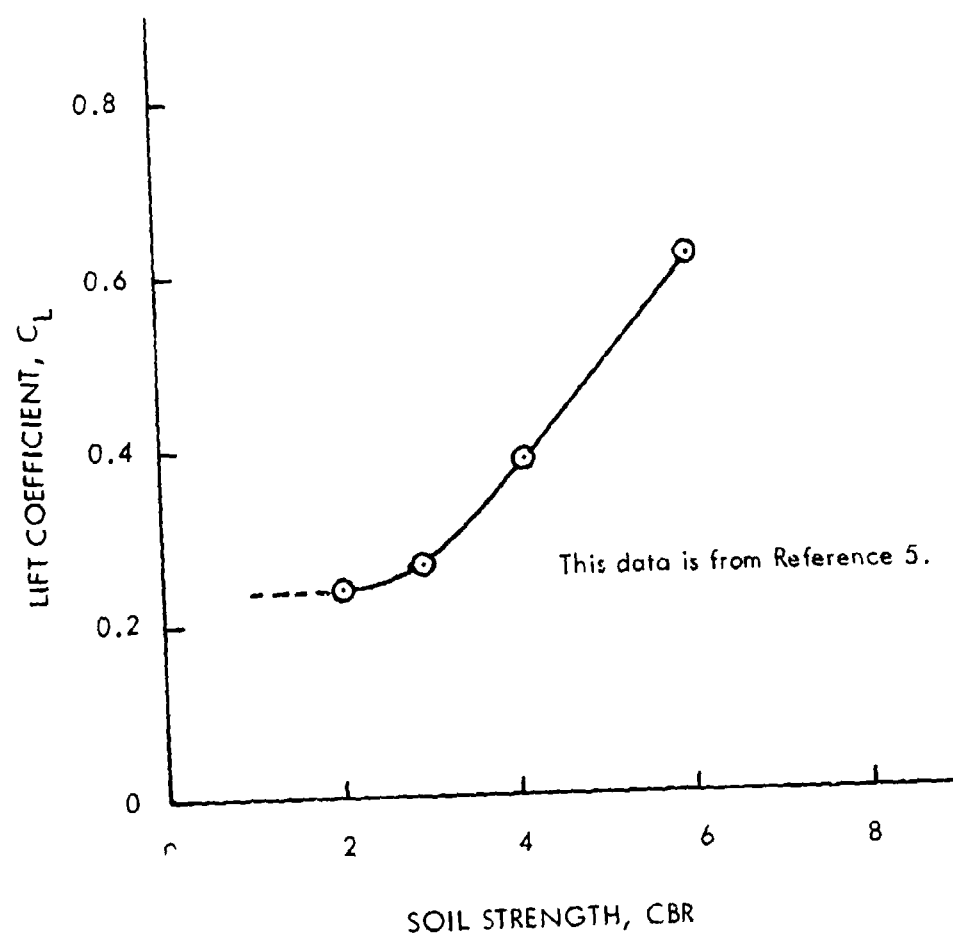


Figure 14. Lift Coefficient as a Function of Soil Strength

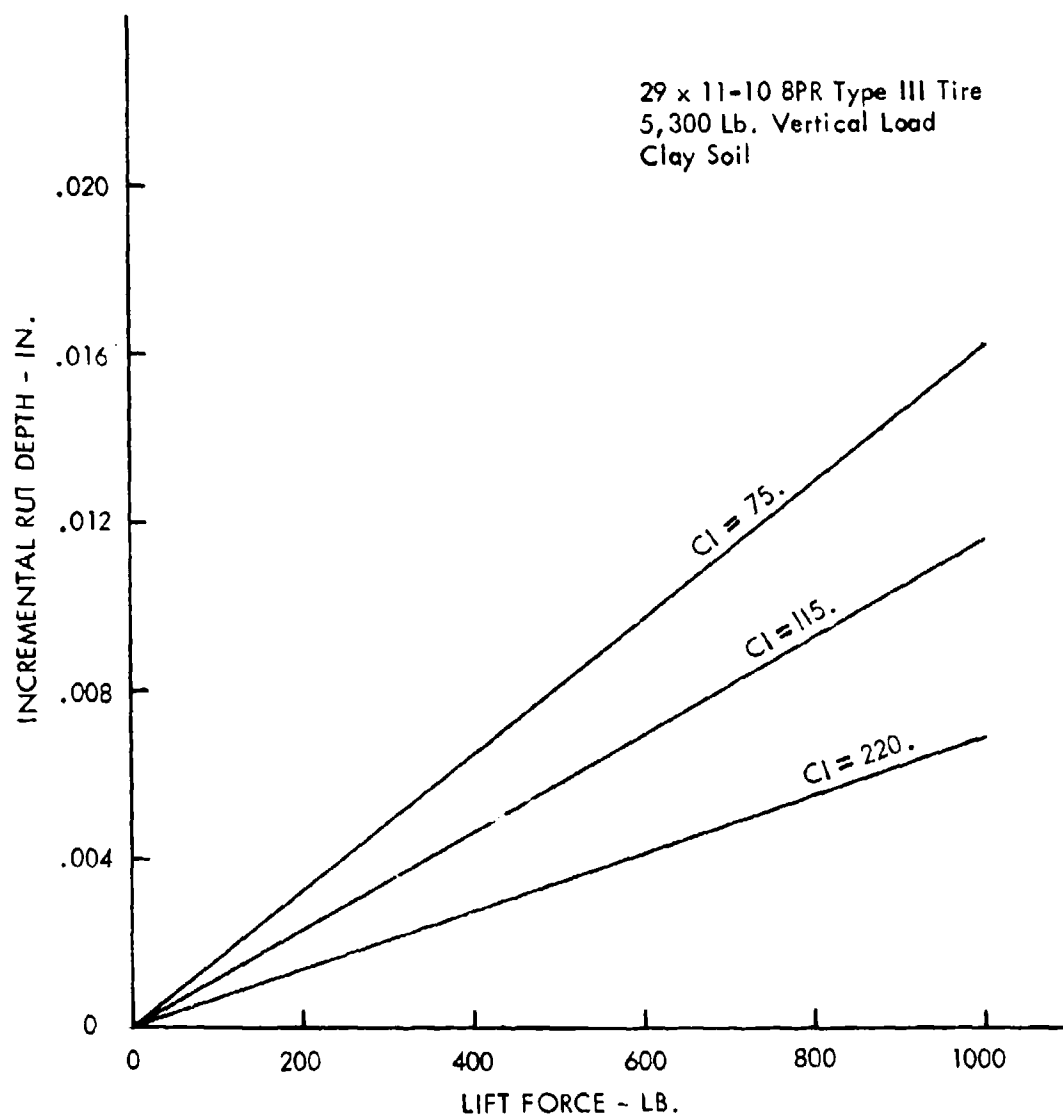


Figure 15. Incremental Rut Depth Caused by Inertial Lift Force

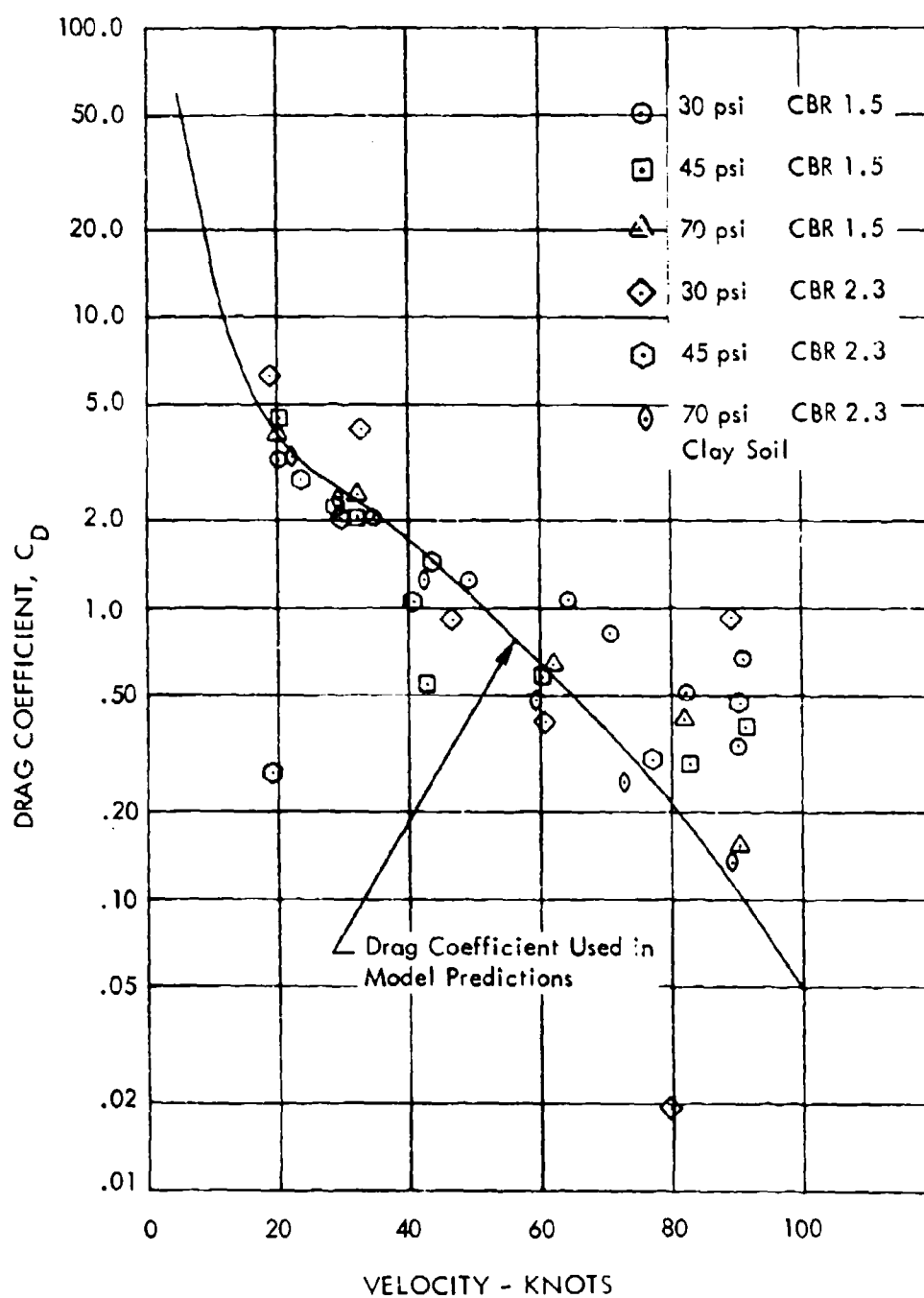


Figure 16. Drag Coefficient as a Function of Wheel Forward Velocity

analytical model. Superimposed on the function used are experimental values of C_D computed by rearranging Equation 18 to the form:

$$C_D = \frac{F_x - \left(\mu_o + \frac{Z_s}{L_t} \right) F_t}{1/2 \rho b Z_s V^2} \quad (19)$$

and using measured values of F_x , Z_s , and V . 5300 lb. was used for F_t in all cases. The curve used in the analytical calculation approximates the test data well from 20 knots to around 80 knots. The analytical curve falls below the average of the test data above 80 knots. It is suspected that this is caused by the lift term's being too low, which would in turn cause higher predicted ruts that must be reduced by a reduced drag coefficient.

f. Selection of Interaction Coefficients

Interaction coefficients were first developed by trial and error for the 29 x 11-10 8PR tire. These coefficients will also be needed for other tire sizes in order to have the model generally applicable. A pressure deflection curve will be needed for the soil material loaded by the particular tire being studied. This can be obtained from pressure sinkage theory or preferably from tests.

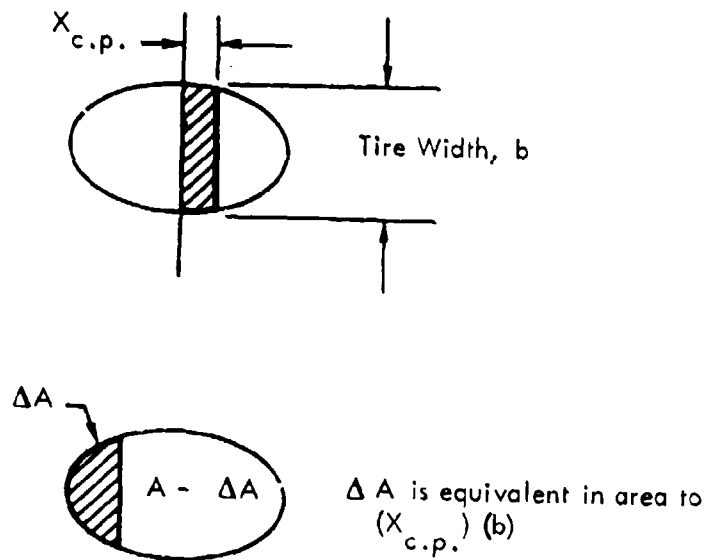
(1) Drag Interaction Coefficient

The drag interaction coefficient has been successfully calculated for the 29 x 11-10 8PR tire by assuming that the drag interaction is proportional to a footprint pressure increase which may be equated to a footprint area reduction as in Figure 17. The center of pressure shift, $X_{c.p.}$, of the vertical load is first calculated according to the equation:

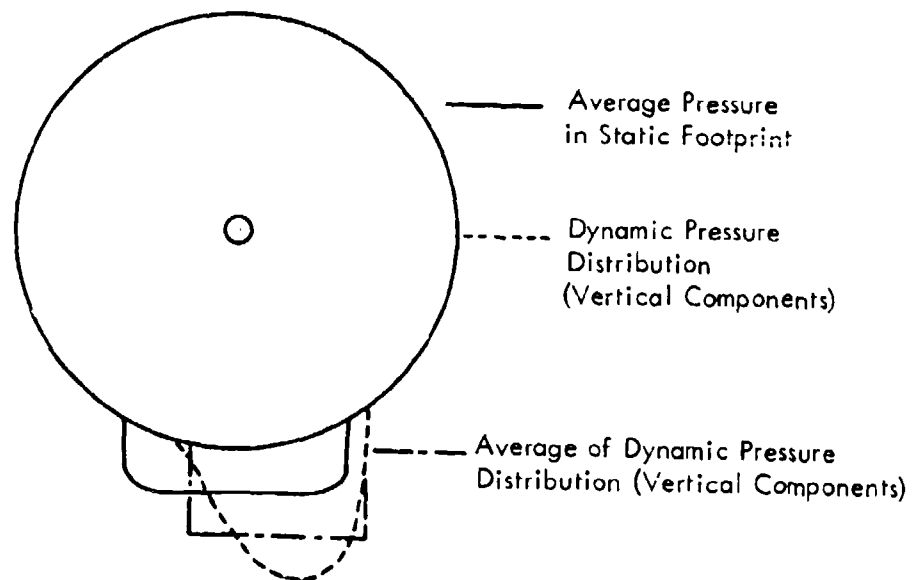
$$X_{c.p.} = \frac{F_x}{F_t} (R_t) \quad (20)$$

The area reduction is then assumed to be the product of the center of pressure shift and the tire footprint width:

$$\Delta A = X_{c.p.} (b) \quad (21)$$



(a) Top View of Tire Footprint



(b) Side View Showing Dynamic and Average Pressure Distribution

Figure 17. Equivalent Tire Footprint Area Reduction with Center of Pressure Shift

The pressure increase caused by this area reduction is then:

$$\Delta P = \frac{F_t}{\left(\frac{F_t}{P_o} - \frac{b F_x R_r}{F_t} \right)} - P_o \quad (22)$$

ΔP is considered as a pressure increase, and the incremental rut depth caused by this pressure increase can be estimated from the load sinkage curve shown in Figure 18.

(2) Lift Coefficient

Without the benefit of tests run at constant depth of penetration instead of at constant load, it is not possible to calculate an accurate lift coefficient. In the absence of any better test data, or additional theoretical calculations, the lift coefficient shown in Figure 14 should be used.

(3) Mobility Number Changes

Figures 19 and 20 show the range of the dynamic mobility numbers calculated for CBR 1.5 and CBR 2.3 clay soil using Equations 23 through 33. The location of the cross hatched vertical bars in relation to each other defines the relative magnitudes of sinkage that will be predicted for the different tire pressures shown. If these bars are close together the predicted results will be close together for the different tire pressures as was found when the WES prediction was used as in Figure 9. The only term in the mobility equation which changes with tire pressure is the tire deflection, δ_t . As tire pressure changes the value of δ_t changes. In the WES mobility numbers the value of the number is proportional to δ_t which is less than a linear variation. It was found in tests that the 29 x 11-10 8PR tire varied more in sinkage than would be expected from the δ_t variation in the mobility number. Consequently the value of the exponent on δ_t was changed from 0.5 to 1.2 for the calculations shown in Figures 19 and 20. Multiplication of the mobility number by a constant will shift the mobility number to the left or right. This was done to offset the effect of changing the exponent on δ_t .

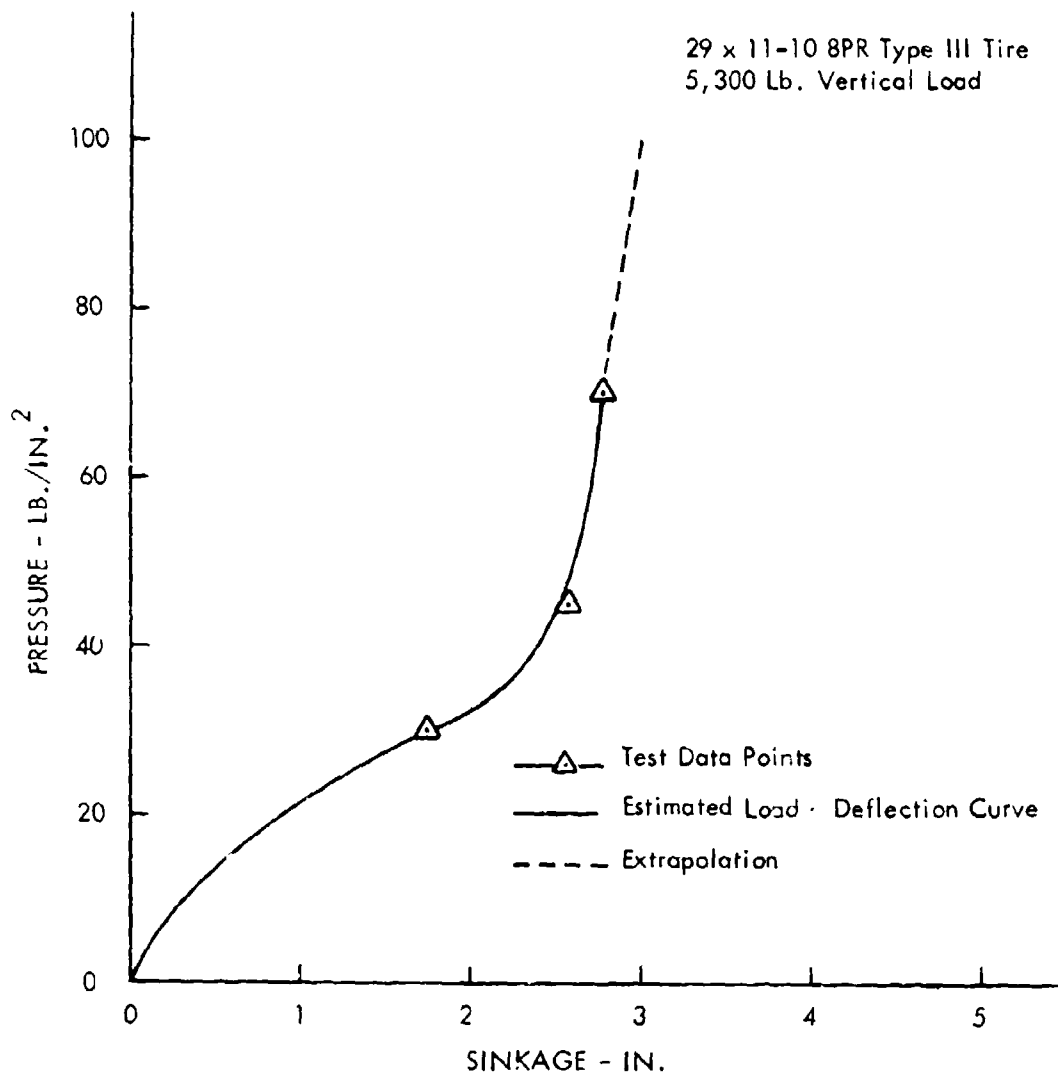


Figure 18. Static Pressure Sinkage Relation.
for CBR 1.5 Buckshot Clay

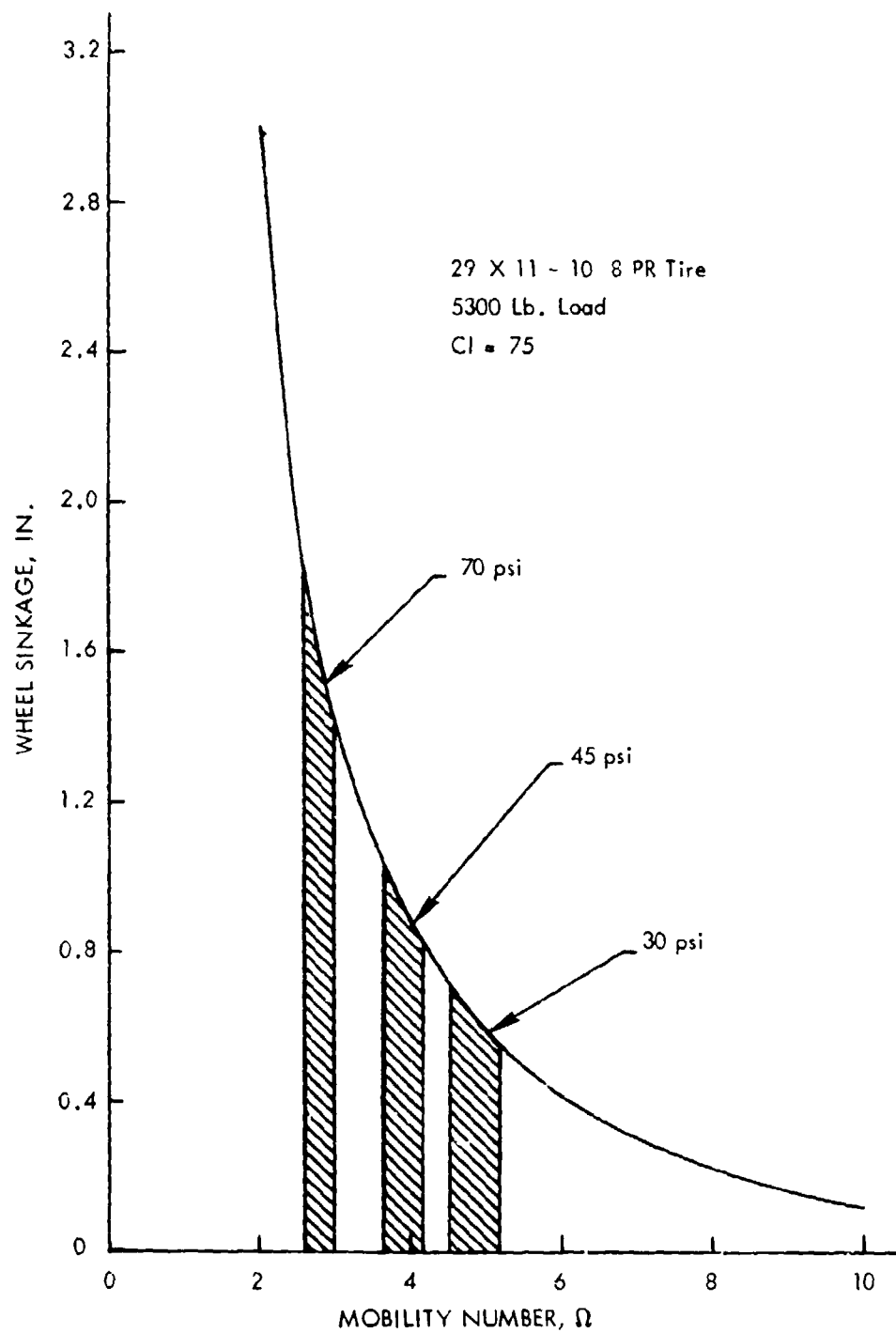


Figure 19. Predicted Sinkage vs. Dynamic Mobility Number, Clay Surface, CI = 75

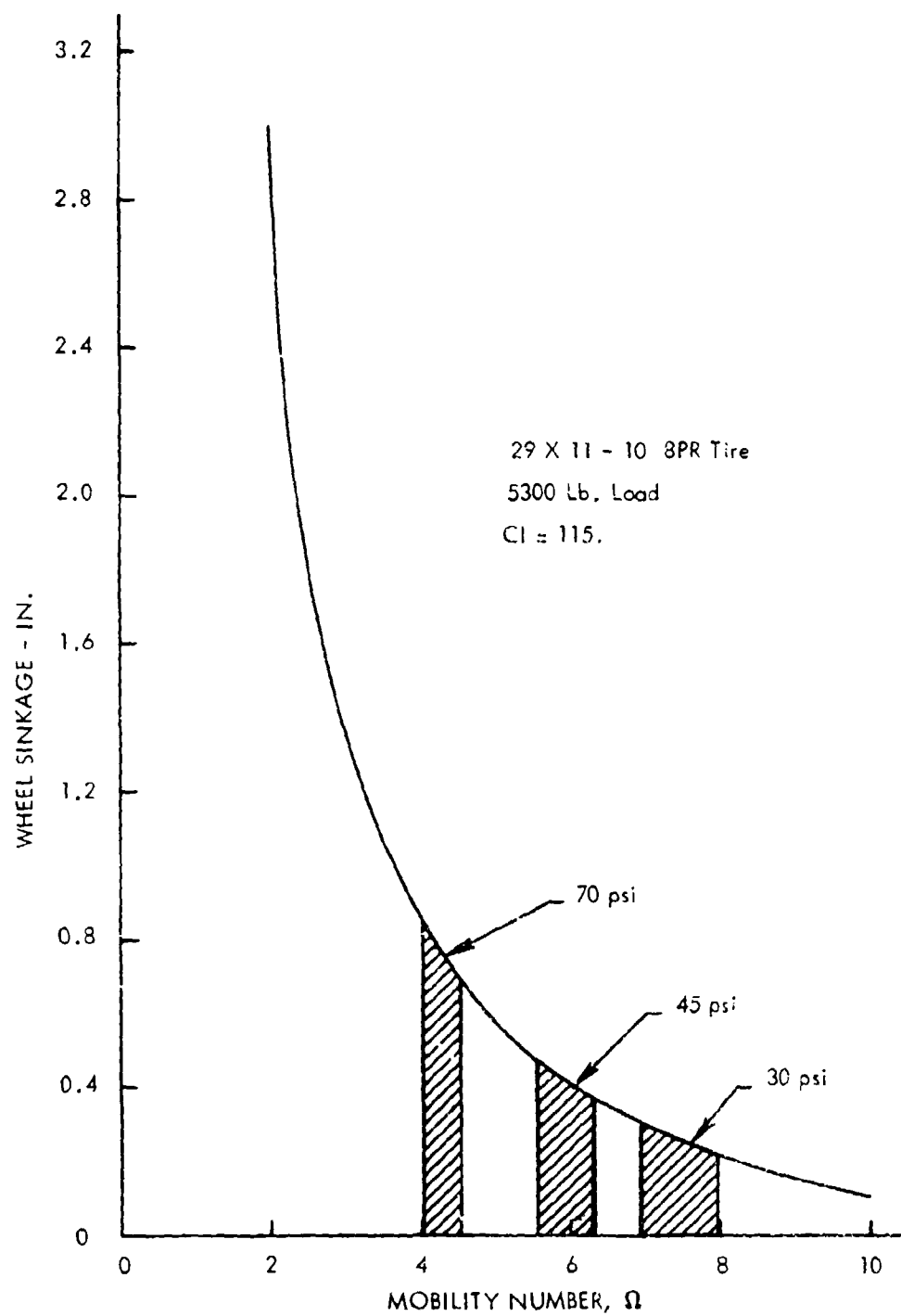


Figure 20. Predicted Sinkage vs. Dynamic Mobility Number, Clay Surface, CI = 115

g. Method of Solution for Rut Depths and Drag Loads

The equations which are solved for rut depth and drag loads are summarized here:

(1) Soil Spring Equations (for Clay)

$$Z_o = \delta_t + Z_s \quad (23)$$

$$L_t = 2 \sqrt{d Z_o - Z_o^2} \quad (24)$$

$$r_p = \frac{L_t}{V} \quad (25)$$

$$D = 1.0 + 1.34 e^{-1.27 r_p} \quad (26)$$

$$\Omega'_c = \frac{D}{1.6} \cdot \frac{CI (bd) (\delta_t)^{1.2}}{F_t (h_t)^{1/2}} \quad (.534) \quad (27)$$

$$\Delta Z_{s_{\text{soil spring}}} = \left[\frac{.1208}{\Omega'_c - .9468} - .0095 \right] d \quad (28)$$

(2) Drag Load Equation

$$F_x = \left[\mu_o + \frac{Z_s}{L_t} \right] F_t + 1/2 \rho b Z_s C_d V^2 \quad (29)$$

(3) Inertia Lift Force Equation

$$F_l = 1/2 \rho b L_t C_L V^2 \quad (30)$$

(4) Drag Load and Inertia Lift Interactions

$$\Delta Z_{s_{\text{drag}}} = \frac{K_d F_x}{(CI)^{0.8}} \quad (31)$$

$$\Delta Z_{s, \text{lift}} = \frac{K_1 F_l}{(C_l)^{0.8}} \quad (32)$$

(5) Rut Depth Equation (Summation of Deflection Components)

$$Z_s = \Delta Z_{s, \text{soil spring}} + \Delta Z_{s, \text{drag}} - \Delta Z_{s, \text{lift}} \quad (33)$$

Equation 33 is solved implicitly for Z_s by rearranging to the form

$$\Delta Z_{s, \text{soil spring}} + \Delta Z_{s, \text{drag}} - \Delta Z_{s, \text{lift}} - Z_s = 0 \quad (34)$$

These equations are shown in flow chart form in Figure 21. The computer program used to obtain the solution is listed in Appendix C. Sample calculations are shown in Appendix D.

(6) Assumptions Used in the Equations

The wheel is assumed to be in a steady state condition with no rotational or linear accelerations. This is not a severe restriction as changes in tire deflection, rut depth, cone index, or velocity can be treated as step increments and a new equilibrium solution to the equations established.

There is not enough information known about the transient response of tires to predict the effects of the rate of change of these parameters, but they are expected to be small since the soil will act as a smoothing filter to attenuate any high frequencies.

(7) Comparisons to an Alternate Model

The point of reference for the solution of the equations above is the wheel axle. The soil is considered to flow past the wheel at a velocity equal to the forward velocity of the wheel. A similar coordinate system is used in the study of aircraft flight and in the solution of some hydrodynamics problems.

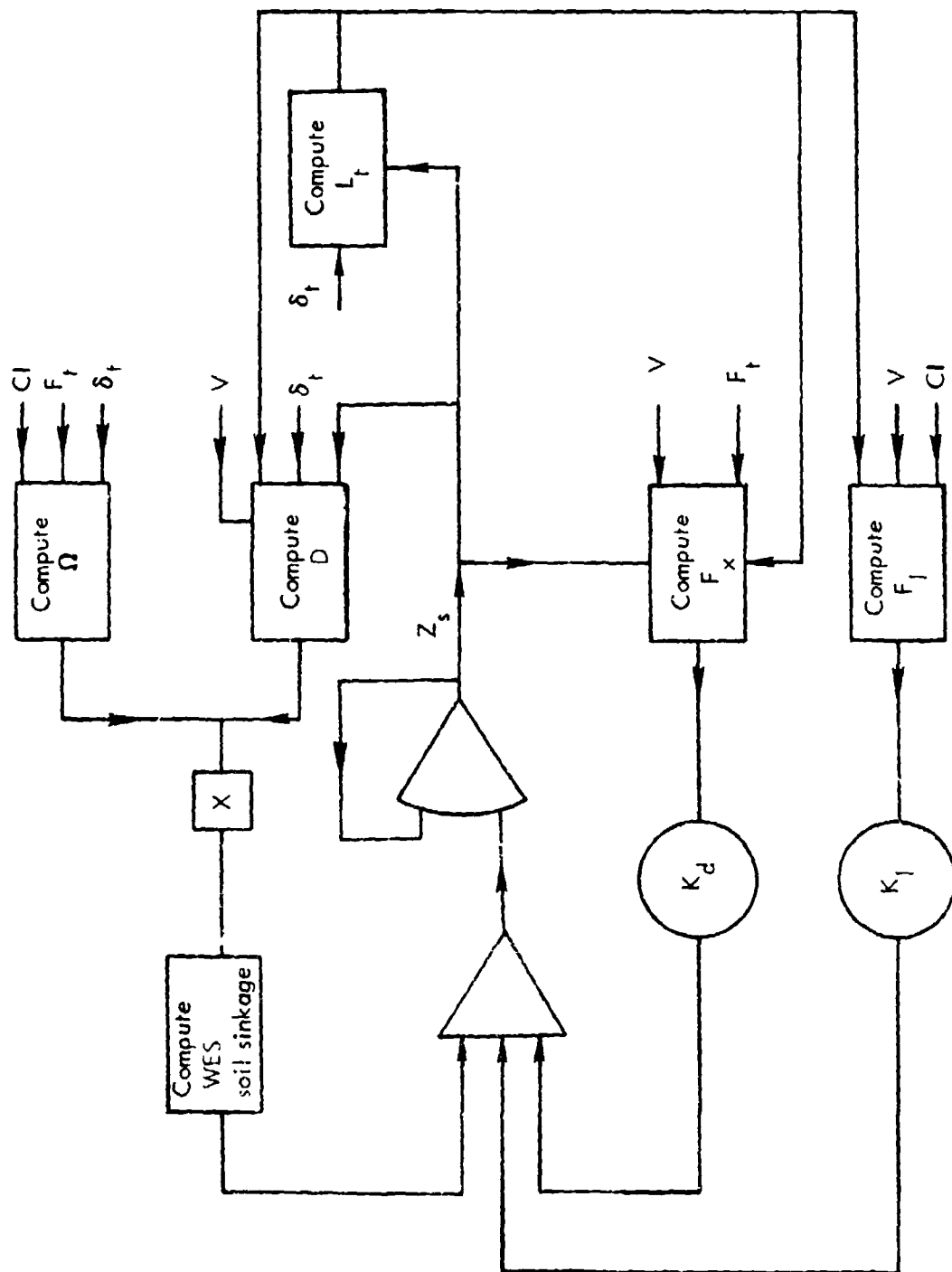


Figure 21. Flow Chart of the Soil Model Computation

A somewhat different approach has been suggested (5) in which the soil and wheel are made up of a series of springs that are deformed in a time sequence. The point of reference is external to the wheel and the time history of a single point in the soil is considered. The total wheel response becomes the summation of all of the deformations of these points in sequence. This procedure has been previously used in the study of the vibrations of building foundations (22). The approach is quite well suited to the study of fixed structures where the only coordinate to be considered is the vertical motion. When it is extended to the case of two coordinates with the motions in the horizontal direction being many orders of magnitude larger than the motion in the vertical direction, computational problems arise and the steady state solution becomes somewhat easier to use.

3. A MODEL FOR BRAKING

The braking conditions studied herein are for a locked towed wheel. Intermediate slip behavior has not been considered because of the short time to reach full brake pressure, usually around 0.3 seconds. More consistent results for the locked wheel could also have been obtained at the higher velocities if more distance in the soil bed had been available for braking, but an attempt was made to obtain both free rolling and braking coefficients in a single run.

Drag loads and rut depths caused by a locked wheel are higher than the corresponding values for a free rolling wheel. At 20 knots the increase is 167% for the drag load ratio and 141% for the rut depth with a single wheel at zero degrees yaw on Test Bed IV. At 90 knots the increases are less, being 72% for the drag load ratio, and the rut depths are approximately equal. This behavior is illustrated in the test results in Section III below, particularly Figures 42 through 47.

It has been found that the braking loads and rut depths can be predicted using the free rolling model with a change in the drag coefficient, C_D . The revised coefficient is shown in Figure 22. It produces a good comparison with both rut depth and drag load test data at 70 psi tire pressure but predicts lower values than observed in tests for 45

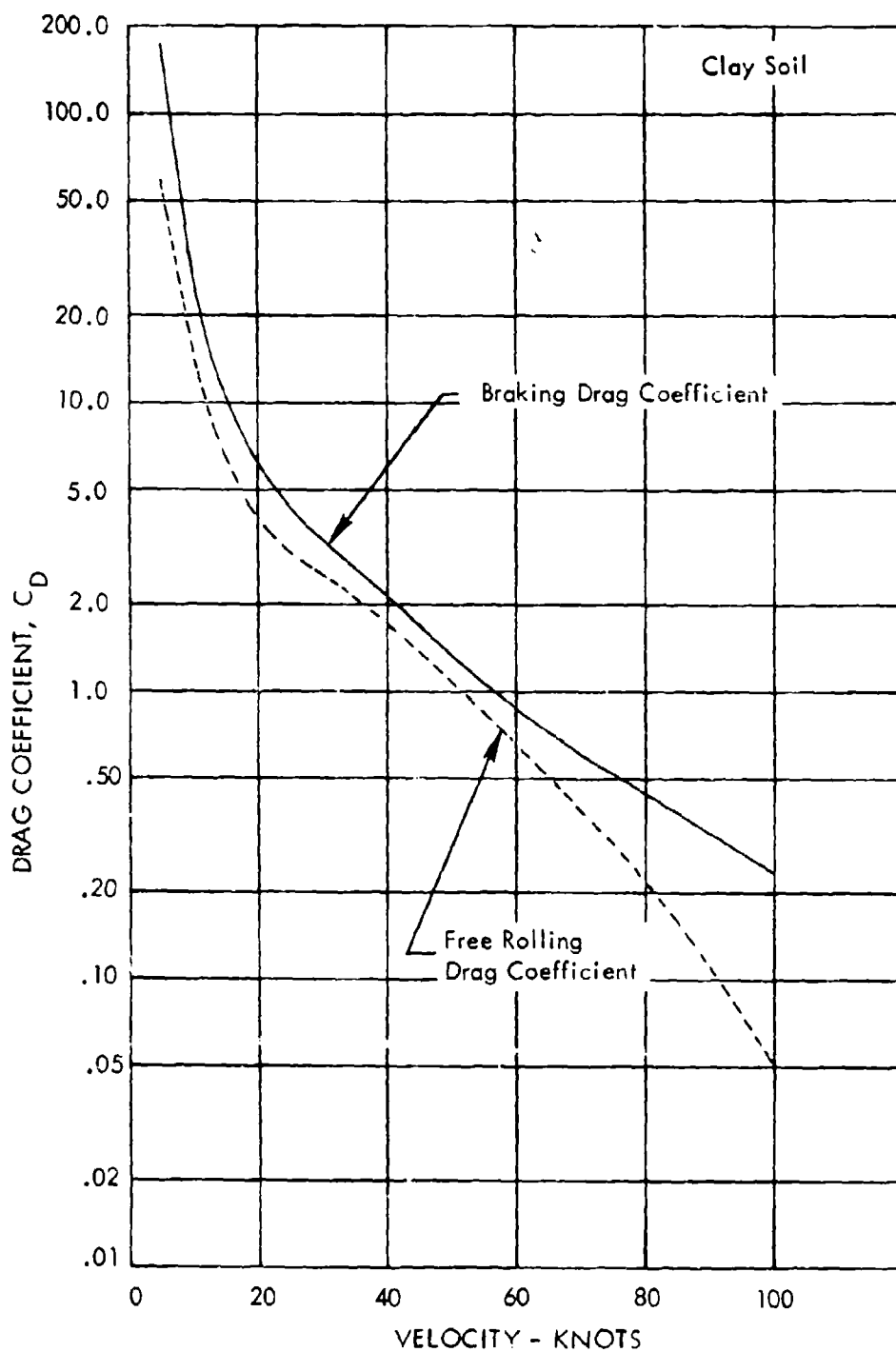


Figure 22. Drag Coefficient for a Braked Wheel

and 30 psi tire pressure particularly at speeds below about 60 knots. These lower tire pressure conditions could be predicted much closer with a coefficient which increased with decreasing tire pressure. No variation with pressure was indicated for the free rolling coefficient.

A possible explanation of the apparent increase in C_D for 45 and 30 psi tire pressures is that the tire sidewall is less stiff at lower tire pressures and distortion of the tire causes the increase when brakes are applied. This deserves further study, as it has an important influence on the use of large low pressure tires for future aircraft.

4. A SECOND PASS MODEL

No second pass information was gathered during the testing phase of this program so therefore only estimates of the wheel behavior can be made at this time.

a. Second Pass Equation

The rut depth equation for clay that should be used for second pass prediction is:

$$Z_s = \left[\frac{.0405}{\epsilon'_c - 1.5789} - .0038 \right] d + \Delta Z_{s_{\text{drag}}} - \Delta Z_{s_{\text{lift}}} \quad (35)$$

The empirical constants are from Reference 5 and are a curve fit to WES experimental data. $\Delta Z_{s_{\text{drag}}}$ and $\Delta Z_{s_{\text{lift}}}$ use the same coefficients as in the first pass model. Predictions of second pass behavior of the wheel are shown in Figures 35 and 36 of Item 6 below.

b. Recommendations

It is recommended that Equation 35 be used for second pass predictions until further information becomes available. An area of soil response which has not received much study is that of a compactible soil. This material is more likely to occur under natural conditions than would be indicated from the amount of attention it has received in laboratory tests. The lower rut depth increment predicted by Equation 35 should account

for part of the second pass response of a compactible material. As the number of passes accumulates, the soil should become harder and then Equation 35 would predict more rutting than might occur on subsequent passes. Little compactive effects were observed in the clay test beds below CBR 4 because the water content was high enough that remoulding of the material could take place without a corresponding strength change.

5. LANDING IMPACT

It is frequently assumed that since a landing impact may generate vertical loads greater than 1 "g", the rutting at impact would be greater than during free rolling. This assumption is not validated by either aircraft landing tests (with C-130 aircraft) or by a limited number of tests at the Langley Landing Loads Track. The ruts actually start at zero depth and increase to the free rolling value after spin-up. There is evidence of skidding during spin-up in the form of material ejected to each side of the rut and loosening of material in the bottom of the rut.

If drop tests are made at zero forward speed the sinkage is greater than that of a free rolling rut because of the added increment of vertical load from dynamic response of the landing gear.

The forward speed of most aircraft at touchdown will be in the vicinity of 100 knots or more and at these speeds drag loads and rut depths are well below their peak at the mid velocity range. Vertical load also starts to build up from zero as the aircraft is moving forward. The vehicle will travel forward several feet before full gear load is applied, thus accounting for the gradual increase in rut depth. Wing lift during touchdown also tends to keep the rutting low.

Since the wheel is not rotating at impact, a drag torque must be applied by the soil to rotate the wheel. As far as can be determined, this is equivalent to applying braking torque except that in the case of spin-up slip begins at 100% and decreases instead of starting near zero increasing to 100% as for braking. During spin-up there is probably a smooth transition from the locked wheel drag coefficient to the free rolling drag coefficient proportional to the percent slip.

From the limited amount of information available, it is concluded that conventional landing operations will produce no deeper ruts during impact than free rolling ruts on an undisturbed surface. Repeated landing impacts at the same location on an unpaved surface would tend to cause accumulative surface damage from a weakening of the soil structure by the spin-up loads, but this damage is likely to accumulate less rapidly than in the area where brakes are applied.

6. COMPARISONS OF THE SOIL MODEL RESULTS WITH TEST DATA

Equations 23 through 33 of Item g. above were programmed for computer solution. The independent variable, velocity, was varied from 5 to 100 knots in 5 knot increments. Computer results were then compared with test data from the Landing Loads Track.

The drag load interaction and inertial lift interaction coefficients were first determined from the 70 psi CBR 1.5 clay tests using the drag coefficient, C_D , from Reference 5, adjusted so that 1.0 on the normalized velocity axis corresponded to the velocity of the peak drag load on the test curve. When it was realized that this drag coefficient was too low at speeds below 1.0 on the normalized curve, a free rolling drag coefficient was selected by trial and error with the computer program. This coefficient improved the model results at speeds from around 5 to 30 knots where both drag and rutting predictions were too low (21).

The modifications of the mobility numbers in Equations 12 and 13 were made on the basis of the spread in the rut depths for the 70, 45, and 30 psi tire pressures on CBR 1.5 clay and on sand.

Variation of the interaction factors inversely with cone index was not determined from test data but was incorporated as a logical way to change the constants after poor results were obtained when interaction was held constant while soil strength changed.

A test of the validity of the model is whether it is capable of predicting results of other test conditions not used in the model derivation. Comparisons have been made for data obtained at the Landing Loads Track. Unfortunately a sufficiently large number of wheel sizes, soil strengths, and wheel loads have not been tested to refine the model with respect to wheel geometry.

Usually the differences in a model and an experiment can be attributed to random error when the model is known to be theoretically correct and measurements are made to verify well defined constants. In such cases the variations are subject to statistical analyses to determine probable error and confidence. The analytical model in this report consists of the primary variables which determine rutting and drag. There are secondary variables which affect the solution to a lesser degree but nevertheless provide a bias in the data which is identifiable as being non-random in a simplified statistical analysis. These second order terms include such items as the true variation of lift and drag coefficients with tire pressure, soil strength, and applied drag load; the actual cross-sectional area of the tire which is only approximated by the quantity $\left[bZ_s \right]$; and localized variations in the soil loading rate instead of an assumed average loading rate.

Another bias is introduced by arbitrary lift and drag coefficients rather than values derived as a "best fit" to all of the experimental data available. There is also a lack of well defined mean values for the test data. In most cases only one experiment was run for each test condition and, at most, two points were obtained for a few tests. The means which have been drawn through the test data must of necessity be estimates.

All of these items contribute to differences between data and analyses which are not random. The best error evaluation that can be made in this case is the overall average difference without establishing confidence limits. As these deficiencies are corrected through additional test data and through better identification of the secondary variables in the analytical model, errors can be more closely evaluated using statistical techniques.

a. Comparisons for Free Rolling on Clay Surfaces.

Figures 23 and 24 compare rut depths and drag loads from the analytical model with test data on a CBR 1.5 clay surface. Figures 25 and 26 show corresponding data for a CBR 2.3 clay surface. These comparisons show that for some test conditions rut depths and drag loads are higher or lower than the analytical model predictions for the reasons discussed above.

The model predicted rut depths in CBR 1.5 clay, on the average, 11% higher than the measured values. The average of the overprediction difference was 24%, and the average of the underprediction difference was 11%. For drag loads on CBR 1.5, the model underpredicts the measured values by an average of 6%. The average of both overprediction and underprediction differences was 13%.

On the CBR 2.3 clay surface the rut depths predicted by the model were, for the overall average, less than 1% higher than the measured values. The average of the overprediction difference was 34% and the average of the underprediction difference was 36%. Overall, the predicted drag loads averaged 9% higher than the measured values. The average differences were 30% for overprediction and 17% for underprediction.

Examination of the individual comparison plots indicates where the analytical model and test data differences occur. In Figure 23 the analytical model predicts too high for ruts beyond 50 knots. This indicates that lift is too small at high speed. If lift is increased, the drag coefficient will also have to be increased in this speed range to compensate for reduced rutting since Figure 24 shows that existing predictions of drag load are correct. Rut differences between analysis and test at 45 and 30 psi are attributed in part to increasing errors in measured ruts as their accuracy becomes increasingly poor as absolute magnitudes become small. Comparisons of ruts and drag loads on CBR 2.3 show that 70 psi tests are consistently under predicted. No trend is evident from 45 and 30 psi, but it is noted that test data scatter is larger at these test conditions.

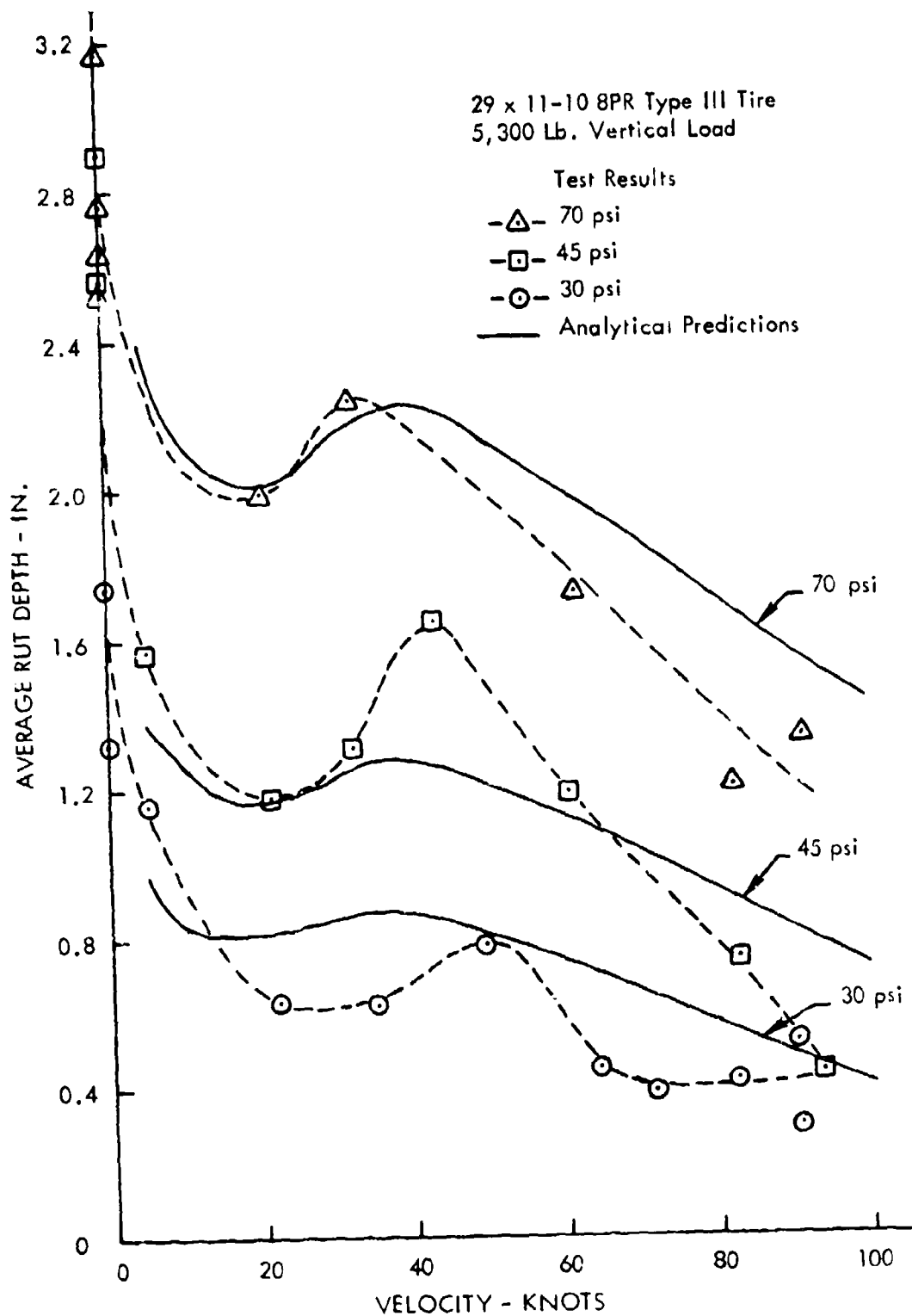


Figure 23. Comparison of Analytical and Test Rut Depths for CBR 1.5 Clay

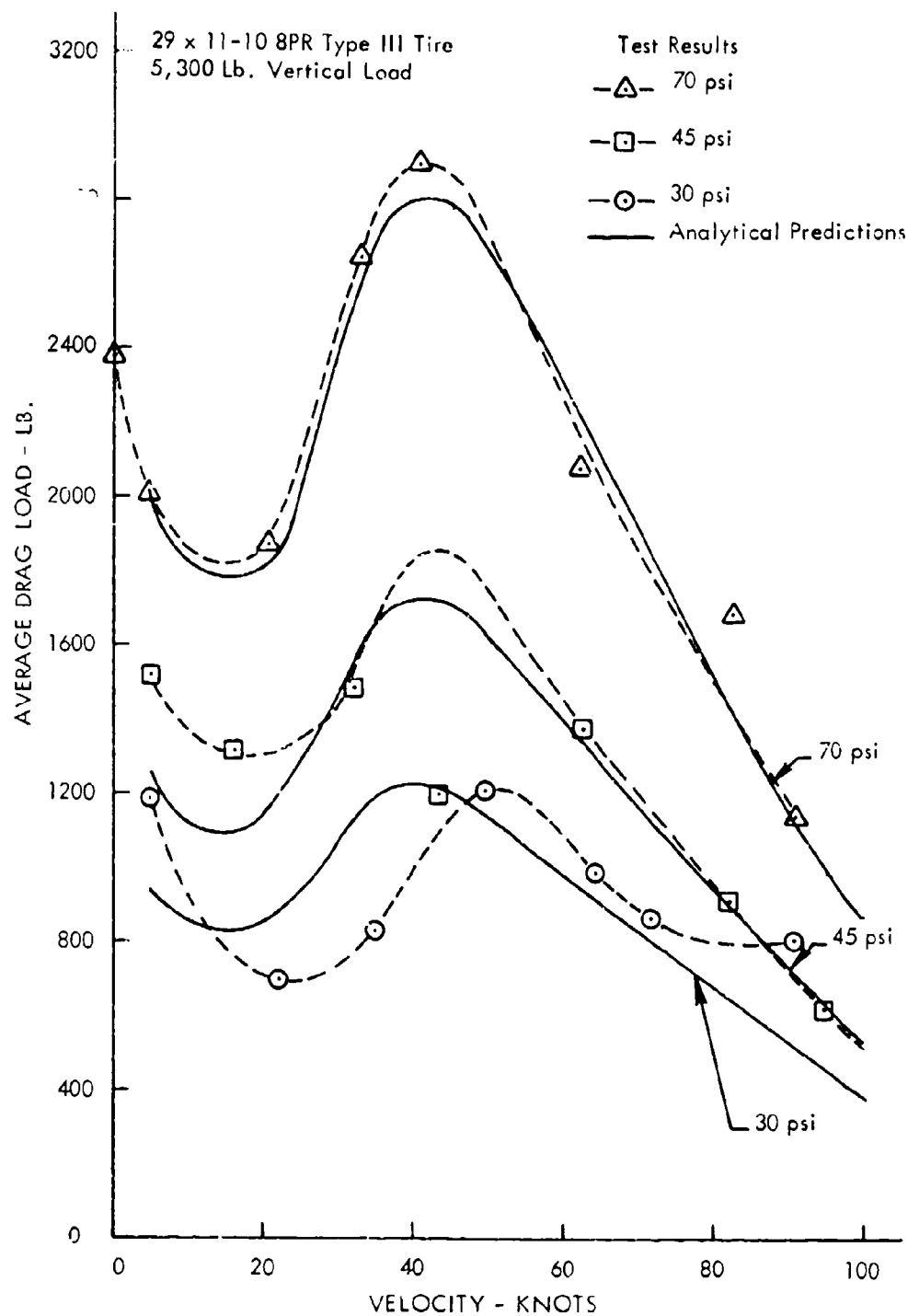


Figure 24. Comparison of Analytical and Test Drag Loads for CBR 1.5 Clay

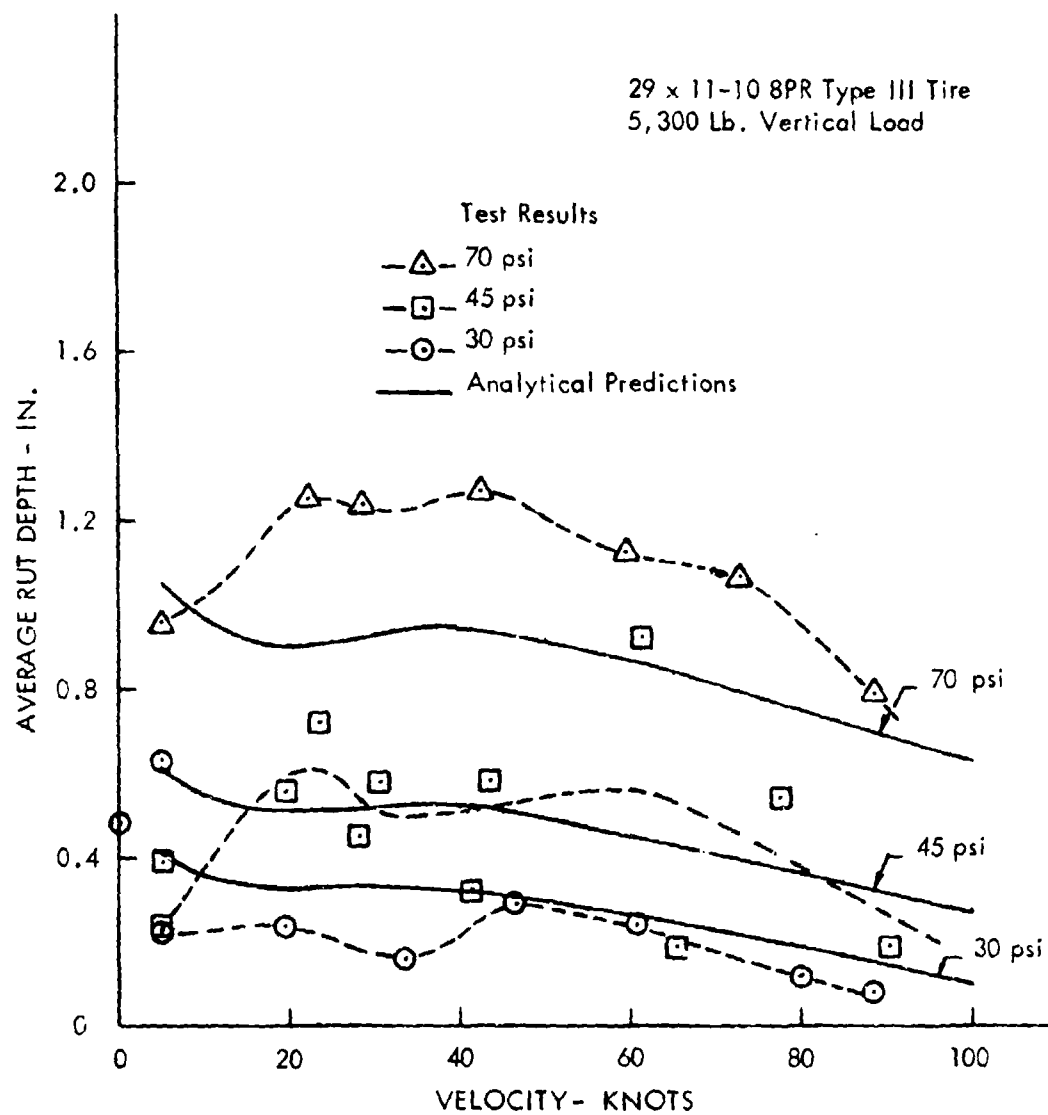


Figure 25. Comparison of Analytical and Test Rut Depths for CBR 2.3 Clay

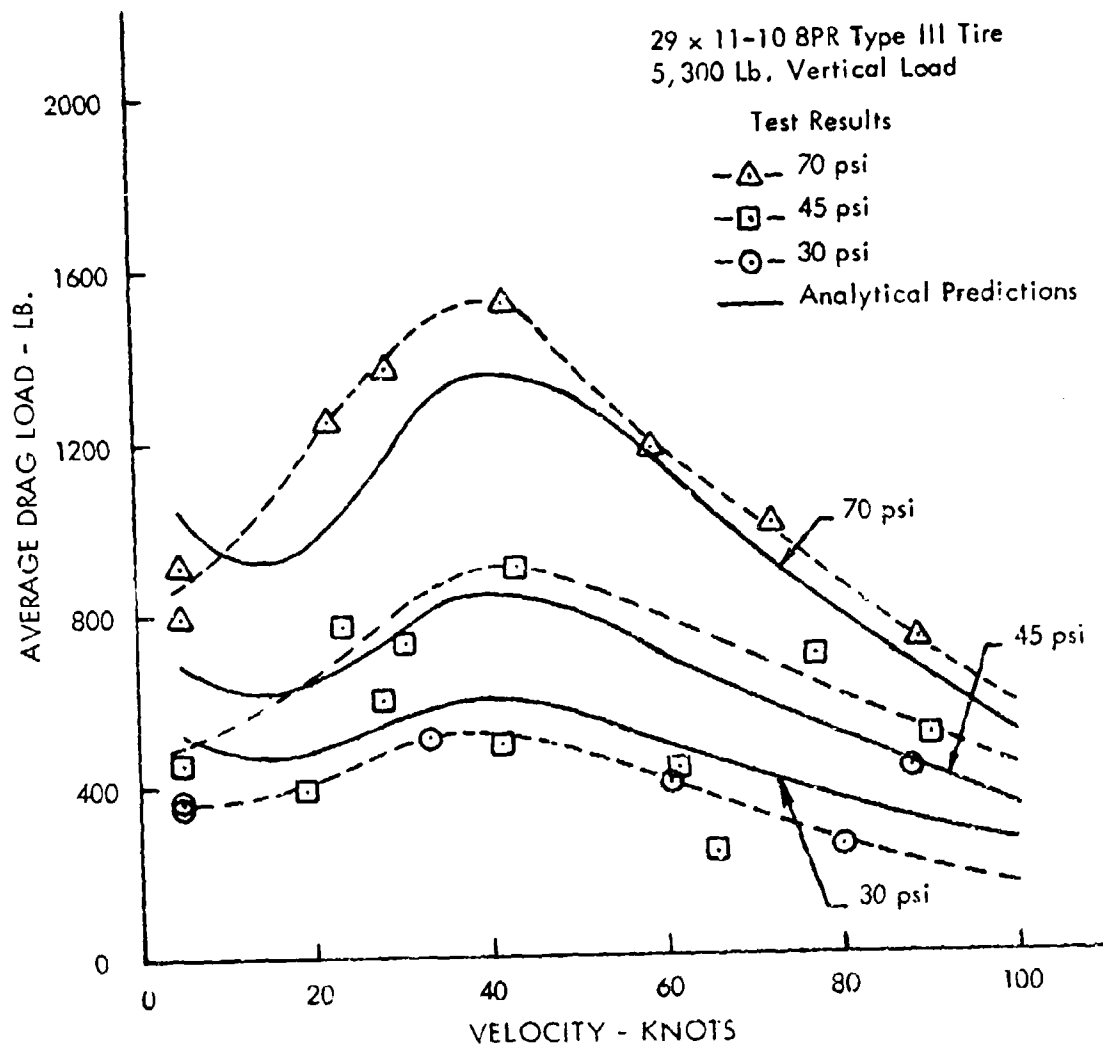


Figure 26. Comparison of Analytical and Test Drag Loads for CBR 2.3 Clay

Figures 27 and 28 show data for CBR 4.4 clay. Rut depth test measurements were not obtained for these tests, but they were quite small (on the order of 0.5 in. and less). Drag load measurements that were made compare reasonably well with test data on an absolute magnitude basis.

b. Comparisons for Free Rolling on a Sand Surface.

Figures 29 and 30 compare rut depths and drag loads on a sand surface with analysis. Only one series of tests was run on sand so comparisons for a strength variation could not be made. For the single strength tested reasonably good agreement was obtained between the model and test data.

Figure 29 shows that the overall behavior of the model and test results are similar with respect to velocity and tire pressure changes. Test points are above and below analytical predicted values. The average of test points greater than predicted is 22%. The average of test points less than predicted is 21%. The overall average of the test point differences is 1.5% more than predicted.

Similar differences are seen in Figure 30 for drag loads. Test points above predictions average 13% greater while those which are below the predictions average 21% less. The overall average is 12% below predictions. To obtain this agreement, some changes in the coefficients K_y and K_f were required. The drag coefficient, C_D , is also much lower for sand than for clay. The coefficient published in Reference 5, which was initially used for the clay soil model, is still being used for the sand model.

Improvement in accuracy of the model for sand can be expected when data is obtained over a range of strengths and for a range of wheel sizes and loadings.

c. Comparison for Braking on Clay

Considerable difficulty was encountered in obtaining good results with the braking model (21). It has been found that the best agreement can be obtained by keeping the model identical with the free rolling model except for a change in the drag

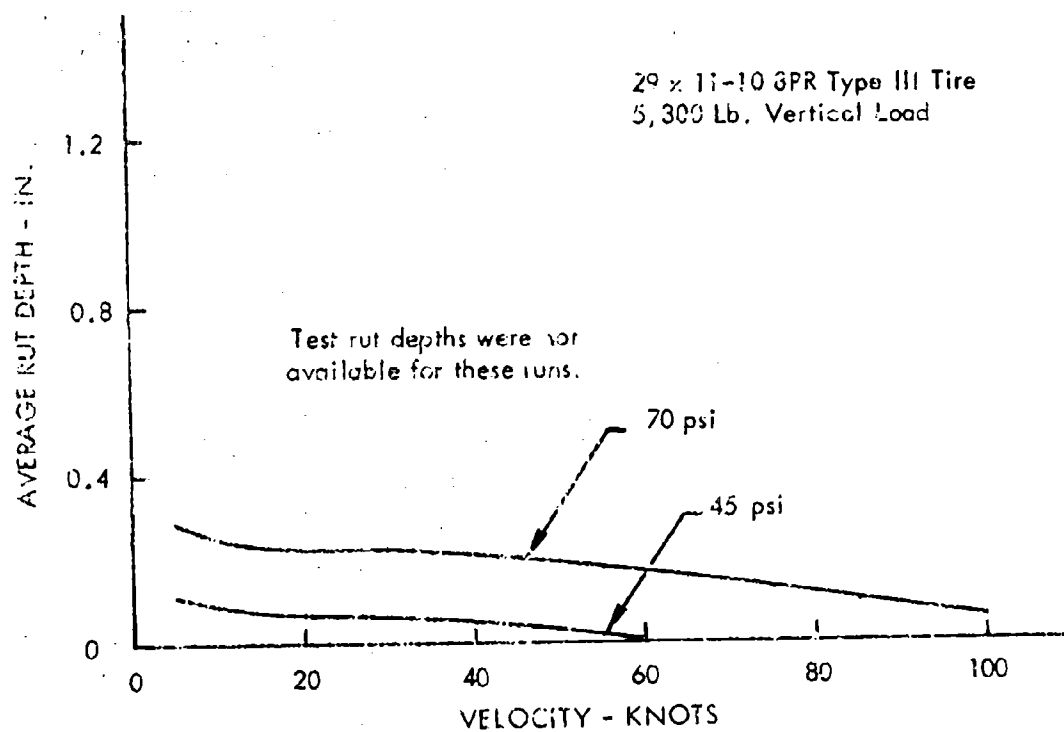


Figure 27. Analytical Predictions of Rut Depths
for CBR 4.4 Clay

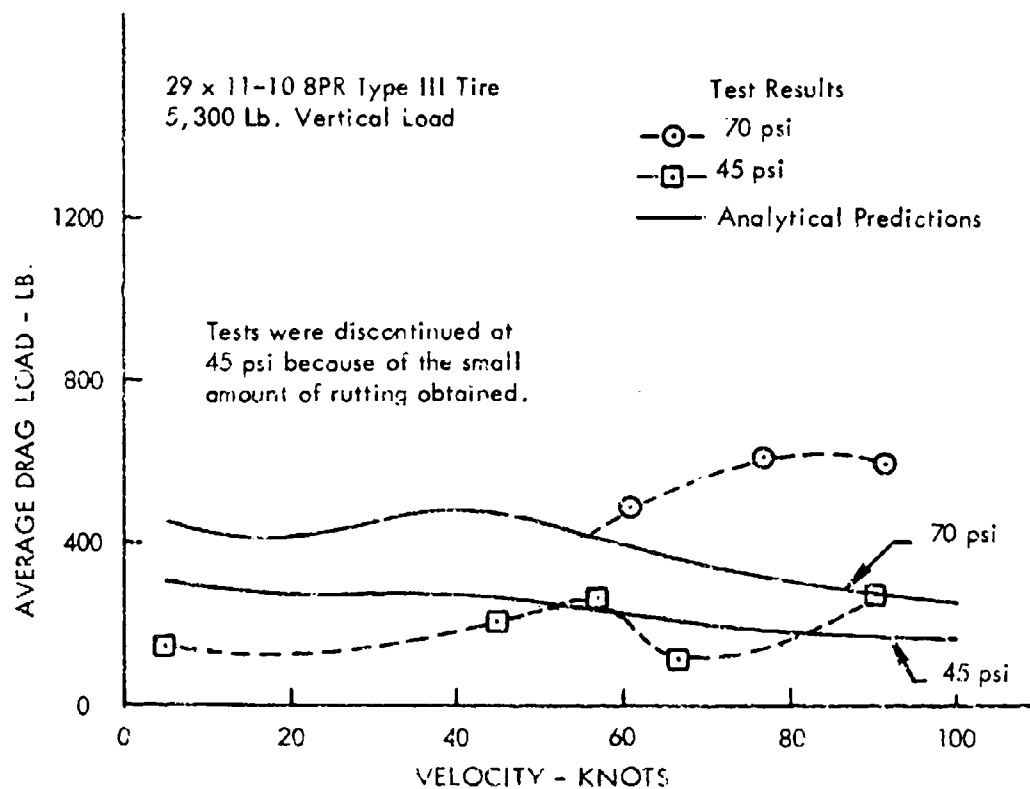


Figure 28. Comparison of Analytical and Test Drag Loads for CBR 4.4 Clay

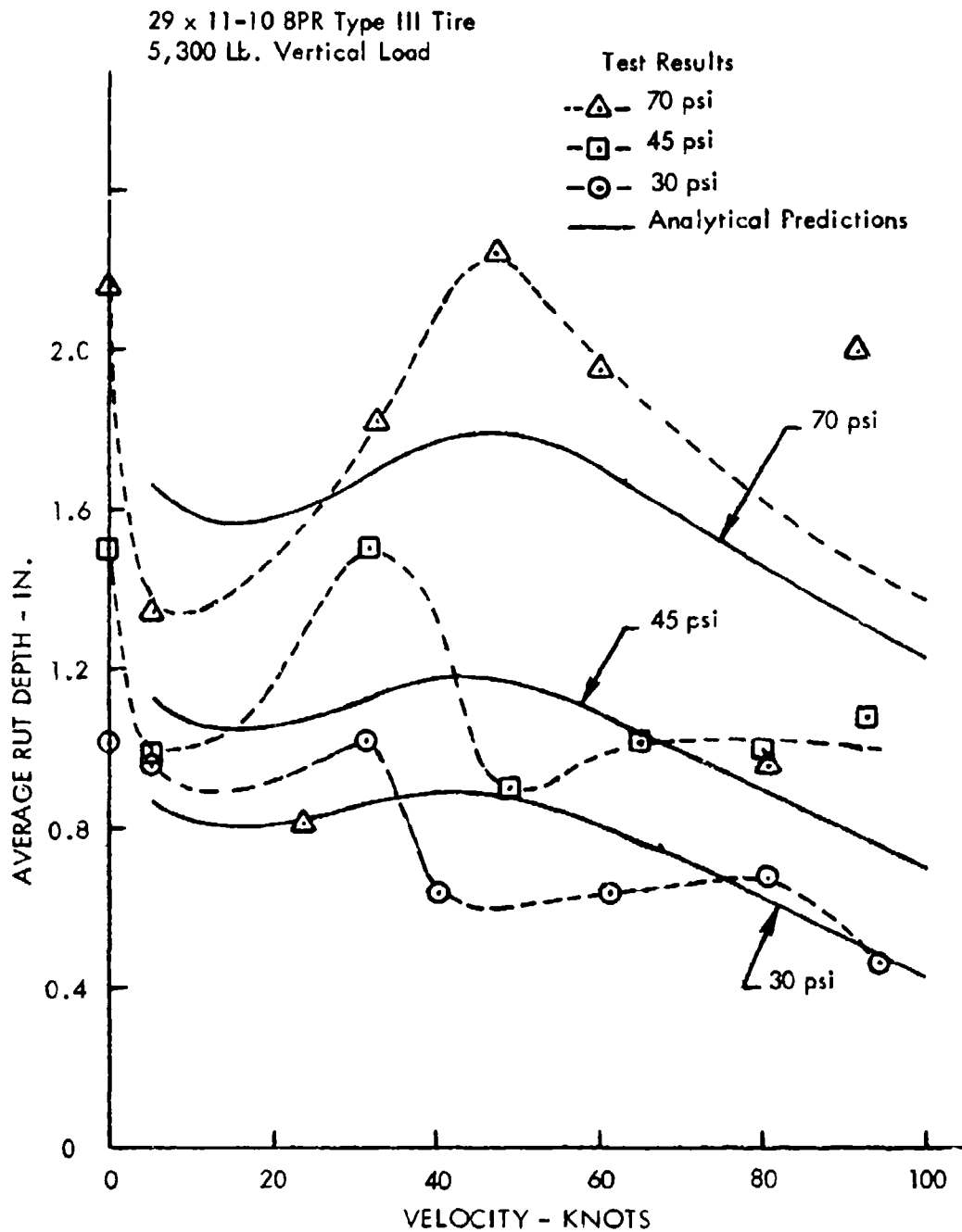


Figure 29. Comparison of Analytical and Test Rut Depths on Sand

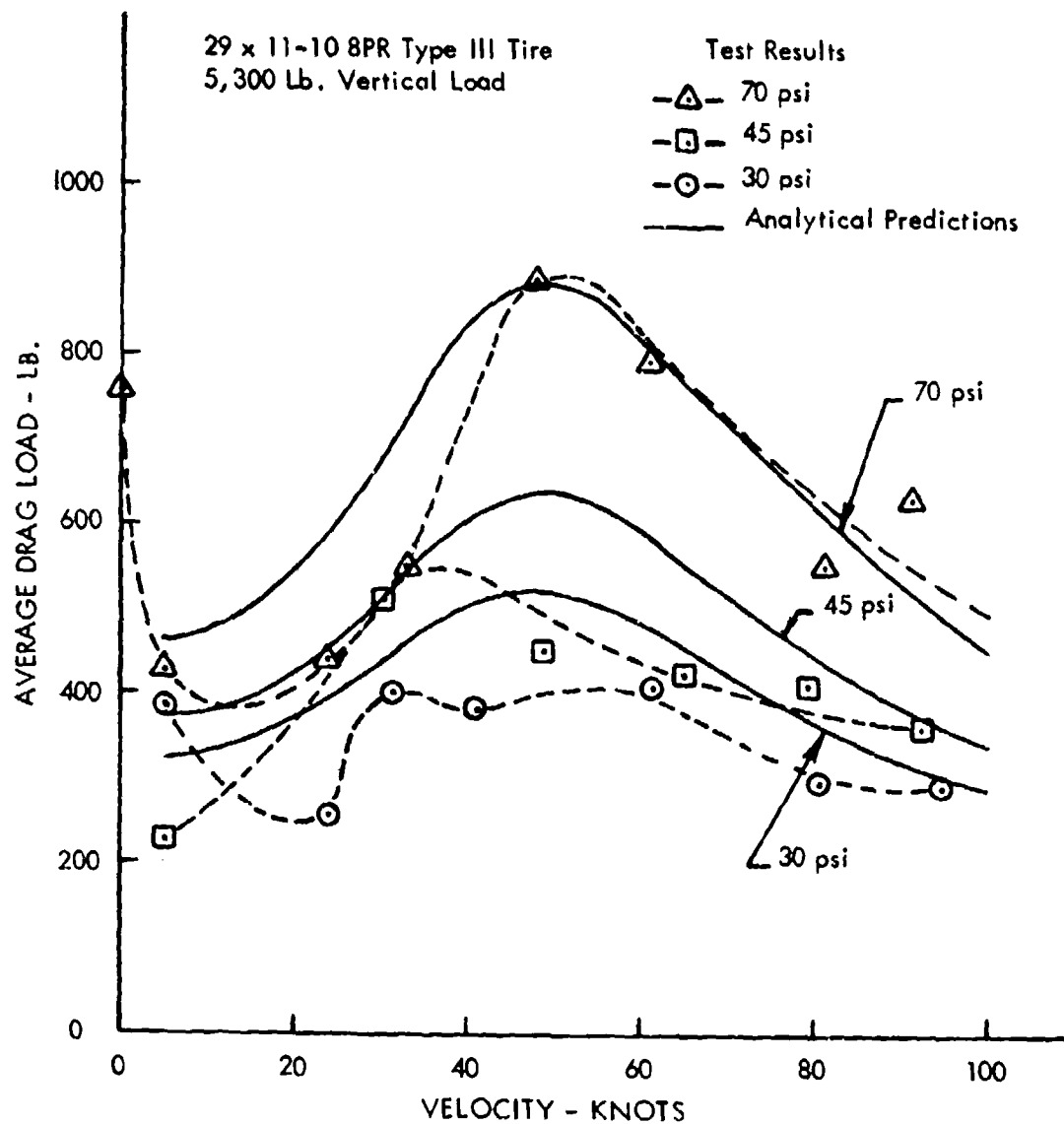


Figure 30. Comparison of Analytical and Test Drag Loads on Sand

coefficient. From the improvement noted in the comparison of the model with drag load test data at 70 psi it now appears that brake torque at all speeds can be accounted for through the drag coefficient. If this assumption is correct, it means that braking effects are caused almost entirely by the relative velocity of the tire with respect to the soil. Once methods for evaluating this coefficient are obtained (through testing probably), improved predictions can be made.

Figures 31 and 32 compare analyses with test data for CBR 1.5, and Figures 33 and 34 compare analyses with test data for CBR 2.3. Good comparisons are obtained for drag loads at 70 psi tire pressure using the drag coefficient from Figure 22. Not enough rut data points were obtained to define adequately a velocity variation at this tire pressure, but agreement with the available points seems to be rather poor as indicated in Figure 31. Drag loads at 45 and 30 psi are only about 50% as high as measured values over the whole velocity range. This suggests that a drag coefficient variation with tire pressure exists which offsets the normal decrease in rutting with reduced tire pressure that is seen from free rolling tests. Further computations with a drag coefficient which is allowed to change with tire pressure should be made to determine the amount of improvement in drag prediction and its effect upon rut predictions.

Figures 33 and 34 show comparisons of the model and test data for CBR 2.3 clay. Some improvement in the comparisons for rut depth over that for CBR 1.5 may have been obtained at the lowest tire pressure, but substantial data scatter is present. Drag loads are again only about 50% of the test values.

d. Second Pass Prediction:

Figures 35 and 36 show a comparison between ruts and drag loads predicted for first and second pass at 70 psi tire pressure on a CBR 1.5 clay surface using Equation 35. Ruts decrease from 2.4 in. on the first pass to 1.36 in. for the second pass at 5 knots; from 2.21 to 1.17 at 40 knots; and from 1.44 to 0.64 at 100 knots. The average reduction in rutting for these three velocities is 47%. The drag loads decrease from 2000 pounds to 725 pounds at 5 knots, from 2810 pounds to 900 pounds at 40 knots, and from 820 pounds to 300 pounds at 100 knots. The average drag load reduction for these three speeds is 65%.

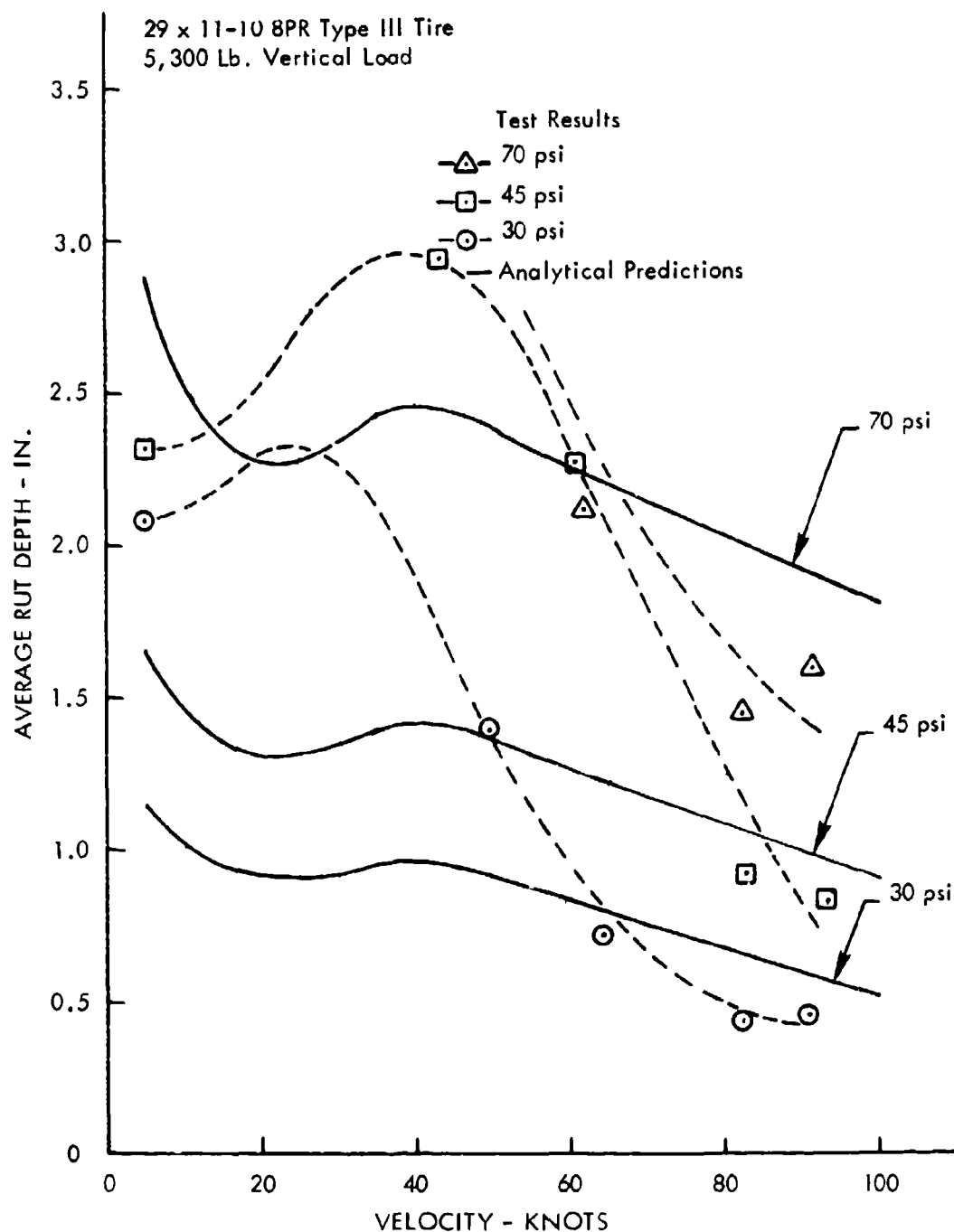


Figure 31. Comparison of Analytical and Test Rut Depths
for Braking on CBR 1.5 Clay

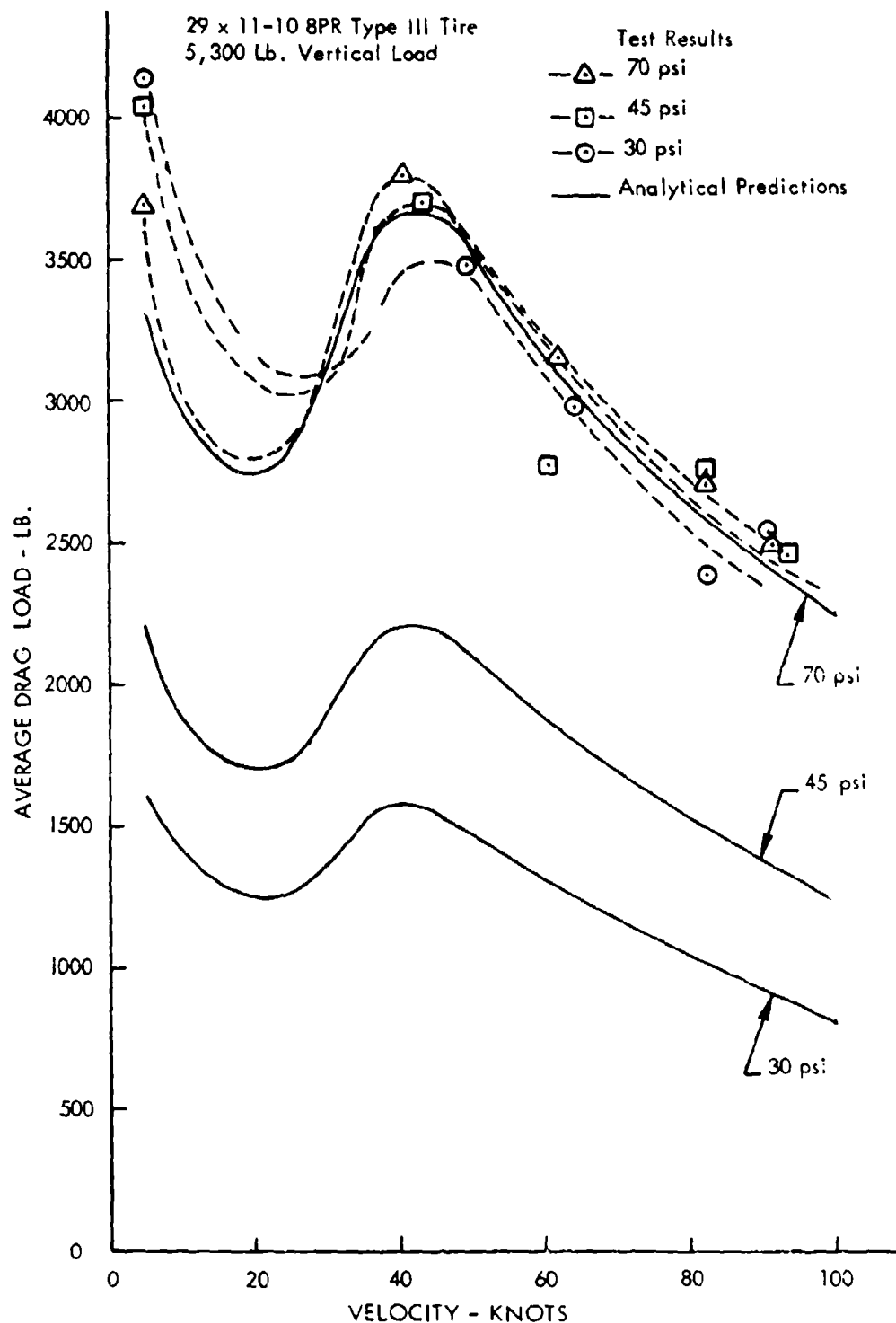


Figure 32. Comparison of Analytical and Test Drag Loads for Braking on CBR 1.5 Clay

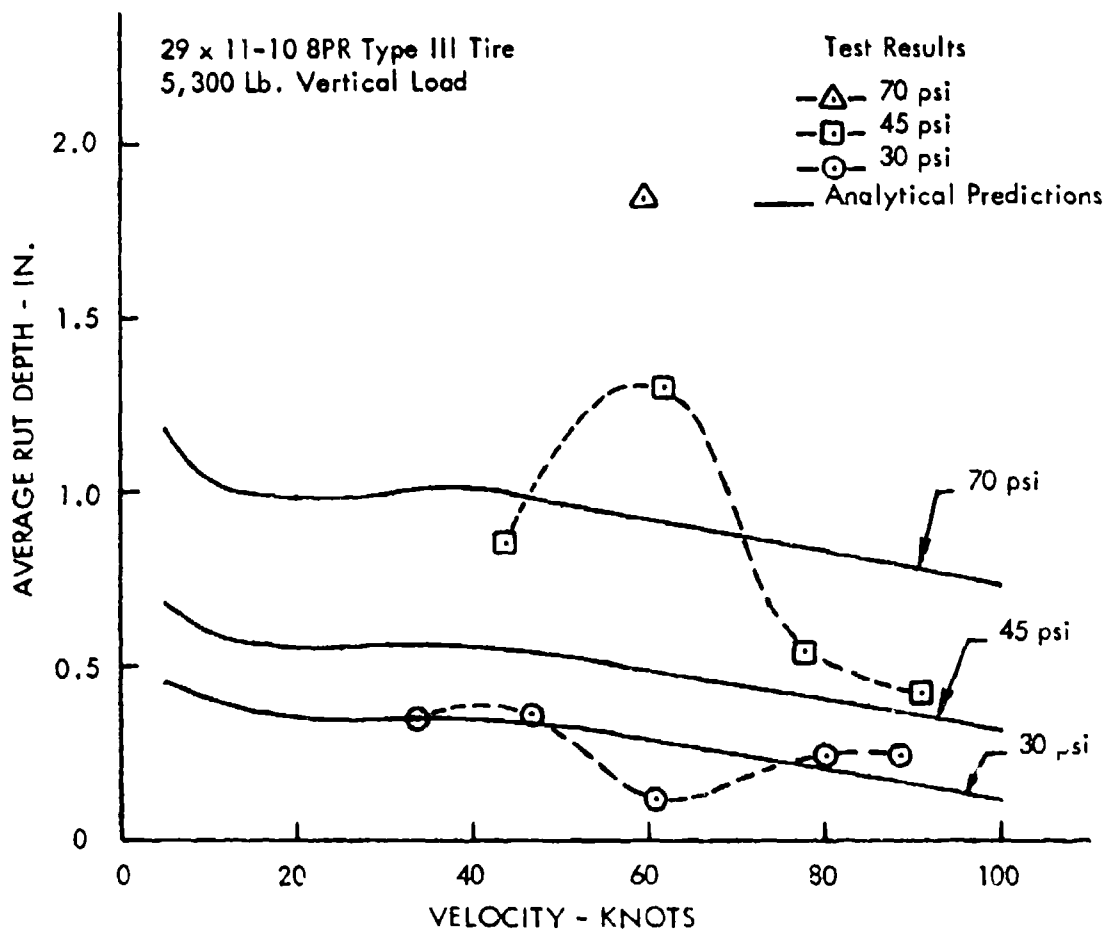


Figure 33. Comparison of Analytical and Test Rut Depths for Braking on CBR 2.3 Clay

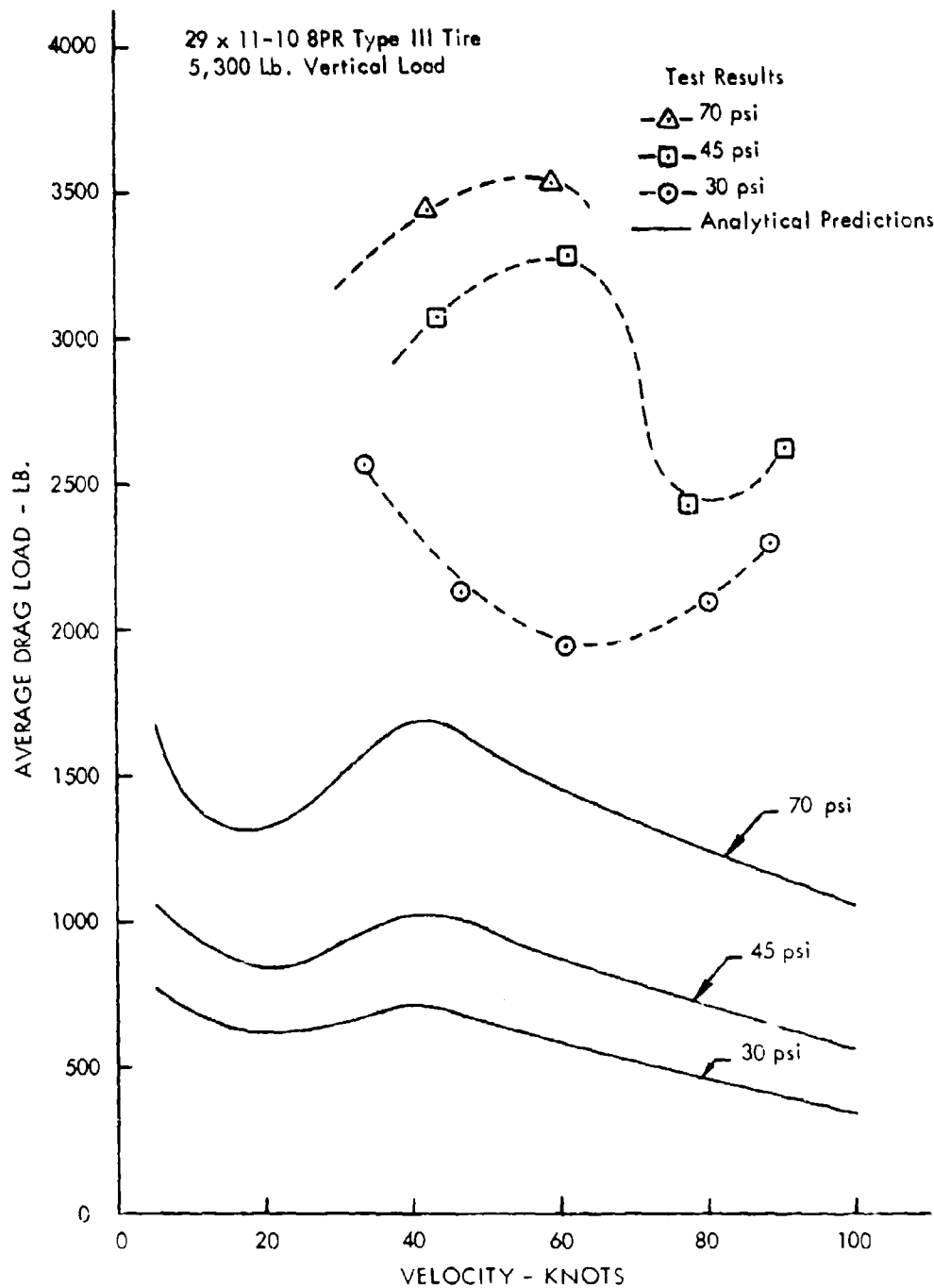


Figure 34. Comparison of Analytical and Test Drag Loads for Braking on CBR 2.3 Clay

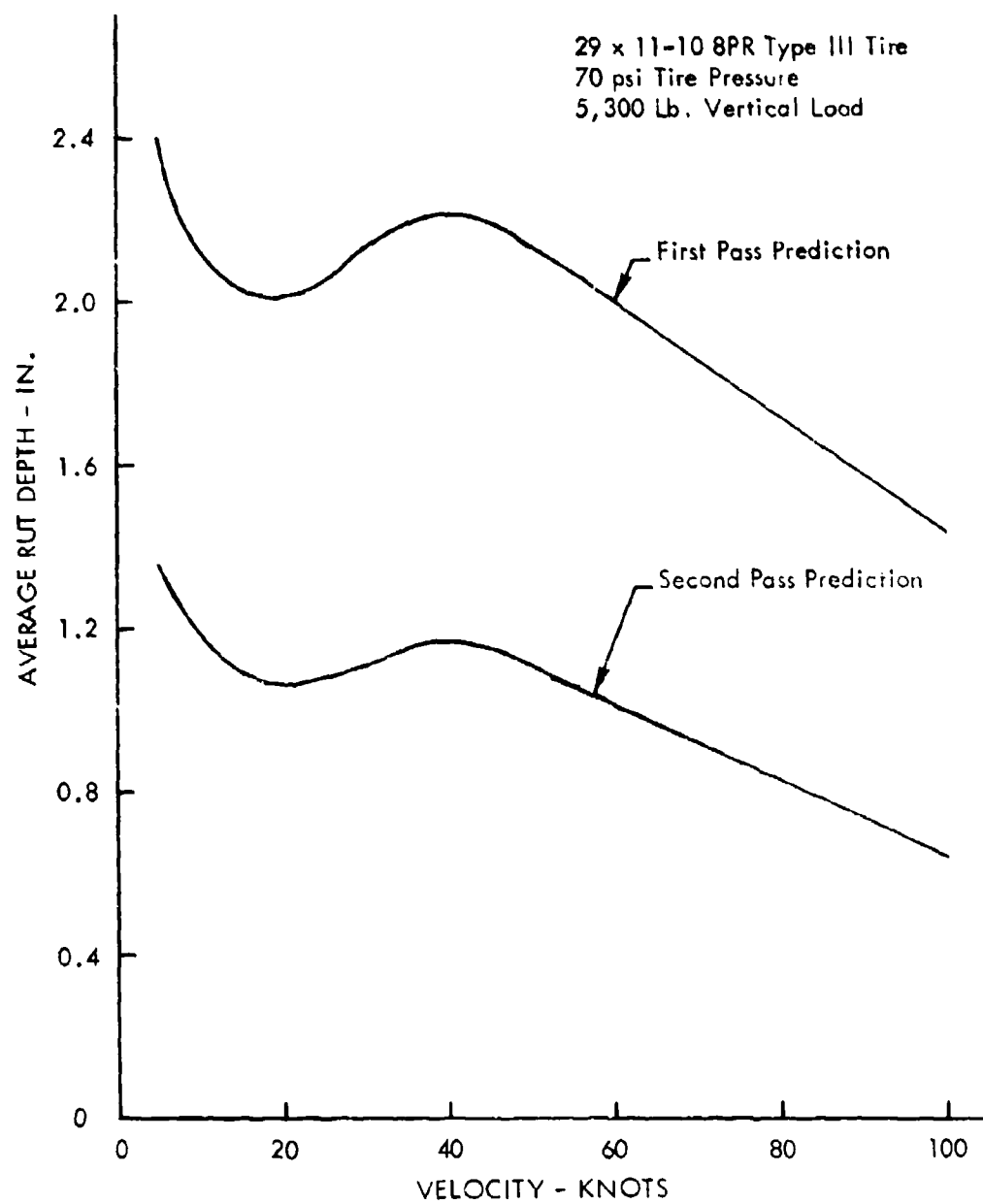


Figure 35. Predictions of Second Pass Rut Depths, CBR 1.5 Clay

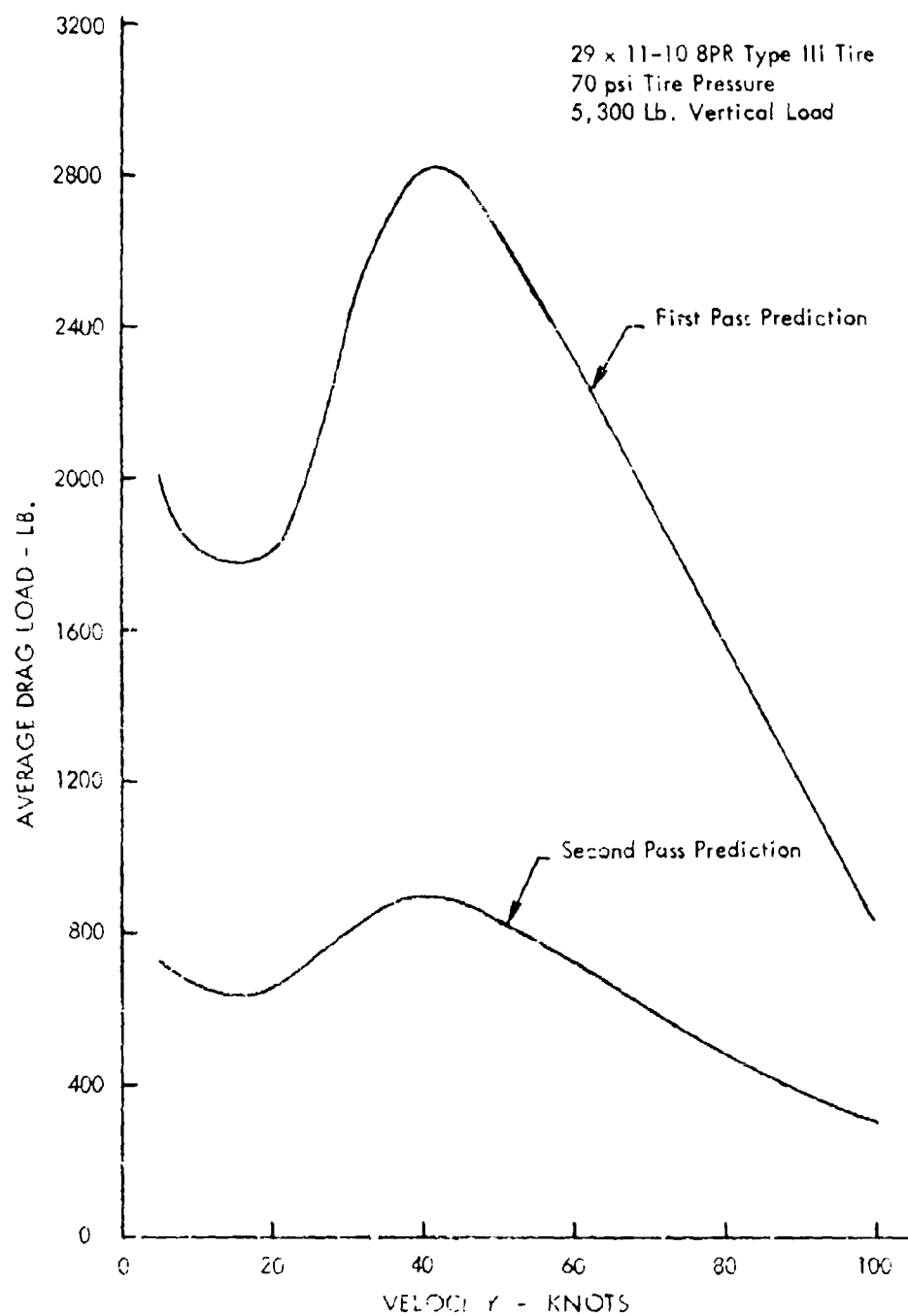


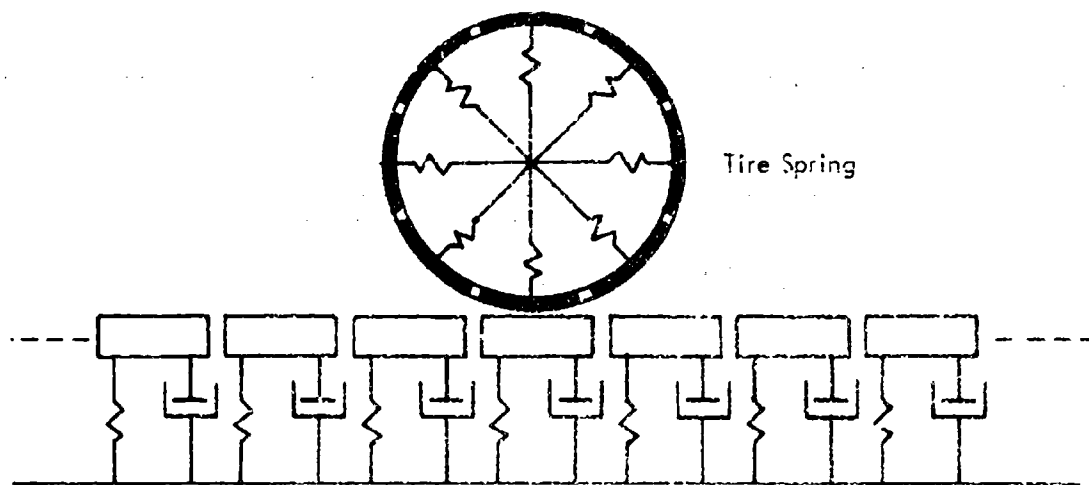
Figure 36. Predictions - Second Pass Drag Loads, CBR 1.5 Clay

As discussed above in Section II, these values are estimates based on the analytical model.

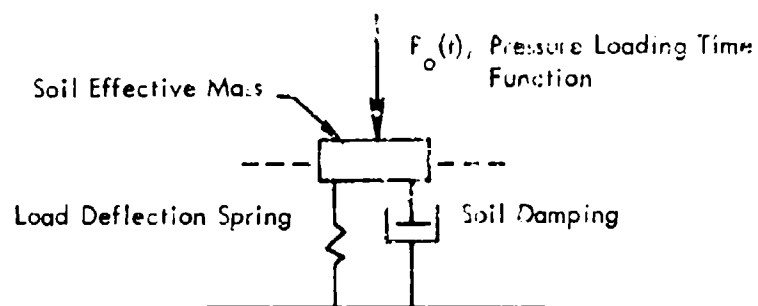
7. AN ALTERNATE SOIL MODEL

The soil model presented above is based on the concept of constant soil rutting at a constant forward velocity analogous to considering a tire deflection constant even though the individual particles of the tire are undergoing a cyclic variation in their deflection. The model is dependent upon the frame of reference used; in the recommended model the frame of reference is the wheel axle. An alternate approach was suggested in Reference 20 and shown here in Figure 37. In this approach the observer is located at a single point as the wheel passes. A time history of the deformation and load at this point is developed. Such a frame of reference is equally valid for studying wheel response, but incorporation of the model into simulation of a complete vehicle presents problems not encountered in the recommended method.

The recommended soil model uses iteration to convergence of a steady state value of rut depth and drag load for a given vertical load, tire pressure, soil condition, and velocity. Convergence usually takes place within 10 iterations. This method provides a direct calculation of the maximum value of rut depth and of the drag load on the wheel axle. The alternate model starts with zero initial soil deflection and computes a differential equation time history solution to reach the maximum deflection at a point in the soil. This maximum deflection must be known before any other time dependent computations can be incremented. Since the differential equation time history solution is likely to be slower than the iterative solution, some means must be developed to provide proper time sequencing between various parts of the problem (i. e. between the wheel loads and the aircraft structural loads). Although direct comparisons have not been made, it is believed that the iterative process is much faster than the differential equation solution.



(a) Idealization of the Continuous Soil Medium and the Wheel by Discrete Elements



(b) A Single Soil Element

Figure 37. Proposed Alternate Spring-Mass-Damper Soil Model

The alternate model consists of repeated solutions of the differential equation:

$$M_e \ddot{Z}_s = p_o(t) - F_{spring} - C \dot{Z}_s \quad (36)$$

where M_e is the soil effective mass, $p_o(t)$ is the wheel footprint pressure time history, and C is the soil damping factor. The values of M_e and C are from Reference 20.

F_{spring} was taken as the static load deflection curve for CBR 1.5 clay as measured at the Landing Loads Track. The forcing function, $p_o(t)$, was assumed to be a $(1 - \cos \alpha)$ shape pulse of duration L_f varying linearly with the forward speed of the wheel. These pulses are shown in $\frac{L_f}{2V}$ Figure 38 for four speeds.

Figure 39 shows time history solutions of Equations 36 at different wheel velocities. As the wheel velocity increases, the time during which the soil is loaded decreases and the deflection decreases. Figure 40 is a plot of the maximum deflection vs. wheel velocity. It is a continuously decreasing function and does not exhibit any evidence of resonant response to the single pulse load.

The magnitude of the sinkage predicted by this model is less than that predicted by the WES mobility number approach but by proper adjustment of the mass, spring, and damper numerical values, the curves could probably be brought into close agreement.

This model again points to the need for a drag interaction term which increases the pressure pulse in proportion to the drag load. It is believed that with additional development of this model and incorporation of the corrections already applied to the WES mobility approach, it could produce about the same accuracy as the recommended model. The computation time problem mentioned earlier would, however, remain. Figure 41 is a sketch of a possible modification of the alternate soil model to incorporate the drag force interaction and inertial lift.

A listing of the computer program used to obtain the results contained in Figures 38-40 is shown in Appendix C.

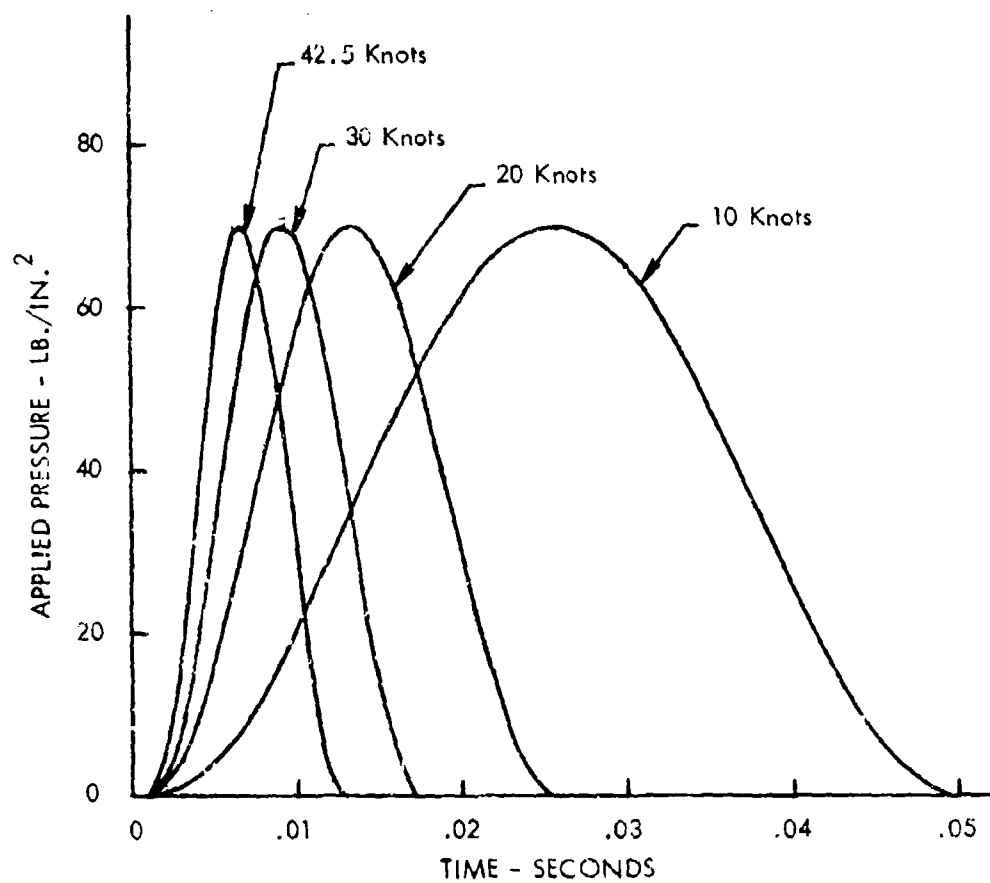


Figure 38. Pressure Pulse Forcing Functions

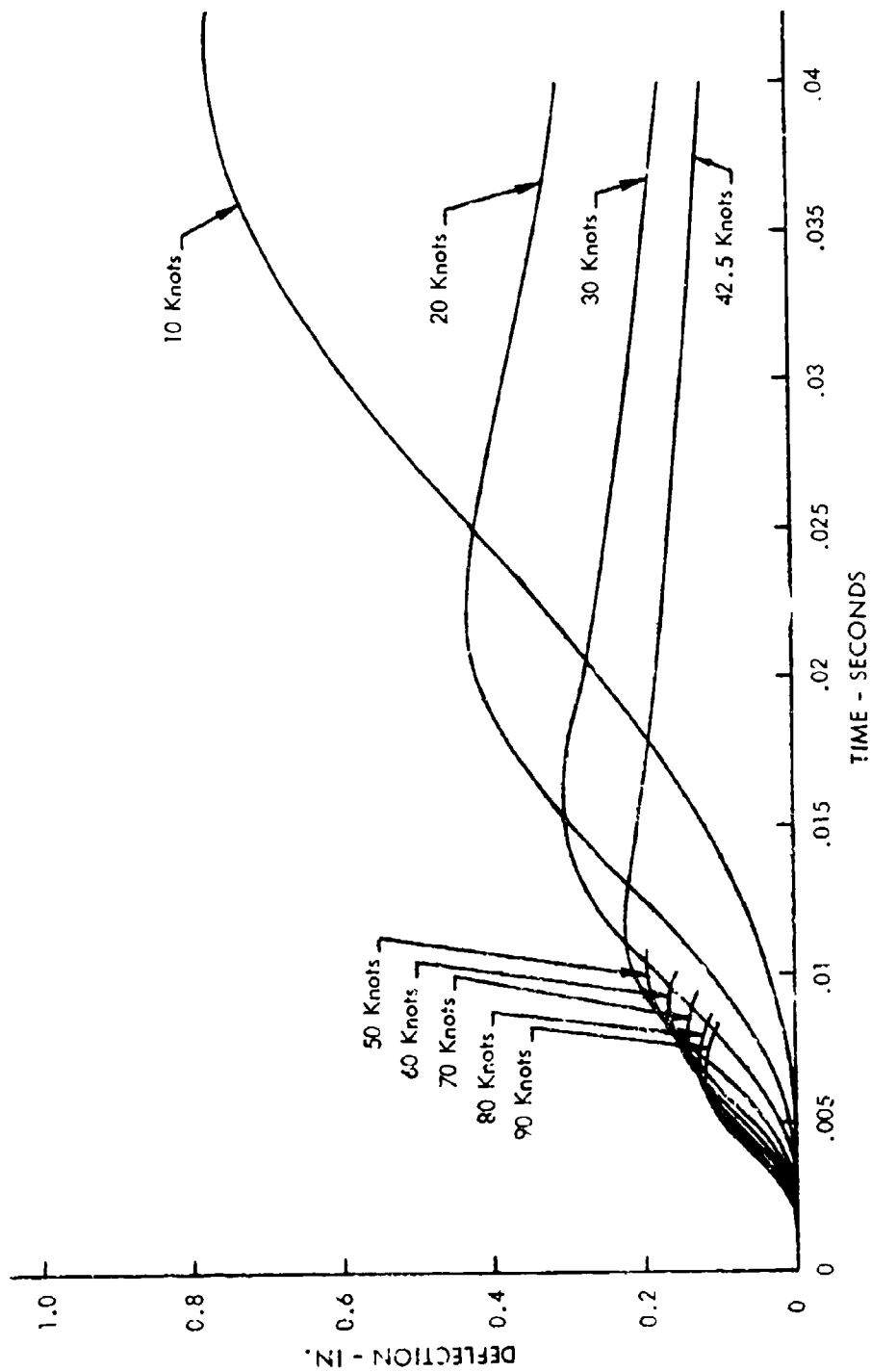


Figure 39. Soil Element Deflection Time Histories

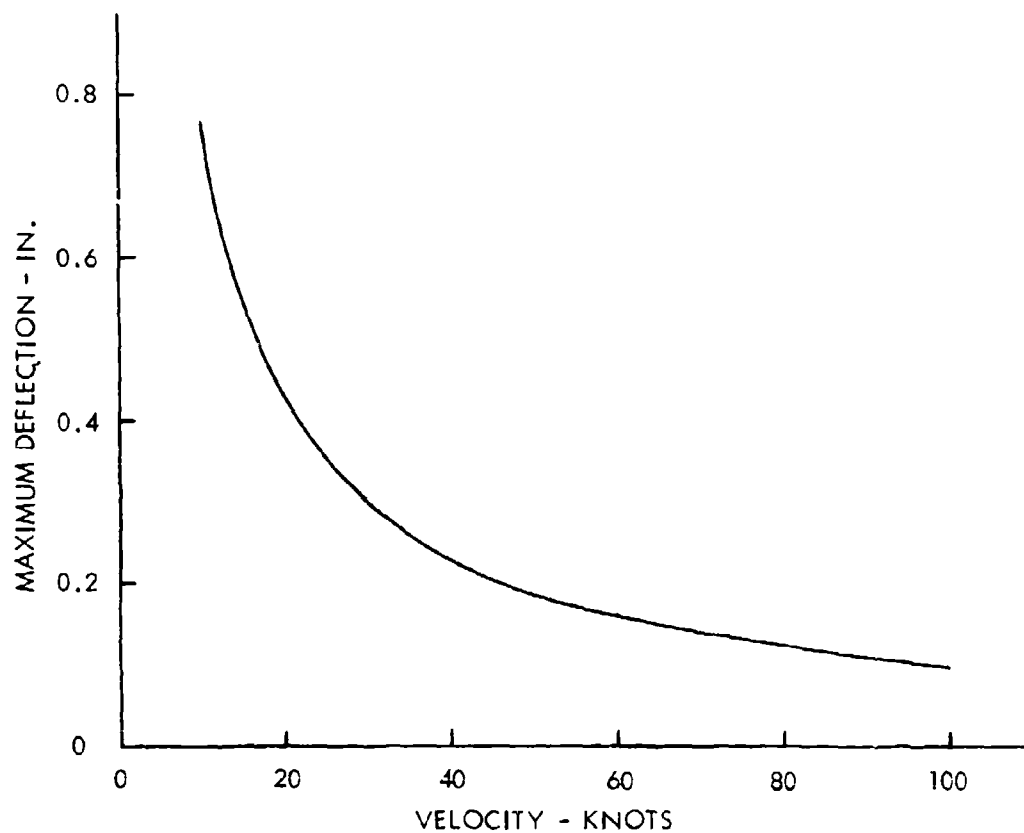
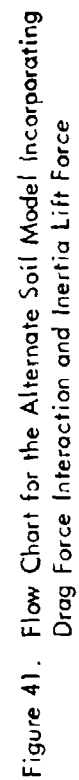


Figure 40. Maximum Soil Element Deflections vs. Wheel Velocity



Because of the failure to predict observed rut depth variations with velocity, and the lack of a drag interaction term in the equations, this model is not recommended for computation of aircraft wheel loads.

SECTION III

TEST RESULTS

The data reported herein are from the third series of tests that were made at the NASA Landing Loads Track. Table I shows soil strengths and wheel geometry used for all of the tests. In this test series a study was made of the yawed rolling properties of single wheels for yaw angles up to six degrees. A tandem configuration was studied for 5,300 pounds and 11,200 pounds loading on the two wheels. A few tests were run with a rigid single wheel to compare with the pneumatic tire results.

All tests in this series were run on a buckshot clay test bed with an estimated average strength of approximately CBR 2.4.

1. TESTS WITH A SINGLE WHEEL

Rut depths produced by free rolling and braking wheels are shown in Figures 42 - 44 for zero, three and six degrees yaw angle, respectively, for test velocities ranging up to 90 knots. The effect of yaw angle on rut depth is negligible for these conditions. Free rolling rut depths varied from 2.4 in. to 0.86 in., and braking rut depths varied from 3.8 in. to 0.72 in. In all cases the braked wheel rut depths are higher than the free rolling wheel rut depths at low speeds but approach the latter at about 75 knots. Some rut depths are lower for braking at 80 - 90 knots. This was caused by dynamic response of the test fixture. At high speeds the time during which the wheel is braked is quite small, and the average vertical load may be less during braking than it is during free rolling. In these cases the resulting rut depth may be less. Locking the wheel has little effect on the rut magnitude in the 80 - 90 knot range.

At three and six degrees yaw angle the sensors used to measure drag load and lateral load are rotated through the yaw angle and measure loads parallel and perpendicular to the wheel axis instead of parallel and perpendicular to the direction of motion of the test carriage. The convention reported here is consistent with aircraft loads usage for

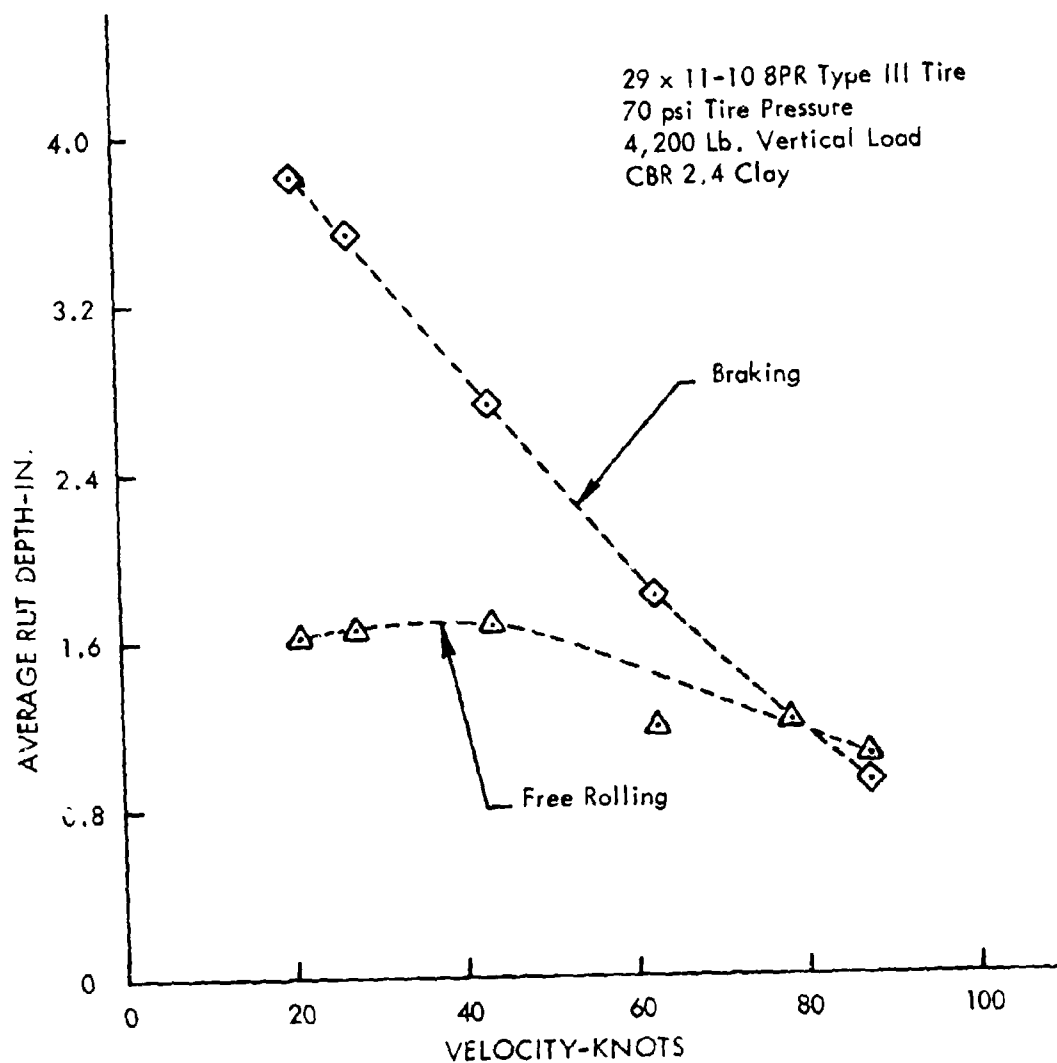


Figure 42. Free Rolling and Braking Rut Depths for Single Wheel - Zero Degrees Wheel Yaw Angle

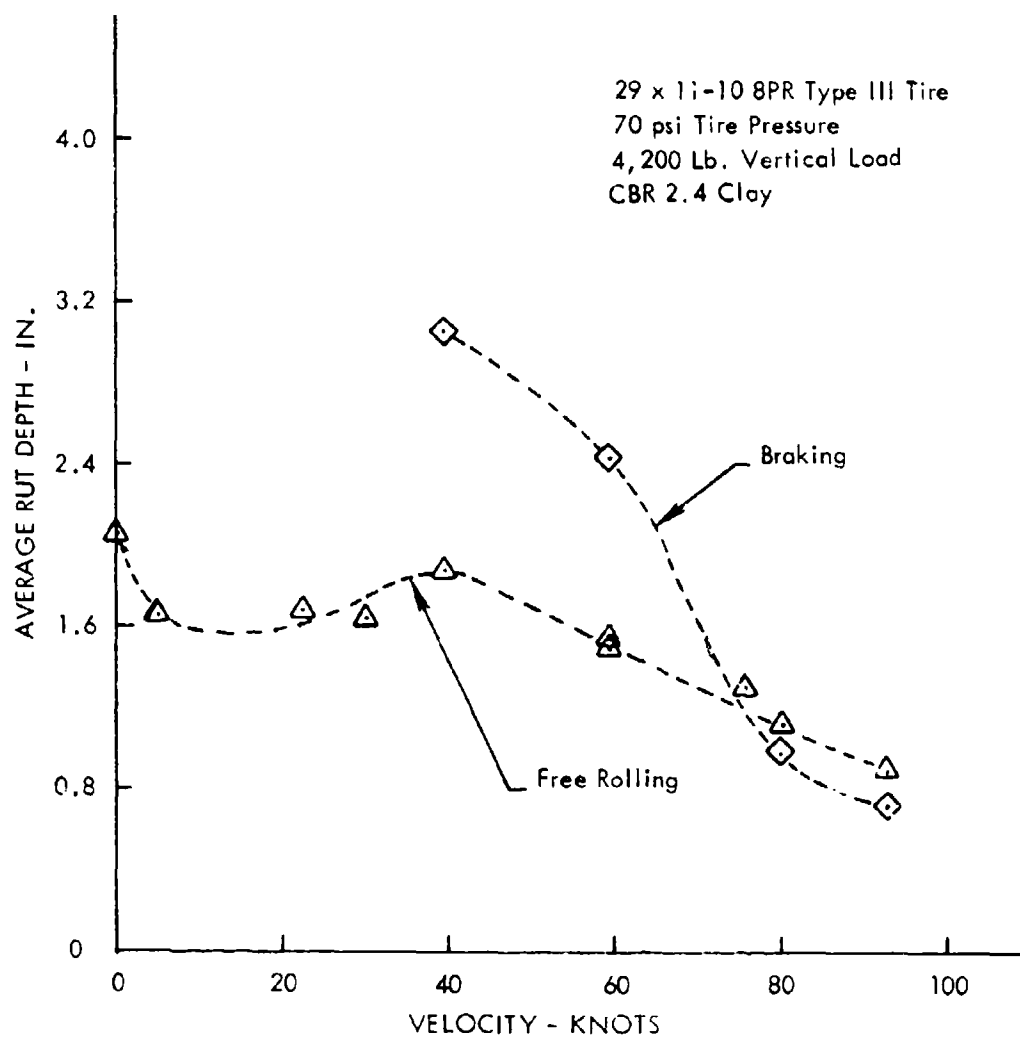


Figure 43. Free Rolling and Braking Rut Depths for Single Wheel - Three Degrees Wheel Yaw Angle

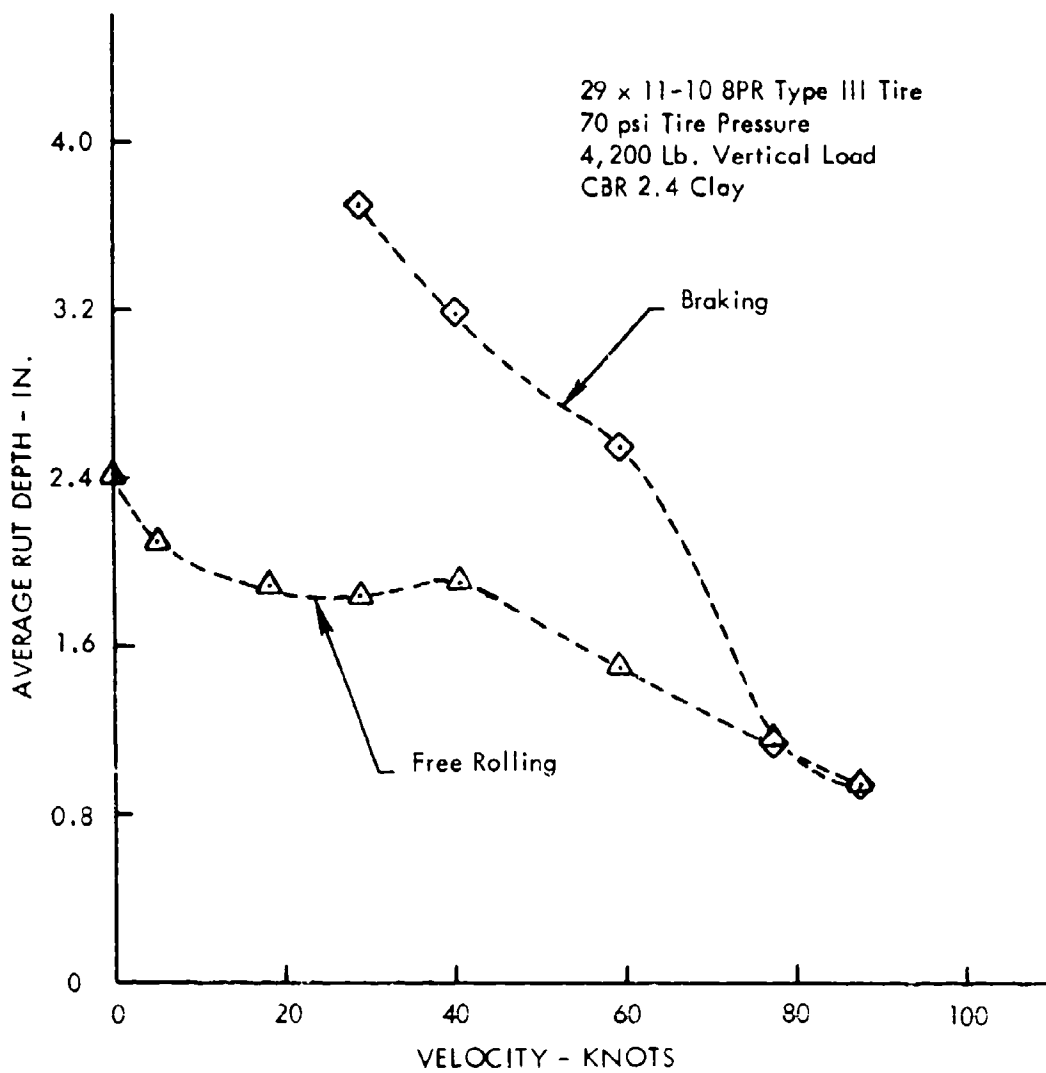


Figure 44. Free Rolling and Braking Rut Depths for Single Wheel - Six Degrees Wheel Yaw Angle

calculation of internal loads on fixed gear aircraft. For nose or main gears which rotate with respect to the aircraft coordinate system or for calculations of accelerations along axes that do not coincide with the principal directions of the aircraft axis system, it may be necessary to transfer lateral and drag loads to a new axis system during yaw conditions.

Figures 45 - 47 show drag load ratios for braking and free rolling at zero, three, and six degrees yaw angle. Yaw angles of these magnitudes have little effect upon drag ratios. Free rolling drag ratios varied from 0.52 to 0.14 depending on the wheel velocity. Braking drag ratios varied from 1.03 to 0.32 and decreased with increasing speed.

An evaluation of the effect of yaw angle on the measured drag loads was made from a straight-line least squares fit of the drag loads versus corresponding rut depths. For equivalent sinkages, ranging from 0.5 in. to 2.4 in., drag load at zero degrees yaw averaged 125 pounds more than at three degrees yaw and 65 pounds more than at six degrees yaw. The results show that when averaging over this sinkage range, there is no consistent trend in the drag load results with yaw angle. Additional data at higher yaw angles might better define the relations among these test conditions and thus indicate a trend, but below six degrees, any change in the drag loads with angle will be quite small.

A similar least squares straight line fit of drag load versus rut depth was made for yawed wheel braking. This analysis showed that drag load at zero degrees yaw averaged 75 pounds higher than at three degrees yaw and 220 pounds higher than at six degrees yaw for equivalent sinkage between 0.5 and 2.4 in.

The braking drag loads for zero degrees yaw averaged 950 pounds higher than the free rolling drag loads for sinkages between 0.5 in. and 2.4 in.

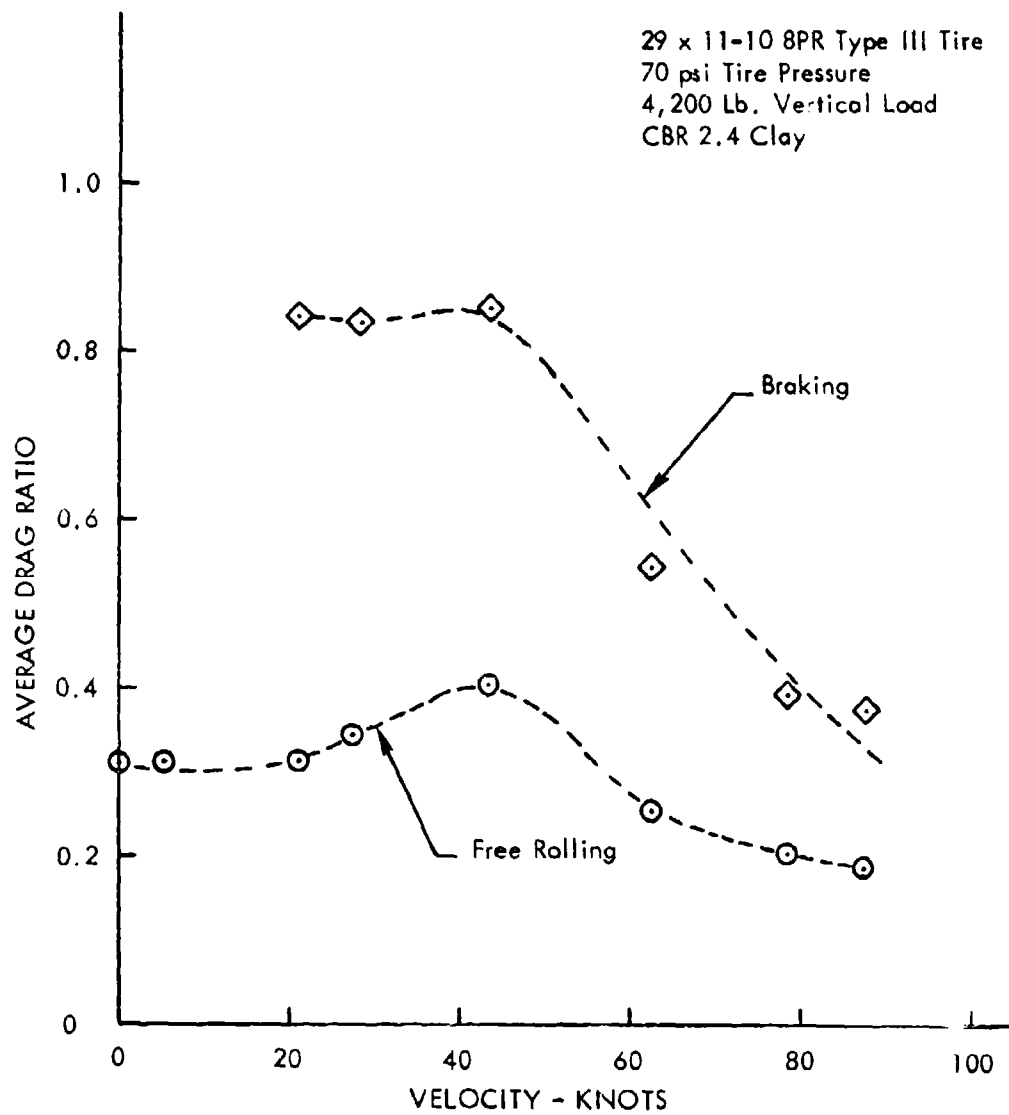


Figure 45. Free Rolling and Braking Drag Ratios for Single Wheel - Zero Degrees Wheel Yaw Angle

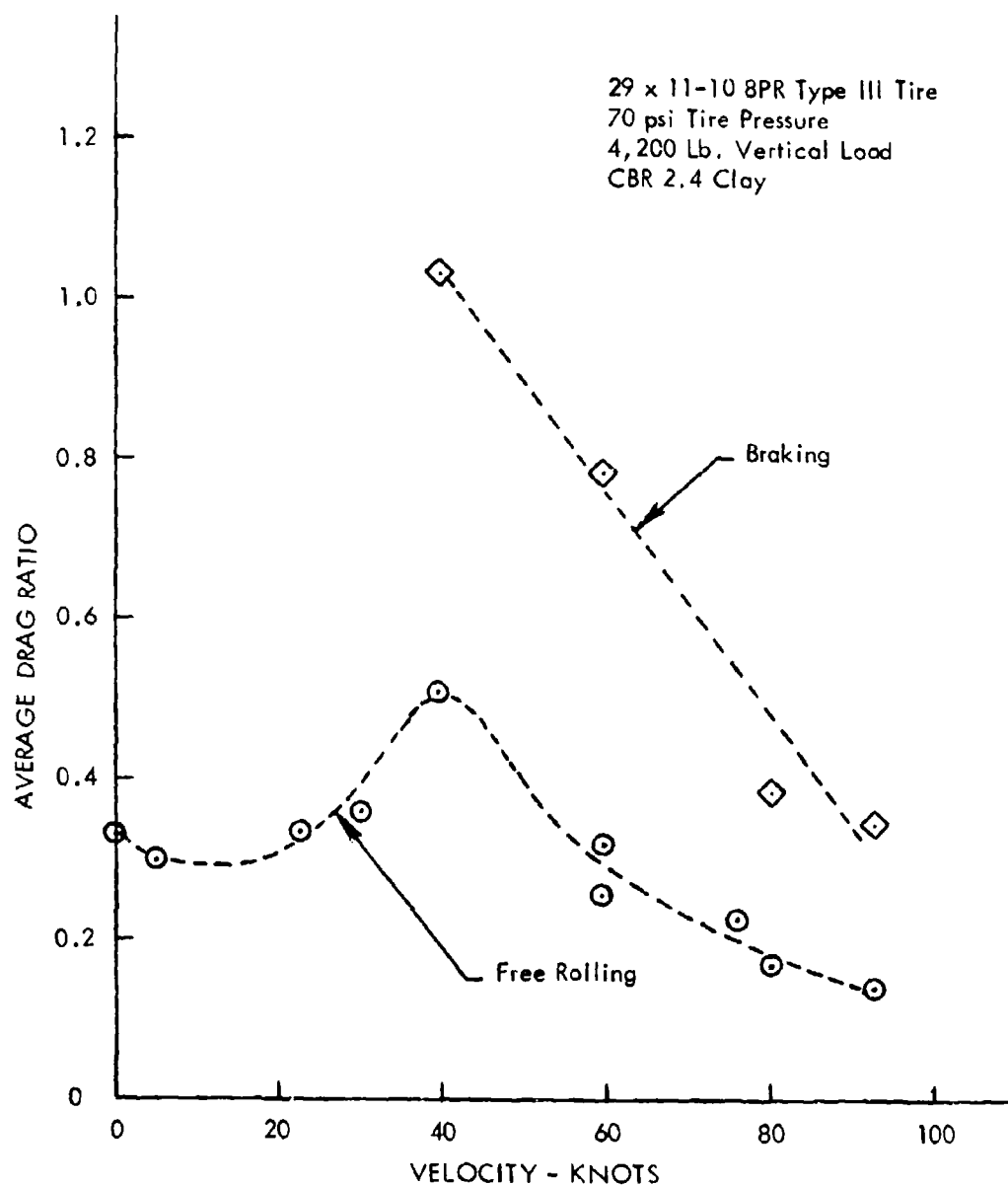


Figure 46. Free Rolling and Braking Drag Ratios for Single Wheel - Three Degrees Wheel Yaw Angle

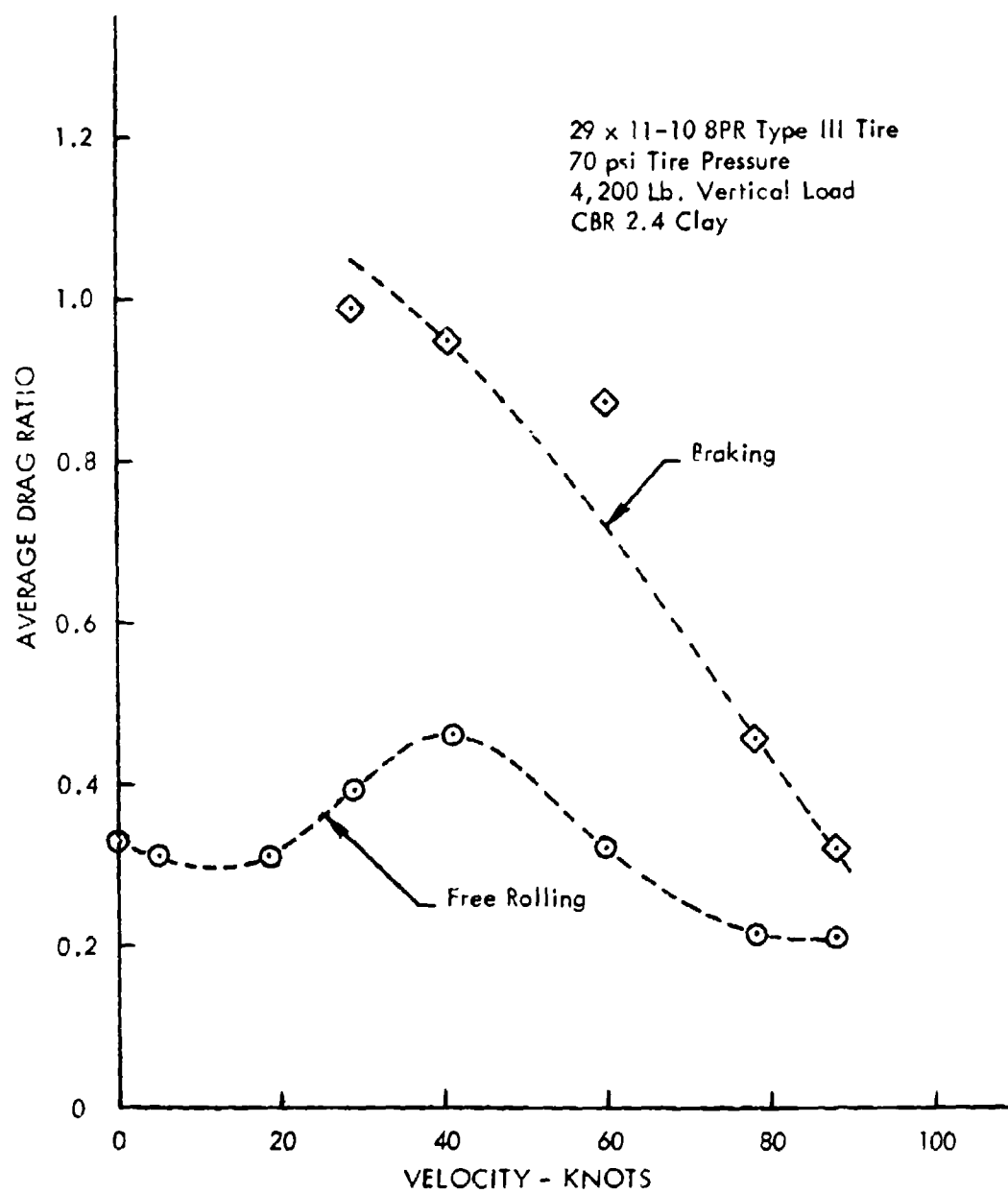


Figure 47. Free Rolling and Braking Drag Ratios for Single Wheel - Six Degrees Wheel Yaw Angle

Significant lateral loads are developed on a wheel when it is yawed at an angle to the direction of motion. Figure 48 shows the lateral load to vertical load ratio developed for free rolling on clay and on concrete for three and six degree yaw angles. Variation with velocity is small compared to the variation with velocity found for drag loads. Lateral loads on concrete are significantly higher than on clay. At three degrees yaw angle the clay lateral load ratio is only 35% of the lateral load ratio for concrete, or about 0.125, compared to 0.36 for concrete. At six degrees yaw angle the clay ratio is also 35% of the concrete ratio, but the magnitudes have increased to 0.22 for clay and 0.625 for concrete.

Figure 49 compares lateral load ratios for free rolling with the lateral load ratios for braking on clay. At three degrees the braking ratio is about 32% of the free rolling ratio, and at six degrees the braking ratio is about 54% of the free rolling ratio.

These percentages are meaningful only in the coordinate system parallel and perpendicular to the wheel. If the lateral load is resolved to an axis perpendicular to the direction of motion it should be near zero since the locked wheel cannot, in theory, develop a side force.

It is concluded from these tests that for wheel yaw angles up to 6° the lateral loads are always lower on a soft soil surface than on a concrete surface. Braking lateral loads are lower than free rolling lateral loads on the soil surface. The behavior is illustrated by time histories contained in Appendix A.

The decrease in lateral loads in soil over those encountered on hard surfaces at the same yaw angle does not imply that an aircraft landing gear designed for maximum hard surface lateral loads would be adequate for operation in soft soil. It must be remembered that the lateral loads on the soil surface occur simultaneously with drag loads which are much higher than are encountered on a hard surface for either free rolling or braking. Each gear configuration must be individually evaluated to obtain

29 x 11-10 8PR Type III Tire
70 psi Tire Pressure
4,200 Lb. Vertical Load

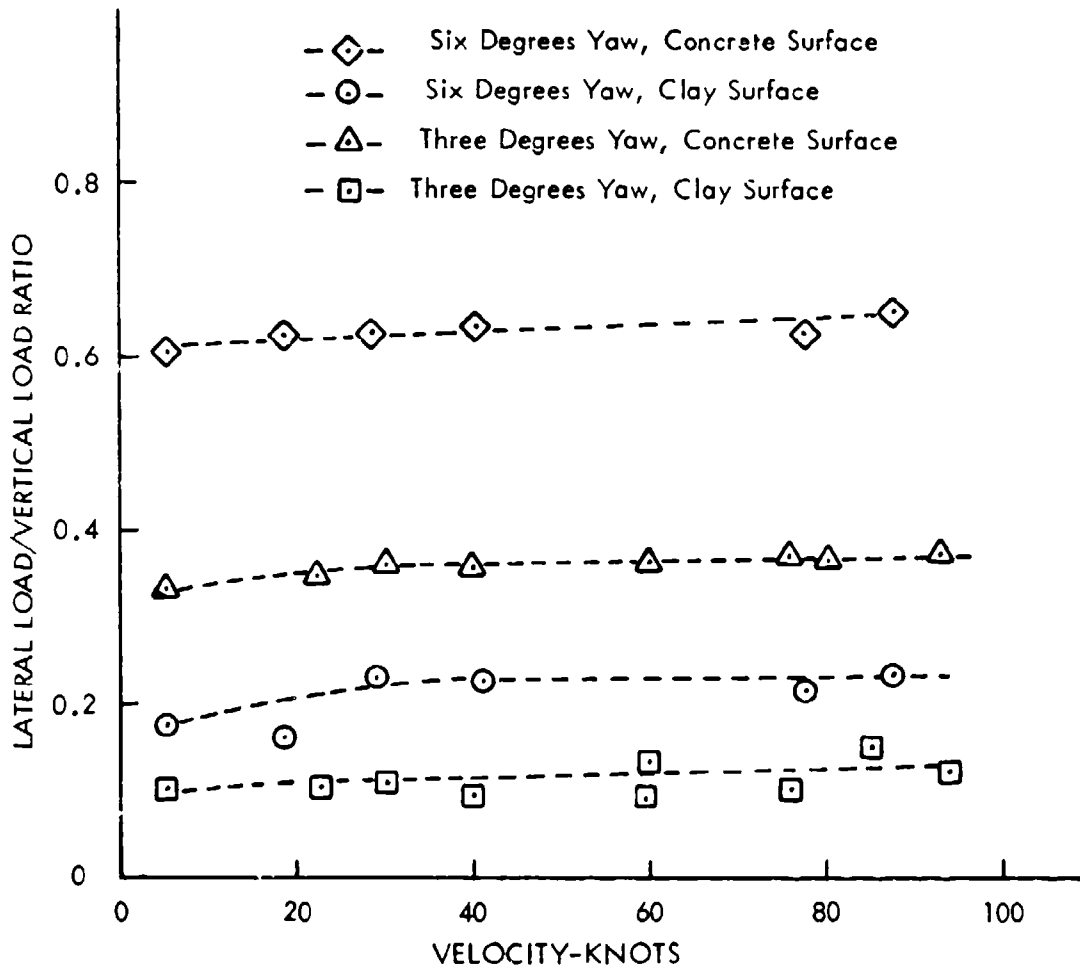


Figure 48. Comparison of Free Rolling Lateral Load Ratios on Concrete and Clay for Three and Six Degrees Yaw Angle

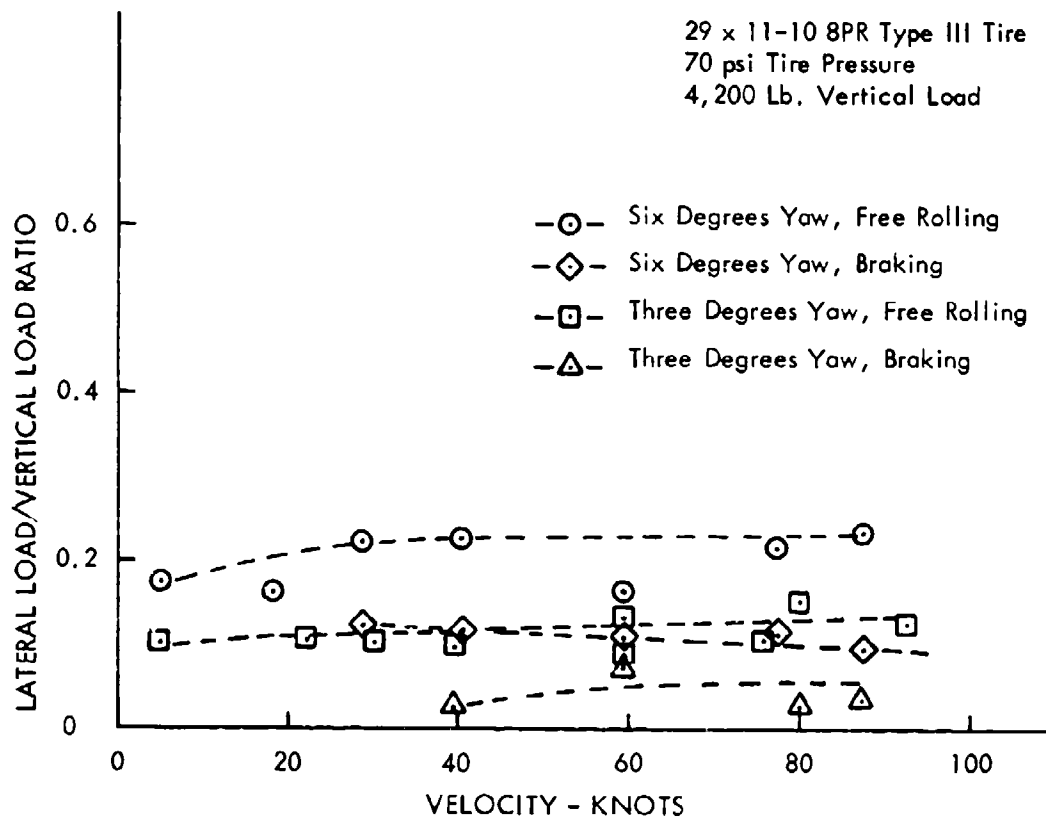


Figure 49. Comparison of Lateral Load Ratios for Free Rolling and Braking on Clay at Three and Six Degrees Wheel Yaw Angle

its capability for sustaining simultaneous loads. There may also be potential problems of maneuverability on soft soil during crosswind operations or during taxi or turning maneuvers.

2. TESTS WITH A TANDEM WHEEL

Two 29 x 11-10 8PR tires were tested in tandem with a 40 in. axle centerline spacing. Vertical load was 5,300 pounds on the tandem pair for a series of tests at 70, 45, and 30 psi tire pressure and 11,200 pounds for a series of tests at 30 psi.

Free rolling and braking rut depths are shown in Figures 50, 51, and 52 for 70, 45, and 30 psi. Peak ruts occur between 40 and 60 knots for free rolling and are 1.6 in., 1.1 in., and 0.58 in. respectively for the three tire pressures. Braking rut depths decreased continually with increasing velocity at a slope of about 0.24 in. per 10 knots above about 25 knots. The 45 psi and 30 psi rut depths for braking were quite close to the free rolling values at 90 knots, but the braking rut at 70 psi was approximately 0.6 in. deeper than the free rolling rut at 90 knots.

Maximum braking ruts occurred at about 20 - 30 knots in a range that was not studied in great detail. It appears that there may be a peak in the braking rut depths in this speed range consistent with the evidence seen in the single wheel tests, but not enough data points are available for good definition at either wheel configuration. Maximum ruts for braking at a speed of 30 knots were estimated to be 3.6 in., 1.8 in. and 1.0 in. respectively for 70, 45, and 30 psi. The 70 psi braking rut depth of 3.6 in. compares with an estimated 3.2 in. depth for the single wheel zero degree yaw case shown in Figure 42. The difference from 3.2 in. to 3.6 in. is small enough to be caused by data scatter and the 1100 pound difference in vertical load for the single wheel and the tandem pair. It is concluded from Figures 42 and 50 that for equal tire pressures there are no significant differences in the ruts formed by a single wheel and a tandem pair when both assemblies are loaded to similar values.

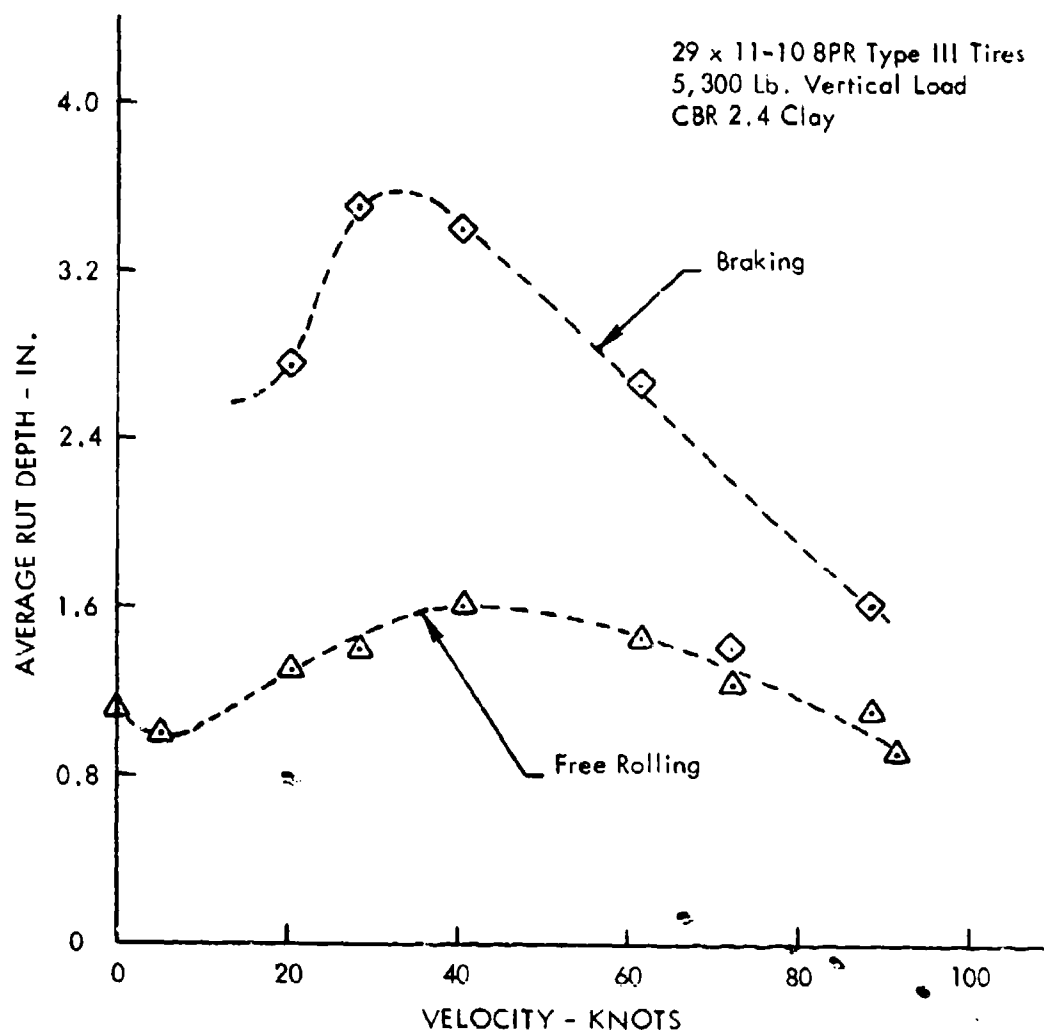


Figure 50. Free Rolling and Braking Rut Depths for Tandem Wheels - 70 psi Tire Pressure

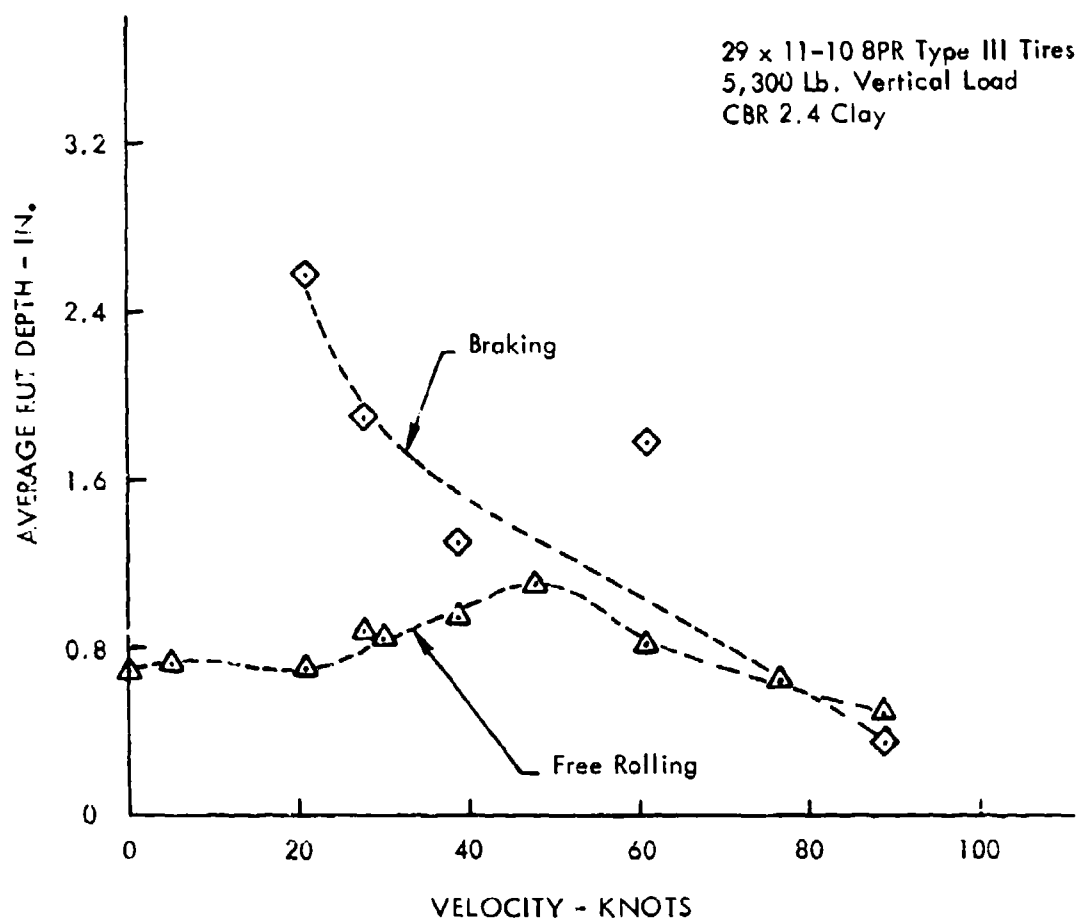


Figure 51. Free Rolling and Braking Rut Depths for Tandem
Wheels - 45 psi Tire Pressure

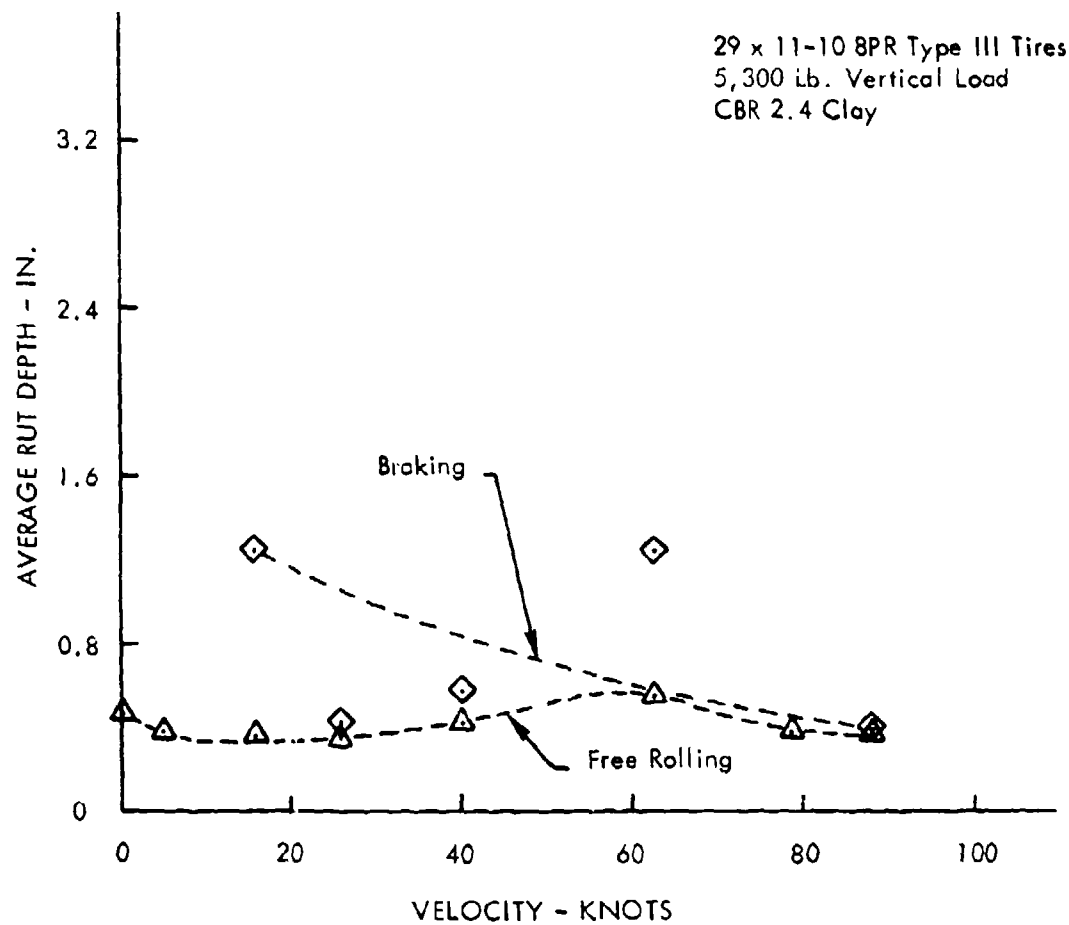


Figure 52. Free Rolling and Braking Rut Depths for Tandem Wheels - 30 psi Tire Pressure

Figures 53, 54, and 55 show the tandem wheel drag ratios. Peak free rolling drag ratios for the leading and trailing wheels are approximately equal at each of the three tire pressures tested. Drag ratios are approximately 0.42, 0.275, and 0.26 for 70, 45 and 30 psi. In all cases the peak drag load is reached on the leading wheel at a lower speed than on the trailing wheel. The average difference in speed at the peaks is 19 knots. If 70 psi single wheel drag ratios from Figure 45 are compared with those for the tandem wheel in Figure 53, it is seen that the trailing wheel peak drag ratio occurs at approximately the same speed as that for the single wheel. The magnitude of the drag ratio for the single wheel and the tandem wheels is seen to be quite close when Figures 45 and 53 are compared.

At 70 and 45 psi braking drag ratios are higher for the trailing wheel. The average difference is about 0.15 at 70 psi and about .08 at 45 psi. The data scatter in the 30 psi braking drag ratios precludes a definite conclusion as to the difference between leading and trailing wheels for this tire pressure. The peak drag ratios for braking at 30 knots are 0.77, 0.77, and 0.64 for 70, 45, and 30 psi respectively. The data points at 60 knots for 45 psi and at 63 and 88 knots for 30 psi were ignored since these are beyond what is considered normal data scatter.

Figure 56 compares the 30 psi tandem wheel drag ratios for 11,200 pound and 5,300 pound ballast weights. There do not appear to be any significant differences in these ratios. Figure 57 compares drag ratios for the single wheel and the tandem wheels for both free rolling and braking at 70 psi tire pressure.

Differences are quite small for free rolling; both the single and tandem wheel drag ratios reach a peak value of about 0.41. The velocity for maximum drag ratio is about 35 knots for the tandem wheels and about 43 knots for the single wheel. Over the velocity range from 20 to 90 knots the average tandem ratio is 0.30 and the average single wheel ratio is 0.29. Allowing for the differences in the wheel vertical load, the tandem wheels average 220 pounds more drag per wheel than the single wheel. For braking, the tandem wheel drag ratio average is 25% to 35% higher than the single wheel ratio.

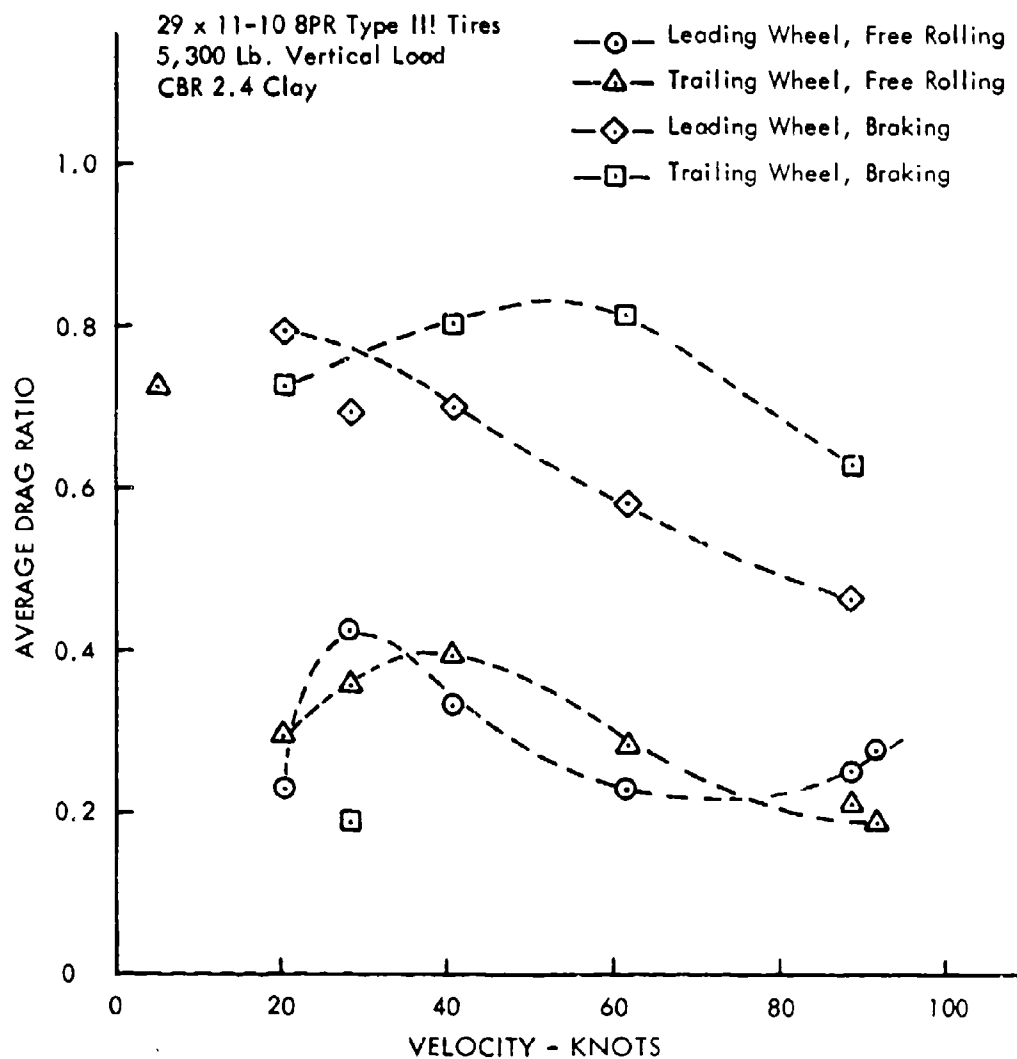


Figure 53. Free Rolling and Braking Drag Ratios for Tandem Wheels - 70 psi Tire Pressure

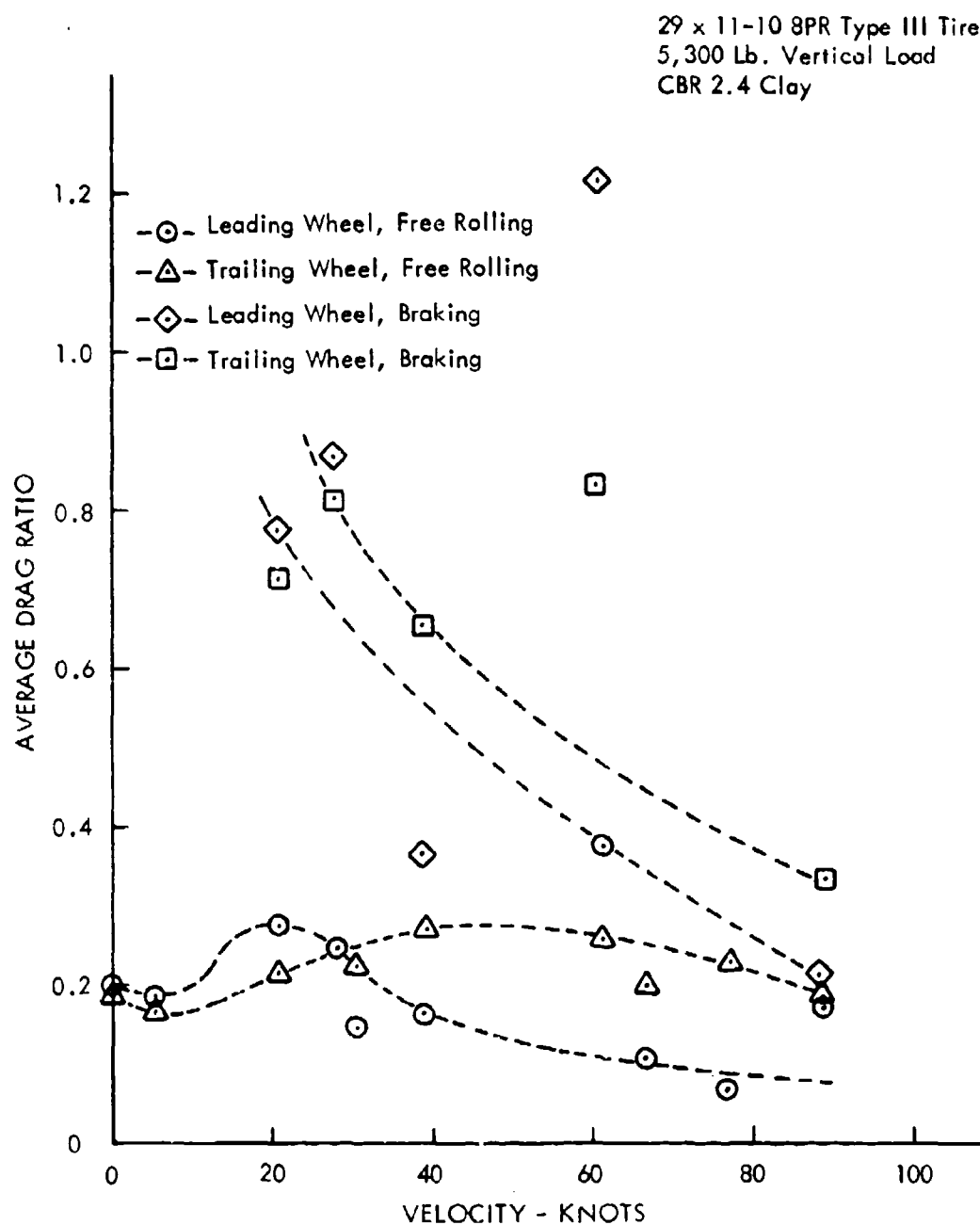


Figure 54. Free Rolling and Braking Drag Ratios for Tandem Wheels - 45 psi Tire Pressure

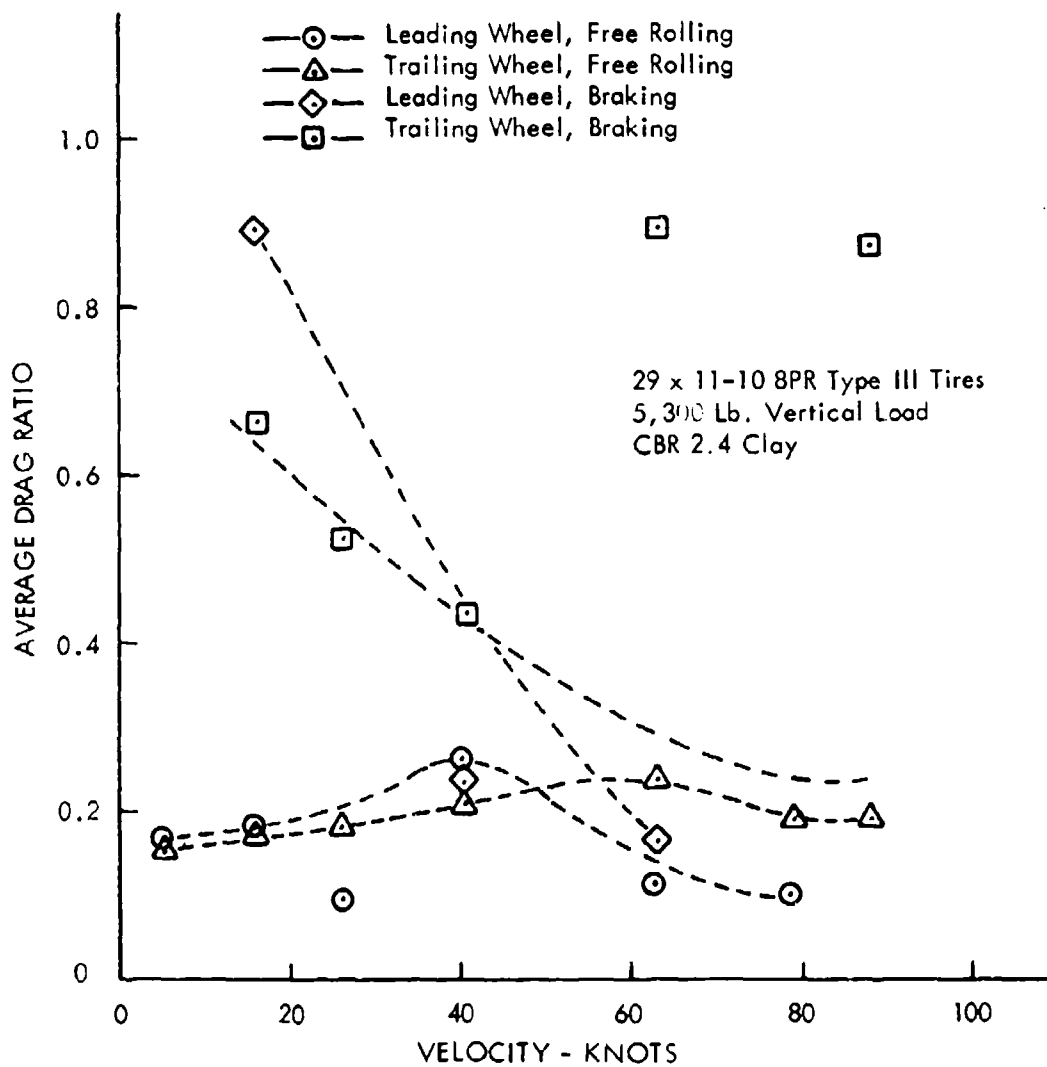


Figure 55. Free Rolling and Braking Drag Ratios for Tandem Wheels - 30 psi Tire Pressure

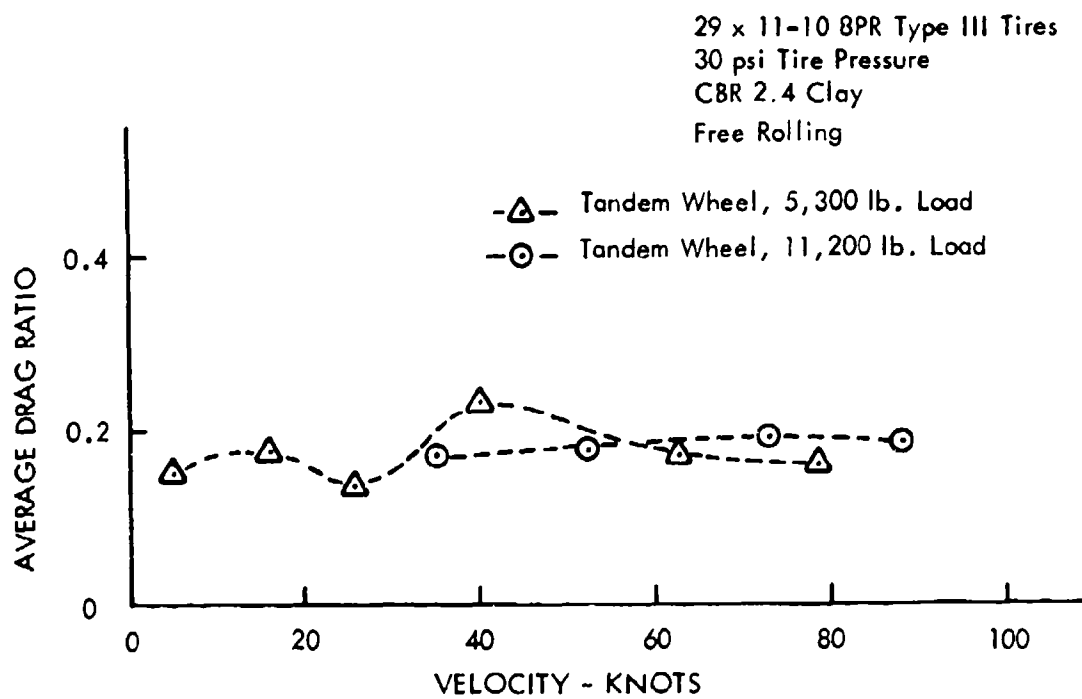


Figure 56. Comparison of Drag Ratios for 5,300 Lb. and 11,200 Lb. Tandem Wheel Loads

29 x 11-10 8PR Type III Tires
 70 psi Tire Pressure
 5,300 Lb. Tandem Wheel Load
 4,200 Lb. Single Wheel Load
 CBR 2.4 Clay

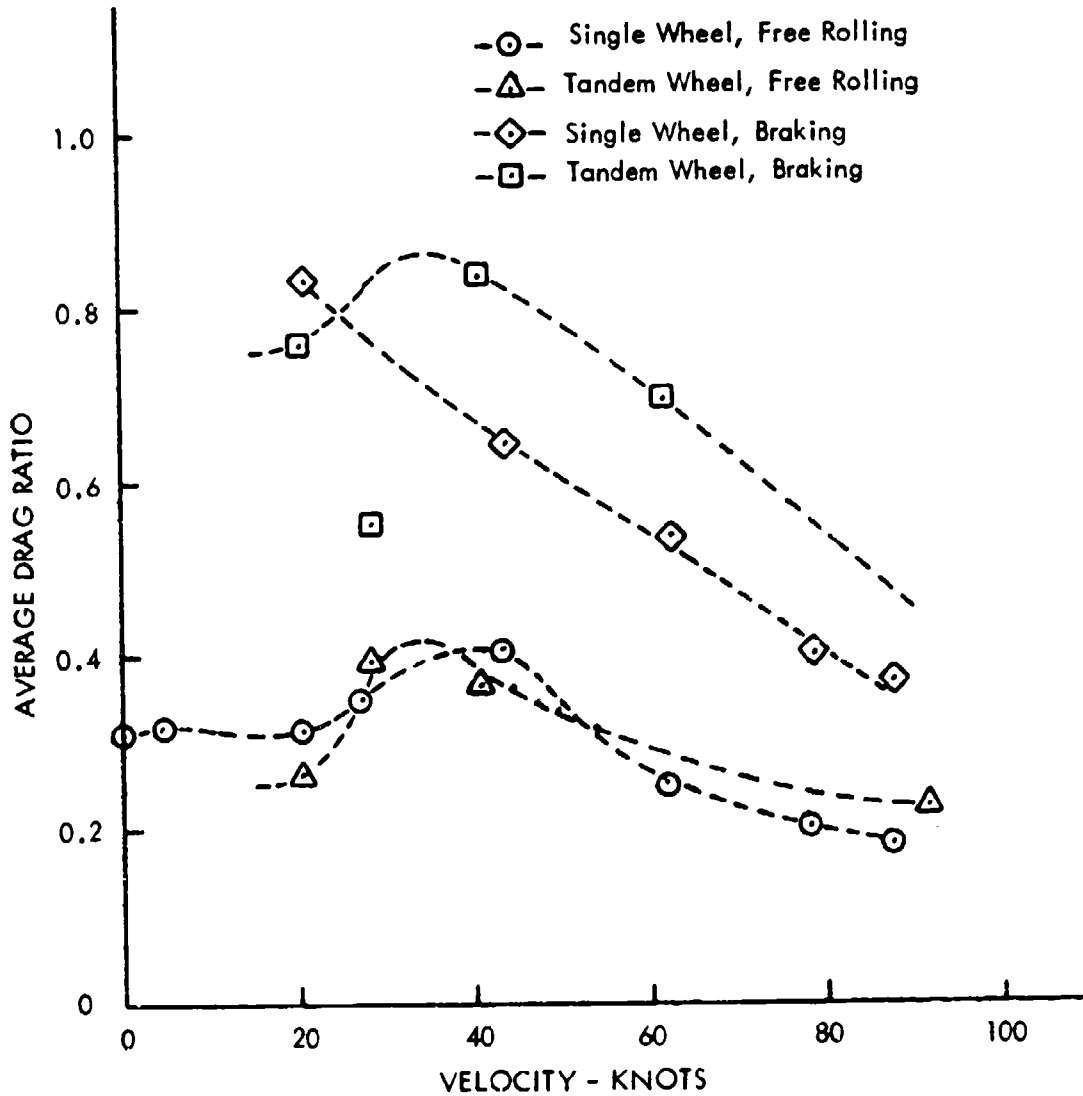


Figure 57. Comparison of Single and Tandem Wheel Drag Ratios

3. TESTS WITH A RIGID TIRE

A 29 x 11-10 8PR tire was filled with a rigid plastic foam having crushing strength of approximately 2500 psi to provide a rigid tire of the same cross sectional profile as an undeflected pneumatic tire. Because of time limitations only 6 tests were made with this wheel, but the results show significant differences from those obtained with a pneumatic tire. The primary differences are the much higher rut depths and drag loads and the different mode of failure of the soil.

Figures 58 and 59 show the rut depths and drag ratios for the rigid wheel. The pneumatic tire drag ratios for 70 psi tire pressure are shown for comparison. There appears to be a tendency for the rigid tire drag ratio to vary as the square of the velocity except for the data points at 55 and 76 knots. It is possible that there is a peak in rut depth and drag load between 55 and 76 knots and that the load will decrease at higher speeds as shown by the estimated curves. The rigid tire drag ratio increases from about 0.5 in the 0 to 30 knot range to 0.85 at 75 knots.

From 20 knots to 75 knots the rigid tire rut depth is approximately 2.5 in. The 70 psi pneumatic tire rut is about 60% of this depth and averages about 1.5 in.

The failure of the soil in the rut was significantly different for the rigid tire than for the pneumatic tire. A pneumatic tire compresses the soil and forces it to flow laterally around and underneath the tire. As brakes are applied on a pneumatic tire it begins to shear the material and push it aside in large pieces. The bottom of the rut underneath a braked wheel is filled with large lateral cracks indicating strong shearing forces.

The free rolling rigid tire produces a failure of the soil that appears quite similar to the failure underneath a braked pneumatic tire. The pieces of clay ejected from the rut were usually smaller for the rigid tire than those from a braked pneumatic tire, but at 60 knots and above they were thrown as far as 30 feet from the soil bed. Additional data points at

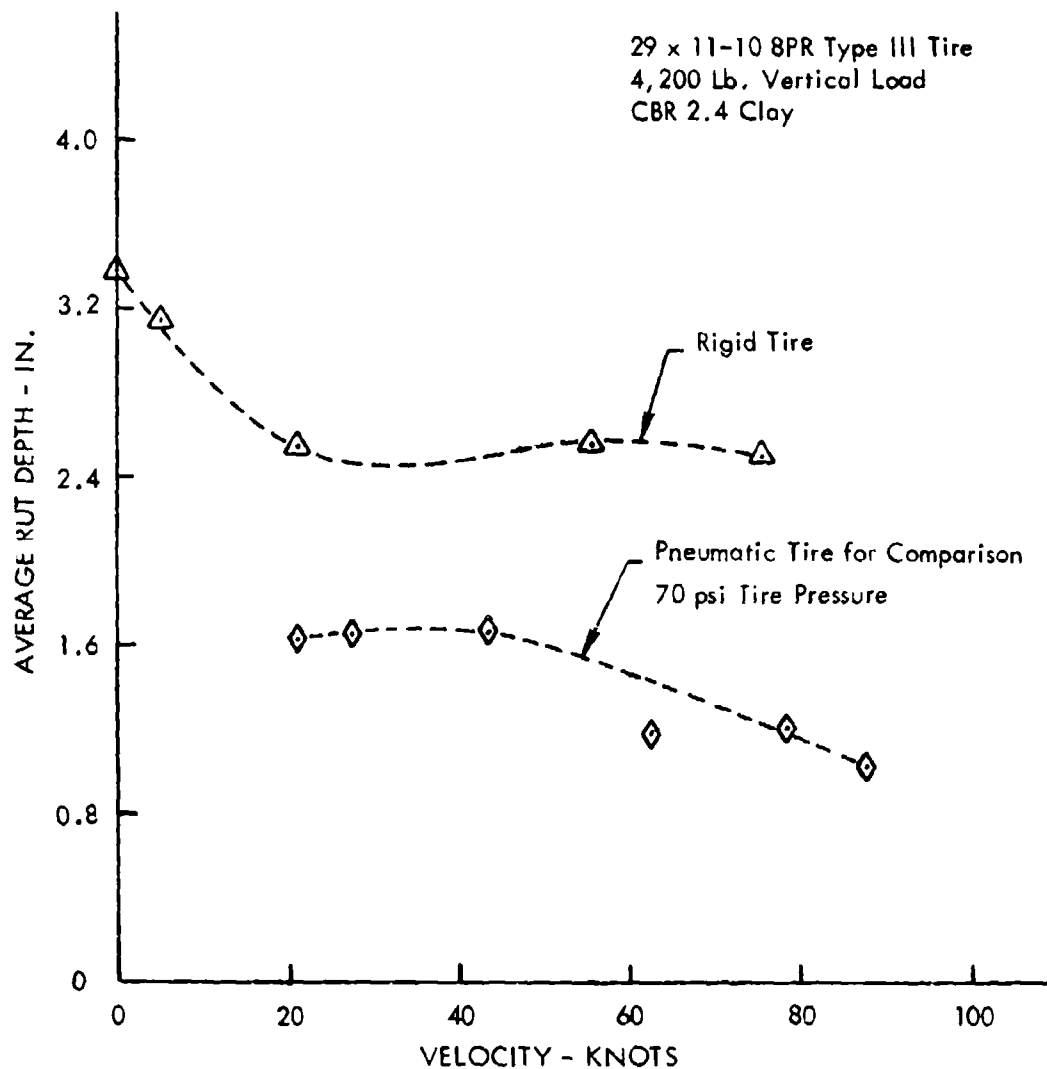


Figure 58. Rut Depths for a Single Rigid Wheel

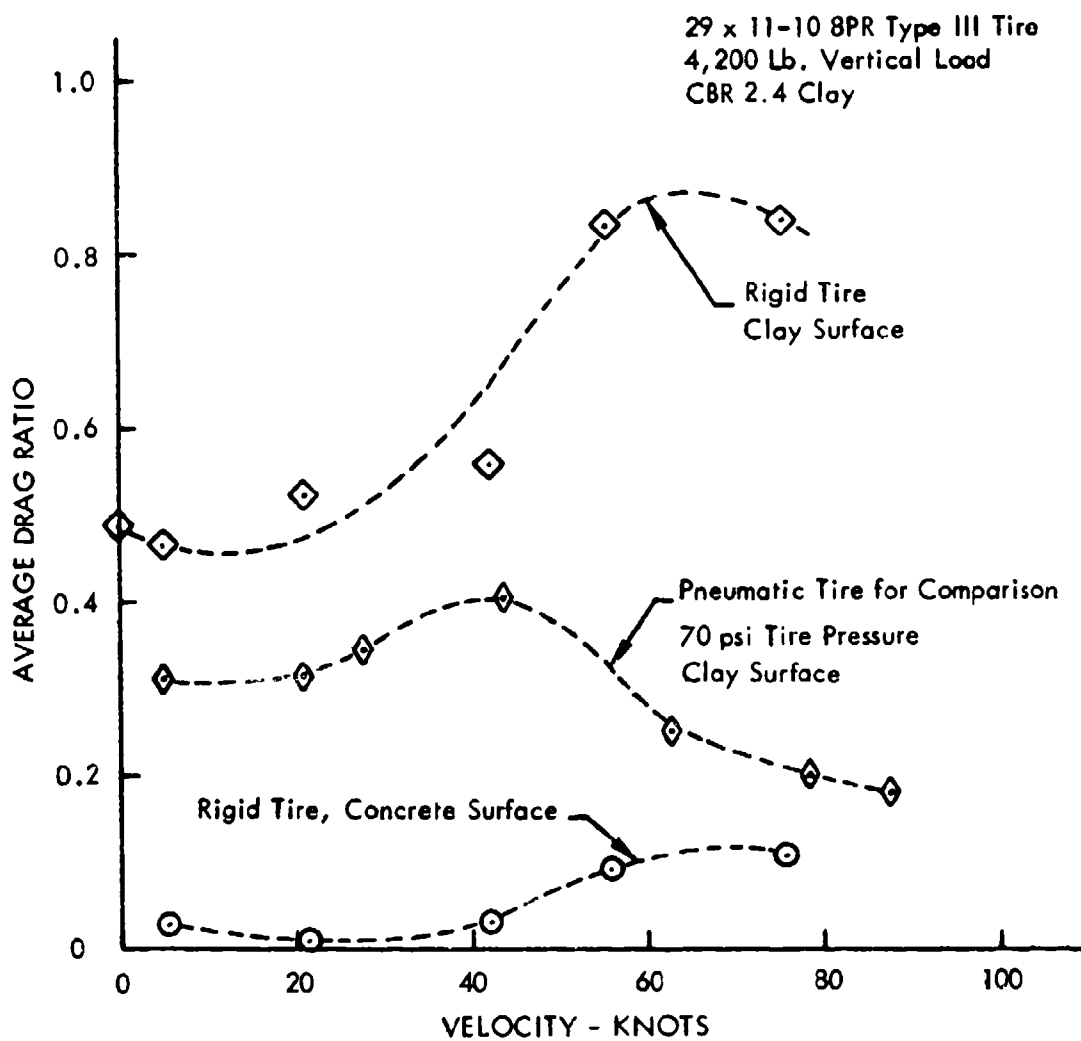


Figure 59. Drag Load Ratios for a Single Rigid Wheel

all speed ranges and further study of the soil mode of failure will be required before this behavior of the rigid tire or its relation to the behavior of a pneumatic tire can be explained.

SECTION IV

INCORPORATION OF THE SOIL MODEL INTO AN AIRCRAFT TAXI SIMULATION

An analog computer program was developed which incorporated the soil model discussed above in Section II. The aircraft simulated was the C-130 shown below in Figure 60 and was a proposed assault transport version equipped with a special landing gear designed for rough field operation. The schematic of this landing gear strut is also shown in Figure 60. It consists of two air chambers, one of which by-passes the strut damper orifice to limit high damper loads during operation on rough surfaces.

The aircraft simulation included three landing gear struts, representing one half of a symmetrical airplane, rigid body pitch and translation, three flexible wing modes, and a deformable surface for each gear. A flow chart for this simulation is shown in Figure 61.

Runway roughness consisted of the centerline profile of an unprepared runway at Fort Campbell, Kentucky, designated as site U-8 by the U. S. Air Force (5). It is considered moderately rough. Computer simulations were made for constant speed taxi over the entire length of the runway at speeds of 20, 40, and 80 ft./sec. and for take-off runs beginning at one end of the runway.

1. TAKE-OFF DISTANCE DETERMINATION

The take-off studies were made to determine if the surface roughness significantly affected take-off distance and how much the soil strength changed the take-off distance. Results are shown in Figure 62.

Surface roughness does not produce any appreciable differences in the take-off distances. As would be expected, the distances required to reach take-off speed increase rapidly at the lower CBR strengths. At a value of $CI = 200$ (CBR 4) the increase is 18% over the hard surface value.

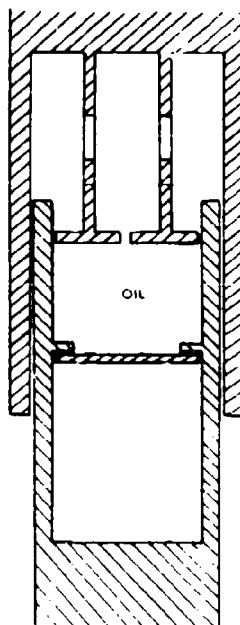
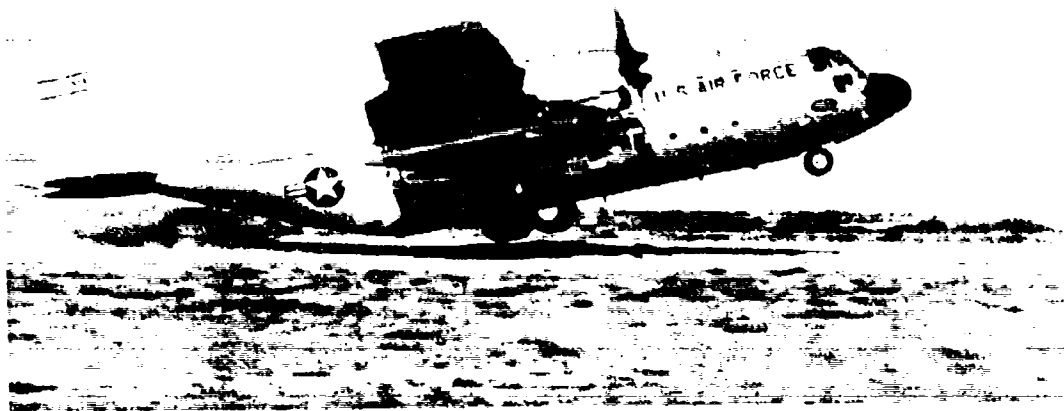


Figure 60. C-130 Aircraft and Assault Landing Gear Schematic

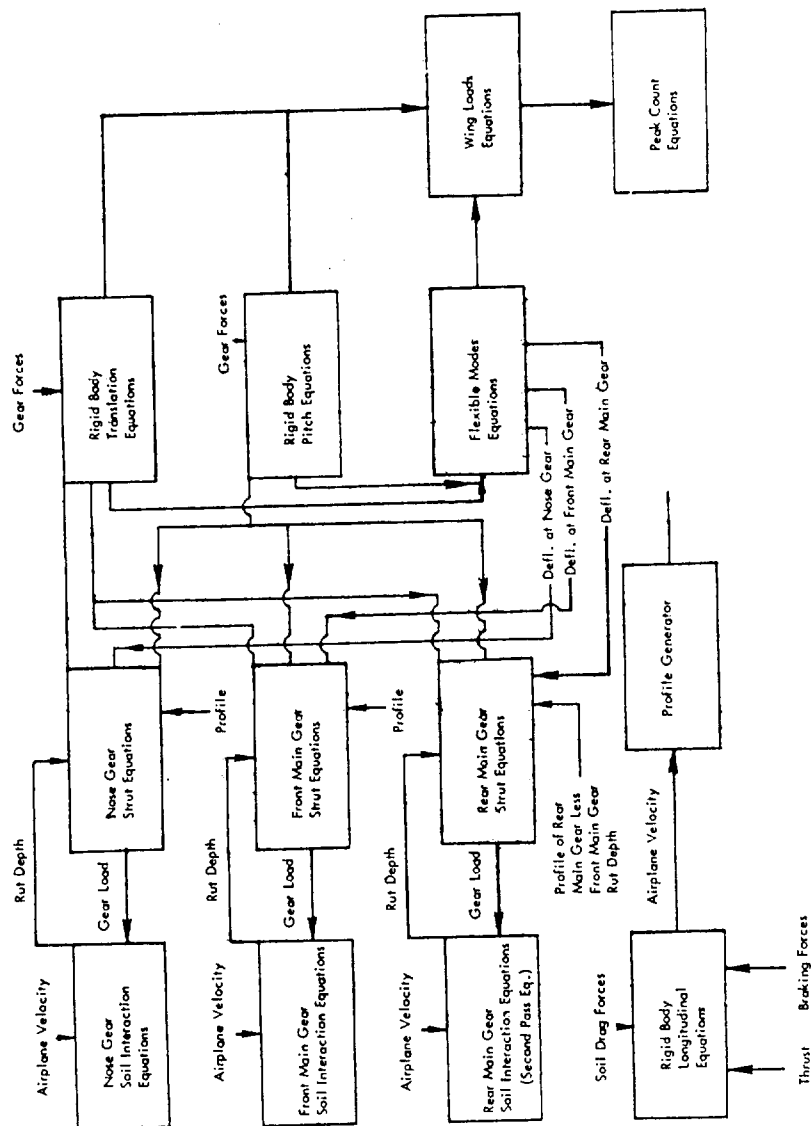


Figure 61. Hybrid Simulation Flow Chart for Soil - Aircraft Interaction

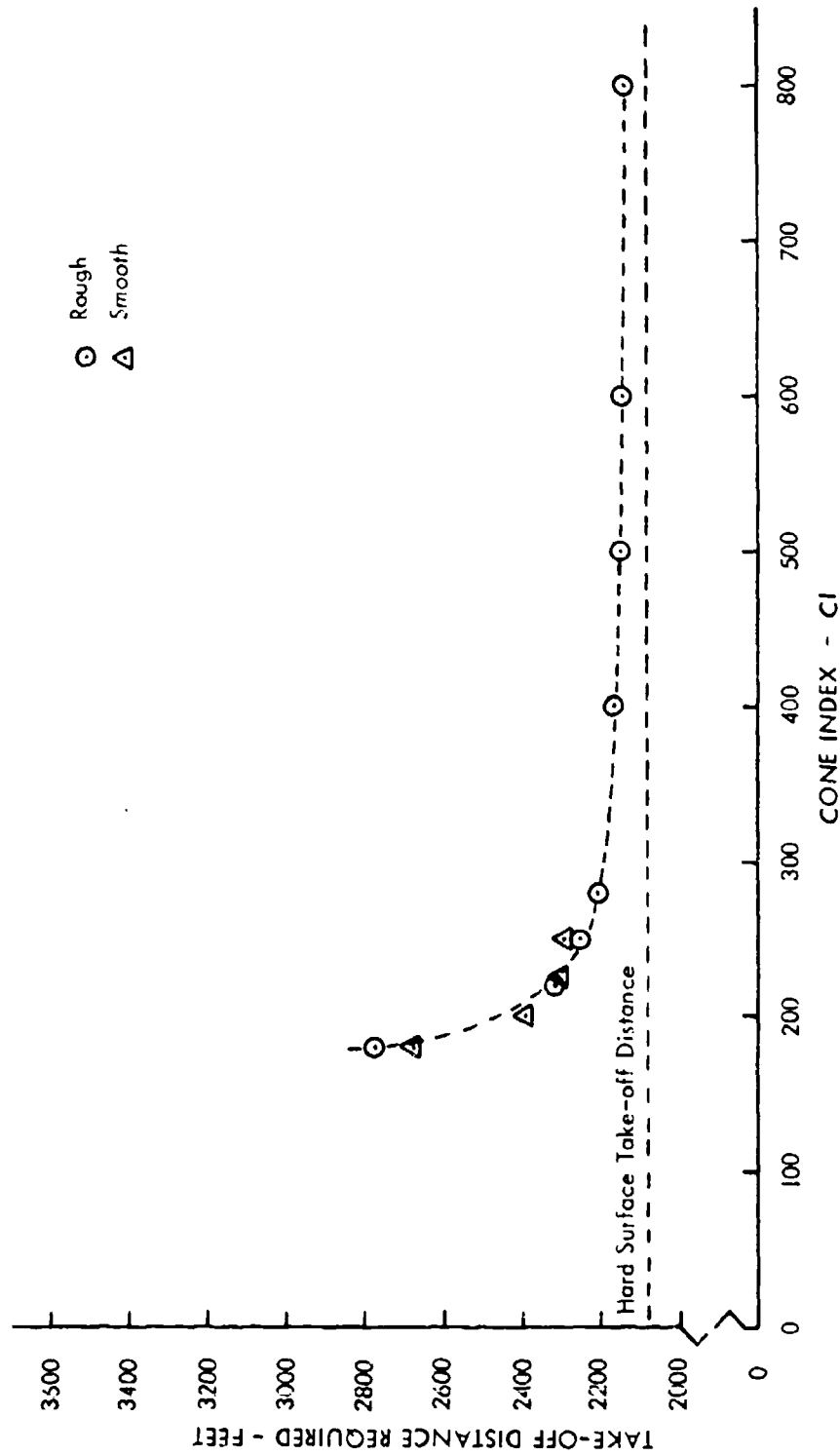


Figure 62. Take-off Distance vs. Soil Strength - Rough and Smooth Surfaces

2. WING LOAD PEAK COUNTS FOR TAKE-OFF

Figures 63 and 64 show the shear and bending peak load exceedances during take-off runs for wing station 550. Figure 65 shows the location of wing station 550 on a general arrangement of the C-130E. This station was chosen because the dynamic taxi condition produces the design loads at this location. The magnitudes of the highest loads are less than for constant speed taxi over the entire runway and the number of exceedances at each load level is less than those for the highest speed taxi runs. The number of exceedances at a given load level is slightly higher on the soil surface at $CI = 200$ than on the rigid surface because of the longer distance traveled on the runway and the greater amount of roughness encountered.

Wing loads encountered on take-off are low and do not exceed the design limits of 16.8×10^3 lb. for shear and 1.9×10^6 in. lb. for bending.

3. WING LOAD PEAK COUNTS FOR CONSTANT SPEED TAXI

Figures 66 and 67 show the shear and bending peak counts for constant speed taxi at 20, 40, and 80 ft./sec. These loads are higher than during take-off because of the longer distances on the rough surface, but the loads are still below the design limits.

Wing loads increase with increasing taxi speed, but the increase is partially offset by wing lift. Wing lift buildup reduces the dynamic loads through decreased gear dynamic response because the gear operates about a lower slope on the strut airspring as lift builds up. At 80 ft./sec. on a rigid surface the loads are reduced to approximately 50% to 75% of their value when wing lift is not included (1).

4. INCREMENTAL GEAR LOADS FOR (1-cosine) SHAPED BUMPS

Figure 68 shows the incremental gear loads from constant speed taxi over (1-cosine) shaped bumps at several frequencies for the front main gear. The crosshatched area in Figure 68 represents the estimated spread in load caused by different wavelength bumps and the interaction of the three gears with the bump. For a single gear simulation, bump wavelength and airplane speed can be combined and expressed

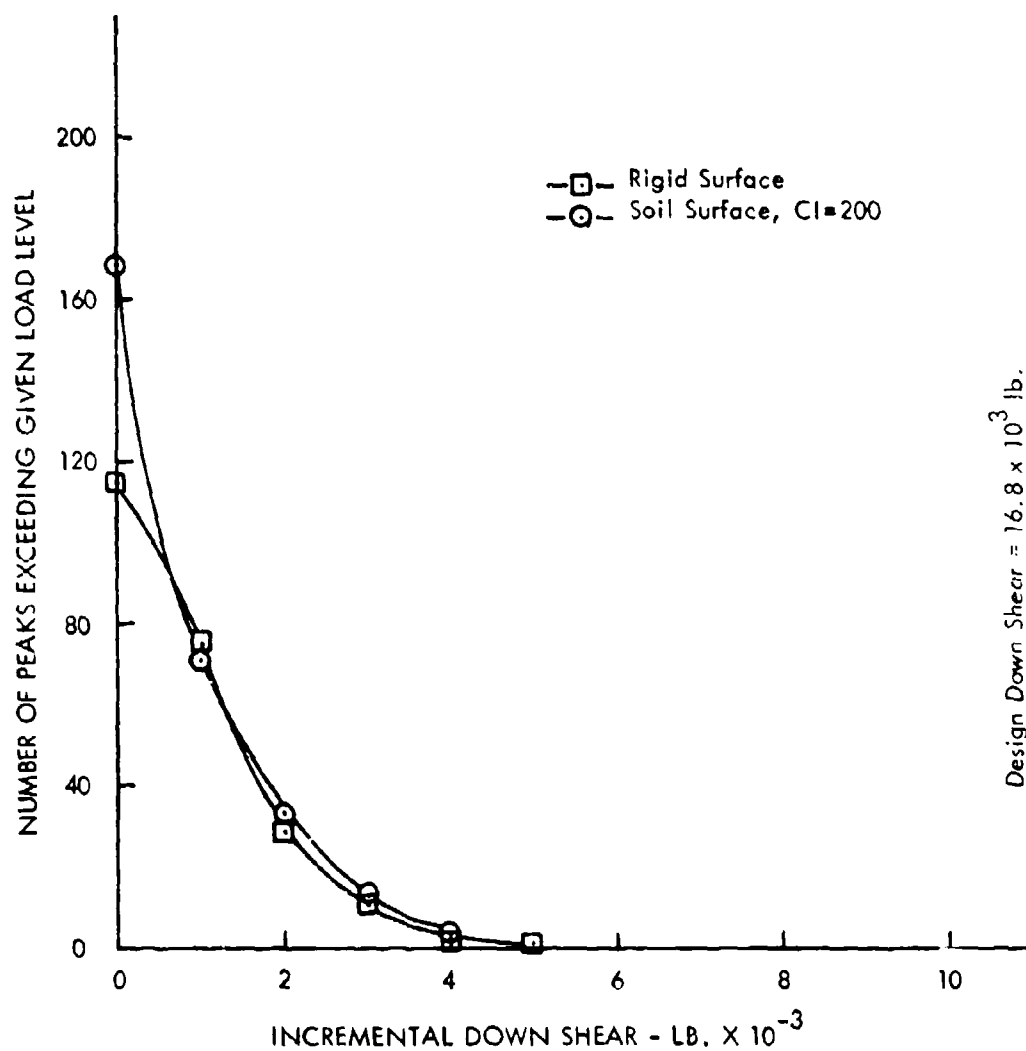


Figure 63. Shear Peak Counts for Take-off

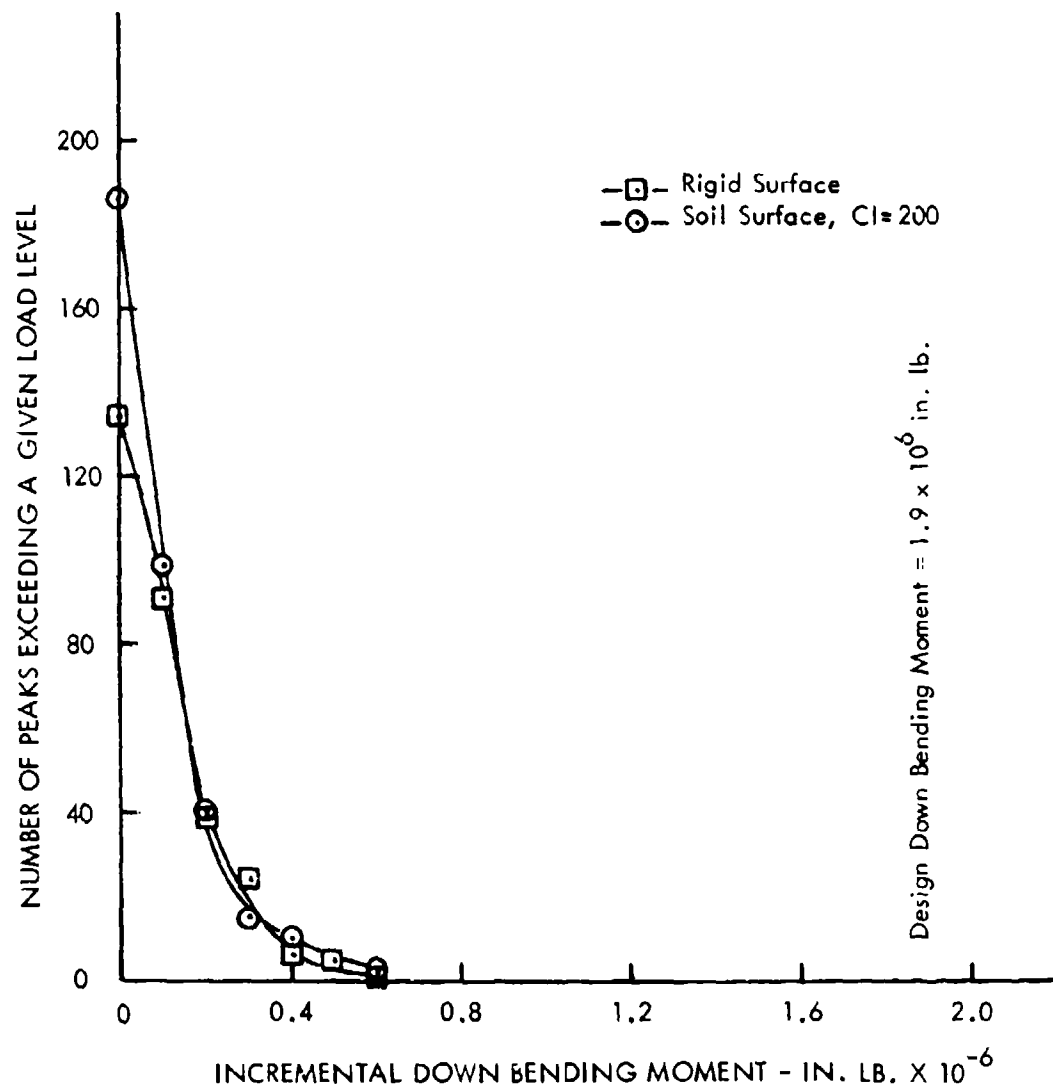


Figure 64. Bending Peak Counts for Take-off

C-130E GENERAL ARRANGEMENT

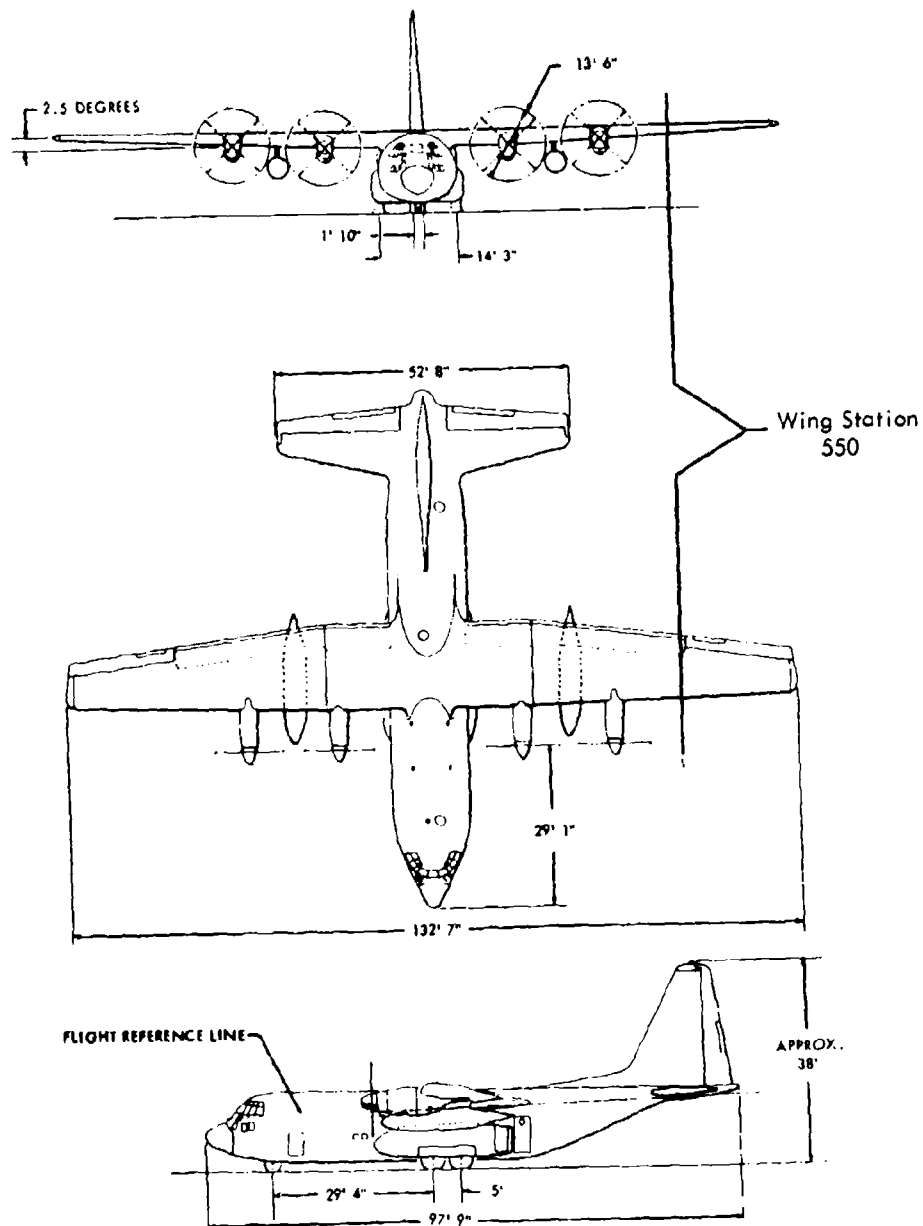


Figure 65. C-130 Aircraft Configuration

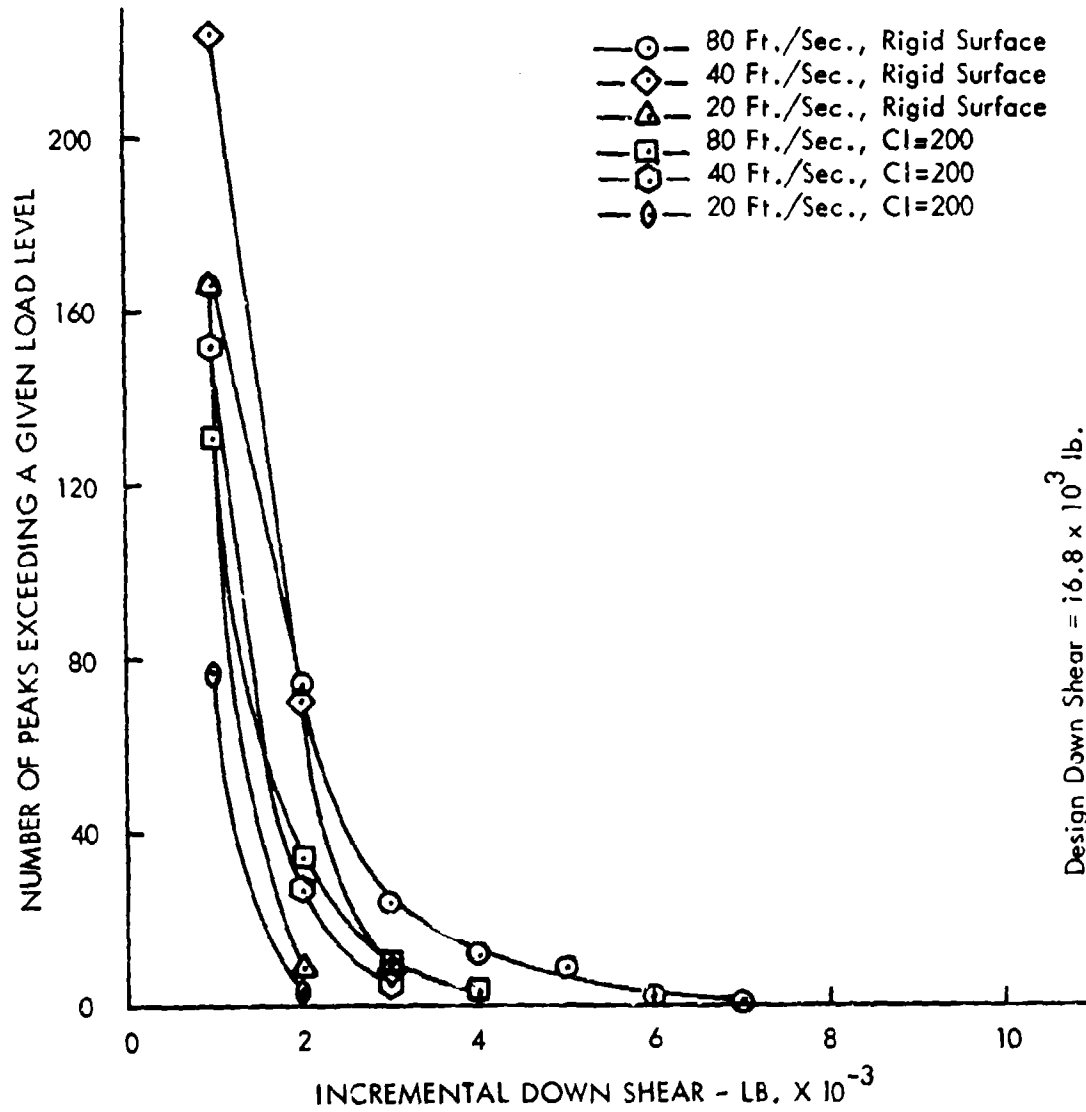


Figure 66. Shear Peak Counts for Constant Speed Taxi

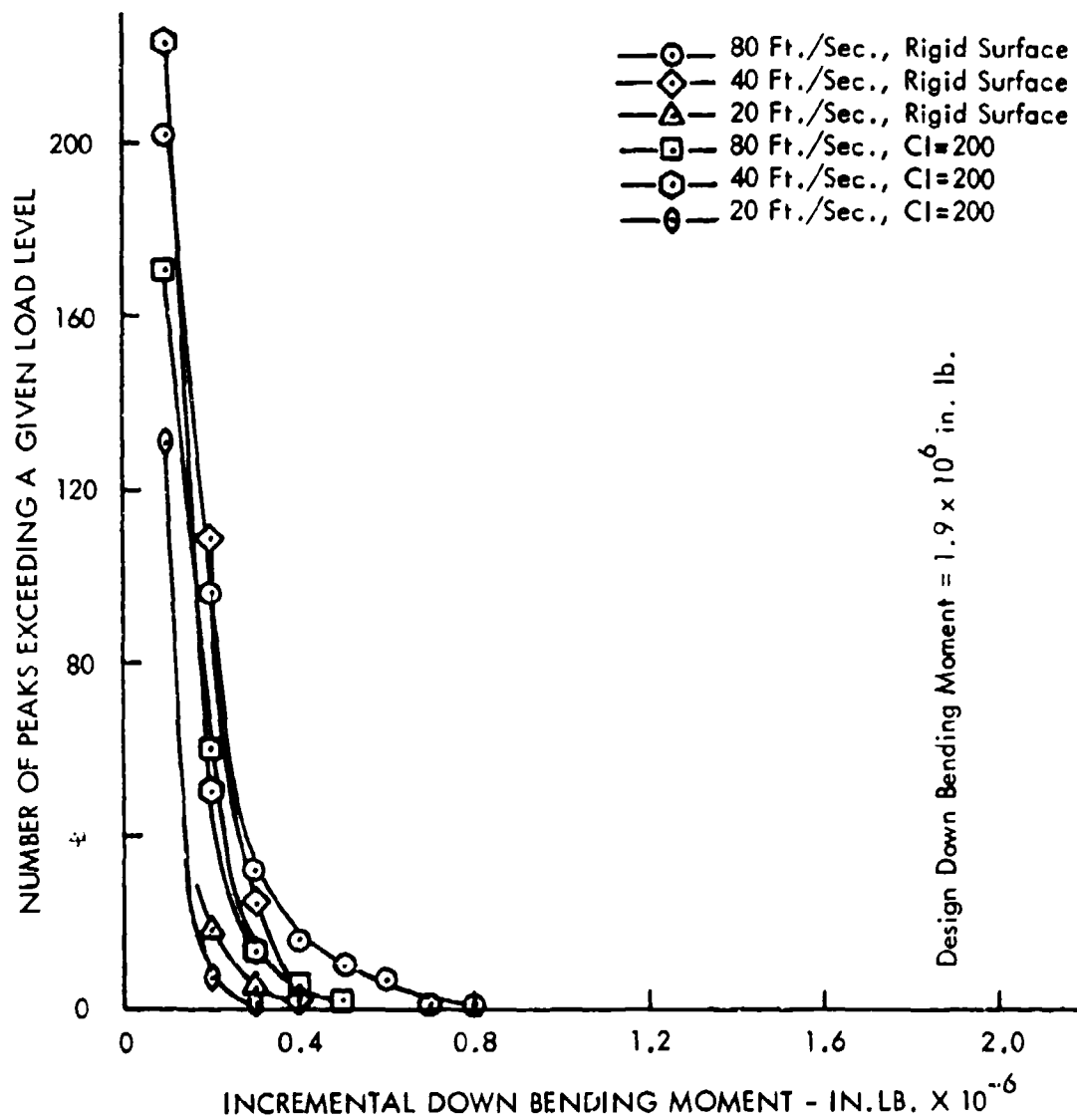


Figure 67. Bending Peak Counts for Constant Speed Taxi

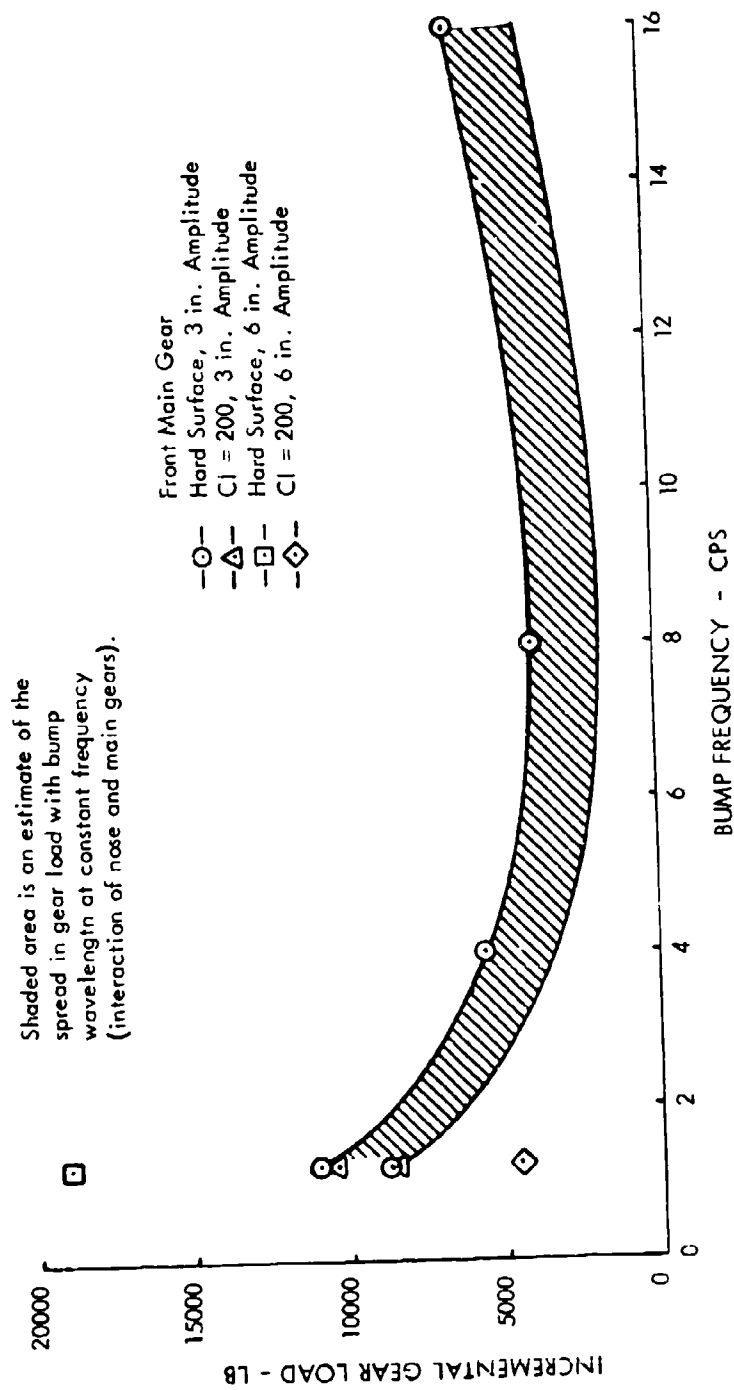


Figure 68. Incremental Gear Load vs. Frequency

as frequency. However, as shown here, interaction on a multi-gear aircraft causes more deviation from the idealized case.

5. RECOMMENDATIONS FOR FURTHER COMPUTER SIMULATION

a. Incorporation of Roughness in Take-off Analyses

This model has shown that since inclusion of roughness has little effect on the take-off distance, for studies not including consideration of wing or gear loads the program could be simplified to one using a smooth surface and static gear loads.

b. Pilot Inputs

No pilot inputs have been included in this computation. It is likely that there would be some influence on take-off distance because of the pilot control over aircraft lift, and the magnitude of the differences to be expected should be evaluated.

SECTION V

CONCLUSIONS

1. A soil/wheel interaction model has been developed which identifies the four primary factors that determine wheel ruts and drag loads. These are the tire load-deflection spring rate, the soil load-deflection relation, and two inertia forces. The inertia forces are lift and drag generated by the soil resistance to penetration at high rates of loading.
2. Secondary factors have been identified which require additional testing and analyses for adequate definition. The most significant secondary factors are the drag and lift coefficient variation with tire pressure, tire cross sectional area and forward velocity, tire/soil interface pressure distribution underneath the wheel, and tire shape (cross sectional area and effective rolling radius) in the soil.
3. An alternate soil model as shown by Figure 37 was compared with the recommended soil model as shown by Figure 8. Trial solutions with the alternate soil model did not produce the characteristic soil deflection-velocity relationships observed in the test data as seen from Figure 40. The differences are believed to be caused by the lack of a drag load interaction term. A suggested method of improving the alternate soil model by including drag interaction is presented, but an evaluation of the amount of possible improvement was not made.
4. Pressure-sinkage curves for additional wheel sizes and soil conditions are needed in order to estimate drag load/rut depth interaction by the method in Equations 20-22 and Figures 17 and 18. Improvements in estimates of the drag load interaction can be expected if dynamic pressure sinkage curves are available. These should include rates up to 150-200 in./sec.

5. The predicted and experimental ground loads and ruts for a free-rolling wheel were compared for the 29 x 11-10 8PR Type III tire for two clay soil strengths and one sand soil. For each of the three soils the average (over track length, tire pressure, and velocity) of the difference between calculated and experimental results was less than 12%. Positive and negative differences (also averaged over track length, tire pressure, and velocity) were between 11% and 36%.
6. Single wheel tests show very small effects of yaw angle (up to 6°) on drag load. The ratio of lateral load to vertical load on soil is only 35% of the ratio on concrete for yaw angles of 3° and 6°. The ratio for braking on clay is 32% and 54% of the ratio for free-rolling on clay at yaw angles of 3° and 6° respectively. While lateral loads decrease in braking, drag loads increase.
7. Only small differences in individual wheel drag ratios are found between single and tandem wheels loaded to equivalent weights on each wheel. Peak free rolling drag ratios encountered were from 0.25 to 0.41 and are dependent upon tire pressure. Peak braking drag ratios encountered were from 0.68 to 0.98. Maximum free rolling rut depths with a tandem wheel varied from 0.58 to 1.6 in. The maximum braking rut depth for the tandem wheel was about 3.6 in. at 70 psi tire pressure. Comparisons of both free rolling and braking rut depths show that for equal tire pressures there were no significant differences in the rut depths formed by a single wheel and by a tandem pair when the load on the single wheel equals the total load on the tandem pair.
8. Drag loads were greater for a rigid tire than for a pneumatic tire at the highest pressure tested. Rut depths were 66% greater. Soil failure underneath a free rolling rigid tire resembles the failure underneath a braked pneumatic tire. A satisfactory explanation for this behavior of the rigid wheel has not been found.

9. Analog computer studies of the C-130 aircraft show that the difference in take-off distance between a smooth soft surface and a rough soft surface is small and in most cases can be neglected. Take-off distance increases with decreasing soil strength as shown by Figure 62. From a hard surface to $CI = 200$ (CBR 4) the increase is 18%. Wing load peak counts for take-off are less than for constant speed taxi over the entire runway because of the shorter length of runway covered.

APPENDIX A

TABULATIONS OF TEST DATA AND TYPICAL TEST LOAD HISTORIES

The data from the test program was in the form of time histories of the sensor outputs. Since changing from one condition to another (such as from free rolling to locked wheel braking) introduced oscillations into the data, portions where the loads were relatively steady were selected and the average values in these regions were used for analysis. The quantities used are presented below in tabular form and referenced to the test conditions of velocity, tire pressure, and wheel loading geometry.

1. SINGLE WHEEL TESTS

Three sets of wheel geometry were tested using the NASA single wheel dynamometer support device (See Appendix B). These were run for zero, three, and six degrees wheel yaw and 70 psi tire pressure. The average drag load, vertical load, lateral load (where significant), and rut depths are contained in Tables II and III.

2. TANDEM WHEEL TESTS

One tandem wheel configuration and three tire pressures, 70, 45, and 30 psi were tested. The tandem axles were spaced 40 inches apart. Results of the average loads and rut depth measurements for the clay tests are summarized in Tables IV and V. The average loads measured during free rolling tests on the concrete surface are summarized in Table VI for both tandem and single wheel configurations.

3. RIGID WHEEL TESTS

A few runs were made with a rigid foam filled tire in an attempt to determine the limiting condition of no tire deflection. As discussed in the main body of the report, these tests were so few in number that conclusive statements cannot be made, but the wheel behavior was quite different from that of the pneumatic tires. Table VII summarizes the rigid wheel load averages and rut depths.

TABLE II

Summary of Single Wheel Free Rolling Tests - Test Bed IV

Time Pressure psi	Test Number	Velocity Knots	Yaw Angle Degrees	Drag Load Lb.	Vertical Load Lb.	Lateral Load Lb.	Rui Depth In.
70	24601	Sink	0	136	4100		1.68
	24602	S. T.		1360	4380		2.04
	24604	Tow		1340	4260		1.32
	24605	21.0		1320	4220		1.62
	24802	27.3		1400	4080		1.65
	24702	43.5		1760	4350		1.67
	24705	62.5		10.7	4200		1.18
	24708	78.2		880	4320		1.20
	24711	87.3		760	4050		1.04
	24810	Sink	3	144	4060	---	1.80
70	24811	S. T.		1480	4540	-348	2.05
	24809	Tow		1260	4240	-430	1.65
	25205	22.3		1440	4280	-450	1.68
	25202	30.0		1560	4350	-450	1.64
	25105	39.5		2080	4140	-400	1.88
	24814	59.5		1080	4250	-380	1.50
	25410	59.5		1300	4080	-540	1.55
	24817	75.7		940	4180	-440	1.31
	25708	80.0		560	3300	-500	1.12
	25102	92.6		540	3800	-480	0.89
70	25406	Sink	6	110	3940	---	1.80
	25407	S. T.		1460	4380	-825	2.42
	25405	Tow		1340	4220	-740	2.10
	25402	18.1		1340	4220	-680	1.89
	25314	28.8		1700	4300	-940	1.84
	25311	40.2		2000	4320	-990	1.90
	25302	59.2		1280	3950	-640	1.50
	25305	77.3		860	3900	-840	1.16
	25308	87.4		810	3800	-880	0.94

TABLE III
Summary of Single Wheel Braking Tests - Test Bed IV

Tire Pressure psi	Test Number	Velocity Knots	Yaw Angle Degrees	Average Values for Braking			
				Drop Load Lb.	Vertical Load Lb.	Lateral Load Lb.	Rut Depth In.
70	24805	21.0	0	2240	3840		3.80
	24802	27.3		3270	3850		3.53
	24707	43.5		3400	4000		2.71
	24705	62.5		2600	4800		1.80
	24708	78.2		1670	4140		—
70	24711	87.3	3	1600	4250		0.91
	25105	39.5		3880	3740	-100	3.05
	25410	59.5		3180	4080	-306	2.43
	25208	80.0		1500	3950	-80	0.98
	25102	92.6		1460	4200	-140	0.72
70	25314	28.8	6	3460	3700	-460	3.70
	25311	40.2		3790	3880	-450	3.18
	25302	59.2		3560	4050	-440	2.55
	25305	77.3		1800	3950	-440	1.18
	25308	87.4		1220	3800	-360	0.94

TABLE IV
Summary of Tandem Wheel Free Rolling Tests - Test Bed IV

Tire Pressure psi.	Test Number	Velocity Knots	5,300 Lb. Nominal Vertical Load				Rur Depth In.
			Drag Load Leading Wheel Lb.	Vertical Load Leading Wheel Lb.	Drag Load Trailing Wheel Lb.	Vertical Load Trailing Wheel Lb.	
30	24112	Sink	370	2900	240	2570	0.3
	24115	Sink	700	2690	---	---	---
	24113	S. T.	---	---	---	---	0.47
	24114	Tom	550	3280	384	2590	0.38
	23908	15.8	590	2140	440	2580	0.36
	23902	25.9	570	2420	440	2490	0.35
	23808	40.0	560	2170	540	2390	0.42
	23711	62.5	250	2200	530	2300	0.55
	23822	78.7	280	2660	490	2380	0.58
	23905	88.0	340	2540	480	2570	0.56
45	23802	Sink	340	2880	475	2640	0.30
	24075	Sink	300	2970	524	2450	0.49
	24015	S. T.	670	3200	485	2570	0.72
	24017	Tom	670	3340	450	2570	0.70
	23914	20.9	510	1840	540	2480	0.88
	24005	27.8	570	2160	580	2500	0.84
	23102	30.0	400	2700	595	2640	0.94
	24007	38.8	360	2360	680	2500	1.10
	23105	47.6	---	---	---	---	0.81
	23917	60.9	840	2270	680	2670	---
70	23109	66.3	240	2200	520	2640	6.64
	23302	76.5	160	2280	520	2770	0.48
	24102	88.8	560	3300	460	2440	0.75
	23706	Sink	128	2350	120	2370	1.10
	23707	S. T.	---	---	---	---	1.06
	23708	Tom	---	---	1300	1790	1.36
	23705	20.2	560	2440	720	2460	1.40
	23702	28.7	1060	2500	840	2360	1.66
	23408	40.6	780	2350	905	2300	1.45
	23405	61.5	490	2140	660	2340	1.23
30	23911	77.0	---	---	---	---	1.11
	23402	88.5	700	2800	550	2670	0.91
	23308	91.6	530	1900	490	2600	---
	11,700 Lb. Nominal Vertical Load						
	24109	35.0	790	5600	1170	5600	0.73
	24009	57.1	640	5720	1440	6100	0.79
	24012	72.9	840	5600	1325	5690	0.65
	24106	87.3	840	5950	1100	5300	0.75
	23003	Tom	960	6850	1310	5600	---
	---	---	---	---	---	---	---

TABLE V

Summary of Tandem Wheel Braking Tests - Test Bed IV

Test Pressure psi	Test Number	Velocity Kmph	5,200 lb. Nominal Vertical Load				
			Drag Load Leading Wheel Lb.	Vertical Load Leading Wheel Lb.	Drag Load Trailing Wheel Lb.	Vertical Load Trailing Wheel Lb.	Rut Depth in.
30	23908	15.8	1710	1920	1840	2780	1.25
	23902	25.9	800	2420	1520	2880	0.42
	23808	40.0	620	2600	1220	2810	0.52
	23711	62.5	2300	1400	2600	2900	1.25
	23905	88.0	2380	---	2600	2760	0.38
45	23914	20.8	1600	2080	1880	2640	2.57
	24005	27.8	1560	1800	2160	2660	1.90
	24002	38.8	660	1800	1880	2860	1.30
	23917	60.9	2520	2060	2520	3050	1.77
	24102	88.8	660	3100	960	2840	0.34
70	23705	20.2	1940	2440	2100	2900	2.75
	23702	28.2	4660	6700	480	2560	3.50
	23408	40.6	2200	3150	2165	2700	3.40
	23405	61.5	1830	3140	2360	2900	2.66
	23402	88.5	1440	3080	1750	2780	1.61
			11,200 lb. Nominal Vertical Load				
30	24109	25.0	1050	6600	3640	7600	2.43
	24009	52.1	2900	5700	4520	7800	3.03
	24012	72.9	3640	2700	5925	8150	2.40

TABLE VI

Summary of Free Rolling Tests on Concrete - Single and Tandem Wheel

			Average Values for Tandem Wheel			
			5,300 Lb. Nominal Vertical Load			
Tire Pressure psi	Test Number	Velocity Km/hr	Drag Load Leading Wheel Lb.	Vertical Load Leading Wheel Lb.	Drag Load Trailing Wheel Lb.	Vertical Load Trailing Wheel Lb.
30	23908	15.8	330	2360	320	2520
	23902	25.4	420	2280	280	2440
	23808	40.0	300	1960	300	2450
	23711	62.5	100	1600	320	2100
	23802	78.7	220	1300	250	1420
	23905	88.0	290	1360	200	1920
45	23914	20.8	380	1760	260	2480
	24005	27.8	240	2040	280	2510
	24002	38.8	120	2240	320	2450
	23917	60.9	360	2020	300	2540
	23109	66.3	220	1720	420	2280
	24102	88.8	400	5050	260	2320
70	23702	28.2	660	2500	440	2360
	23408	40.0	140	2450	230	2340
	23405	61.5	50	1960	240	2380
	23402	88.5	360	2120	150	2020
			11,200 Lb. Nominal Vertical Load			
30	24109	35.0	550	5300	680	5500
	24006	52.1	390	5070	800	5620
	24012	72.9	520	5450	820	5620
	24106	87.3	560	5150	660	4800
			Average Values for Single Wheel			
			4,200 Lb. Nominal Vertical Load			
			Yaw Angle Degrees	Drag Load Lb.	Vertical Load Lb.	Lateral Load Lb.
70	24805	21.0	0	120	4020	
	24822	27.3		190	3950	
	24702	43.5		150	4050	
	24705	62.5		160	4000	
	24708	78.2		160	3920	
	24711	87.3		170	4000	
	25205	22.3	3	140	4080	-1410
	25202	30.0		160	4150	-1500
	25105	39.5		480	3960	-1470
	24814	59.5		160	4000	-1440
	25410	59.5		0	4040	-1500
	24817	75.7		180	3860	-1440
	25208	80.0		220	3900	-1440
	25102	92.6		60	3830	-1440
	25405	10.0	6	130	4200	-2550
	25402	18.1		440	4140	-2500
	25314	28.8		130	4200	-2540
	25311	40.2		290	4160	-2540
	25302	59.2		160	4050	-2620
	25305	77.1		140	3950	-2480
	25308	87.4		260	3850	-2520

TABLE VII

Summary of Rigid Wheel Tests - Free Rolling on Concrete and on Test Bed IV

		4,200 Lb. Nominal Vertical Load					
Yaw Angle Degrees	Test Number	Velocity Knots	Average Values Concrete Surface		Average Values Clay Surface		Rut Depth In.
			Drag Load Lb.	Vertical Load Lb.	Drag Load Lb.	Vertical Load Lb.	
0	25503	S	---	---	144	4050	2.05
	25504	S. T.	---	---	2180	4420	3.38
	25502	Tow	100	4350	2020	4350	3.15
	25512	21.0	0	4200	2200	4200	2.55
	25507	42.0	100	4300	2420	4300	---
	25413	55.1	340	3900	3260	3900	2.56
	25509	75.6	400	3900	3280	3900	2.50

4. TYPICAL TEST LOAD HISTORIES

Histories of drag, lateral and vertical loads for single wheel tests at six degrees yaw are presented in Figures 69 - 89. These results include tests ranging in velocity from 5 to approximately 90 knots. The test sequence was as follows: Touchdown occurred on the concrete surface. The wheel rolled freely across the concrete and onto the clay surface. Braking occurred over the final portion of the clay surface.

Portions of the loads time histories used for averaging are identified on each figure for the concrete surface, for free rolling on clay, and, where applicable, for braking on clay.

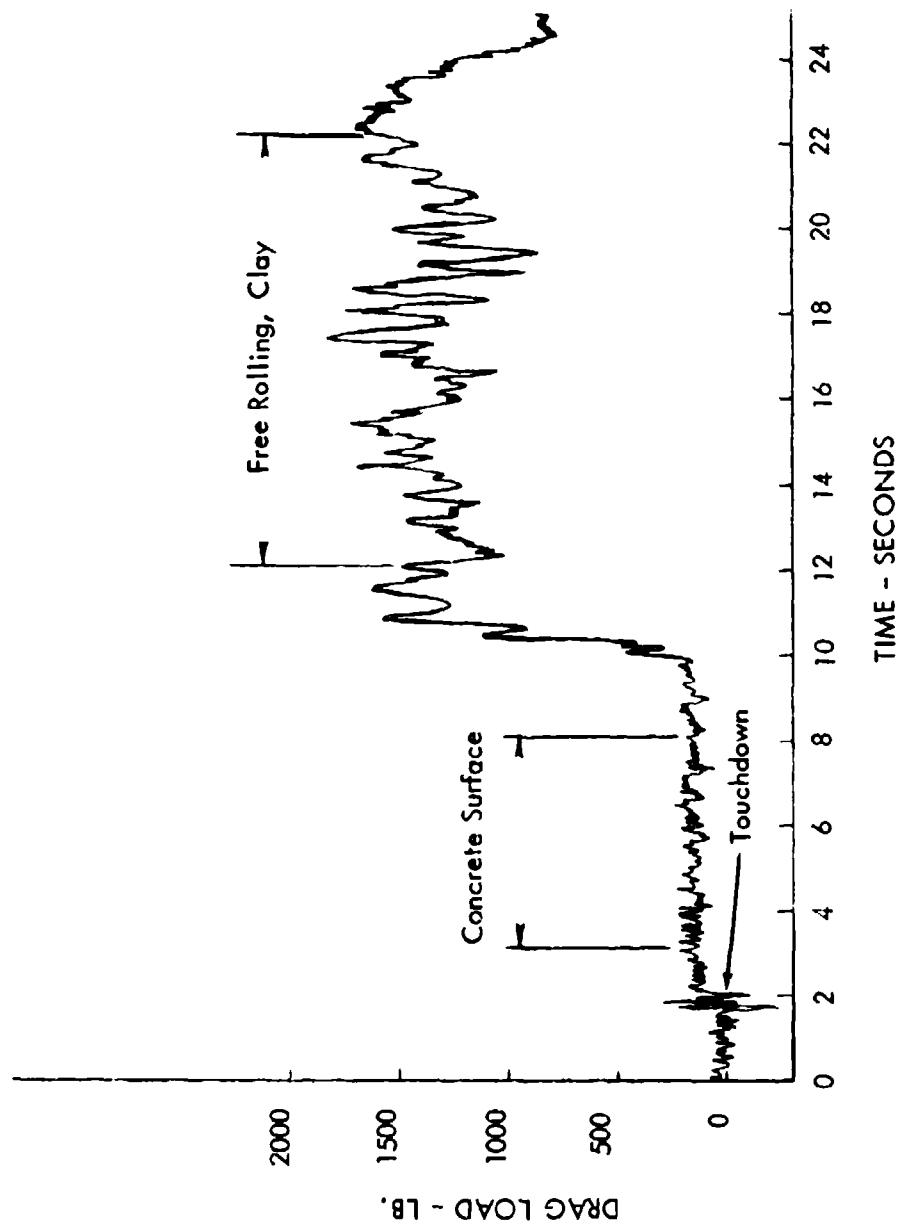


Figure 69. Drag Load Time History for Single Wheel at Six Degrees Yaw - Tow

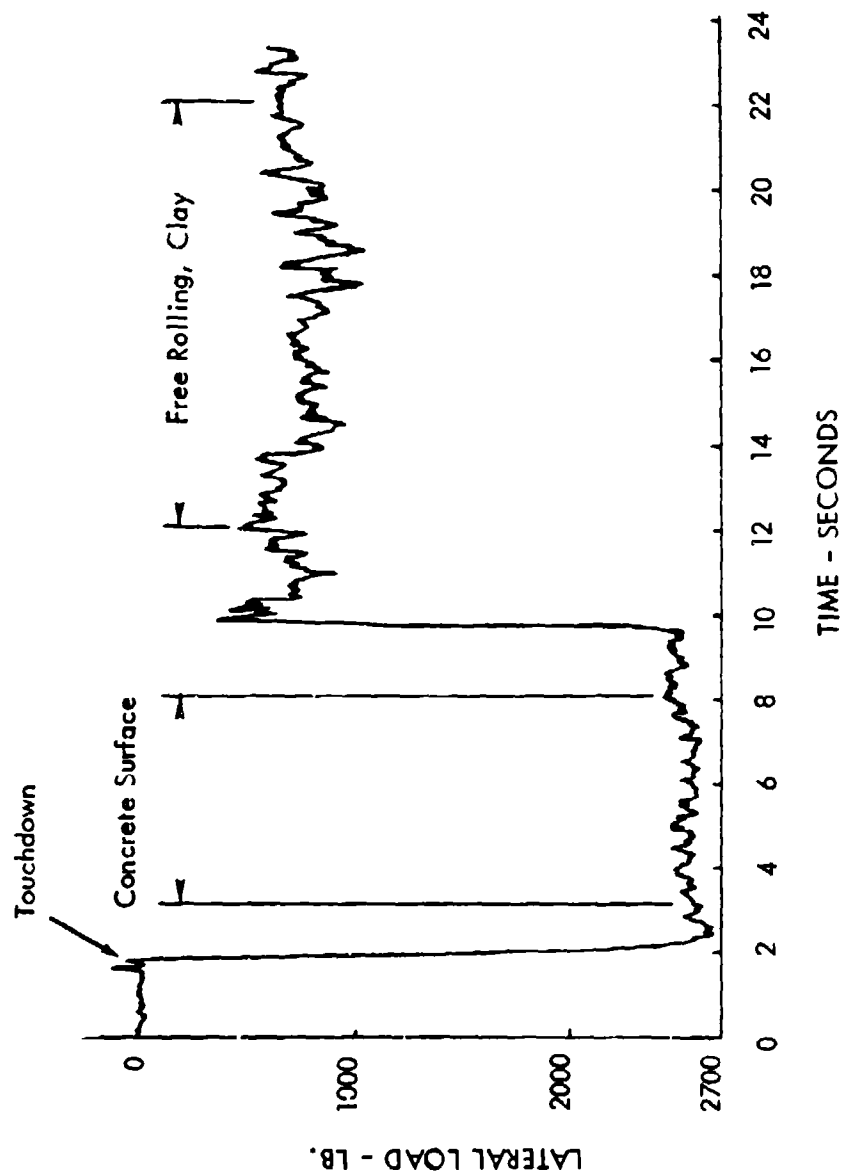


Figure 70. Lateral Load Time History for Single Wheel at Six Degrees Yaw - Tow

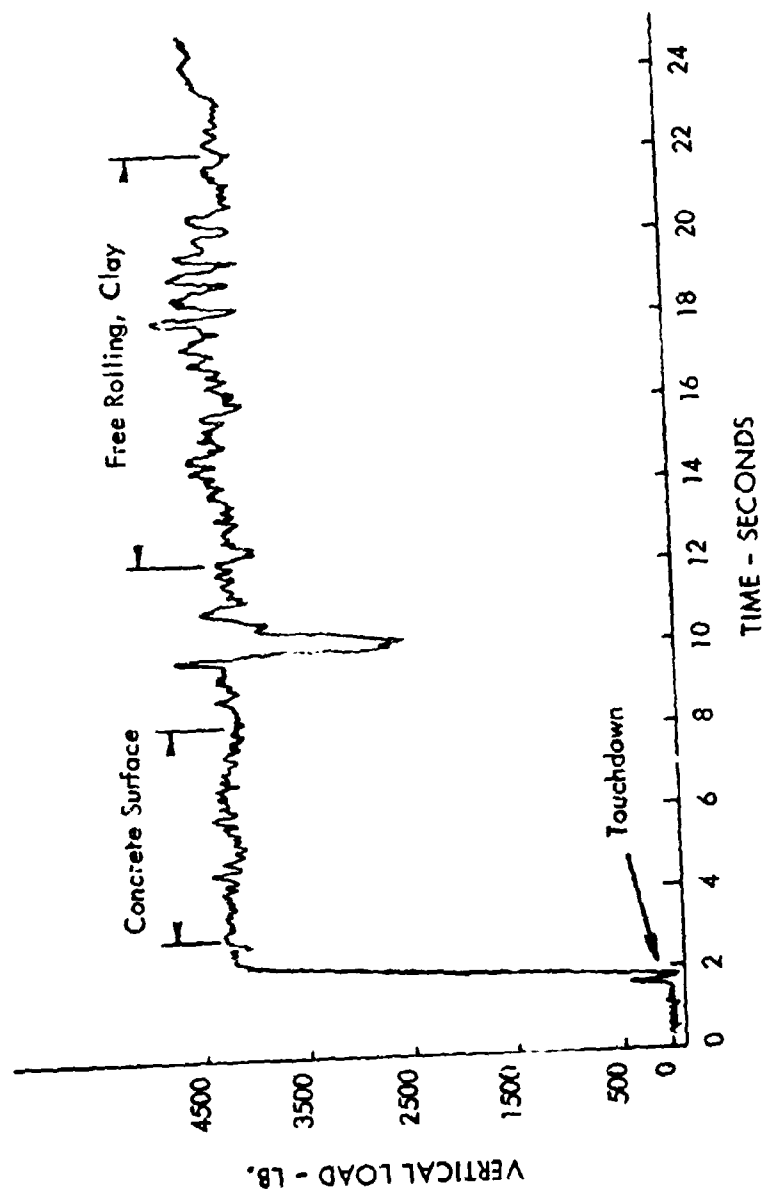


Figure 71. Vertical Load Time History for Single Wheel at Six Degrees Yaw - Tow

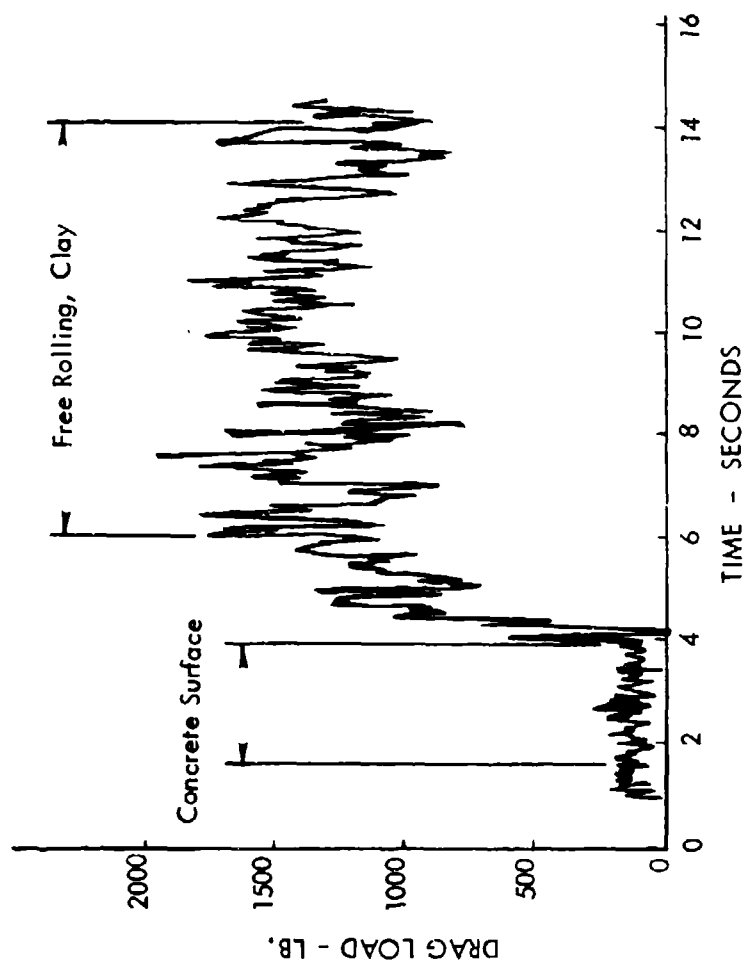


Figure 72. Drag Load Time History for Single Wheel at Six Degrees Yaw - 18.1 Knots

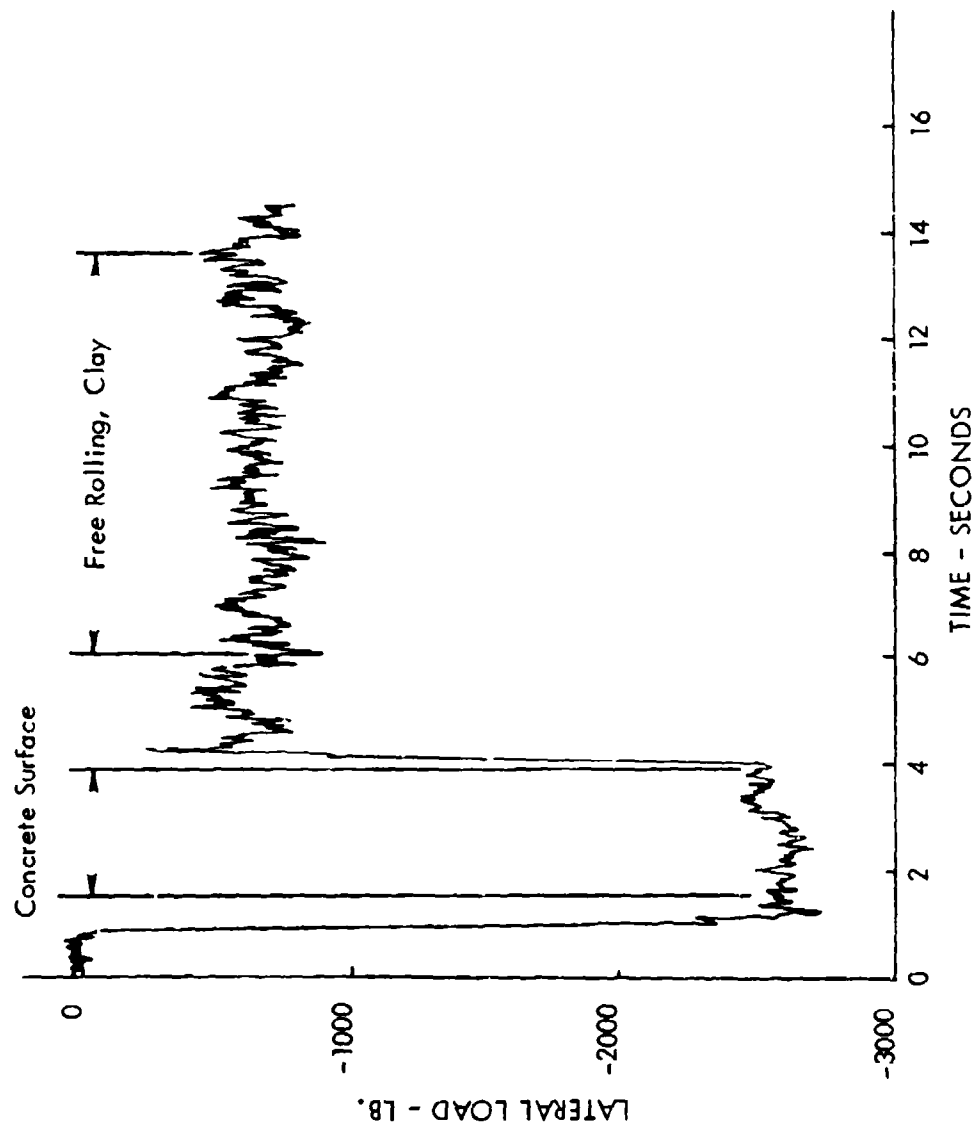


Figure 73. Lateral Load Time History for Single Wheel at Six Degrees Yaw - 18.1 Knots

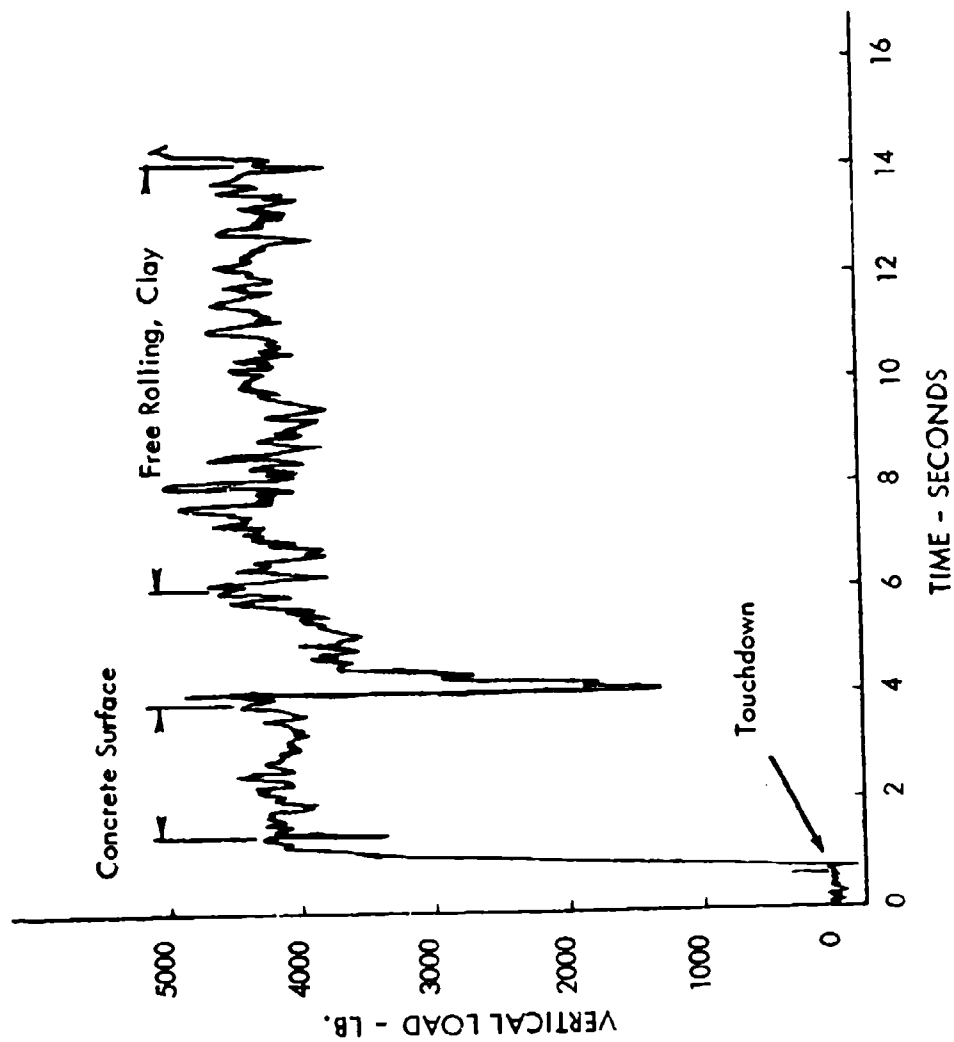


Figure 74. Vertical Load Time History for Single Wheel at Six Degrees Yaw - 18.1 Knots

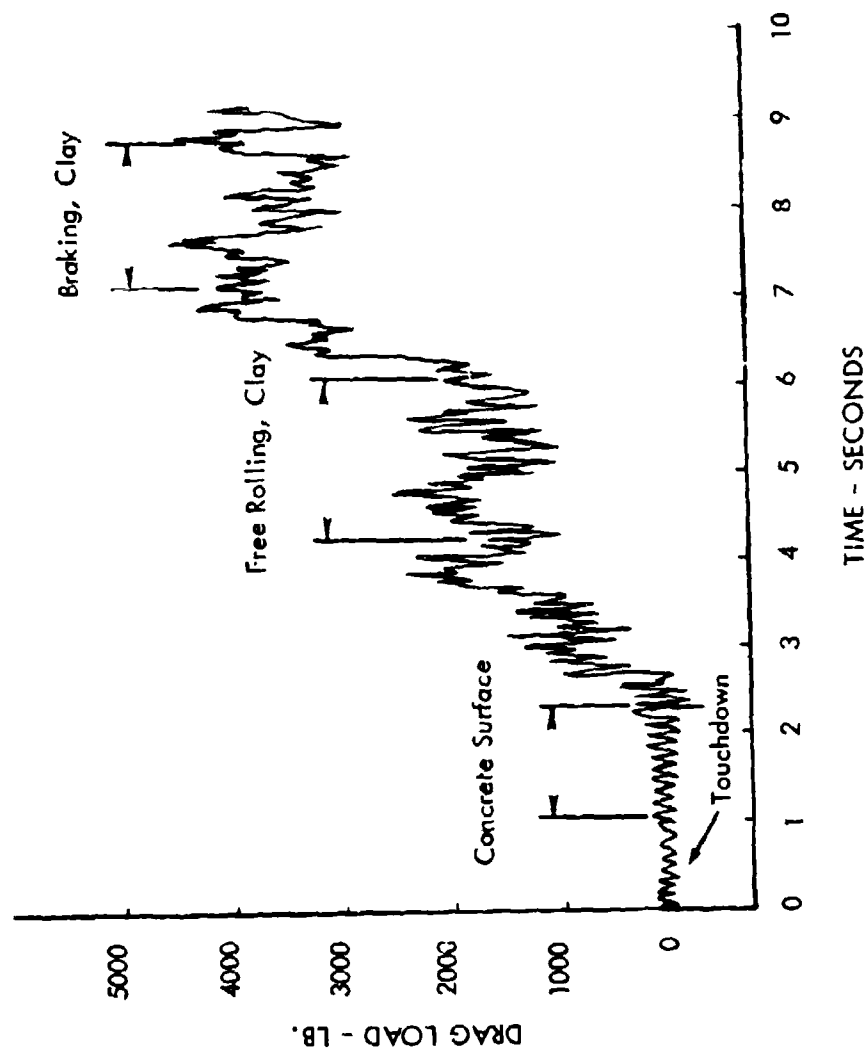


Figure 75. Drag Load Time History for Single Wheel at Six Degrees Yaw - 28.8 Knots

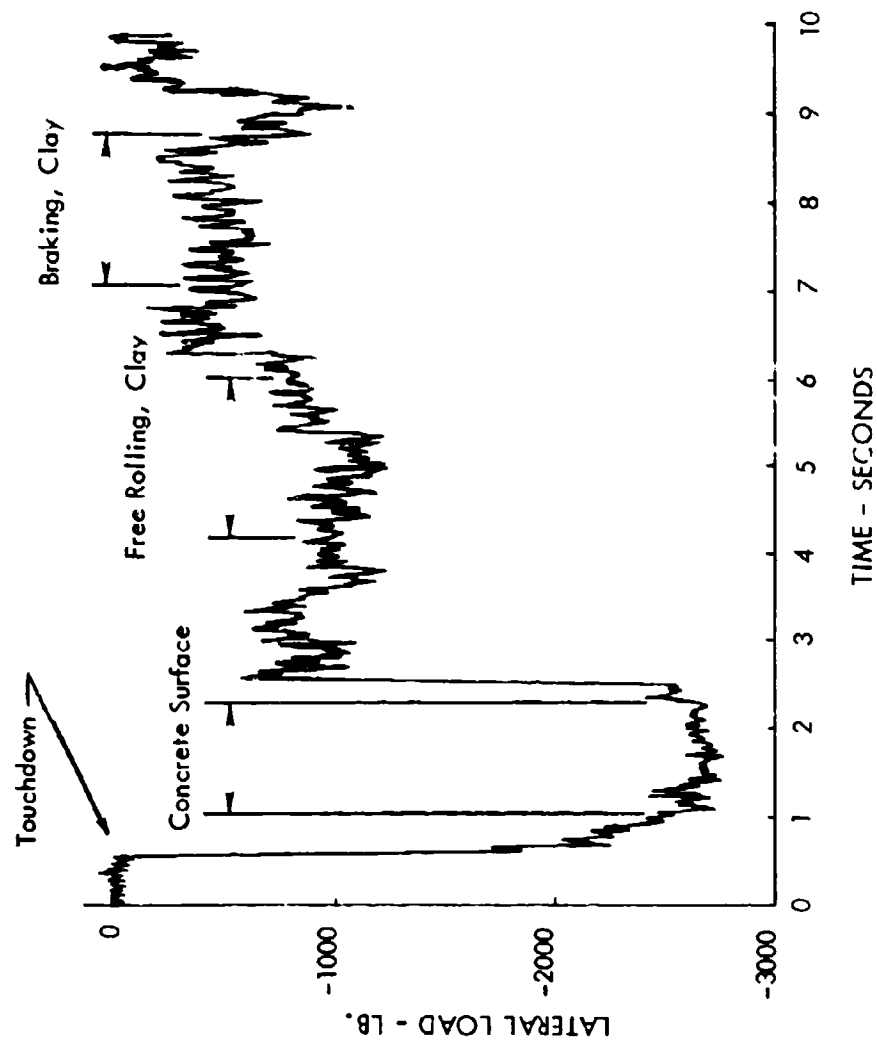


Figure 76. Lateral Load Time History for Single Wheel at Six Degrees Yaw - 28.8 Knots

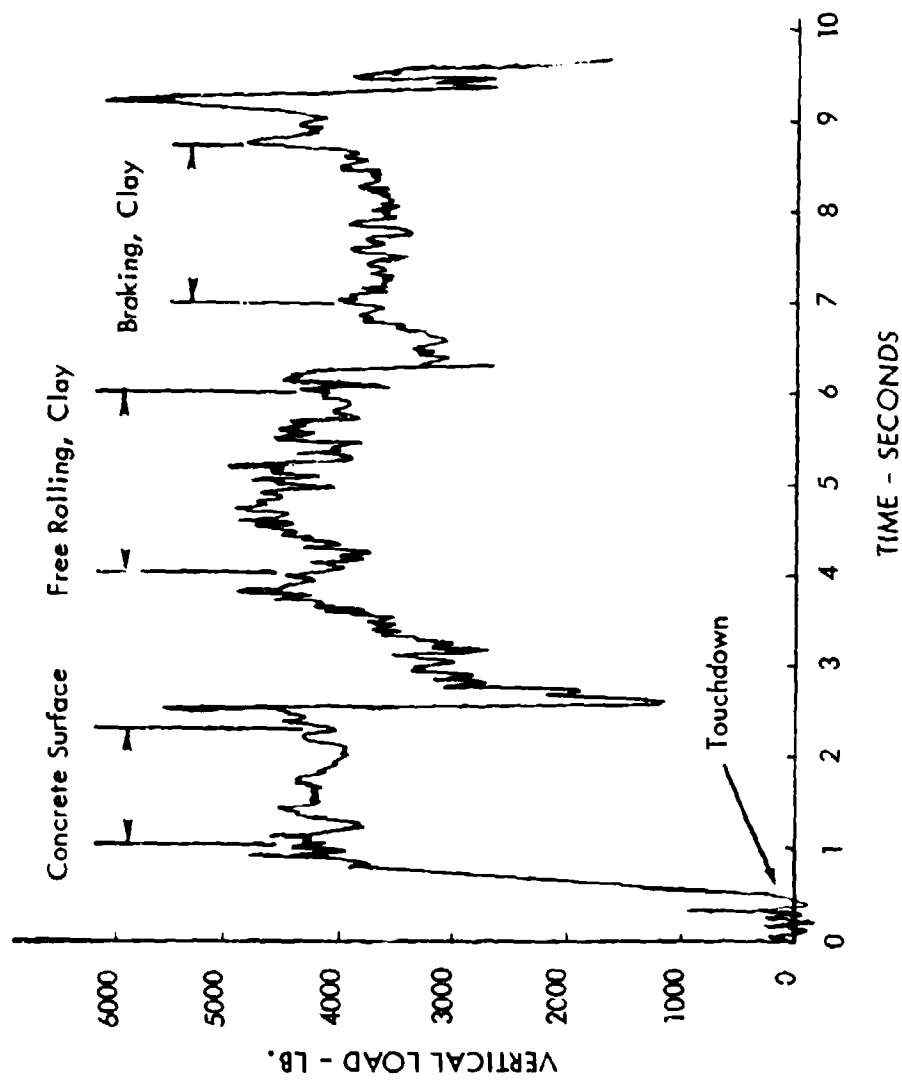


Figure 77. Vertical Load Time History for Single Wheel at Six Degrees Yaw - 28.8 Knots

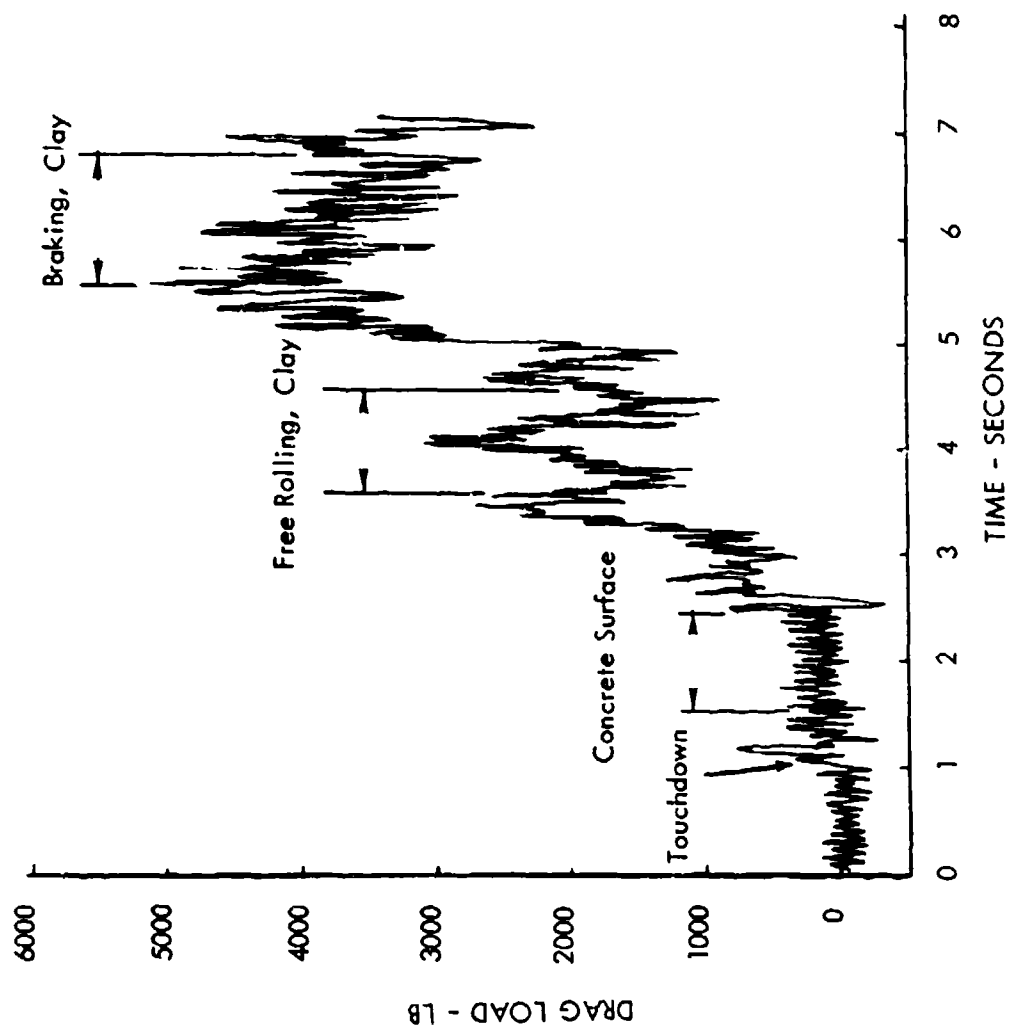


Figure 78. Drag Load Time History for Single Wheel at Six Degrees Yaw - 40.2 Knots

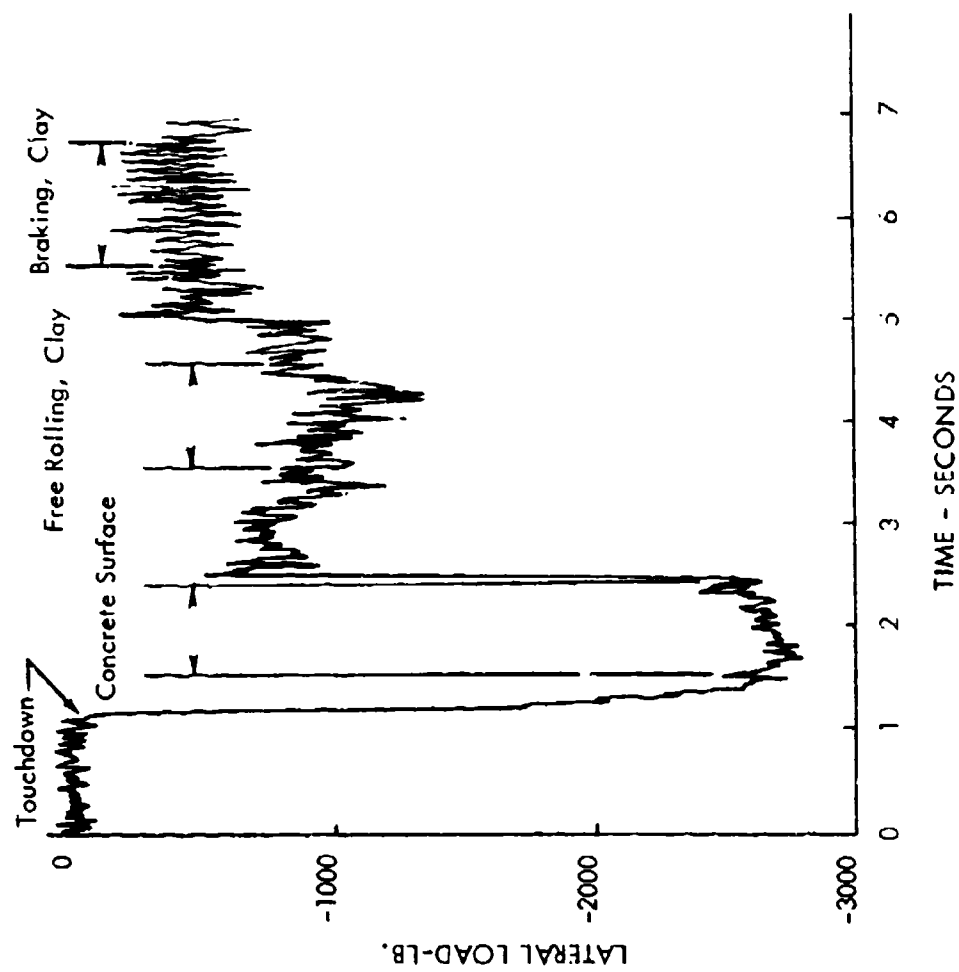


Figure 79. Lateral Load Time History for Single Wheel at Six Degrees Yaw - 40.2 Knots

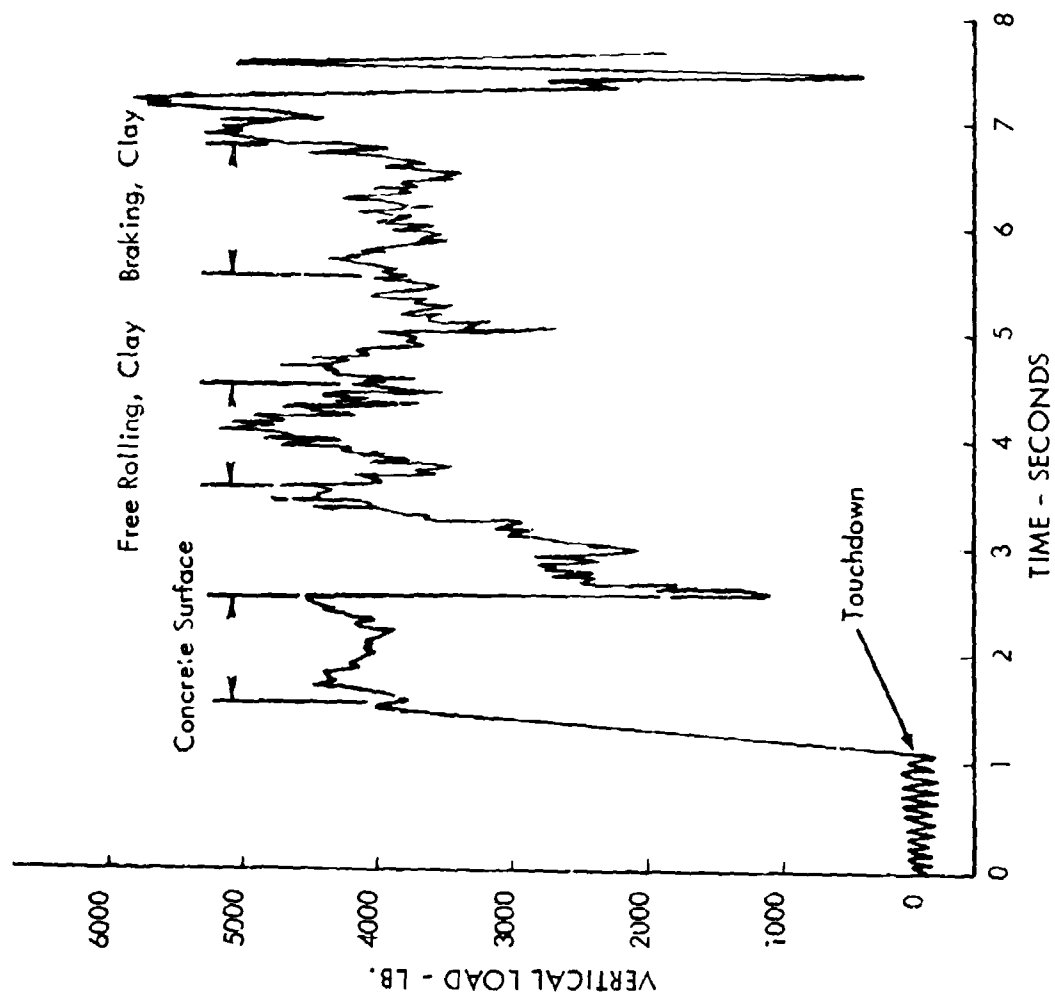


Figure 80. Vertical Load Time History for Single Wheel at Six Degrees Yaw - 40.2 Knots

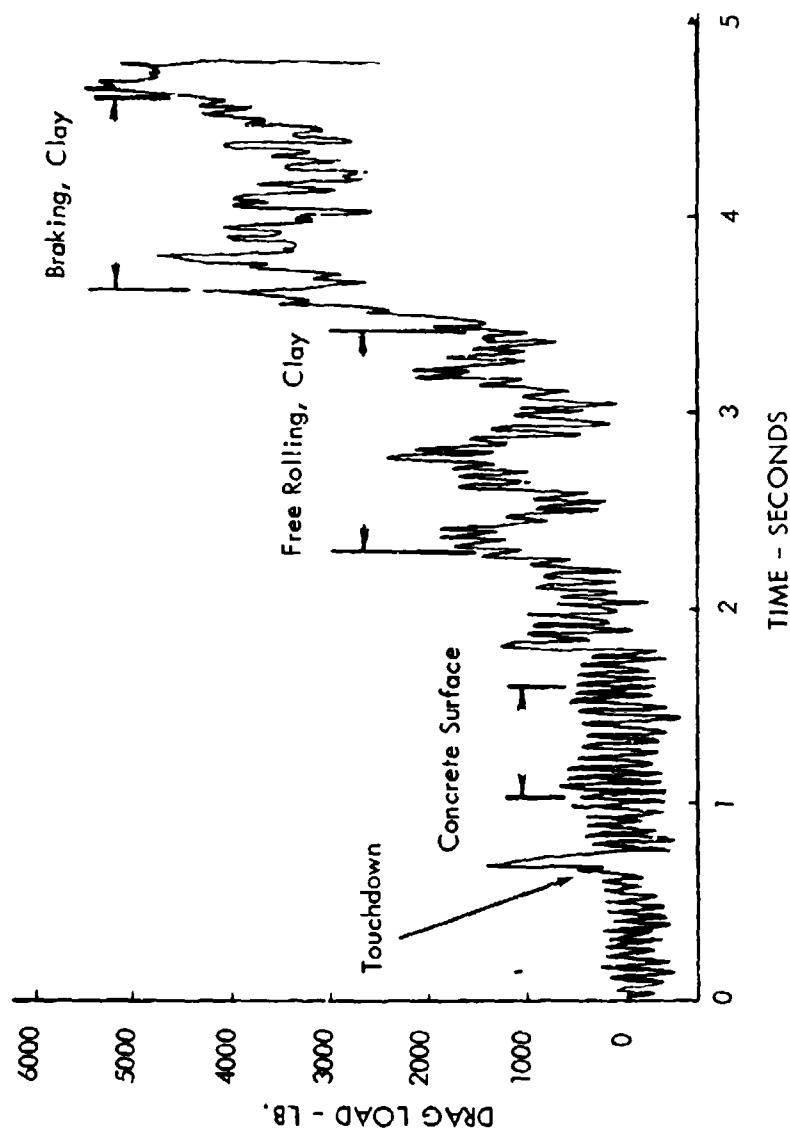


Figure 81. Drag Load Time History for Single Wheel at Six Degrees Yaw - 59.2 Knots

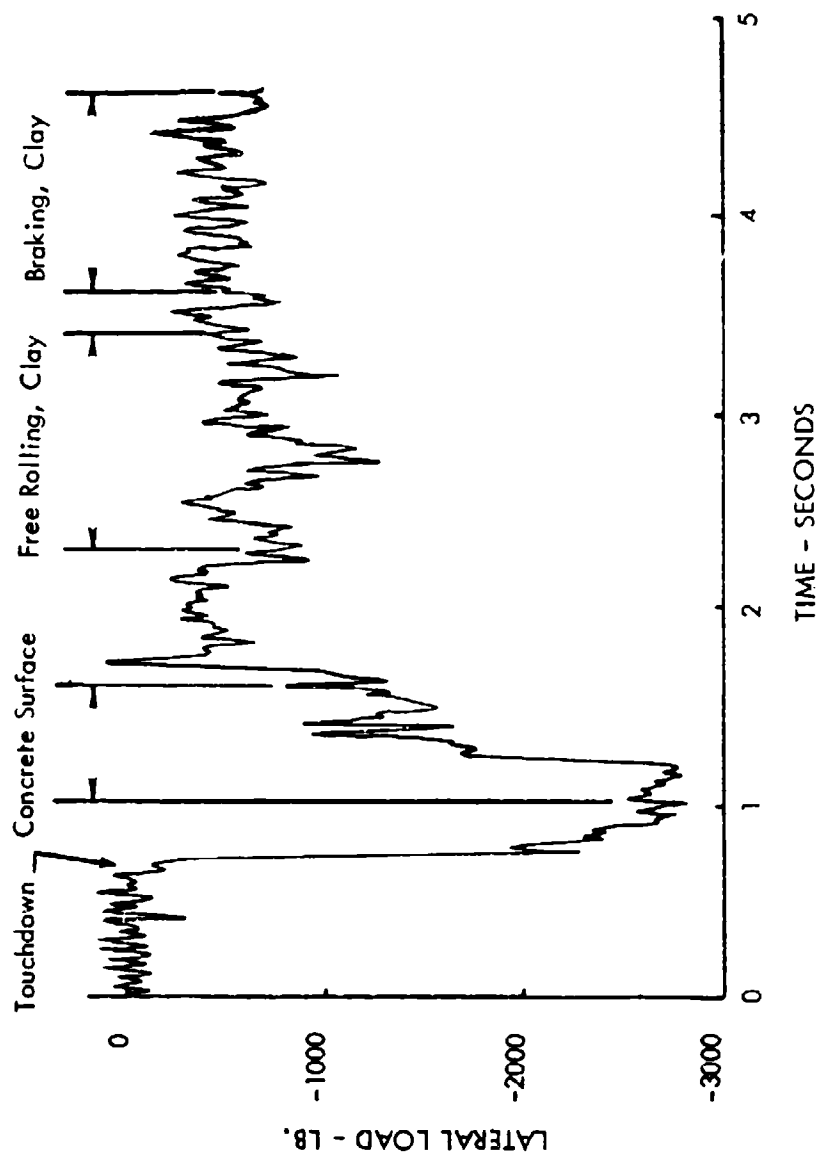


Figure 82. Lateral Load Time History for Single Wheel at Six Degrees Yaw - 59.2 Knots

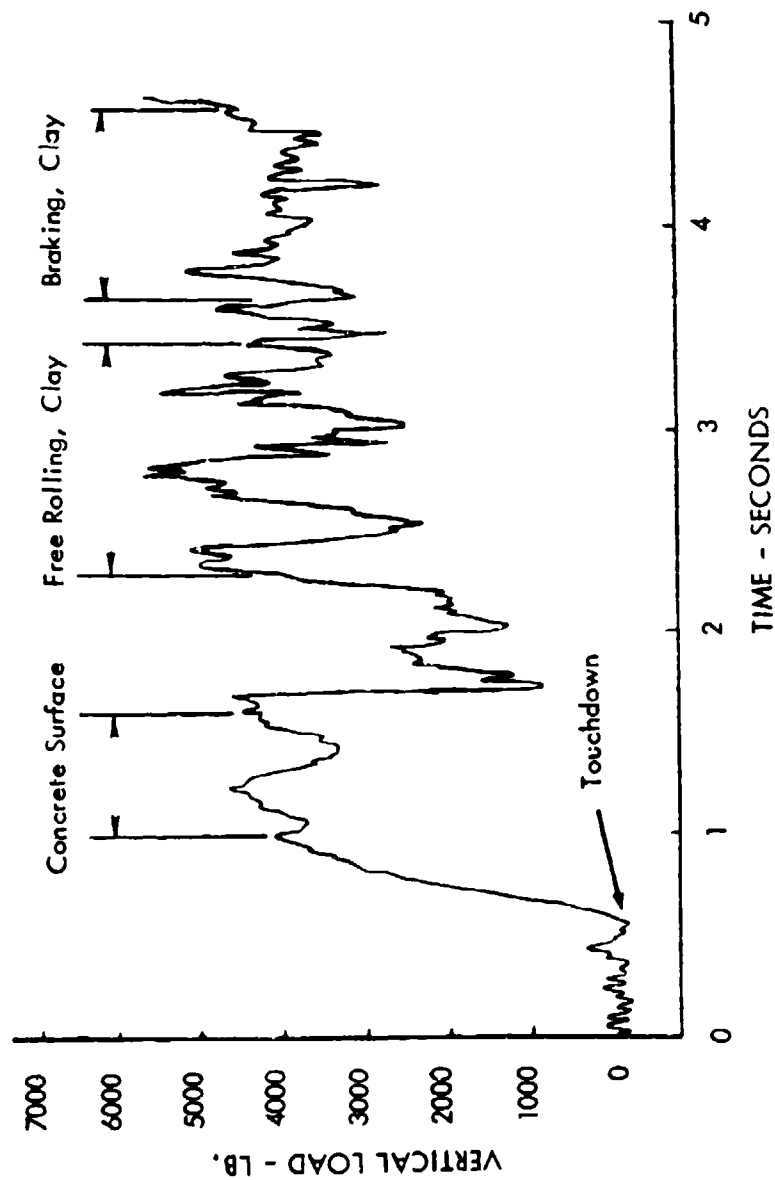


Figure 83. Vertical Load Time History for Single Wheel at Six Degrees Yaw - 59.2 Knots

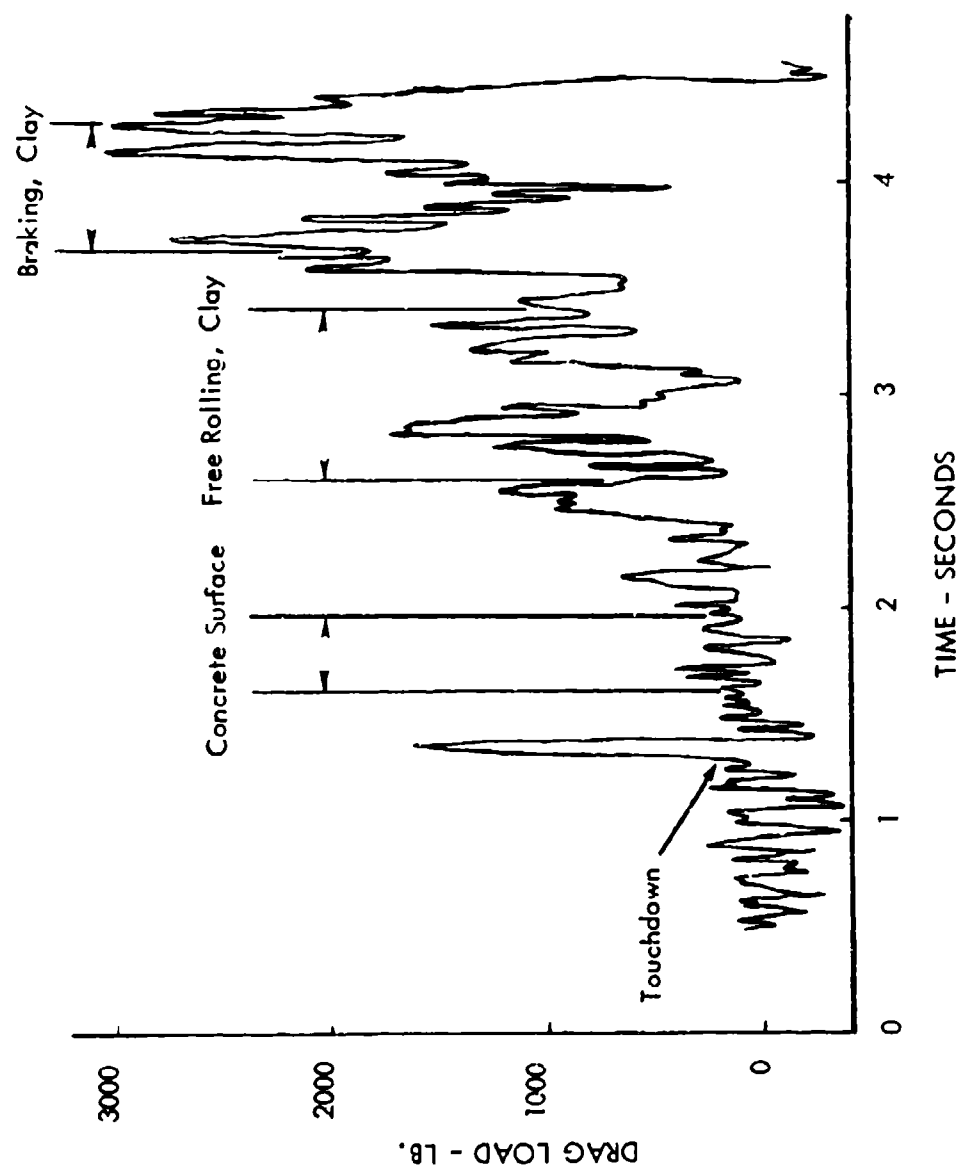


Figure 84. Drag Load Time History for Single Wheel at Six Degrees Yaw - 77.3 Knots

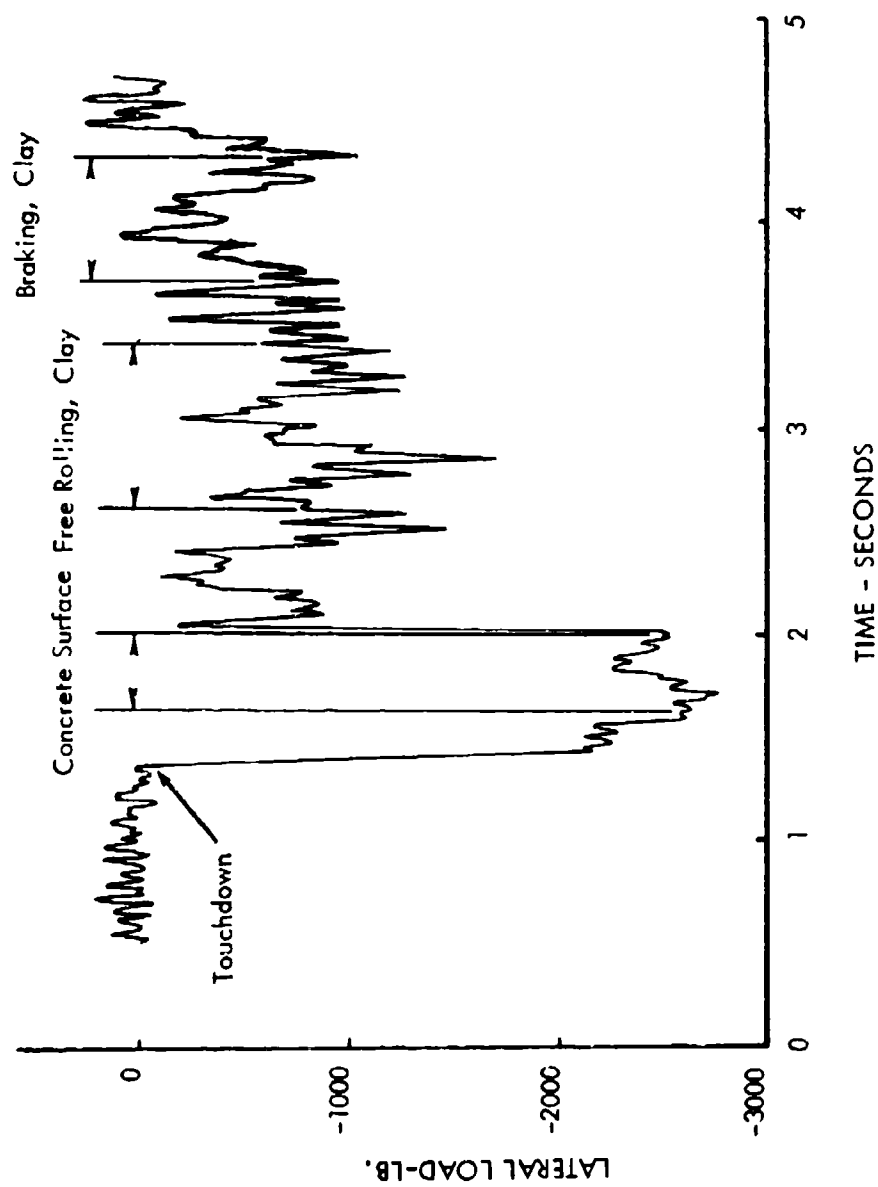


Figure 85. Lateral Load Time History for Single Wheel at Six Degrees Yaw - 77.3 Knots

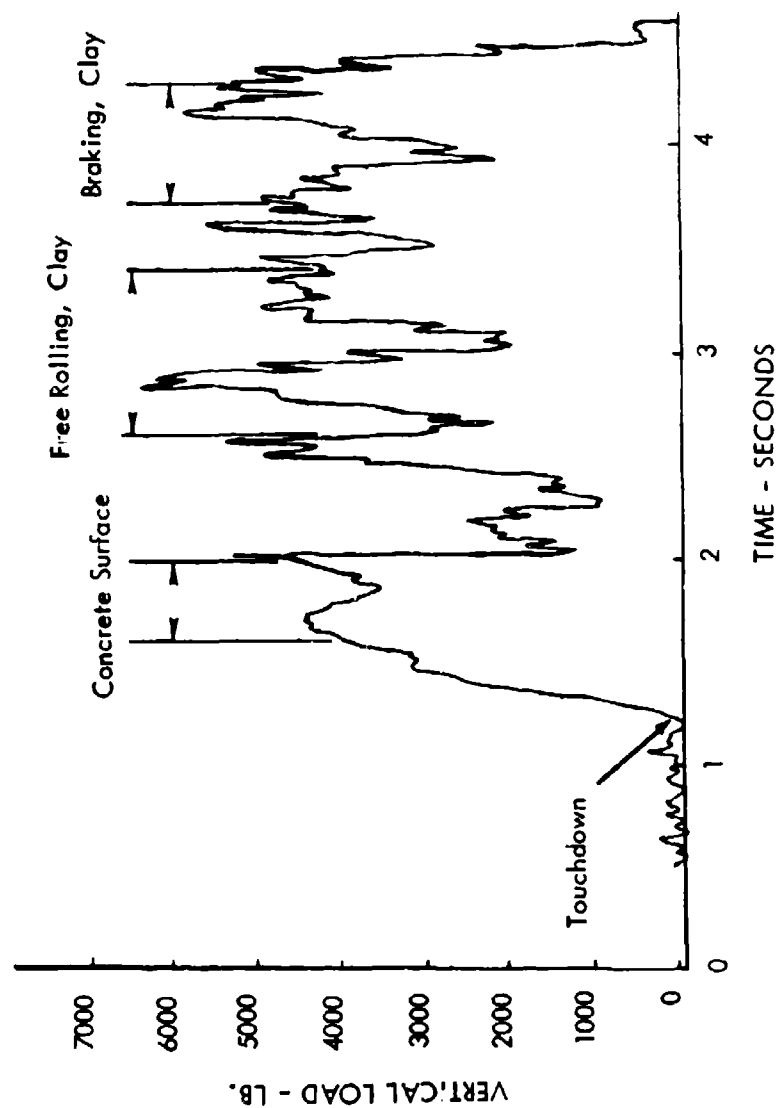


Figure 86. Vertical Load Time History for Single Wheel at Six Degrees Yaw - 77.3 Knots

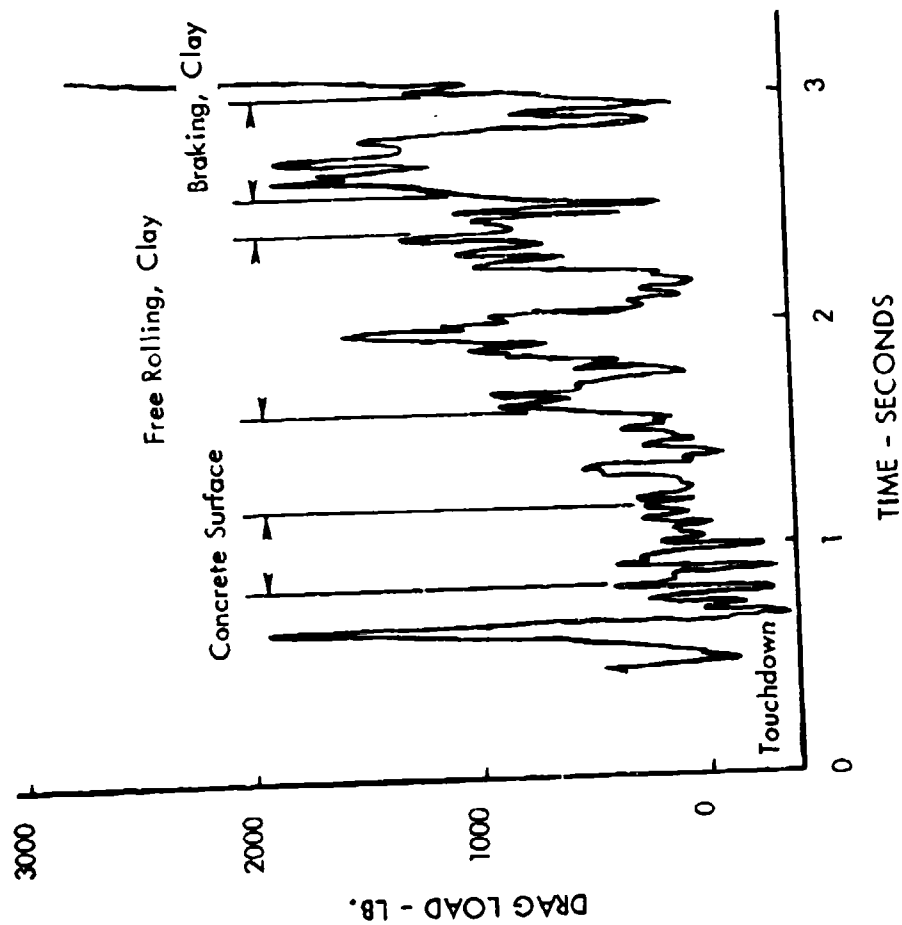


Figure 87. Drag Load Time History for Single Wheel at Six Degrees Yaw - 87.4 Knots

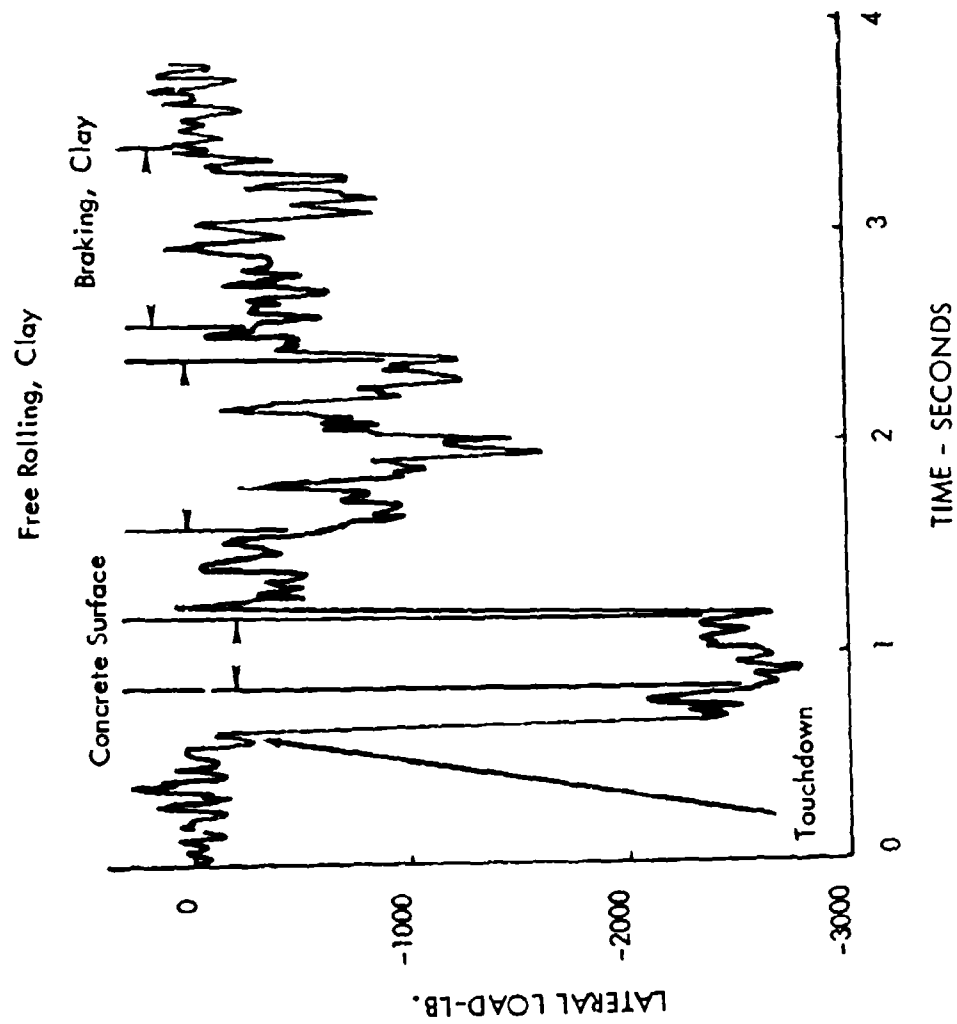


Figure 88. Lateral Load Time History for Single Wheel at Six Degrees Yaw - 87.4 Knots

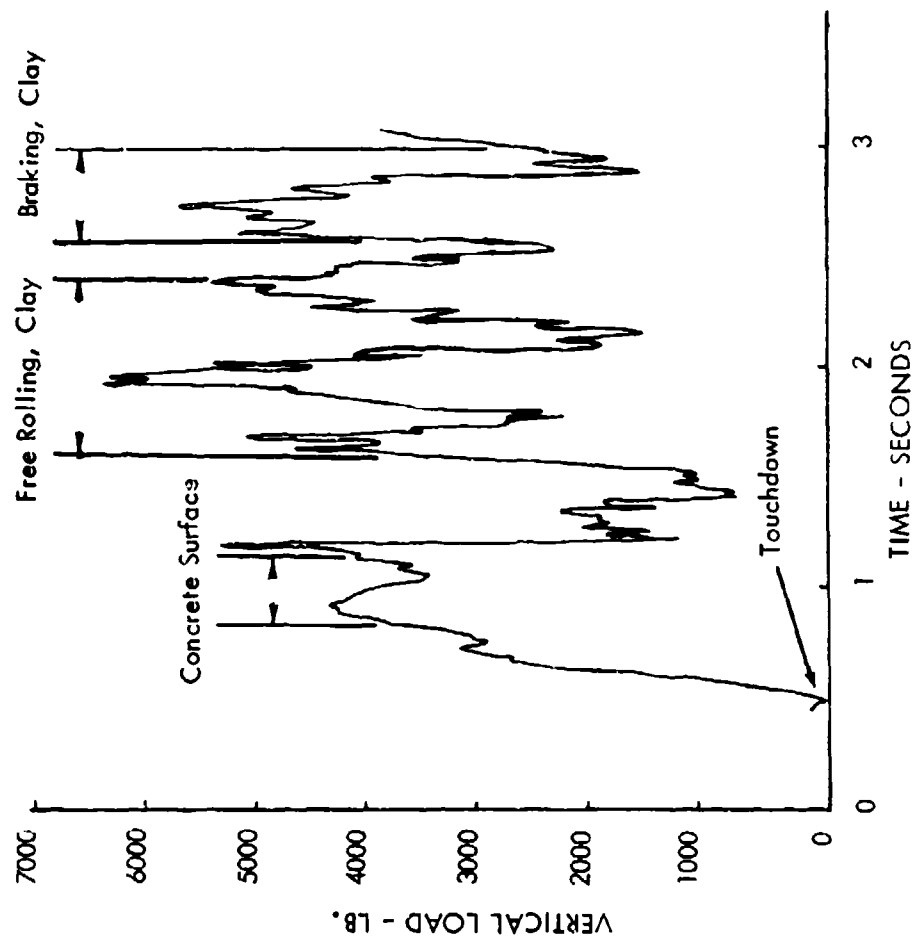


Figure 89. Vertical Load Time History for Single Wheel at Six Degrees Yaw - 87.4 Knots

APPENDIX B

ACQUISITION OF TEST DATA

Testing wheels on a soil material requires a device which supports and tows the wheels. Precise lateral positioning on the surface is needed so that undisturbed surface profiles and subsurface properties in the wheel path may be measured prior to a test. Vibration and motions of the wheel support structure should be minimized to insure that measured loads truly represent the wheel-surface interaction.

1. DESCRIPTION OF THE TEST TRACK

The facility used to perform these tests is located at the NASA/Langley Research Center, Hampton, Virginia. It consists of a 2200 ft. steel rail test track along which a test carriage is propelled by means of a water jet catapult. Carriage braking is accomplished by a cable arresting system. Test speeds were from zero (starting) to approximately 90 knots.

The test carriage weighs approximately 80,000 lb. In addition a wheel test support and ballast weight of approximately 10,000 lb. is cantilevered from the right side of the test carriage. Tests were conducted in a 6 ft. deep by 8 ft. wide tank alongside the track rails. Soil was placed in this tank for a distance of approximately 250 ft., ending at the arresting system. A concrete section was poured just ahead of the soil test bed. Height of the concrete section was equal to that of the soil bed in order to minimize dynamic loading during transition from concrete onto the soil. Rolling drag coefficients on concrete were obtained for baseline data.

A test track schematic layout is shown in Figure 90. Figure 91 shows operations on the soil test bed. The test wheel is on the concrete approach ramp. A tug used to tow the carriage back to the catapult point and to conduct low speed towing tests is attached to the test carriage. The deep rut in the soil bed resulted from braking on a previous test.

Additional detailed test track information may be found in Reference 23.

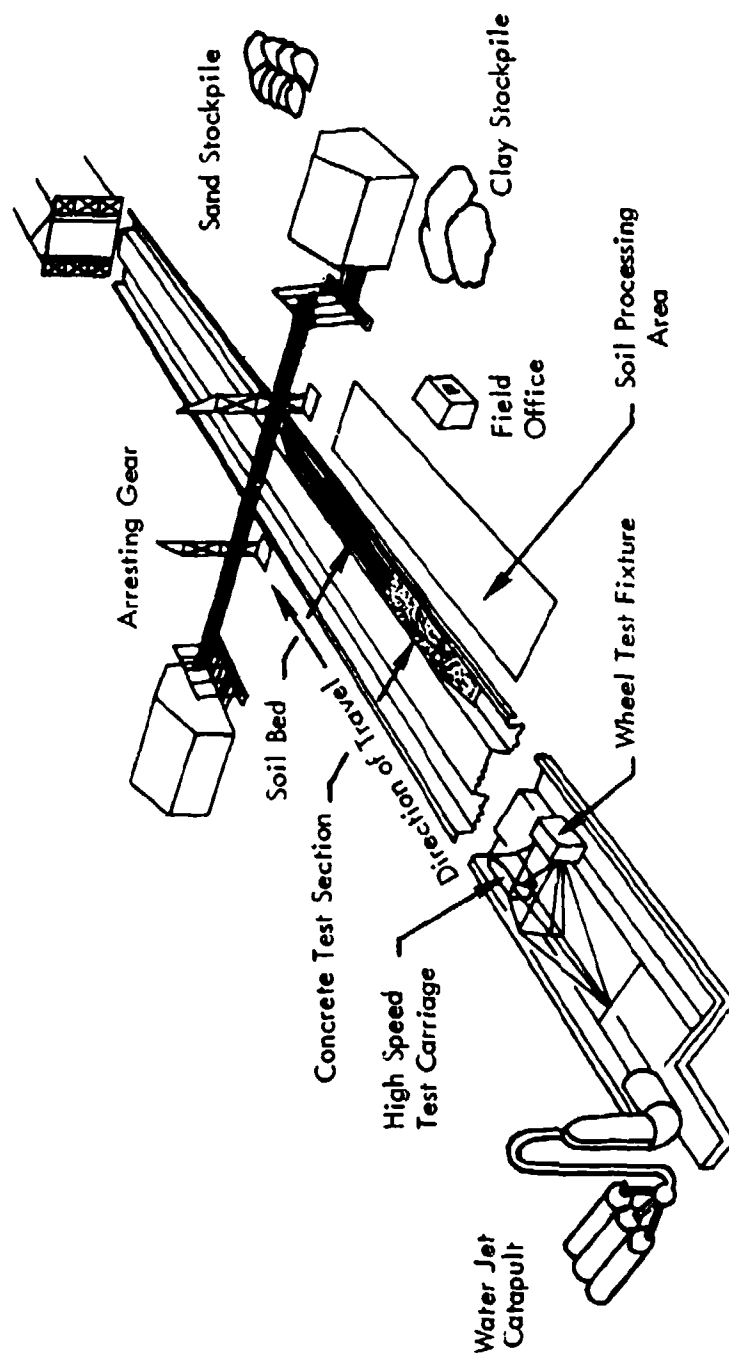


Figure 90. Schematic Diagram of the NASA/Langley Landing and Impact Loads Test Facility

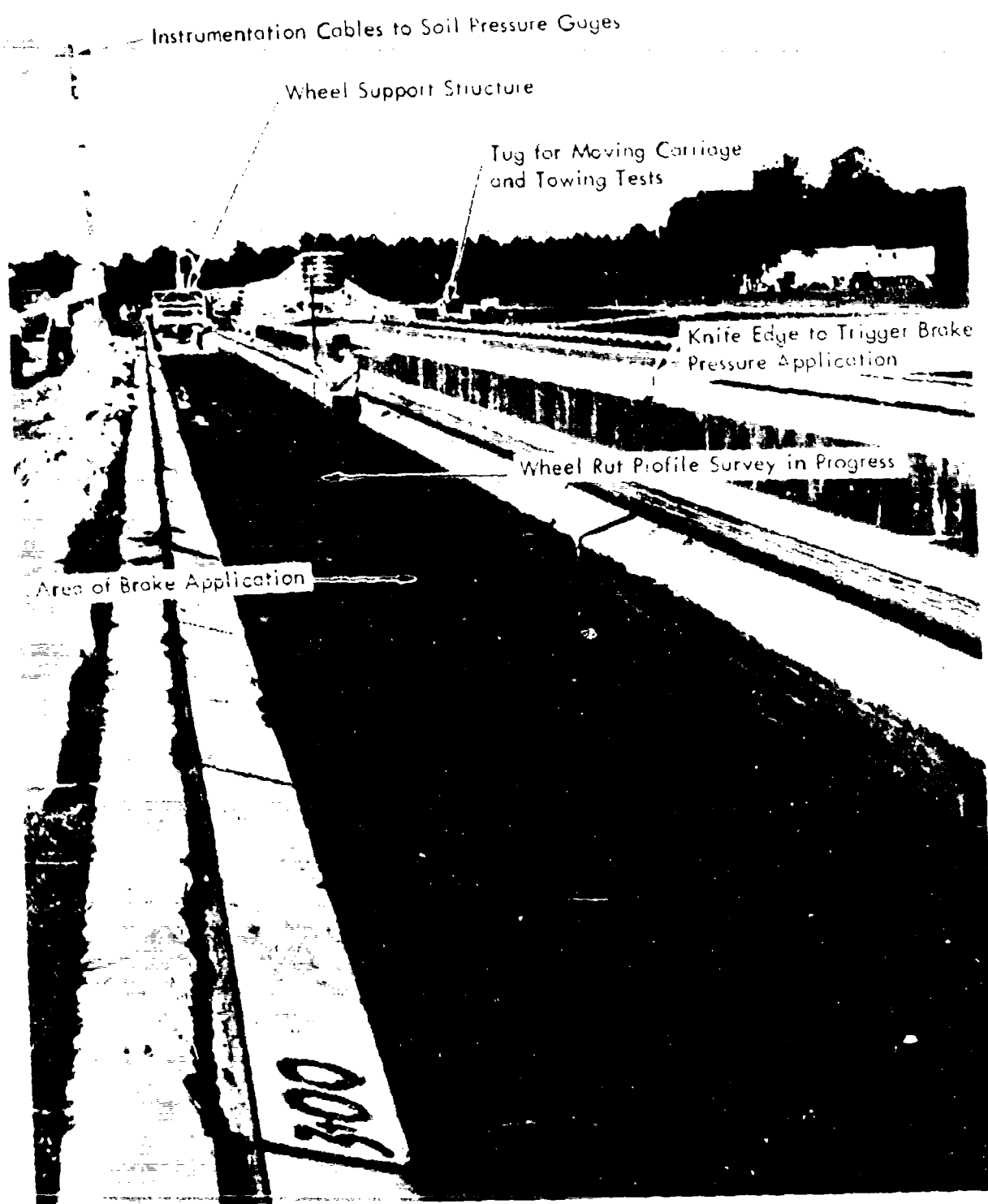


Figure 91. Landing Loads Track during the Soil Test Program

2. WHEEL SUPPORT DEVICES

Three interchangeable wheel support devices have been used for testing. They were attached to a support structure and ballast weight basket shown below in Figure 92. They were a single wheel cantilever axle mounted directly underneath the ballast weight basket, a two wheel tandem configuration on a beam pivoted directly underneath the ballast weight basket, and a single wheel mounted in a dynamometer frame capable of being yawed with respect to the direction of motion. These test fixtures are shown in Figures 93 and 94.

The test wheel was held in a retracted position to prevent it from striking the leading edge of the test section. After the wheel was over the test section, a hydraulic cylinder was used to lower the assembly and act as a shock absorber to minimize wheel bounce.

Lateral translation of the test wheel and ballast weight to allow several tests without soil surface re-processing to remove ruts was utilized for initial testing, but was not used on the last test series because of added mechanical restraints in connection with testing the wheel in a yawed configuration.

3. DATA RECORDING SYSTEM

Sensors were used to obtain load, acceleration, and velocity data as the wheel traversed the test section. Outputs of these sensors were conditioned and recorded on a magnetic tape recorder aboard the test carriage. Figure 95 shows the instrumentation signal conditioning and recording system.

Further data processing was done at the NASA Computer Center, and final output was scaled plots of each variable versus time.

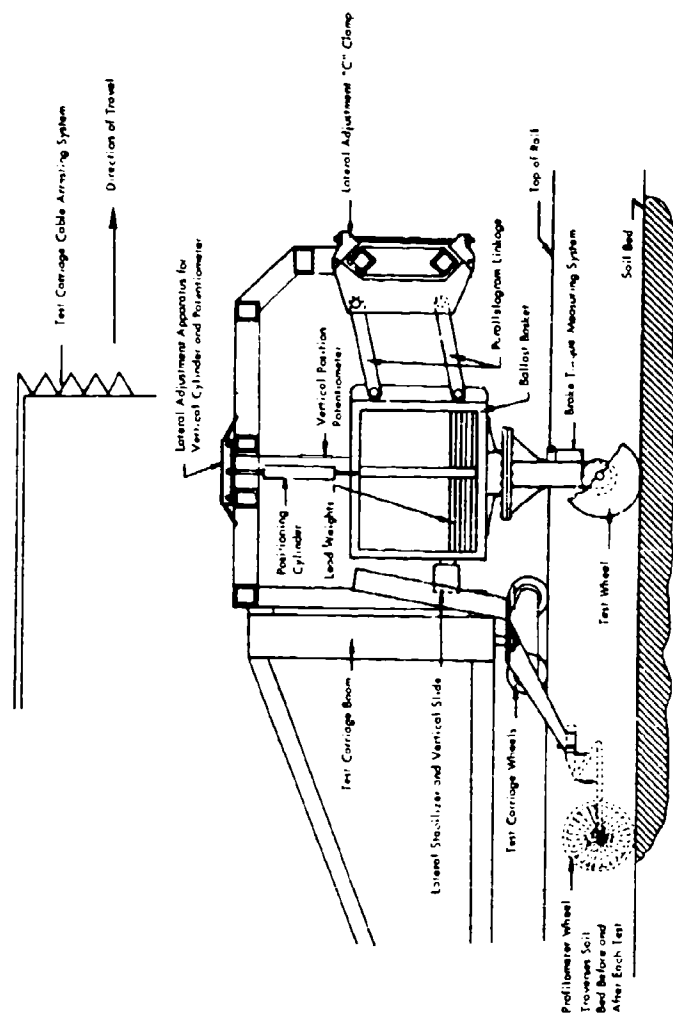


Figure 92. Schematic of the Test Fixture Mounted to the Test Carriage

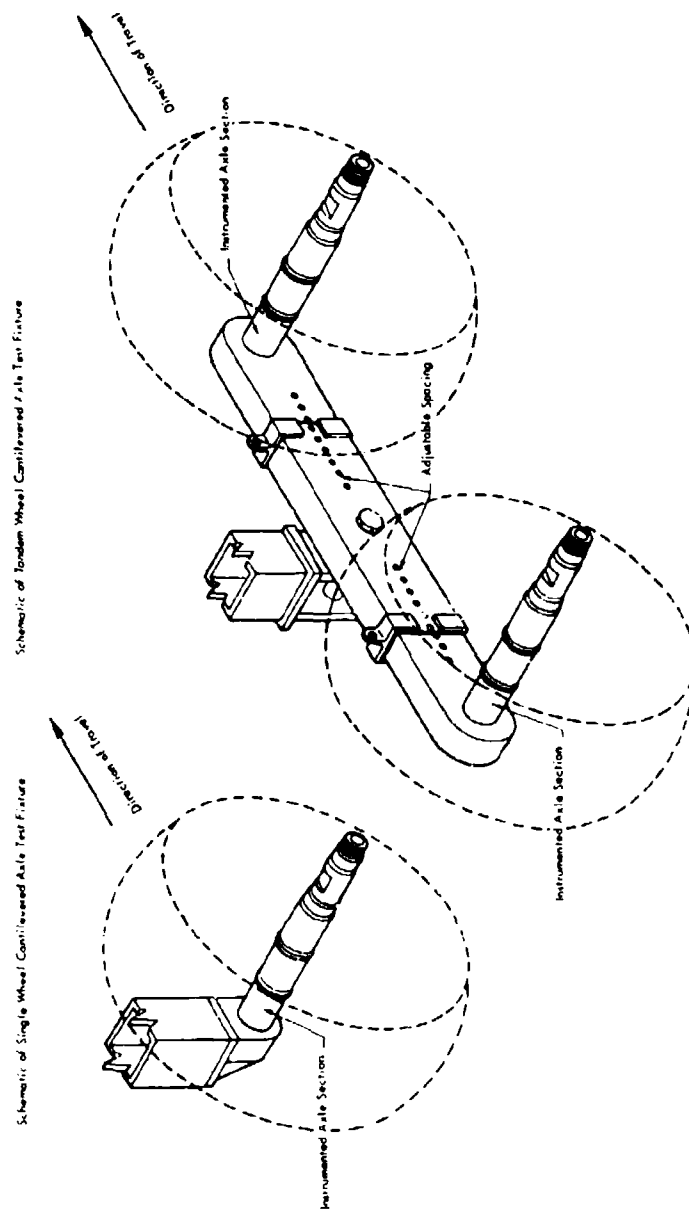


Figure 93. Schematic of the Single and Tandem Wheel Cantilevered Axle Test Fixtures

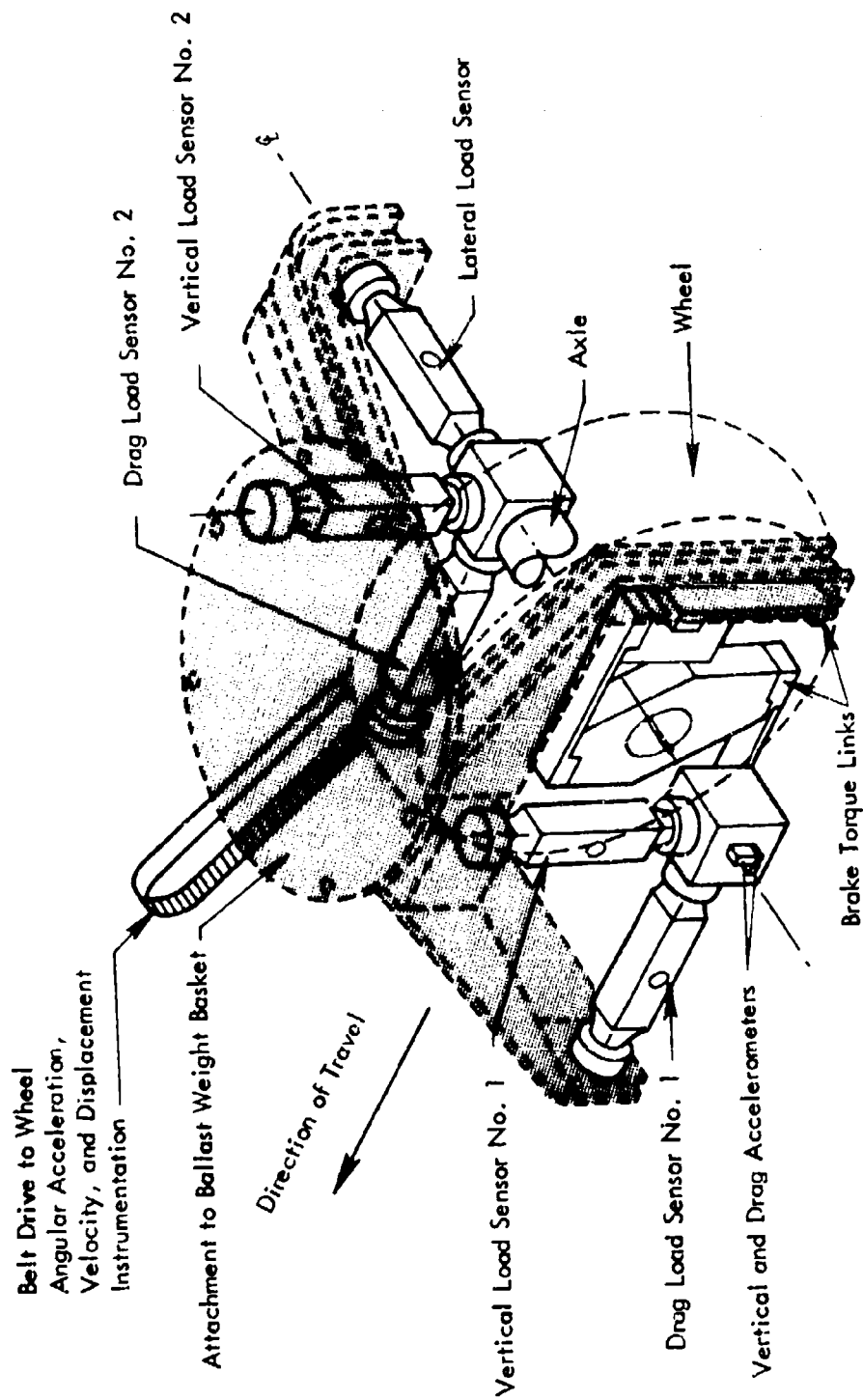


Figure 94. Schematic of the NASA Single Wheel Dynamometer

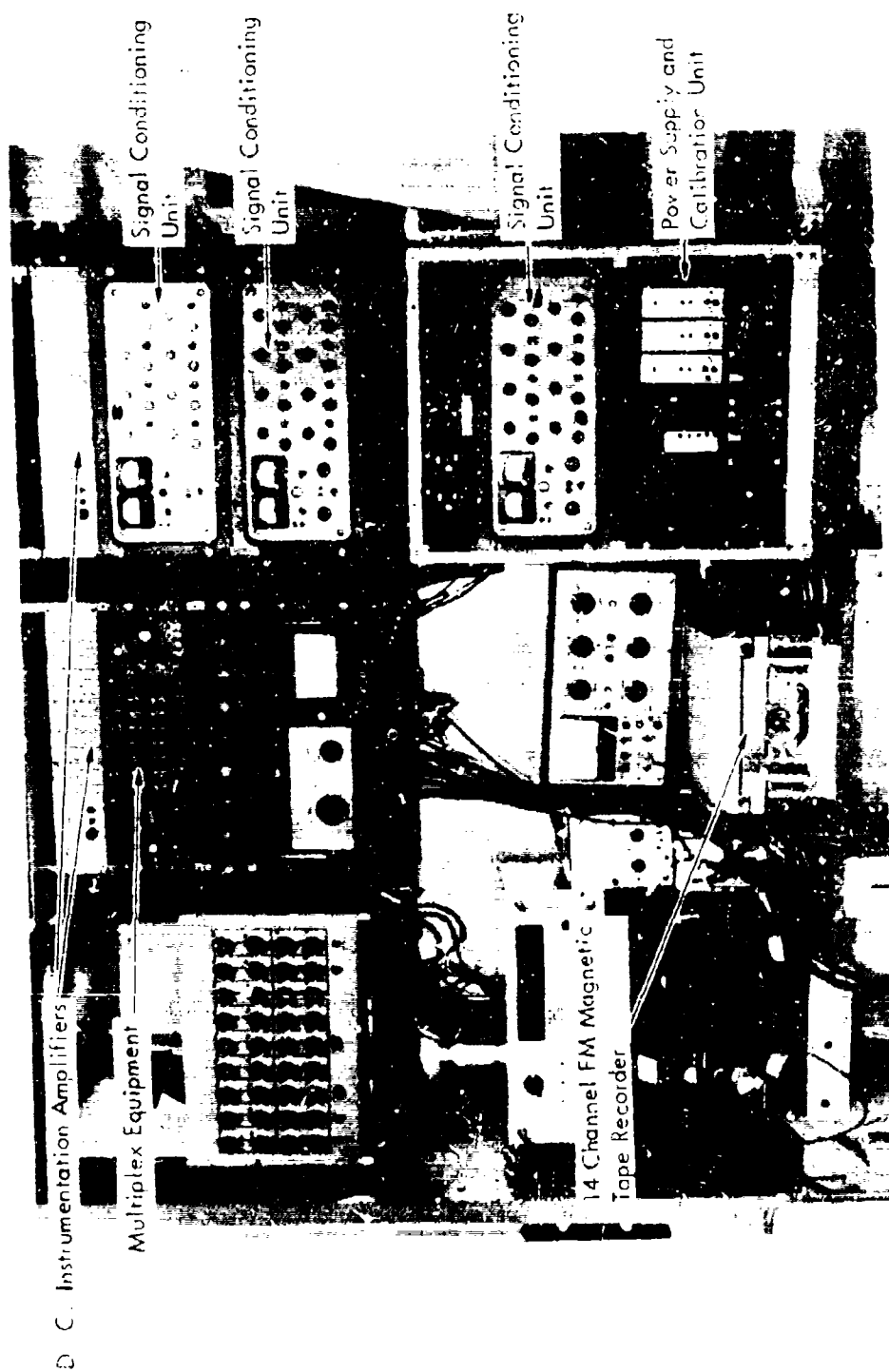


Figure 95. Instrumentation Signal Conditioning and Recording System

APPENDIX C

COMPUTER PROGRAM LISTINGS FOR SOIL MODELS

This appendix contains computer program listings for numerical computations needed with the proposed soil models. "MIMIC" simulation language is used. A description of the "MIMIC" system and programming instructions are contained in Reference 24.

Table VIII shows the computer program listing for the recommended soil model which utilizes the drag interaction concept and an iterative solution of the equilibrium, or steady state, rut depth. Table IX shows the computer program for the alternate soil model which is a differential equation solution for the time history of a soil mass as it undergoes deformation by the wheel.

TABLE VIII

Computer Program Listing for the Recommended Soil Model

MIMIC SOURCE-LANGUAGE PROGRAM

```

CON(DT,DTMIN,DTMAX)
CON(K1,K2,K3)
CON(Z,DIA,P,HT,KD)
CON(MU,K5,K6,K4)
DRAG CFN(17.)
LIFT CFN(8.)
TIRE CFN(9.)
PAR(FV)
PAR(CI)
PSWIT,FALSE,TRUE,FALSE)
P A (CI*B*DIA)/(1.6*FV*SQR(HT))
D DELT FUN(TIRE,FV)
D DELT
ZA1 LIM(DELT*Z,-100.,DIA)
ZA LIM(ZA1,DELT,100.)
LT 2.*SQR(DTA*ZA-ZA*ZA)
TP LT/(V*20.3)
DYN 1.0+1.34*EXP(-1.27*TP)
OMEGAP DYN*A*EXP(1.2*DELT)*.614*.87
CC (MU*Z/LT)*FV
CD FUN(DRAG,V)
DD K4*Z*V*20.3*V*20.3*CD
FD1 CC+DD
FD LIM(FD1,0.,5700.)
CL FUN(LIFT,CI)
D K5*CL*LT*V*20.3*V*20.3
RDRAG K5*FD/EXP(0.8*CI)
RLIFT DD/EXP(0.8*CI)
DOEZ (K1/(OMEGAP-K2)-K3)*DIA
Z IMP(Z,DOEZ+RDRAG-RLIFT)
V T*KD*5.
FIN(V,100.)
HDR(VELO,RUT,DRAG,OMEGAP,DYN,LIFT)
HDR(LOSD,V20,TP)
HDR(DOEZ,RDRAG,RLIFT)
OUT(V,Z,FD,OMEGAP,DYN,BB)
OUT(CC,DD,TP)
OUT(DOEZ,RDRAG,RLIFT)
END

```

END CCMPTLE BEGIN SORT
END SORT DEPTH ASSEMBLY

TABLE IX

Computer Program Listing for the Alternate Soil Model

```

***MIMIC SOURCE=LANGUAGE PROGRAM***

MIMIC.
CON(DT)
CON(DYMIN,DYMAX)
CON(RHO,LT)
CON(FV,PO)
CON(C1,B0,B1,A0,NU,E)
CON(PRESS)
      SP=1
      CFN(13.)
      PAR(V)
      P      FSHIT,FALSE,TRUE,FALSE)
      P      ME      C1*RHO*EXP(1.5,A/3.14)
      P      A      FV/PO
      P      C      (A/3.14)*(B0+B1*A0)*SQRT(E*RHO/2.*(1.+NU))
      K1      PRESS/2.
      T01     DSP(T,0.,.001)
      K2      6.283*2.*V/LT
      SPRING  FUN(SPR1,ZS)
      ZSDDOT  SUM(-A*SPRING/ME,A*PRES/ME,-C*ZSDOT/ME)
      ZSDOT   INT(ZSDDOT,0.)
      ZS      INT(ZSDOT,0.)
      PRES    MPY(1.-COS(LIM(T01*K2,0.,6.283)),K1)
              FIN(T,.01)
              HDR(T,ZSDDOT,ZSDOT,ZS,PRES,SPRING)
              OUT(T,ZSDDOT,ZSDOT,ZS,PRES,SPRING)
              END
END COMPILE BEGIN SORT
END SORT BEGIN ASSEMBLY

```

APPENDIX D

A SAMPLE CALCULATION FOR RUT DEPTH AND DRAG LOAD

The computations discussed here are for the recommended soil model which includes drag load interaction and inertial lift in the rut depth computations. Equilibrium rut depths are determined by an iterative process and are too lengthy for routine hand calculations. The procedure for determining the input data necessary for the computer program described in Appendix C and the process by which a single step in the iterative process takes place are outlined below.

The sample calculation is for a 29 x 11-10 8PR Type III tire loaded to 5,300 lb. operating at 40 knots over a CBR 1.5 clay surface. Calculations for other assumed conditions or for a different soil are similar.

1. INPUT DATA

Tire data is obtained from manufacturers' published data or from measurements and tests of a tire. In this report manufacturers' data have been used. The information needed consists of the following:

- ° Diameter
- ° Width
- ° Section height
- ° Load deflection curve as a function of tire pressure
- ° Tire loading and tire pressure which are selected by the analyst

Only two types of soil are used in rut depth calculations. These are sand and clay which represent pure frictional or pure cohesive soils. Mixtures of cohesive and frictional soil are assumed to have responses intermediate to the responses of these two types of soil in their separate forms.

Strength of cohesive soil (clay) is measured by cone index, CI. Cone index is related to the other common measurement of soil strength, CBR, by the relation

CI = 50 (CBR). The measure of strength for a frictional material (sand) is the quantity, G , which is the average of the rate of increase in cone index over a depth in the soil equal to the width of the tire.

2. CALCULATIONS

Tire deflection is obtained from the manufacturers' published data. For a load of 5,300 lb. and 70 psi tire pressure the value of δ_t is found to be 2.29 in. from Figure 96.

Other geometric data given for the 29 x 11-10 8PR Type III tire are:

- ° Tire diameter, $d = 28.65$ in.
- ° Tire width, $b = 10.71$ in.
- ° Tire section height, $h_t = 9.32$ in.

a. Mobility Number

The above data are substituted into the WES equation for mobility number (as modified to change the exponent on δ_t):

$$\Omega_c = \frac{. CI (bd)}{F_t} \frac{(\delta_t)^{1.2}}{(h_t)^{1/2}} \quad (.534) \quad (37)$$

$$= \frac{(75)(10.71)(28.65)(2.29)^{1.2}}{5,300 (9.32)^{1/2}} \quad (.534)$$

$$= 2.0524$$

b. Dynamic Factor

The dynamic factor is a function of the length of time a point in the soil is loaded. This time is approximated by the equation:

$$t_p = \frac{L_t}{V} \quad (38)$$

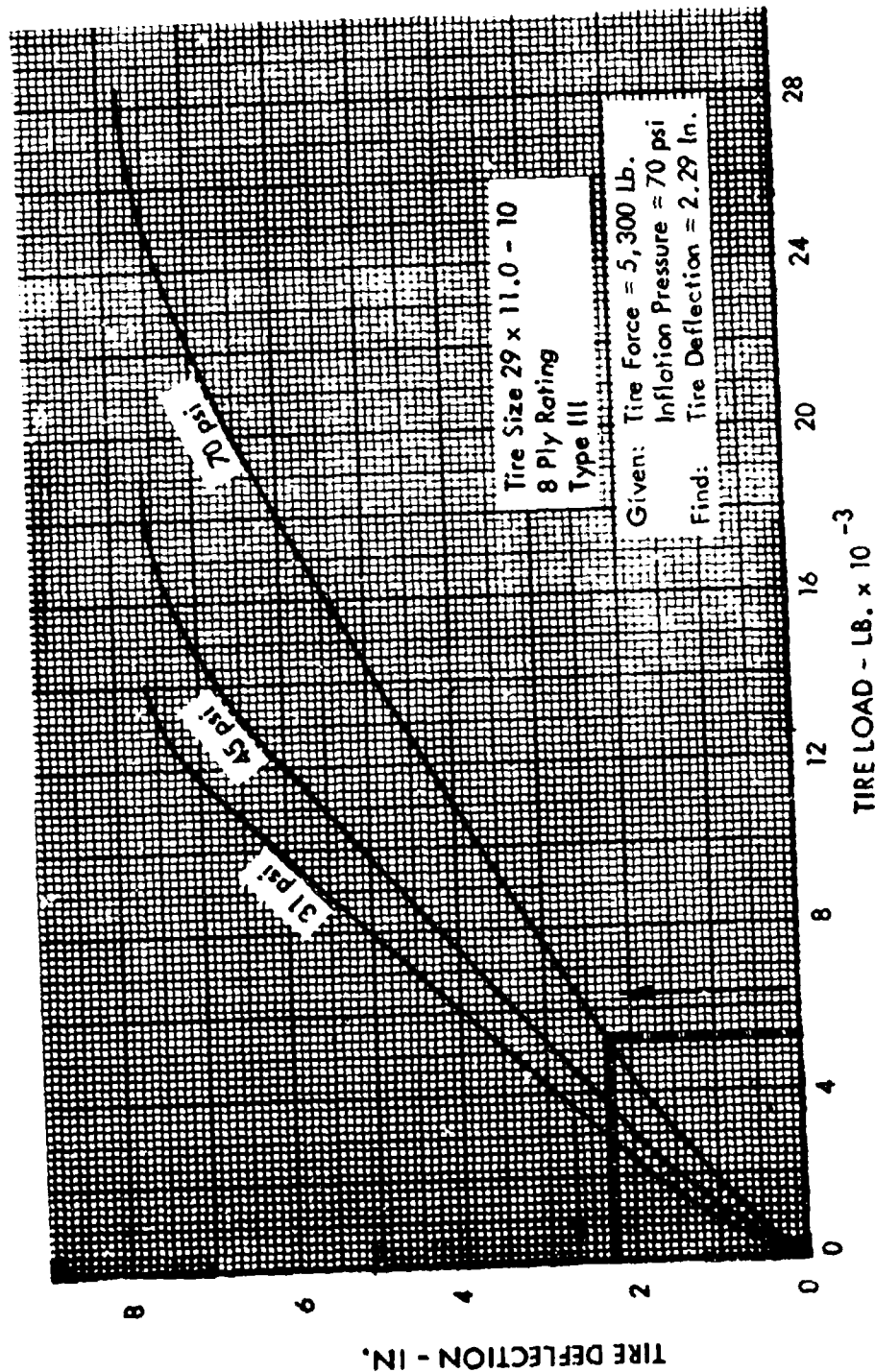


Figure 96. Determination of Tire Deflection for a Given Wheel Load and Tire Inflation Pressure

Footprint length, L_f , is pre-computed in Figure 97 for several tire pressures as a function of sinkage (rut depth). At this point an initial rut depth must be assumed to start the iterative calculation. This is arbitrarily chosen as 2.5 in. For 70 psi tire pressure the footprint length is found from Figure 97 to be 21.4 in.

For illustration, 40 knots wheel speed will be used. The pulse time, t_p , is then:

$$t_p = \frac{21.4}{40 \times 1.69 \times 12} = .0264 \text{ sec.}$$

where 1.69×12 converts knots to in./sec.

The dynamic factor is next calculated from the equation:

$$\begin{aligned} D &= 1.0 + 1.34e^{-1.27t_p} \\ &= 1.0 + 1.34e^{-1.27(.0264)} \\ &= 2.295 \end{aligned} \quad (39)$$

The dynamic mobility number, Ω'_c , is:

$$\begin{aligned} \Omega'_c &= \frac{D}{1.6} \Omega_c \\ &= \frac{2.295 (2.0524)}{1.6} \\ &= 2.944 \end{aligned} \quad (40)$$

where 1.6 is an adjustment factor to remove the dynamic effects from the original test data used to derive the dynamic factor.

c. Soil Spring Sinkage

Soil spring sinkage is obtained from the equation:

$$\begin{aligned} \Delta Z_{s_{\text{soil spring}}} &= \left[\frac{.1208}{\Omega'_c - .9468} - .0095 \right] d \\ &= \left[\frac{.1208}{2.944 - .9468} - .0095 \right] 28.65 \\ &= 1.4608 \end{aligned} \quad (41)$$

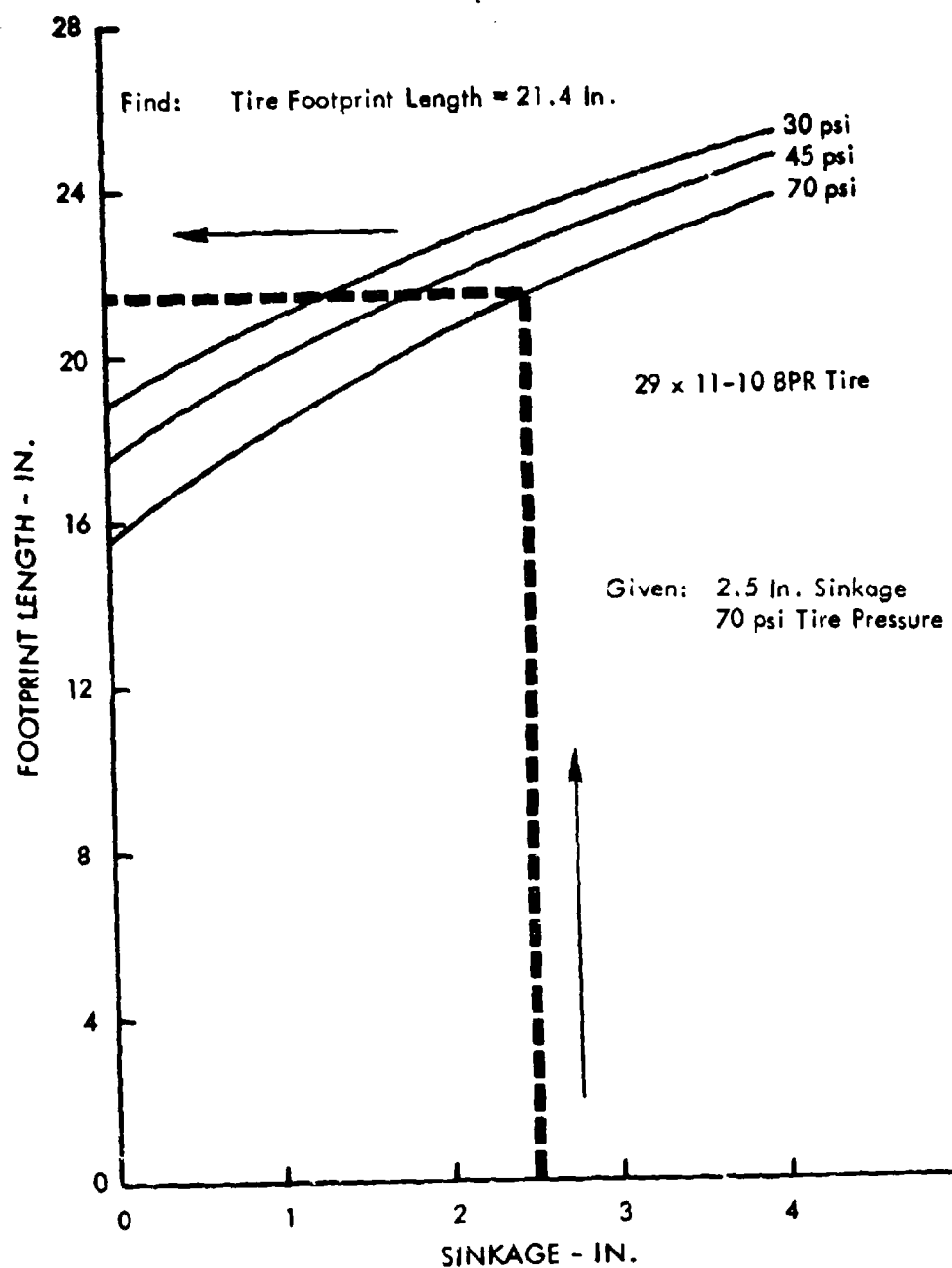


Figure 97. Determination of Tire Footprint Length for a Given Sinkage and Tire Inflation Pressure

To this point the computations are identical to those developed from the testing reported in Reference 5. Incremental terms to represent drag load interaction and lift interaction must be added.

d. Drag Load and Drag Interaction

In order to calculate the drag load/rut depth interaction the drag load is needed. This is computed from:

$$F_x = \left(\mu_o + \frac{Z_s}{L_t} \right) F_t + 1/2 \rho b Z_s C_D V^2 \quad (42)$$

Rut depth, Z_s , in the drag equation is unknown since it is a function of drag. To make an assumed calculation, the guessed value of rut depth previously used for Equation (38) will again be used. A drag coefficient, C_D , is read from the curve of C_D vs. velocity in Figure 98.

$$\begin{aligned} F_x &= \left(.04 + \frac{2.5}{21.4} \right) 5300 + 1/2 (.0001499) (10.71)(2.5)(1.72)(811.2)^2 \\ &= 3102.5 \text{ Lb.} \end{aligned}$$

The drag induced rut depth, $\Delta Z_{s_{\text{drag}}}$, is read from Figure 99 at 3100 lb. load and is found to be 0.86 in.

e. Inertial Lift Force

To calculate the inertial lift/rut depth interaction the lift is computed from:

$$F_l = 1/2 \rho b L_t C_L V^2 \quad (43)$$

The lift coefficient, C_L , is read from Figure 100 and is found to be 0.238.

$$\begin{aligned} F_l &= 1/2 (.0001499) (10.71) (21.4) (.238) (811.2)^2 \\ &= 2690.34 \text{ Lb.} \end{aligned}$$

A rut depth increment caused by inertial lift, $\Delta Z_{s_{\text{lift}}}$, is read from Figure 101 at $Cl = 75$ and 2690 lb. load. Its value is found to be 0.0435 in.

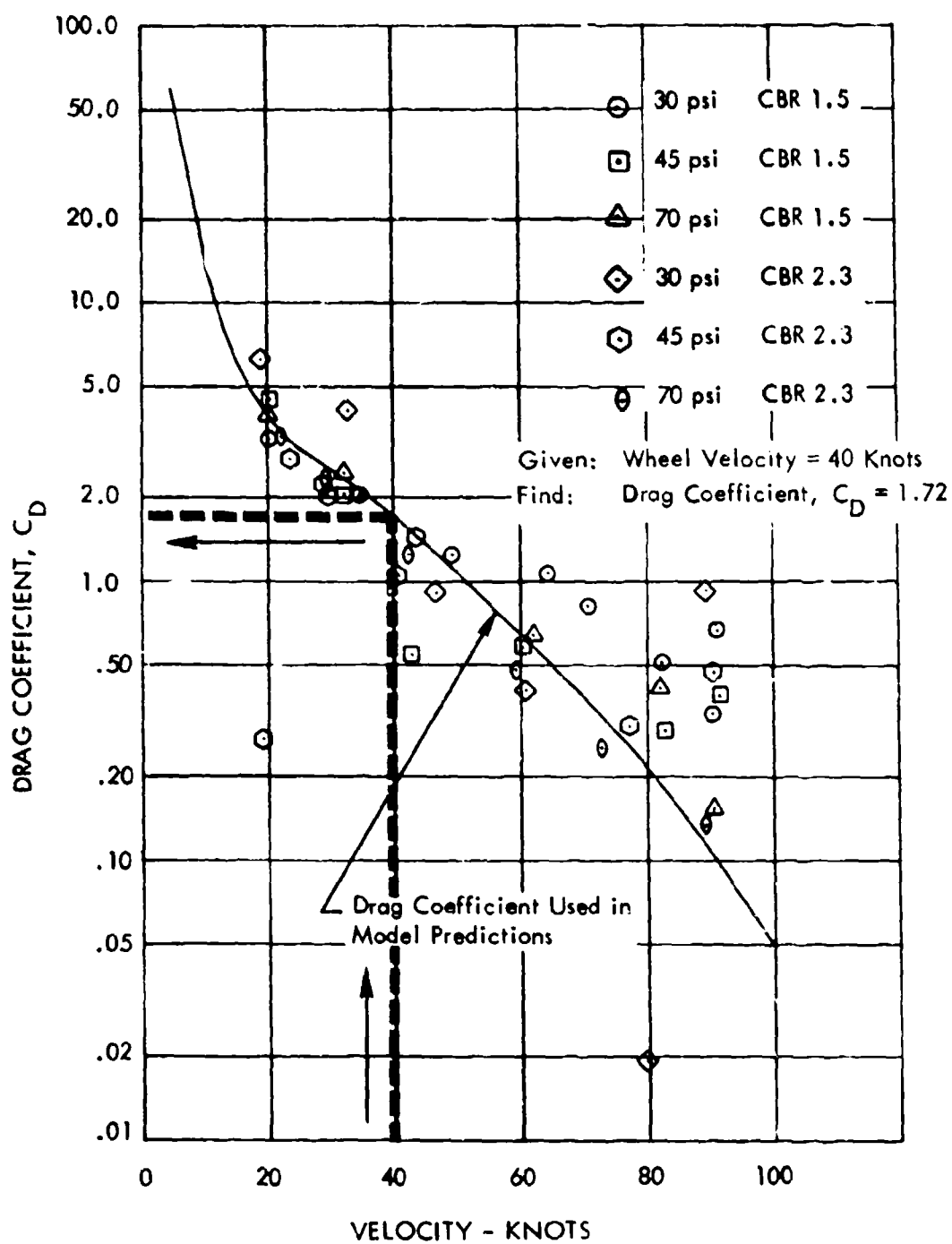


Figure 98. Determination of the Drag Coefficient, C_D , for a Given Velocity

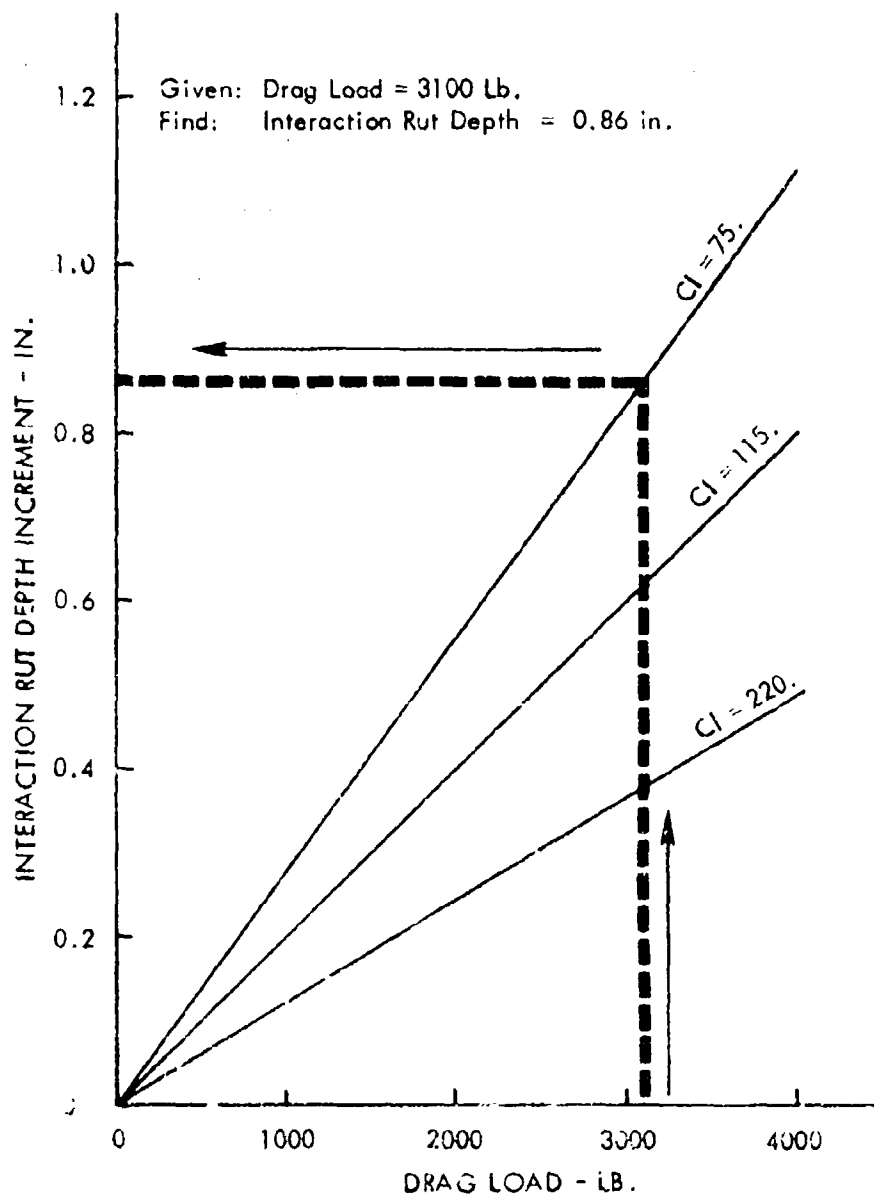


Figure 99. Determination of the Drag Interaction Rut Depth for a Given Drag Load

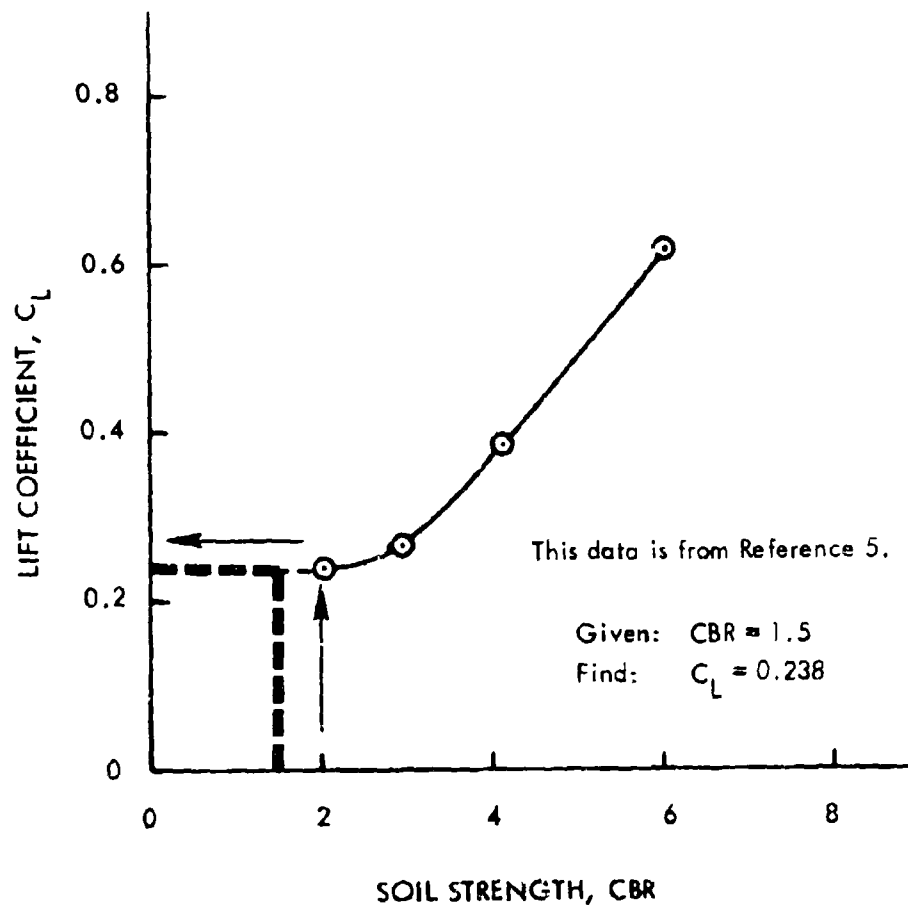


Figure 100. Determination of the Lift Coefficient, C_L , for a Given Soil Strength

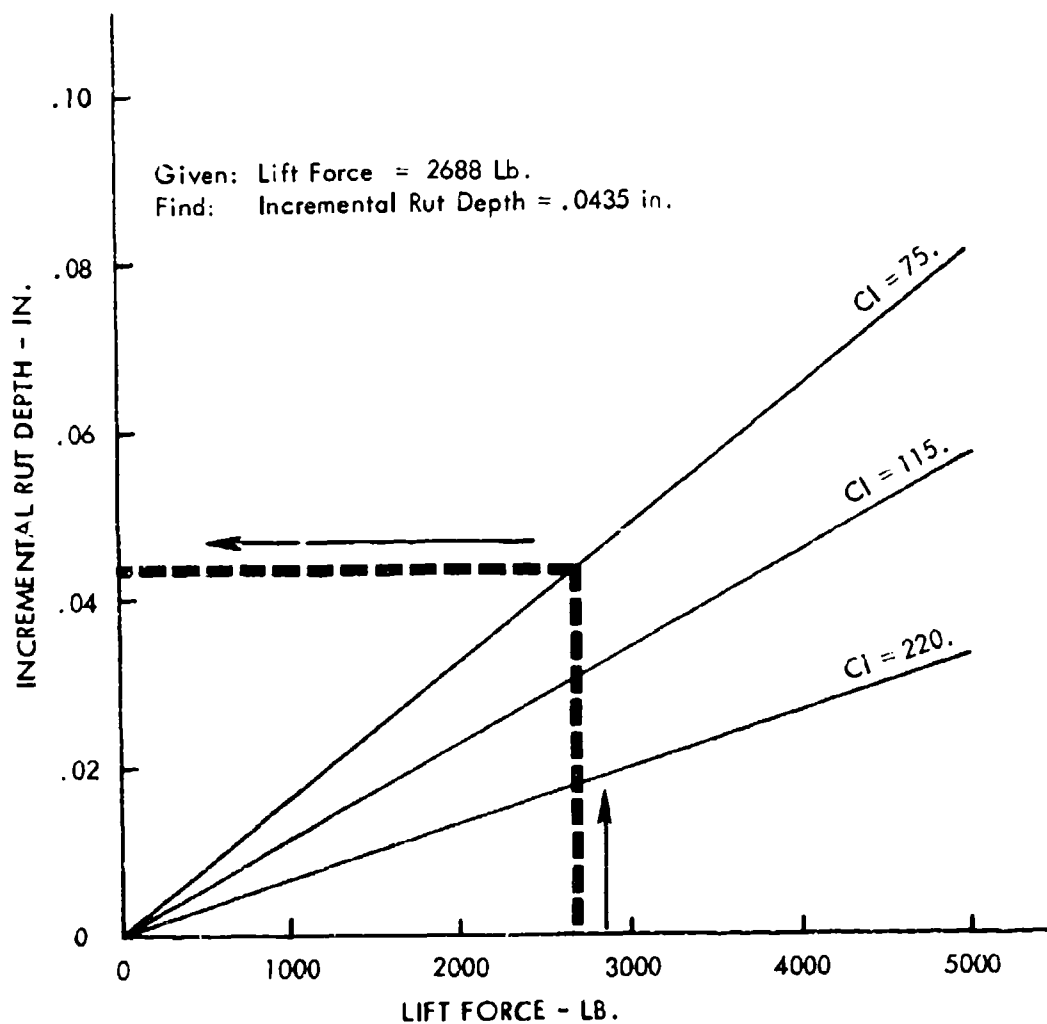


Figure 101. Determination of the Lift Interaction Rut Depth for a Given Inertia Lift Force

f. The Equilibrium Rut Depth

To calculate the total rut depth, all of the components are summed:

$$Z_s = \Delta Z_{s_{\text{soil spring}}} + \Delta Z_{s_{\text{drag}}} - \Delta Z_{s_{\text{lift}}} \quad (44)$$

This equation is of the form $x = f(x, y)$ and the equilibrium rut depths are thus the roots of the equation:

$$\Delta Z_{s_{\text{soil spring}}} + \Delta Z_{s_{\text{drag}}} - \Delta Z_{s_{\text{lift}}} - Z_s = 0 \quad (45)$$

The numerical solution of the equation uses the iteration formula from the MIMIC Programming Manual, Reference 24, page 36. This is:

$$x_{n+1} = \frac{f_n - c_n x_n}{1 - c_n} \quad (46)$$

where

$$c_n = \frac{f_n - f_{n-1}}{x_n - x_{n-1}} \quad (47)$$

This computation continues until $|x_n - f_n| \leq 5 \times 10^{-6} |x_n|$.
In terms of Equation (47),

$$f_n = \text{the } n^{\text{th}} \text{ value of } (\Delta Z_{s_{\text{soil spring}}} + \Delta Z_{s_{\text{drag}}} - \Delta Z_{s_{\text{lift}}})$$

$$f_{n-1} = \text{the } (n-1)^{\text{th}} \text{ value of } (\Delta Z_{s_{\text{soil spring}}} + \Delta Z_{s_{\text{drag}}} - \Delta Z_{s_{\text{lift}}})$$

$$x_n = \text{the value of } Z_s \text{ used in the evaluation of } f_n$$

$$x_{n-1} = \text{the value of } Z_s \text{ used in the evaluation of } f_{n-1}.$$

To begin the iteration a value of Z_s and x_{n-1} must be assumed. As used above, Z_s is assumed to be 2.5 in. x_{n-1} is assumed arbitrarily to be 0.5. The value of f_{n-1} must be evaluated for $x_{n-1} = 0.5$. This means the computation of $(\Delta Z_{s \text{ soil spring}} + \Delta Z_{s \text{ drag}} - \Delta Z_{s \text{ lift}})$ for $Z_s = 0.5$ in. The numerical value is 1.6411 in.

Using these values,

$$f_n = (1.4608 + 0.86 - .0435) \\ = 2.2773$$

$$f_{n-1} = (1.4501 + 0.225 - 0.034) \\ = 1.6411$$

$$c_n = \frac{2.2773 - 1.6411}{2.5 - 0.5} = 0.318$$

and

$$x_{n+1} = \frac{2.2773 - 0.318(2.5)}{1 - 0.318} = 2.17$$

Therefore the assumed value for the second iteration on rut depth is 2.17 in.

REFERENCES

1. Crenshaw, B. M., Butterworth, C. K., and Truesdale, W. B., Aircraft Landing Gear Dynamic Loads from Operation on Clay and Sandy Soil, AFFDL-TR-69-51, Lockheed-Georgia Company and IIT Research Institute, February, 1971.
2. Hegedus, E., Pressure Distribution and Slip-Sinkage Relationship under Driven Rigid Wheels, Report No. 8090, AD 695 669, United States Army Tank-Automotive Center, June, 1963.
3. Subgrade, Subbase, and Test Method for Pavement Base -Course Materials, MIL-STD-621A, 22 December, 1964.
4. Equipment Manual for Penetrometer, Soil, Spring Indicating (Airfield Cone), FSN 6635-900-8563, Rainhart Co., P. O. Box 4533, Austin, Texas.
5. Richmond, L. D., Brueske, N. W., De Bord, K. J., et al., Aircraft Dynamic Loads from Substandard Landing Sites, AFFDL-TR-67-145, The Boeing Company, September, 1968.
6. Ipsen, D. C., Units, Dimensions, and Dimensionless Numbers, McGraw-Hill Book Company, Inc., New York, 1960.
7. Guzdar, Adi R., Erickson, Alve J., and Howland, John S., Criteria for Establishing a Relative Design Merit Index for Aircraft Landing Gear Ground Flotation, AFFDL-TR-68-108, Air Force Flight Dynamics Laboratory, WPAFB, Ohio, March, 1968.
8. Kraft, David C., Analytical Landing Gear - Soils Interaction - Phase I, AFFDL-TR-68-88, University of Dayton Research Institute, May, 1968.
9. Green, A. J., Performance of Soils under Tire Loads, Report 5, Development and Evaluation of Mobility Numbers for Coarse-Grained Soils, Technical Report No. 3-666, U. S. Army Engineer Waterways Experiment Station, Corps of Engineers, Vicksburg, Mississippi, July, 1967.

10. Onafeko, O., and Reece, A. R., "Soil Stresses and Deformations beneath Rigid Wheels," *Journal of Terramechanics*, 1967, Vol. 4, No. 1, pp 59-80.
11. B. F. Goodrich Company, Aircraft Tires, Engineering Data, Third Edition.
12. Smiley, Robert F. and Horne, Walter B., Mechanical Properties of Pneumatic Tires with Special Reference to Modern Aircraft Tires, NACA Technical Report R-64, 1960.
13. B. F. Goodrich Company, "Load Deflection Curve," p 3, Qualification Report No. 3020-1, Issued November 11, 1966.
14. Sela, A. D. and Erlich, I. R., Load Support Capability of Flat Plates of Various Shapes, Paper No. 710178, Automotive Engineering Congress, Society of Automotive Engineers, January, 1971.
15. Green, A. J., Normal Stresses at the Tire-Soil Interface in Yielding Soils, U. S. Army Waterways Experiment Station, Corps of Engineers, Vicksburg, Mississippi, December, 1963.
16. Krick, G., "Radial and Shear Distribution under Rigid Wheels and Pneumatic Tires Operating on Yielding Soils with Consideration of Tire Deflection," *Journal of Terramechanics*, 1969, Vol. 6, No. 3.
17. Schuring, D., "Mathematical Models of the Rigid Wheel on Soft Soil," *Proceedings of the Third International Conference of the International Society for Terrain-Vehicle Systems, Inc.*, Essen, West Germany, 1969.
18. Performance of Soils under Tire Loads, Reports 1-6, U. S. Army Engineer Waterways Experiment Station, Corps of Engineers, Vicksburg, Mississippi, January, 1965-October, 1967.
19. Reece, Alan R., Problems of Soil Vehicle Mechanics, Report No. 97, U. S. Army Tank-Automotive Center, Warren, Michigan, March, 1964.

20. Van Deusen, B. D., A Statistical Technique for the Dynamic Analysis of Vehicles Traversing Rough Yielding and Non-yielding Surfaces, NASA CR-659, National Aeronautics and Space Administration, Washington, D. C., March, 1967.
21. Crenshaw, B. M., Soil/Wheel Interaction at High Speed, Paper No. 710181, Automotive Engineering Congress, Society of Automotive Engineers, January, 1971.
22. Weissmann, G. F., "A Mathematical Model of a Vibrating Soil-Foundation System," The Bell System Technical Journal, January, 1966.
23. Joyner, Upshur T., Horne, Walter, B., and Leland, Trafford, J. W., Investigations of the Ground Performance of Aircraft Relating to Wet Runway Braking and Slush Drag, AGARD Report 429, January 1963.
24. Sansom, Frederick J., and Peterson, Harry E., Mimic Programming Manual, SEG-TR-67-31, Systems Engineering Group, Aeronautical Systems Division, Air Force Systems Command, Wright-Patterson Air Force Base, Ohio, July, 1967.

UNCLASSIFIED

Security Classification

DOCUMENT CONTROL DATA - R & D

(Security classification of title, body of abstract and indexing annotation must be entered when the overall report is classified)

1. ORIGINATING ACTIVITY (Corporate author) Lockheed-Georgia Company		2a. REPORT SECURITY CLASSIFICATION Unclassified	
		2b. GROUP	
3. REPORT TITLE Aircraft Landing Gear Dynamic Loads Induced by Soil Landing Fields Volume I. Prediction Model and Wheel Loads			
4. DESCRIPTIVE NOTES (Type of report and inclusive dates) Final Report February 1969 to June 1971			
5. AUTHOR(S) (First name, middle initial, last name) B. M. Crenshaw			
6. REPORT DATE June 1972		7a. TOTAL NO. OF PAGES 173	7b. NO. OF REFS 24
8a. CONTRACT OR GRANT NO. F33615-69-C-1349		9a. ORIGINATOR'S REPORT NUMBER(S)	
b. PROJECT NO. 1370			
c. Task No. 137008		9b. OTHER REPORT NO(S) (Any other numbers that may be assigned this report) AFFDL-TR-70-169, Volume I	
d.			
10. DISTRIBUTION STATEMENT Distribution limited to U. S. Government agencies only; test and evaluation statement applied September 1971. Other requests for this document must be referred to AF Flight Dynamics Laboratory, (FY), Wright-Patterson AFB, Ohio 45433.			
11. SUPPLEMENTARY NOTES		12. SPONSORING MILITARY ACTIVITY Air Force Flight Dynamics Laboratory/FY Wright-Patterson AFB, Ohio 45433.	
13. ABSTRACT A mathematical model to predict sinkage and the resulting loads for aircraft wheels operating on bare soil surfaces is presented together with experimental results for a 29 x 11-10 8PR Type III tire. Four primary factors which determine soil rutting and drag have been identified. They consist of the tire spring rate, the soil load deflection relation, a drag inertia force, and a lift inertia force. Soil load deflections are based on the mobility number concept developed by the U. S. Army Corps of Engineers Waterways Experiment Station. Empirical constants obtained from tests conducted at the NASA Langley Landing Loads Track were used to compute the inertia forces. Comparisons of predicted and measured rut depths and drag loads are made for a clay soil with CBR's ranging from 1.5 to 2.3 and speeds from 0 to 90 knots for tire inflation pressures of 30, 45, and 70 psi. Similar comparisons are made for sand having a surface strength of CBR 1.5. The experimental program included 173 tests with a single wheel and 39 tests with two wheels in tandem on buckshot clay and 24 single wheel tests on sand. Overall average differences in predictions and test data for rut depths were the following: 11% on CBR 1.5, less than 1% on CBR 2.3, and 1.5% on sand. Overall average differences for drag loads were the following: 6% on CBR 1.5, 9% on CBR 2.3, and 12% on sand. Average positive and negative differences were somewhat higher and were between 11% and 36%. An alternate computation using a spring-mass-damper model as used in vibrating foundation studies is also included. This alternate model is not recommended as it does not account for			

DD FORM 1 NOV 65 1473

UNCLASSIFIED

Security Classification

UNCLASSIFIED

Security Classification

DOCUMENT CONTROL DATA - R & D (Cont'd)

(Security classification of title, body of abstract and indexing annotation must be entered when the overall report is classified)

13. ABSTRACT (cont'd)

drag load interaction and thus is not representative of the physical system. Methods for improvement of the alternate model are discussed. A computer program is described which incorporates the soil/wheel interaction model with a simulation of the C-130 aircraft during taxi and take-off. Analyses with this program show that moderate roughness has negligible effect on take-off distance for either soft fields or hard surfaces.

It has been shown in this report that after starting taxi, the wheel rises up out of the static sinkage rut and continues to do so as velocity increases until a minimum of rut depth and wheel drag load is reached. This is in keeping with previous theories. However, in contradiction to previous theories, after the minimum is reached the rut depth and drag load continue to increase with further increases in velocity until a maximum is reached which in some cases may be as large as those experienced at starting taxi. Further increases in velocity again result in decreasing rut depth and drag load. Hence, it is intended that the methods described in this report, which account for the phenomena, be used by airplane designers to better estimate the performance of military aircraft required to operate from soil airfields.

14.

KEY WORDS

LINK A

LINK B

LINK C

ROLE

WT

ROLE

WT

ROLE

WT

Landing Gear

Soil Testing

Substandard Runway Operations

UNCLASSIFIED

Security Classification